Stem cell modelling of α-synuclein aggregation and its pathology

Benedict Tanudjojo

Linacre College
University of Oxford



Supervised by Prof. George Tofaris

This dissertation is submitted for the degree of Doctor of Philosophy

October 2021

Abstract

α-Synuclein is a key player in the pathogenesis of Parkinson's disease and related disorders, yet it remains unclear how its aggregation triggers the degeneration of human dopaminergic neurons. In this study, I induced α-synuclein aggregation in human iPSC-derived dopaminergic neurons using α-synuclein fibrils generated from *de novo* or amplified in the presence of post-mortem brain homogenates from either Parkinson's disease or multiple system atrophy. Increased levels of α-synuclein monomer promoted its seeded aggregation in a dose- and time-dependent manner, which was further associated with the induction of α-synuclein gene expression. Progressive neuronal death was observed with exposure to brain-amplified α-synuclein fibrils and reversed by the reduction of endogenous α-synuclein abundance. Bulk RNA-Seq analysis of human dopaminergic neurons with aggregates at one- and two-weeks post-seeding identified progressive involvement of pathways implicated in organelle homeostasis. Using Gene Ontology, Unfolded Protein Response, endoplasmic reticulum stress, membrane proteolysis, and mitochondrial membrane protein insertion were upregulated. Biotin proximity labelling of α-synuclein identified 56 differentially interacting proteins with aggregates templated by brain-amplified fibrils, including the evasion of Parkinson's disease-associated deglycase, DJ-1. Ablation of DJ-1 enhanced fibril-induced aggregation and exacerbated neuronal death in iPSC-derived dopaminergic neurons. Altogether, my results demonstrate that the toxicity of α-synuclein strains is contingent upon aggregate burden, which is determined by endogenous monomer levels of α-synuclein, and strain conformation, which dictates differential interactomes. This study underscores how Parkinson's disease-associated genes influence the phenotypic manifestation of α-synuclein strains in human neurons.

Declaration of Originality

This dissertation is the result of my own work and includes nothing which is the outcome of work done in collaboration except as declared and specified in this dissertation.

It is not substantially the same as any that I have submitted or is being concurrently submitted for a degree or diploma or other qualification at the University of Oxford or any other University or similar institution except as declared in this dissertation. I further state that no substantial part of my dissertation has already been submitted, or is being concurrently submitted for any such degree, diploma or other qualification at the University of Oxford or any other University or similar institution except as declared and specified in this dissertation.

It does not exceed the prescribed word limit for the relevant Degree Committee.



28 October, 2021

Acknowledgements

First and foremost, I would like to express my sincere gratitude to my supervisor and mentor, George Tofaris, for his unwavering support and constant guidance throughout my doctoral studies. I am greatly indebted for the time George and I have spent together, which has imparted on me the values of stamina and tenacity.

During the course of my studies, the laboratory has been a place of scientific discovery, but also one of personal growth. I also owe the completion of my degree to the other members of our group: who are my colleagues, teammates, and dear friends. I would like to give special thanks to Dr. Samiha Shaikh and Dr. Jade Marsh for their prowess, and contribution towards my publication. I would also like to thank Dr. Dmitry Zenko, Dr. Cheng Jiang, and soon-to-be *Dr.* Antigoni Katsikoudi for their technical and importantly, fraternal support. I am grateful to Dr. Stephanie Halford and Vicky Anderton from Graduate Studies for their willingness to help and for their unbiased care for students. I would also like to thank Prof. Kevin Talbot for his general guidance and motivation when times were challenging.

Lastly, I would like to dedicate this dissertation to my parents, Marie Mayang Tanudjojo and Jean Satrijo Tanudjojo. I do not deserve the tremendous sacrifices they have made for me, however, I do hope that they will be proud of my hard work.

+ Oremus pro invicem +

Glossary of Abbreviations

α-Syn	α-Synuclein
α-Syn-BirA*	Biotin ligase tagged α-Synuclein
AA	Ascorbic acid
AGE	Advanced glycation end-products
Aldh1a1	Aldehyde dehydrogenase 1 family member A1
ATP	Adenosine triphosphate
BCA	Bicinchoninic acid
BDNF	Brain-derived neurotrophic factor neurotrophic factor
BioID	Biotin ligase
BMP	Bone morphogenetic protein
Cal1/2	Calbindin 1/2
Cck	Cholecystokinin
CRISPR	Clustered regularly interspaced short palindromic repeats
Cryo-EM	Cryogenic electron microscopy
db-cAMP	Dibutyryl cyclic adenosine monophosphate
DDC	Dopa decarboxalase
DIV	Days *in vitro*
DLB	Dementia with Lewy bodies
DNA	Deoxyribonucleic acid
DNMT1	DNA methyltransferase 1
FBS	Fetal bovine serum
FGF8a	Fibroblast growth factor 8a
Fib	*De novo* generated α-Synuclein preformed fibrils

FRET	Fluorescence resonance energy transfer
GBA1	Gene encoding β-glucocerebrosidase
GCI	Glial cytoplasmic inclusion
GDNF	Glia-derived neurotrophic factor neurotrophic factor
Girk2	G-protein-regulated inward-rectifier potassium channel 2
GO	Glyoxal
GRK	G-protein coupled receptor kinases
GSEA	Gene set enrichment analysis
GSH	Glutathione
GWAS	Genome-wide association studies
HC	Healthy control
HLA-DQB1	Gene encoding major histocompatibility complex, class II
HTRF	Homology time resolved fluorescence
ICC	Immunocytochemistry
IP	Immunoprecipitation
iPSC	Induced pluripotent stem cell
KSR	Knockout serum replacement medium
LB	Lewy bodies
LDH	Lactate dehydrogenase
lincRNA	Long intervening non-coding RNA
LN	Lewy neurites
LP	Lewy pathology
LRRK2	Leucine-rich zipper kinase 2
MAP2	Microtubule associated protein 2
MAPT	Gene encoding tau

MGO	Methylglyoxal
MMC	Mitomycin-C
mRNA	Messenger RNA
MSA	Multiple system atrophy
MSA-C	Multiple system atrophy with cerebellar subtype
MSA-P	Multiple system atrophy with parkinsonism subtype
NAC	Non-amyloidogenic component
NfL	Neurofilament light chain
NSC	Non-seeded control
OCR	Oxygen consumption rate
OXPHOS	Oxidative phosphorylation
PARK7	Gene encoding DJ-1
PCA	Principal component analysis
PD	Parkinson's disease
PFA	Paraformaldehyde
PINK1	PTEN-induced kinase 1
PK	Proteinase K
PLK	Polo-like kinases
PMCA	Protein misfolding cyclic amplification
PonS	Ponceau stain
PRKN	Gene encoding Parkin
pSYN	α-Synuclein phosphorylated on serine 129
RAGE	Receptor for AGE
RBD	Rapid Eye Movement behaviour disorder
RIPA	Radioimmunoprecipitation assay (buffer)

RNA	Ribonucleic acid
RNA-seq	RNA sequencing
ROCKi	Y-27632 dihydrochloride
S129A	α-Synuclein with the serine 129 to alanine mutation
SDS	Sodium dodecyl sulfate
sgRNA	Small guide RNA
SHH	Sonic hedgehog
SILAC	Stable isotope labelling using amino acids in cell culture
siRNA	Small-interfering RNA
SNCA	Gene encoding α-Synuclein
SNCA^{A53T}	iPSC line from *SNCA* p.A53T patient
SNCA^{ISOTRIP}	Isogenically corrected *SNCA* triplication patient line
SNCA^{TRIP}	iPSC line from *SNCA* triplication patient
SNCA$^{TRIP/DJ-1\ KO}$	iPSC line from *SNCA* triplication patient with CRISPR/Cas9-mediated knockout of DJ-1
SNpc	Substantia nigra pars compacta
TEM	Transmission electron microscopy
TGFβ3	Transforming growth factor β3
TH	Tyrosine hydroxylase
ThT	Thioflavin T
TUJ1	β-3 tubulin
VTA	Ventral tegmental area
WB	Western blotting, immunoblotting

Table of Contents

ABSTRACT **3**

DECLARATION OF ORIGINALITY **4**

ACKNOWLEDGEMENTS **5**

GLOSSARY OF ABBREVIATIONS **6**

TABLE OF CONTENTS **10**

LIST OF FIGURES **15**

LIST OF TABLES **19**

CHAPTER 1 BACKGROUND **20**

1.1 Parkinson's disease **20**

1.1.1 Diagnosis and prevalence of Parkinson's disease 20

1.1.2 Genetics of Parkinson's disease 22

1.1.3 Neuropathology of Parkinson's disease 25

1.1.4 Current therapeutics for Parkinson's disease 31

1.2 α-Synucleinopathies **32**

1.2.1 α-Synuclein pathobiology 33

1.2.2 Lewy pathology in Parkinson's disease 37

1.2.3 Papp-Lantos pathology in multiple system atrophy 40

1.3 Seeded aggregation of α-synuclein **41**

1.4 Stem cell modelling of α-synuclein aggregation **45**

1.5 Aims and objectives **51**

CHAPTER 2 MATERIALS AND METHODS **52**

2.1 Cell culture **52**

2.1.1 iPSC culture conditions 52

2.1.2 Generation of human iPSC-derived midbrain dopaminergic neurons 53

2.1.3 Addition of exogenous α-synuclein fibrils in dopaminergic neurons 56
2.1.4 HEK293 culture conditions 57

2.2 Live cell assays 58
2.2.1 Measurement of mitochondrial respiration 58

2.3 Biochemical techniques 60
2.3.1 List of antibodies 60
2.3.2 Immunofluorescence staining 61
2.3.3 Immunoblotting and immunoprecipitation 62
2.3.4 Time-resolved FRET 64
2.3.5 siRNA treatment 66
2.3.6 Enzyme-linked immunosorbent assay for DJ-1 67
2.3.7 Neurofilament light chain immunoassay 68

2.4 Molecular Biology techniques 69
2.4.1 Table of primers and sgRNAs 69
2.4.2 Relative gene expression 70
2.4.3 CRISPR/Cas9 knockout in HEK293 cells 71
2.4.4 CRISPR/Cas9 modification in iPSC lines 72

2.5 Transcriptome analysis 74
2.5.1 Bulk RNA sequencing 74
2.5.2 Human substantia nigra transcriptomic cell-type atlas 74
2.5.3 Cell-type deconvolution of bulk RNA sequencing samples 75
2.5.4 Analysis of RNA sequencing data 75

2.6 Interactome analysis 76
2.6.1 Affinity capture of biotinylated proteins 76
2.6.2 Mass spectrometry and analysis 78

2.7 Generation of α-synuclein polymorphs 80
2.7.1 α-Synuclein purification and assembly in fibrillar polymorphs 80
2.7.2 Patient brain homogenate preparation and quantification of pathogenic α-synuclein assemblies 82
2.7.3 Amplification of pathogenic α-synuclein in patient brain homogenates by protein misfolding cyclic amplification 85

2.8 Statistical analysis 86

2.9 Ethical approval 86

CHAPTER 3 MODELLING α-SYNUCLEIN SEEDED AGGREGATION IN HUMAN IPSC-DERIVED DOPAMINERGIC NEURONS WITH RECOMBINANT FIBRILS 87

3.1 Introduction 87

3.1.1 Stem cell modelling of Parkinson's disease 87

3.1.2 Differentiation of dopaminergic neurons 90

3.1.3 α-Synuclein seeded aggregation and phosphorylation on serine 129 95

3.1.4 Assay workflow: α-synuclein seeded aggregation in patient-derived dopaminergic neurons 98

3.2 Results 100

3.2.1 Dopaminergic markers in human iPSC-derived neurons 100

3.2.2 Addition of exogenous α-synuclein fibrils induced the accumulation of pSYN in dopaminergic neurons 105

3.2.3 $SNCA^{TRIP}$ dopaminergic neurons exhibit the highest burden of pSYN-positive inclusions 111

3.2.4 α-Synuclein fibrils induce a time and dose-dependent increase in pSYN accumulation in dopaminergic neurons 113

3.2.5 α-Synuclein fibril-induced aggregation upregulates SNCA mRNA in dopaminergic neurons 115

3.2.6 The conformation of α-synuclein polymorphs influences aggregation 117

3.3 Discussion 119

CHAPTER 4 MODIFIERS OF α-SYNUCLEIN SEEDED AGGREGATION AND TOXICITY IN IPSC-DERIVED DOPAMINERGIC NEURONS 128

4.1 Introduction 128

4.1.1 α-Synuclein strains in α-synucleinopathies 128

4.1.2 Brain-amplified fibrils by protein misfolding cyclic amplification 133

4.1.3 Dysregulated cellular pathways associated with α-synuclein pathology. 136

4.1.4 Assay workflow: phenotypic characterisation of patient brain-amplified α-synuclein fibrillar assemblies 138

4.2 Results 139
4.2.1 Amplification and characterisation of pathogenic α-synuclein from Parkinson's disease and multiple system atrophy patients 139
4.2.2 Brain-amplified α-synuclein assemblies cause progressive degeneration of iPSC-derived dopaminergic neurons 145
4.2.3 Brain-amplified α-synuclein assemblies are neurotoxic in $SNCA^{TRIP}$ dopaminergic neurons 154
4.2.4 α-Synuclein monomer levels is a critical determinant of assembly-induced toxicity in iPSC-derived dopaminergic neurons 161
4.2.5 α-Synuclein fibril-induced aggregation impairs mitochondrial function in iPSC-derived dopaminergic neurons 167
4.2.6 Isogenic correction of α-synuclein levels reduces neurodegeneration 173

4.3 Discussion 175

CHAPTER 5 MECHANISMS OF PARKINSON'S DISEASE-ASSOCIATED α-SYNUCLEIN STRAIN TOXICITY 185

5.1 Introduction 185
5.1.1 α-Synuclein protein interactome through proximity labelling 185
5.1.2 The neuroprotective role of DJ-1 190
5.1.3 Glycating stress and its relevance in Parkinson's disease 192
5.1.4 DJ-1 mutants in Parkinson's disease 194
5.1.5 Assay workflow: phenotypic characterisation of DJ-1 knockout under conditions of α-synuclein seeded aggregation 198

5.2 Results 199
5.2.1 Differential protein interactome of *de novo* versus patient brain-amplified α-synuclein assemblies 199
5.2.2 DJ-1 knockout and GLO1 knockout in HEK293 cells under seeded aggregation 207
5.2.3 Advanced glycation end products in HEK293 cells under seeded aggregation 212
5.2.4 Quantitation of α-synuclein K12 containing peptide with or without GlyGly modification 214
5.2.5 Methylglyoxal treatment in iPSC-derived dopaminergic neurons under seeded aggregation 216

5.2.6 DJ-1 knockout in human iPSC-derived dopaminergic neurons exacerbates aggregate-induced toxicity 217

5.3 Discussion 230

CHAPTER 6 CONCLUSIONS 237

REFERENCES 243

APPENDIX 285

List of Figures

Figure 1.1 Cardinal histopathological features of Parkinson's disease 26

Figure 1.2 Six stages of α-synuclein pathology in idiopathic Parkinson's disease brains 28

Figure 1.3 Schematic diagram of α-synuclein residues and protein structure... 35

Figure 1.4 Templated aggregation and propagation of α-synuclein in related disorders 42

Figure 1.5 Major ranked phenotypes from iPSC-derived dopaminergic neurons from Parkinson's disease patients 46

Figure 2.1 Agilent Seahorse XF Cell Mito Stress Test used to quantify oxygen consumption rate under aggregation conditions 59

Figure 2.2 Homology time resolved fluorescence Cisbio kit 65

Figure 3.1 Protocols for the differentiation of human stem cells and pluripotent stem cells into midbrain dopaminergic neurons 94

Figure 3.2 Modelling α-synuclein aggregation in human iPSC-derived dopaminergic neurons 99

Figure 3.3 Differentiation protocol for generation of dopaminergic neurons from iPSCs 101

Figure 3.4 Image journal of differentiating iPSCs from day 0 to day 35 102

Figure 3.5 Characterisation of human iPSC-derived dopaminergic neurons ... 103

Figure 3.6 Dopaminergic neuron identity by bulk RNA-Seq 104

Figure 3.7 Representative confocal images of pSYN inclusions in human iPSC-derived dopaminergic neurons 106

Figure 3.8 RIPA-insoluble fractions from seeded neuronal lysates were immunoreactive for pSYN by immunoblotting 107

Figure 3.9 Phosphorylated α-synuclein in RIPA-insoluble fraction 108

Figure 3.10 S129A mutant *de novo* fibrils induce p-S129 α-synuclein-positive inclusions 110

Figure 3.11 Seeded aggregation in healthy controls, $SNCA^{A53T}$ and $SNCA^{TRIP}$ iPSC-derived dopaminergic neurons 112

Figure 3.12 A single exposure to α-synuclein fibrils induce a dose and time-dependent response in healthy controls and SNCA^{TRIP} iPSC-derived dopaminergic neurons 114

Figure 3.13 α-Synuclein aggregation upregulates *SNCA* mRNA in iPSC-derived dopaminergic neurons 116

Figure 3.14 α-Synuclein ribbons exhibited higher seeding propensity than fibrils 118

Figure 4.1 Structural differences between brain-amplified α-synuclein fibrils from Parkinson's disease and multiple system atrophy patient..... 130

Figure 4.2 Amplification of α-synuclein from diseased brain homogenates 134

Figure 4.3 Quantification of pathogenic α-synuclein aggregates in patient brains 140

Figure 4.4 Three cycle amplification of pathogenic α-synuclein seeds and electron micrographs of resulting assemblies 142

Figure 4.5 Limited proteolytic patterns of PMCA-amplified α-synuclein assemblies 144

Figure 4.6 Aggregation propensity of *de novo* and brain-amplified α-synuclein fibrils 146

Figure 4.7 De novo and brain-amplified α-synuclein fibrils induce distinct pSYN-positive aggregates in SNCA^{TRIP} dopaminergic neurons 148

Figure 4.8 *De novo* and brain-amplified α-synuclein fibrils induce distinct pSYN-positive aggregates in healthy control dopaminergic neurons 149

Figure 4.9 Electron microscopy measurements of *de novo* generated fibrils and brain-amplified assemblies after sonication..... 151

Figure 4.10 Limited proteolytic patterns of α-synuclein assembly-induced aggregates from iPSC-derived dopaminergic neurons 153

Figure 4.11 Progressive neurodegeneration in PD- and MSA-seeded SNCA^{TRIP} dopaminergic neurons 155

Figure 4.12 α-Synuclein monomer and homogenates from each PD and MSA case did not cause toxicity in contrast to corresponding amplified α-synuclein assemblies in SNCA^{TRIP} dopaminergic neurons..... 157

Figure 4.13 Neurofilament light chain release in dopaminergic neurons exposed to *de novo* and patient brain-amplified α-synuclein fibrils 159

Figure 4.14 Principal component analysis on the 1000 most variable protein-coding genes by bulk RNA-Seq in seeded neurons vs non-seeded controls .. 162

Figure 4.15 Differential gene expression by bulk RNA-Seq in seeded neurons vs. non-seeded controls 164

Figure 4.16 Gene set enrichment analysis by bulk RNA-Seq in seeded neurons vs. non-seeded neurons 166

Figure 4.17 De novo fibrils and patient brain-amplified assembly disrupt mitochondrial respiration 168

Figure 4.18 Assessment of mitochondrial function and OXPHOS complex proteins in response to treatment with *de novo* or brain-amplified α-synuclein fibrils 170

Figure 4.19 Characterisation of aggregation in iPSC-derived dopaminergic neurons treated with 0.1 µM fibrils 172

Figure 4.20 α-Synuclein expression is a critical determinant of assembly-induced toxicity 174

Figure 5.1 Cellular functions of DJ-1 191

Figure 5.2 DJ-1 mutants disrupt its protective function against oxidative stress 195

Figure 5.3 DJ-1 as a therapeutic target in Parkinson's disease 197

Figure 5.4 Biotin ligase (BioID) tagged α-synuclein (α-Syn-BirA*) in HEK293 cells 201

Figure 5.5 Confocal images of cells treated with biotin and biotinylation of SILAC labelled cells..... 203

Figure 5.6 Mass spectrometry of biotinylated proteins under α-synuclein seeded aggregation 205

Figure 5.7 α-Synuclein interacts with DJ-1 in HEK293 cells expressing α-Syn-BirA* 206

Figure 5.8 Pathway of methylglyoxal detoxification involving DJ-1 and GLO1 207

Figure 5.9 Confocal images of seeded aggregation in CRISPR/Cas9 knockout of DJ-1 in HEK293 cells expressing Venus-tagged α-synuclein 209

Figure 5.10 CRISPR/Cas9 knockout of DJ-1 and GLO1 in HEK293 cells expressing Venus-tagged α-synuclein 211

Figure 5.11 Seeded aggregation triggered advanced glycation end products in HEK293 cells 213

Figure 5.12 SILAC quantitation for K12 containing peptide with and without GlyGly modification 215

Figure 5.13 Methylglyoxal treatment exacerbates disease phenotypes in human SNCA^{TRIP} dopaminergic neurons 216

Figure 5.14 Generation of DJ-1 knockout clones in SNCA^{TRIP} iPSCs (*on next page*) 217

Figure 5.15 Validation of deletions in PARK7 (DJ-1) by Sanger sequencing 219

Figure 5.16 Short tandem repeat analysis of CRISPR/Cas9 DJ-1 knockout clones and their corresponding line of origin 220

Figure 5.17 Loss of DJ-1 in selected iPSC clones 221

Figure 5.18 Characterisation of human SNCA$^{TRIP/DJ\text{-}1\ KO}$ dopaminergic neurons 222

Figure 5.19 Baseline α-synuclein levels increased with time in culture in SNCA$^{TRIP/DJ\text{-}1KO}$ compared to SNCA^{TRIP} iPSC-derived dopaminergic neurons 223

Figure 5.20 DJ-1 knockout in SNCA^{TRIP} dopaminergic neurons further impairs mitochondrial respiration 224

Figure 5.21 DJ-1 knockout in SNCA^{TRIP} dopaminergic neurons exacerbates seeded aggregation 226

Figure 5.22 α-Synuclein seeded aggregation causes severe neurotoxicity in SNCA$^{TRIP/DJ\text{-}1\ KO}$ dopaminergic neurons 228

List of Tables

Table 1.1 Summary of neurodegenerative diseases associated with α-synuclein toxicity 32

Table 2.1 iPSC clones used in this study 53

Table 2.2 List of primary and secondary antibodies used in this study 60

Table 2.3 List of primers and sgRNAs used in this study 69

Table 2.4 Post-mortem brain tissues used in this study 84

Chapter 1

Background

1.1 Parkinson's disease

1.1.1 Diagnosis and prevalence of Parkinson's disease

Parkinson's disease is an age-related neurodegenerative disorder. Although not typically considered a life limiting disease, it causes severe cumulative disability and a marked decrease in the quality of life of the patient and potentially their family or carers (Goedert, Spillantini, Del Tredici, & Braak, 2013). As the second most prevalent neurodegenerative disorder, finding a cure for Parkinson's disease represents a major unmet need. This disease was first described by James Parkinson (1783-1824) in 1817 in his seminal essay on the '*paralysis agitans*' (Parkinson, 2002). Parkinson described afflicted patients exhibiting "involuntary tremulous motion, with lessened muscular power, in parts not in action and even when supported." After gaining international recognition amongst nosologists, *paralysis agitans*, or shaking palsy, was further characterised by Scottish pathologist William Rutherford Sanders (1828-1881) and French neurologist Jean-Martin Charcot (1825-1893), cementing the Parkinson's disease eponym two hundred years following its inception (Charcot & Sigerson, 1879).

Upon physical examination, the unifying motor symptoms of Parkinson's disease include bradykinesia, rigidity, resting tremor and in more advanced cases postural instability. Parkinsonian patients also manifest non-motor symptoms, that affect multiple systems in the body and the mind (Braak & Braak, 2000; Braak et al., 2002; Braak, Ghebremedhin, Rüb, Bratzke, & Del Tredici, 2004). Interestingly, patients commonly report the gradual development of non-motor symptoms 7-10 years prior to the onset of a movement disorder (Chaudhuri, Healy, & Schapira, 2006). These

prodromal features can be elusive due to their non-specific nature and heterogeneity, yet when assessed based on co-occurrence, the risk for Parkinson's disease heightens significantly (Durcan et al., 2019). Rapid Eye Movement (REM) sleep behaviour disorder (RBD) is most strongly associated with Parkinson's disease, whereby 90% of individuals with RBD develop some form of parkinsonism (Schenck, Bundlie, Ettinger, & Mahowald, 1986). Patients also report symptoms such as the loss of smell and taste, gastrointestinal dysfunction, genitourinary dysfunction, and mood disorders like depression (Ansari & Johnson, 1975; Beck, Fowler, & Mathias, 1994; Cummings, 1992; L. Edwards, Pfeiffer, Quigley, Hofman, & Balluff, 1991). Excessive daytime sleepiness and orthostatic hypotension have also been observed (Abbott et al., 2005; Senard et al., 1997). Increasing age with Parkinson's disease is correlated to increased symptom burden—for example, symptoms of mild cognitive impairment irreversibly develops into Parkinson's disease with dementia in 80% of cases after 15-20 years of disease (Leverenz et al., 2009).

Age is the greatest risk factor for Parkinson's disease, which affects 2-3% of the population above 65 years of age (Reeve, Simcox, & Turnbull, 2014). Around 6 million individuals globally were diagnosed with PD in 2016, 2.4-fold higher than in 1990. And alarmingly, 12 million individuals are expected to be affected by 2040 (Dorsey, Sherer, Okun, & Bloem, 2018). This rise in prevalence may be linked to ageing populations or possibly change in dietary habits or increased exposure to environmental toxins. Exposure to pesticides/herbicides and heavy metals were found to increase the risk of Parkinson's disease, whilst regular exercise and caffeine exerted protective effects (H. Chen, Zhang, Schwarzschild, Hernan, & Ascherio, 2005; Mak, Wong-Yu, Shen, & Chung, 2017; Postuma et al., 2012). Parkinson's disease is also twice as common in men, suggesting that a sex-specific genetic mechanism may underlie additional risk factors (Cerri, Mus, & Blandini, 2019).

1.1.2 Genetics of Parkinson's disease

Parkinson's disease cases are predominantly idiopathic with a minority of cases reporting a family history (10-15%) and an even smaller minority with Mendelian inheritance (5%) (Blauwendraat, Nalls, & Singleton, 2020). Parkinson's disease has been linked to multiple causal genes, involved in pathways related to mitochondrial quality control, synaptic circuitry, protein trafficking and degradation, and neuronal maintenance (Bandres-Ciga, Diez-Fairen, Kim, & Singleton, 2020). Furthermore, independent of the disease variant in question, additional genetic and environmental factors are likely to contribute towards disease progression as carriers of highly penetrant variants sometimes present with incomplete symptoms and vice versa. These genetic and environmental predispositions remain unidentified and contribute to the complex aetiology of Parkinson's disease.

To date, over 20 variants for monogenic forms of Parkinson's disease have been characterized (Koros, Simitsi, & Stefanis, 2017). These variants often possess large risk effects that either alter protein-coding sequences or gene expression. The first familial cause of Parkinson's disease was identified in 1997, as a dominantly inherited missense mutation (p.A53T) in the α-synuclein coding gene, *SNCA* (Polymeropoulos et al., 1997). In subsequent years, six additional point mutations (p.A30P, p.E46K, p.H50Q, p.G51D, p.A53E, p.A53V) were discovered in separate families, also causing an autosomal dominant form of Parkinson's disease (Appel-Cresswell et al., 2013; Kiely et al., 2013; Krüger et al., 1998; Lesage et al., 2013; Pasanen et al., 2014; Proukakis et al., 2013; Yoshino et al., 2017; Zarranz et al., 2004). The age of onset with such mutations are variable, however families with mutations A53T, A53E, and G15D give rise to early onset forms of disease.

Dominantly inherited duplications and triplications in the chromosomal region which comprises *SNCA* were also found to cause Parkinson's disease (Chartier-Harlin

et al., 2004; Ibanez et al., 2004; Ikeuchi et al., 2008; Singleton et al., 2003). Heterozygous duplication of *SNCA* resulted in a clinical phenotype similar to sporadic Parkinson's disease in the context of age of onset and symptoms. However, triplication of *SNCA,* which increased wild-type α-synuclein expression by 2-fold, resulted in an earlier age of onset and significant cognitive impairments.

The most common Parkinson's disease-causing gene is leucine-rich zipper kinase 2 (*LRRK2*), a kinase involved in the regulation of endosomal-lysosomal trafficking, in which seven mutations have been confirmed as pathogenic (Paisán-Ruíz et al., 2004; Tolosa, Vila, Klein, & Rascol, 2020; Zimprich et al., 2004). The p.G2019S mutation in *LRRK2* accounts for 4% of familial cases and 1% of sporadic cases (W. Chen et al., 2020). Autosomal recessive variants typically present with early onset Parkinson's disease, such as mutations in mitochondrial homeostasis-related genes, *PINK1* (PTEN-induced kinase 1), *PRKN* (Parkin), and *PARK7* (DJ-1) (Bonifati, Rizzu, Van Baren, et al., 2003; Kitada et al., 1998; Valente et al., 2004). PINK1/Parkin work together to modulate mitophagy—PINK1 accumulates on the surface of damaged mitochondria and recruits Parkin via the activity of its E3 ubiquitin ligase (Pickrell & Youle, 2015). DJ-1 has been implicated in multiple roles, including the antioxidant response, but it also functions as a deglycase (Biosa et al., 2017; Richarme et al., 2015). Moreover, mutations in β-glucocerebrosidase (*GBA1*) are the highest genetic risk factor for developing sporadic Parkinson's disease (Aflaki et al., 2016; Neudorfer et al., 1996). *GBA1* mutants are otherwise known to develop into Gaucher's disease, a lysosomal storage disorder. Other genetic risk factors include mutant variants in microtubule associated protein tau (*MAPT*) and major histocompatibility complex, class II (*HLA-DQB1*) (T. L. Edwards et al., 2010; Pandi et al., 2021).

Rare monogenic forms of Parkinson's disease can provide critical mechanistic insight into its pathogenesis, especially if applied towards understanding idiopathic

cases (Spillantini & Goedert, 2018). Genome-wide association studies (GWAS) of sporadic Parkinson's disease revealed that *SNCA* contributes to the highest number of risk loci, these polymorphisms are located outside the coding region and thus likely affect *SNCA* transcription, resulting in increased expression of α-synuclein (Bras et al., 2014; Satake et al., 2009; Simon-Sanchez et al., 2009). Additionally, although the majority of parkinsonian patients are idiopathic, variants in several rare monogenic Parkinson's disease-causing genes were identified in these patients through GWAS (Smolders & Van Broeckhoven, 2020). Analysis of the genetic factors in these GWAS studies revealed defects in vesicular transport pathways, defects in endosomal and lysosomal systems, impaired organelle degradation pathways, mitochondrial impairments, and α-synuclein aggregation (Kalinderi, Bostantjopoulou, & Fidani, 2016; Klemann et al., 2017; Smolders & Van Broeckhoven, 2020). Non-coding variants is another area less explored in Parkinson's disease and more broadly neurodegeneration—such variants may alter transcription factor binding or alternatively, dysregulate long non-coding RNAs or even microRNAs (J. Zhou & Troyanskaya, 2015).

1.1.3 Neuropathology of Parkinson's disease

In 1894, the successor of Jean-Martin Charcot, Edouard Brissaud (1851-1893) proposed that lesions in the substantia nigra was the neuropathological substrate of Parkinson's disease after observing that large tumours in the substantia nigra and its proximal regions were linked to parkinsonism (Blocq & Marinesco, 1893; Brissaud & Meige, 1895). Two decades later, Constantin Trétiakoff (1892-1956) described histopathological inclusions which he coined as 'corps de Lewy' in the substantia nigra of Parkinson's disease patients (Trétiakoff, 1919)—these inclusions were similar to those originally identified by Fritz Jacob Heinrich Lewy (1885-1950) in other regions of patient brains (Lewy, 1912). Lastly, in 1997, α-synuclein was brought to the forefront of Parkinson's disease research following the converging discoveries that a missense p.A53T mutation in *SNCA* caused Parkinson's disease and that α-synuclein was the major constituent of Lewy pathology (Polymeropoulos et al., 1997; Spillantini et al., 1997). Altogether, these findings linked lesions in the substantia nigra to mutations in *SNCA* and to α-synuclein toxicity in Lewy pathology, which were crucial for defining the cardinal histopathological features of Parkinson's disease.

Today, prerequisites for the differential diagnosis of Parkinson's disease in post-mortem brains are firstly, the degeneration of pigmented neurons in the pars compacta of the substantia nigra and secondly, the presence of filamentous inclusions termed as Lewy bodies and Lewy neurites (Figure 1.1) (Poewe & Wenning, 2002).

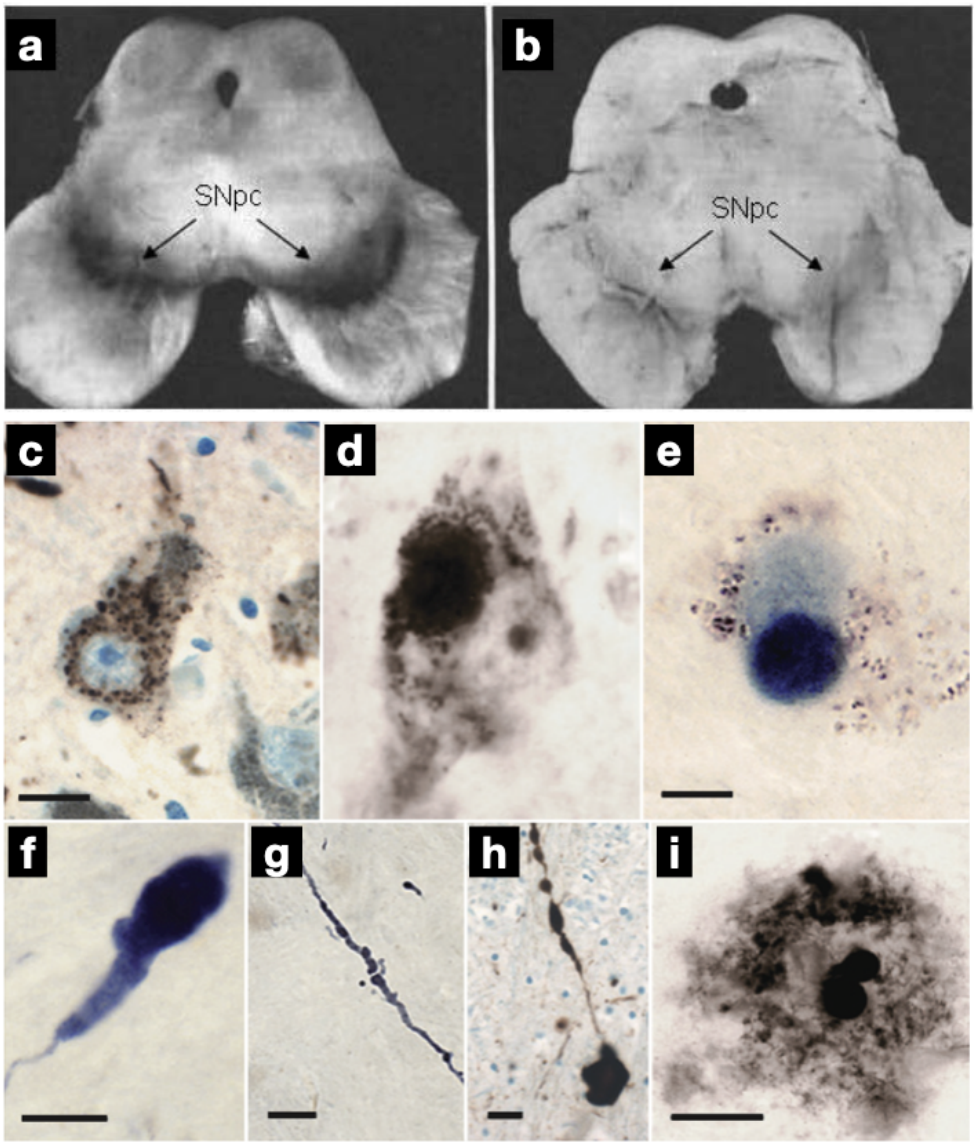


Figure 1.1 Cardinal histopathological features of Parkinson's disease

a, Post-mortem bilateral midbrain sections, showing the black neuromelanin pigment of the substantia nigra pars compacta (SNpc, black arrows) of a healthy individual versus the loss of pigmented dopaminergic neurons in **b,** Parkinson's disease patients (MS Lima et al., 2012). The characteristic black colour of the substantia nigra is caused by the presence of neuromelanin, a product of toxic oxidized dopamine species, which is stored in endosomal autophagic vacuoles in order to protect neurons. Image adapted from (Sulzer et al., 2000). In Parkinson's disease, black pigment in the substantia nigra is reduced upon dopaminergic cell loss, as neuromelanin vacuoles are released extracellularly and broken down by neighbouring microglia (Bush et al., 2006; Zecca, Zucca, Albertini, Rizzio, & Fariello, 2006). Degeneration in the substantia nigra is often accompanied by the presence of α-synuclein-immunoreactive Lewy bodies and Lewy neurites in Parkinson's disease brains. **c,** Speckled inclusions in dopaminergic neurons of the substantia nigra, which likely precede the formation of Lewy bodies. **d,** Mossy cell with Lewy body in Ammon's horn of the hippocampus (CA4). **e,** Lewy body in dopaminergic neurons of the substantia nigra. **f,** Club-shaped, **g,** filiform, and **h,** varicose Lewy neurites. **i,** Lewy plaque consisting of an extracellular amyloid-β core (Campbell-Switzer silver), which is surrounded by α-synuclein-positive dystrophic neurites in the perimeter. Scale bar: 20 μm. Image from adapted from (Braak & Del Tredici, 2008).

Extensive studies have demonstrated that α-synuclein-immunoreactive inclusions emerge in a predictable pattern in different regions of the brain, allowing the possibility to distinguish six stages of α-synuclein deposition (Figure 1.2) (Braak & Del Tredici, 2008; Braak et al., 2004). In stage 1, α-synuclein-positive structures usually occur in the olfactory bulb and/or the dorsal motor nucleus of the glossopharyngeal and vagal nerves. In stage 2, Lewy inclusions develop in the medulla oblongata and the pontine tegmentum. In stage 3, Lewy pathology can be found in the substantia nigra and the amygdala—at which point bradykinesia alongside other motor symptoms begin to appear. Pathology worsens in stage 4 as α-synuclein inclusions reach the temporal cortex. During stages 5 and 6, Lewy bodies and neurites surface in the neocortex, which is attributed for many cognitive impairments associated with advanced Parkinson's disease.

It is important to note that the Braak classification for Parkinson's disease represents the staging of α-synuclein pathology and not the progression of neurodegeneration—Braak's studies were, to a certain extent, biased towards early medullary pathology (Dickson, 2012). Nonetheless, Braak's staging scheme is consistent with the presentation of non-motor symptoms early in the majority of Parkinson's disease patients. RBD, hyposmia, autonomic dysfunction, and depression often precede motor symptoms by many years—and these symptoms correlate with the distribution of Lewy pathology in the brain during early stages (Langston, 2006; Schapira & Tolosa, 2010).

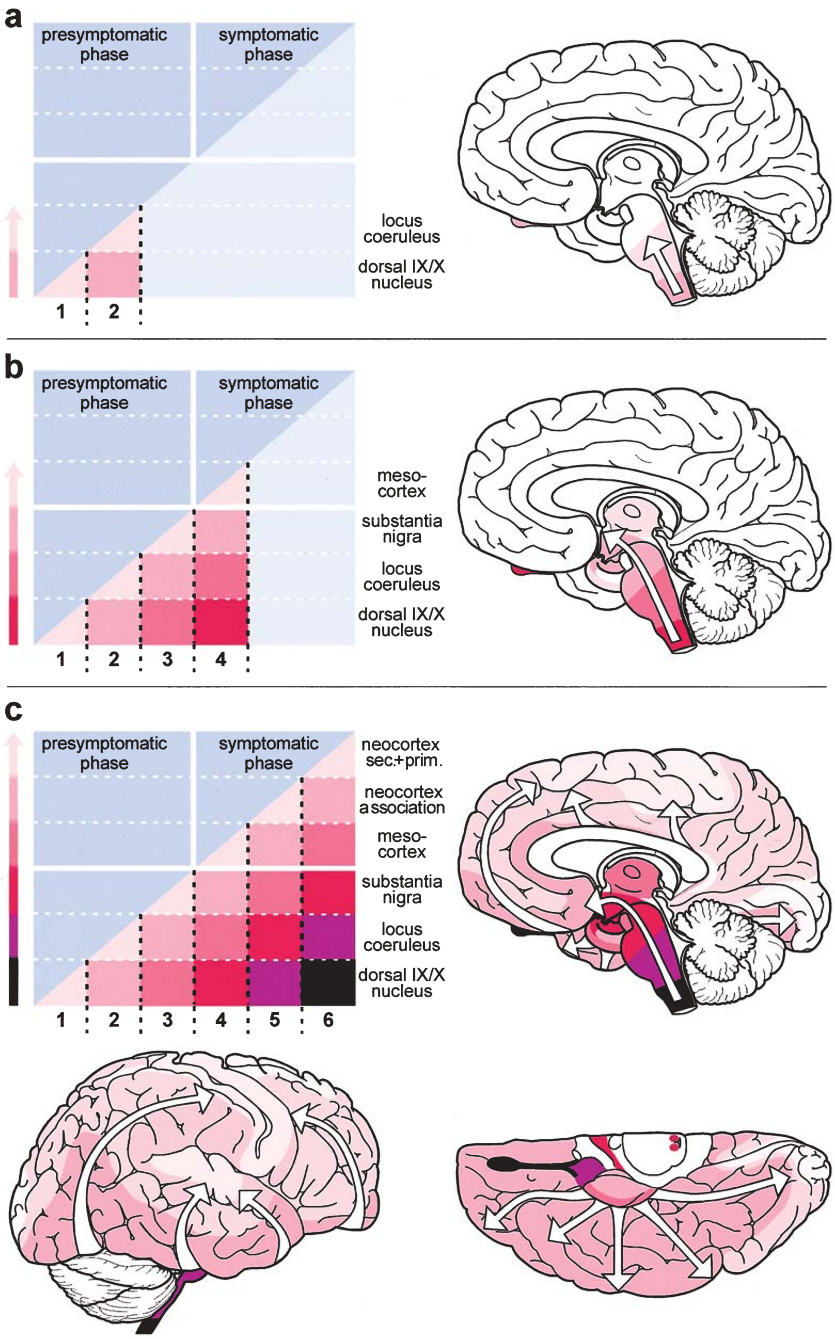


Figure 1.2 Six stages of α-synuclein pathology in idiopathic Parkinson's disease brains

a, The lesions that occur first in stage 1 can be found in the olfactory bulb (anterior olfactory nucleus) and the dorsal motor nucleus (vagus nerve). From these two sites, α-synuclein pathology predominantly follows an ascending path. Stage 2 lesions can be observed in the locus coeruleus, gigantocellular reticular nucleus, and caudal raphe nuclei. b, Stage 3 pathology continues its ascent and lesions the pars compacta of the substantia nigra, the cholinergic nuclei of the basal forebrain, and the cholinergic nuclei of the basal forebrain. The cerebral cortex becomes affect for the first time in stage 4, starting with the anteromedial temporal mesocortex. Classical Parkinson's disease symptoms usually emerge at the juncture between stage 3 and 4. c, Stage 5 involves lesions in higher order association areas followed by first-order association areas in stage 6. Increasing severity of α-synuclein lesions is shown by red, violet, and black shading. Image from (Braak, Rüb, Gai, & Del Tredici, 2003).

α-Synuclein deposition may occur early in the enteric nervous system. Based on the Braak staging system, one hypothesis is that α-synuclein pathology begins in the gut and advances retrogradely to the brain via the vagal nerve (Braak, de Vos, Bohl, & Del Tredici, 2006). Alternatively, α-synuclein pathology may originate in the vagal dorsal motor nucleus and spread anterogradely to the spinal cord and gut (Del Tredici & Braak, 2012b; Holmqvist et al., 2014). Other work has also suggested that pathology could begin in multiple autonomic sites in the periphery and consequently be transmitted to the spinal cord (Braak, Sastre, Bohl, de Vos, & Del Tredici, 2007). Indeed, accumulation of α-synuclein has been detected in nerve cell bodies and axons in the Meissner plexus of the large intestine many years prior to the development of motor symptoms of Parkinson's disease (Annerino et al., 2012). Therefore, α-synuclein inclusions in the large intestine may be a biomarker for prodromal stages of disease.

Parkinson's disease primarily targets dopaminergic neurons in the nigrostriatal pathway, from the substantia nigra to the putamen (Brichta & Greengard, 2014). Anatomically, the substantia nigra (A9) is located adjacent to the ventral tegmental area (A10), which is also comprised of dopaminergic neurons. Interestingly, several reports have suggested that neurodegeneration in the ventral tegmental area is relatively spared during early stages of disease, suggesting differential vulnerabilities even within dopaminergic nuclei in the brain (Alberico, Cassell, & Narayanan, 2015; O'Shea, Popal, Olson, Murty, & Smith, 2021).

The precise relationship between α-synuclein inclusion formation and cell death in vulnerable neurons remains unexplained. Generally, the incidence of Lewy pathology correlates with the severity of clinical symptoms (Henderson, Trojanowski, & Lee, 2019). However, cases of severe parkinsonism have been reported in the absence of Lewy pathology, and in contrast, post-mortem brains with incidental Lewy pathology were discovered in patients in the absence of any symptoms—

demonstrating that nigral neuronal density is independent of the regional distribution of Lewy pathology in the brain (Dickson et al., 2008; Gaig et al., 2007; Jenner, Dexter, Sian, Schapira, & Marsden, 1992; Johansen, Torp, Farrer, Gustavsson, & Aasly, 2018). Importantly, it is likely that cellular dysfunction and neurodegeneration in the substantia nigra precedes Lewy body deposition, as incidental Lewy pathology cases in Braak stages 1 and 2 have exhibited nigral degeneration occurring in parallel (Milber et al., 2012). These findings put into question the pathogenicity of Lewy bodies and Lewy neurites and highlight a major challenge in the field, which is to identify the physico-chemical nature of α-synuclein aggregated oligomers or other primary neurotoxins that mediate disease and ultimately the demise of neurons (Goedert, Jakes, & Spillantini, 2017).

1.1.4 Current therapeutics for Parkinson's disease

The loss of dopaminergic neurons in Parkinson's disease leads to neurotransmitter deficiency (Carlsson, 1959; Carlsson et al., 2001; Ehringer & Hornykiewicz, 1960; Hornykiewicz, 1963). Current approaches to mitigate the motor symptoms of Parkinson's disease involves replenishing dopamine levels in the brain through small molecule oral therapies which are capable of crossing the blood brain barrier (Ellis & Fell, 2017). These include the administration of levodopa (dopamine precursor), dopamine agonists, monoamine oxidase B (dopamine metabolism) inhibitors, and catechol-*O*-methyl transferase (dopamine metabolism) inhibitors. Anticholinergics may also be used to modulate tremor and dystonia in Parkinson's disease patients with limited benefit (Ehrt, Broich, Larsen, Ballard, & Aarsland, 2010). Levodopa remains the gold standard treatment for Parkinson's disease and is combined with decarboxylase inhibitor, carbidopa, to prevent its degradation thereby increasing its concentration in the blood (Fernandez et al., 2018). Although levodopa-carbidopa is to date the most efficacious therapy to counteract motor symptoms, its prolonged use results in multiple adverse effects that may ultimately lead to treatment resistance (Nonnekes et al., 2016). For advanced stages of motor disease, deep brain stimulation has also proven to be highly effective treatment strategy (Benabid, Pollak, Louveau, Henry, & De Rougemont, 1987; Hartmann, Fliegen, Groiss, Wojtecki, & Schnitzler, 2019).

Current treatments for Parkinson's disease ameliorate certain motor and non-motor symptoms, yet they are unable to arrest disease progression or prevent its onset—highlighting the urgent unmet need for mechanism-based curative therapies.

1.2 α-Synucleinopathies

The toxic gain of function of α-synuclein has a central role in several neurodegenerative diseases where α-synuclein accumulates into proteinaceous intraneuronal aggregates—these disorders are now collectively termed α-synucleinopathies (Goedert et al., 2017). The range of α-synucleinopathies is described in more detail in Table 1.1.

Disease	Genes associated	Symptoms	Pathology
Parkinson's disease (PD)	– Autosomal dominant *SNCA LRRK2, VPS35, EIF4G1, DNAJC13, CHCHD2*; *SNCA* duplication/ triplication – Autosomal recessive (*PARK2, PINK1* and *DJ-1*)	– Parkinsonism (bradykinesia, muscular rigidity, resting tremors and postural instability) – Nonmotor symptoms (constipation, impaired olfaction and rapid-eye movement sleep behavior disorder (RBD)) – Cognitive impairment	– SNc dopaminergic degeneration – Variable neuron loss in areas including locus coeruleus (LC), dorsal motor nucleus of the vagus (DMV) and the olfactory bulb – α-synuclein Lewy body and neurite pathology in neurons
Parkinson's disease with dementia (PDD) or dementia with Lewy bodies (DLB)	N/A	– Parkinsonism and dementia – In DLB versus PDD: fewer resting tremors, bilateral parkinsonism	– Cholinergic/SNc dopaminergic degeneration – α-synuclein Lewy body and neurite pathology in neurons – aβ amyloid plaques and tau tangles
Multiple system atrophy (MSA)	– Autosomal dominant (*SHC2* copy-number loss, *SNCA*) – Autosomal recessive (*COQ2*)	– Parkinsonism, cerebellar ataxia, autonomic failure – Nonmotor symptoms (sexual dysfunction, urinary incontinence and RBD)	– SNc/olivopontocerebellar degeneration – α-synuclein pathology in oligodendrocytes
Gaucher's disease (GD)	– Autosomal recessive (*GBA1*)	– Type I adult-onset (thrombocytopenia, anemia, hepatosplenomegaly and bone pain) – Type II (infant)/III (juvenile) neuropathic form (seizures, cognitive impairment and oculomotor problems)	– α-synuclein Lewy body and neurite pathology in some patients
Additional lysosomal storage disorders (LSDs)	– Sanfilippo syndrome (*SGSH*, *NAGLU*) – Tay–Sachs and Sandhoff diseases (*HEXA/HEXB*) – Hunter's syndrome (*I2S*) – Niemann–Pick type C (*NPC1/2*)	– Multisystem disorder	– α-synuclein Lewy body and neurite pathology in some patients
Neurodegeneration with brain iron accumulation (NBIA)	– Autosomal recessive *C19orf12, PLA2G6*	– Variable symptoms that may include dystonia, muscle rigidity, spasticity and ataxia	– Iron accumulation in the globus pallidus and SNc – α-synuclein Lewy body and neurite pathology in some patients
Alzheimer's disease (AD)	– Autosomal dominant (*APP*, *PS1/2*)	– Progressive memory loss – Cognitive impairment	– Cortical and CA1 hippocampal degeneration – aβ amyloid plaques and tau tangles – α-synuclein Lewy body and neurite pathology in some patients

Table 1.1 Summary of neurodegenerative diseases associated with α-synuclein toxicity

Table adapted from (Wong & Krainc, 2017).

1.2.1 α-Synuclein pathobiology

Physiological α-synuclein was originally identified using antibodies that were immunoreactive to cholinergic vesicles from the Pacific electric ray (*Torpedo californica*), providing the first evidence of its role at the presynapse (Luc Maroteaux, Campanelli, & Scheller, 1988; L Maroteaux & Scheller, 1991). In addition to its pre-synaptic localization, α-synuclein was expressed on nuclear envelopes, hence its designation as 'synuclein'. Human α-synuclein is a small protein consisting of 140 amino acids (14 kDa) and belongs to a family of brain synucleins, which comprises β-synuclein (134 aa) and ɣ-synuclein (127 aa) (Buchman et al., 1998; Jakes, Spillantini, & Goedert, 1994). The β-isoform is also located at the presynapse and co-localises with α-synuclein at presynaptic terminals (Lavedan, 1998). ɣ-Synuclein is expressed in glial cells and certain neuronal populations, including dopaminergic neurons (Bendor, Logan, & Edwards, 2013).

The function of α-synuclein is incompletely understood. Single (α-synuclein), double (α-/β-synuclein), and triple (α-/β-/ɣ-synuclein) knockout rodent models surprisingly were not lethal and exhibited late-onset phenotypes and age-related dysfunctions, in behavioural tests, synaptic structure and protein composition (Anwar et al., 2011; Chandra et al., 2004; Greten-Harrison et al., 2010). These results demonstrated that synucleins were not essential components for basic brain function or survival, but rather they may contribute to the long-term maintenance of synaptic function and dopamine levels (Sulzer & Edwards, 2019). *SNCA* knockout mice did not display a neurodegenerative phenotype and demonstrated increased release of striatal dopamine, whereas mice overexpressing α-synuclein displayed reduced neurotransmitter release (Abeliovich et al., 2000; Nemani et al., 2010). It was proposed that α-synuclein modulated neurotransmitter release through chaperone-like activity, in a process involving multimerization at the synapse, which was hypothesised to

cause the redistribution of membrane fusion SNARE proteins and the sequestration of synaptic vesicles (Garcia-Reitböck et al., 2010; L. Wang et al., 2014). Additionally, α-synuclein has been implicated in membrane fusion events that require high curvature, such as in regulating the size of the fusion pore (Logan, Bendor, Toupin, Thorn, & Edwards, 2017; Nellikka, Bhaskar, Sanghrajka, Patil, & Das, 2021).

α-Synuclein is a natively unstructured protein and lacks a defined secondary structure (Bisaglia, Mammi, & Bubacco, 2009; Tofaris & Spillantini, 2005). Its N-terminus (1-60 aa) contains seven distinct eleven residue repeats (KTKEGV) which are highly conserved and predicted to form an amphipathic α-helical structure (Figure 1.3) (Bendor et al., 2013). These repeats are located between residues 7 to 87 on α-synuclein. The KTKEGV motif is unique to α-synuclein and mediates its binding properties to membrane phospholipids (Zarbiv et al., 2014). Additionally, functional studies demonstrated that certain amino acid substitutions in the KTKEGV repeat abrogated α-synuclein tetramerization and reduced cell viability, suggesting that α-synuclein tetramers are important for α-synuclein homeostasis (Dettmer, Newman, von Saucken, Bartels, & Selkoe, 2015). Remarkably, each of the seven missense mutations associated with Parkinson's disease cluster within this amino-terminal domain.

The central region of α-synuclein (61-95 aa), also termed the non-amyloid-β component (NAC) region, is characterised by its hydrophobicity (Figure 1.3) (Gallegos, Pacheco, Peters, Opazo, & Aguayo, 2015). This region can be subject to conformational changes and is required to form cylindrical and amyloid-like β-sheets (Bellucci et al., 2012; Deleersnijder, Gerard, Debyser, & Baekelandt, 2013). The C-terminus (96-140 aa) is polar and abundant in acidic residues and is responsible for the intrinsically disordered nature of α-synuclein (Figure 1.3b) (Bisaglia et al., 2009). The C-terminus is also a domain which undergoes phosphorylation at multiple sites, suggesting the presence of several regulatory mechanisms (Barrett & Greenamyre,

2015; Oueslati, Fournier, & Lashuel, 2010). In addition to phosphorylation, α-synuclein in Lewy pathology was shown to be subjected to several post-translational modifications, such as ubiquitination and sumoylation, as well as nitration (Giasson et al., 2000; Krumova et al., 2011; Tofaris, Razzaq, Ghetti, Lilley, & Spillantini, 2003)—implicating these modifications in the regulation of α-synuclein aggregation and toxicity. Primarily C-terminus, but also N-terminus, truncations are also one of the predominant modifications of α-synuclein in Parkinson's disease (Baba et al., 1998; Tofaris et al., 2003).

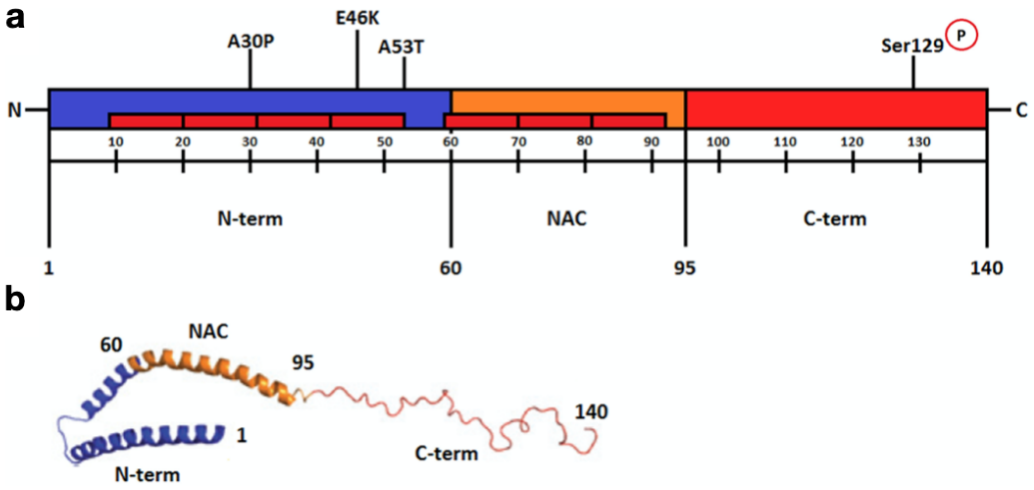


Figure 1.3 Schematic diagram of α-synuclein residues and protein structure

a, The N-terminus (1-60 aa) is an amphipathic region responsible for α-synuclein-membrane interaction. α-Synuclein contains hexamer motifs, as found in apolipoproteins (red rectangles). Dominantly inherited Parkinson's disease-causing point mutations are located in the N-terminus. The central region (61-95 aa), termed non-amyloid-β component, is a hydrophobic region and required for aggregation into a β-sheet secondary structure. The C-terminus (96-140 aa) is rich in acidic residues and is polar. α-Synuclein is phosphorylated on serine 129 in Lewy pathology and under conditions of aggregation. Image adapted from (Plotegher, Greggio, Bisaglia, & Bubacco, 2014). **b,** Schematic diagram of micelle-bound α-synuclein. The N-terminus (blue) displays antiparallel α-helices, the NAC region (orange) is also an α-helix, and the C-terminus is an unstructured coil (red). Numbering refers to amino acid residues. Image adapted from (Lashuel, Overk, Oueslati, & Masliah, 2013).

Histopathological studies in post-mortem Parkinson's disease brains identified increased phosphorylation at serine 129 on α-synuclein as the dominant pathological modification in both familial and sporadic Parkinson's disease (Anderson et al., 2006; Fujiwara et al., 2002; Yuko Saito et al., 2003). Above 90% of aggregated α-synuclein is phosphorylated on serine 129 in disease, whereas only 4% of α-synuclein is phosphorylated in normal brains at that site. α-Synuclein was shown *in vitro* to be phosphorylated on serine 129 by multiple kinases including polo-like kinases, G-protein coupled receptor kinases, and casein kinases (Ishii et al., 2007; Mbefo et al., 2010; Pronin, Morris, Surguchov, & Benovic, 2000). Post-translational modifications on α-synuclein have gained interest as a potential biomarker of disease, but also as putative therapeutic target sites (Barrett & Greenamyre, 2015; Samuel et al., 2016). Antibodies which recognize phosphorylated α-synuclein are specific and sensitive tools used to identify pathological α-synuclein in a range of α-synucleinopathies (Parkinson's disease, dementia with Lewy bodies, multiple system atrophy).

1.2.2 Lewy pathology in Parkinson's disease

Lewy bodies and Lewy neurites are large, dense, eosinophilic inclusions that were shown by electron microscopy to consist of unbranched α-synuclein filaments (length: 200-600 nm, width: 5-10 nm) (Spillantini, Crowther, Jakes, Hasegawa, & Goedert, 1998). The core of these filaments extends over 70 amino acids with the central repeat region of α-synuclein and adopts a cross-β structure. Two types of Lewy bodies have been characterised: brainstem-type Lewy bodies possess a dense acidophilic and argyrophilic core with a pale staining halo, in contrast, cortical Lewy bodies are more strongly immunoreactive for disorganised and scattered α-synuclein filaments and lack a halo, highlighting differences in their ultrastructural properties (Figure 1.1). Lewy neurites in the form of either spindle-like or thread-like structures occur within axons and dendrites of diseased neurons (Figure 1.1). Moreover, Lewy inclusions are immunoreactive for ubiquitin and aggresomal marker p62 (M. Hasegawa et al., 2002; Kuusisto, Parkkinen, & Alafuzoff, 2003; Kuzuhara, Mori, Izumiyama, Yoshimura, & Ihara, 1988; Sampathu, Giasson, Pawlyk, Trojanowski, & Lee, 2003; Tofaris et al., 2003).

There is ongoing debate on whether neurons are capable of surviving for decades in the presence of widespread Lewy pathology or if α-synuclein inclusions trigger cell death in a more acute manner (e.g. within 6 months) (Greffard et al., 2010)—raising the question whether aggregated α-synuclein is a harmless and neuroprotective species or a deleterious neurotoxin (Beach et al., 2008; Dugger & Dickson, 2010; H.-g. Lee, Zhu, Takeda, Perry, & Smith, 2006; Saha et al., 2004). The process by which Lewy pathology arises and its role in neurotoxicity remains a mystery. The leading hypothesis proposes that α-synuclein misfolds as a result of stochastic intracellular events and progressively accumulates into aberrant oligomers which ultimately fibrillate and form Lewy bodies and Lewy neurites. Proteomic studies revealed that isolated Lewy pathology comprises over 300 proteins, of which presently,

90 have been confirmed via immunohistochemistry in post-mortem brains (Fares, Jagannath, & Lashuel, 2021; Voronkov, Salkov, Anufriev, & Khudoerkov, 2018; Wakabayashi et al., 2013). These α-synuclein-interacting proteins have been linked to protein degradation systems, axonal damage, and molecular chaperones. More recently, it has been suggested that Lewy body formation involves a complex interplay between α-synuclein fibrilization, post-translational modifications, and interactions between aggregated α-synuclein and membranous organelles like mitochondria, autophagosomes, and endolysosome (Mahul-Mellier et al., 2020). The summative effect of these processes was shown *in vitro* to cause neurodegeneration, therefore refuting the notion that Lewy pathology in the brain is benign.

Early electron microscopy studies and more recent advanced microscopy technologies have visualised Lewy inclusions at the nanoscale resolution (Duffy & Tennyson, 1965; Shahmoradian et al., 2019). These studies showed that Lewy bodies contain an abundance of crowded membranous structures and lipids, appearing to originate from vesicles and fragmented organelles (e.g. mitochondria and lysosomes). Lewy bodies displayed a systematic onion-like structure with an inner ring rich in C-terminal truncated α-synuclein and an outer ring rich in phosphorylated α-synuclein on serine 129—this structure was surrounded, at the periphery, by a cage-like network of intermediate neurofilaments (Moors et al., 2018). Interestingly, the core of Lewy bodies was shown to encapsulate high levels of protein-lipid moieties (Moors et al., 2018; Shahmoradian et al., 2019). These ultrastructural investigations into the architecture of Lewy bodies strongly suggest that our current understanding of Lewy pathology is in its infancy. The observed relationship between α-synuclein and membranous lipids is consistent with the hypothesis that α-synuclein-membrane interactions are nucleation events which ultimately promote aggregation (Fanning, Selkoe, & Dettmer, 2021; Galvagnion et al., 2015). Parkinson's disease-associated genes have also been linked

to lipid homeostasis and membrane trafficking, lending credence to a role for protein-induced lipotoxicity or rather, α-synuclein-induced lipotoxicity. In this way, the interpretation of Parkinson's disease lesions may be extended to include lipidopathies and vesiculopathies.

1.2.3 Papp-Lantos pathology in multiple system atrophy

Multiple system atrophy is a fatal neurodegenerative disorder which is characterised by autonomic, cerebellar, parkinsonian, pyramidal, and cognitive symptoms in various combinations (Fanciulli & Wenning, 2015). Patients usually carry an average life expectancy of between 5-10 years following the initial diagnosis (Figueroa et al., 2014). Multiple system atrophy is divided into primarily parkinsonian (MSA-P) or cerebellar (MSA-C) subtypes, with MSA-P being the most prevalent (Goedert et al., 2017). The history of multiple system atrophy reflects the heterogeneity in its clinical manifestations—multiple system atrophy was first coined to include three previously known neurological disorders: olivopontocerebellar atrophy, striatonigral degeneration, and Shy-Drager syndrome, which constitutes parkinsonism and autonomic failure (Quinn, 1989). Similar to Parkinson's disease, multiple system atrophy is a sporadic disorder and sequence variation in *SNCA* is a major risk factor.

Papp-Lantos bodies, also termed glial-cytoplasmic inclusions, are the major pathological hallmark of multiple system atrophy and are absent in parkinsonian patients. These inclusions are α-synuclein-immunoreactive and contain α-synuclein filaments. Interestingly, glial-cytoplasmic inclusions are found predominantly in oligodendrocytes, which are large glial cells that produce myelin sheath on neuronal axons, and also nerve cells. Inclusion bodies are mostly localised to the cytoplasm and in some instances, the nucleus. Cryogenic electron microscopy identified that α-synuclein inclusions from multiple system atrophy brains were made from two distinct filaments (Schweighauser et al., 2020). Moreover, pathogenic α-synuclein from glial-cytoplasmic inclusions has been reported *in vitro* to be significantly more potent compared to α-synuclein from Lewy bodies, in seeding the aggregation α-synuclein (Peng, Gathagan, Covell, et al., 2018).

1.3 Seeded aggregation of α-synuclein

Lewy pathology in the brain is thought to progress along interconnected networks, spreading rostrally from the dorsal motor nucleus of the vagal and glossopharyngeal nerves or olfactory bulb (Braak et al., 2002). At the molecular level, this spread of Lewy pathology may involve prion-like propagation of α-synuclein assemblies (Tofaris, Goedert, & Spillantini, 2017). Prions describe proteins that acquire distinct conformations, are transmissible, and gain infectivity (Prusiner, 1998). The prion paradigm in neurodegenerative diseases involving protein misfolding has recently gained impetus as a crucial aspect of disease progression (Figure 1.4). In Parkinson's disease and more broadly in α-synucleinopathies, α-synuclein misfolds into seeds that act as a conformational template to amplify the formation of proteopathic assemblies from endogenous α-synuclein monomer (Brundin & Melki, 2017). Remarkably, α-synuclein seeds can induce aggregation independently, or in a non-cell-autonomous manner, by travelling from cell to cell, of which one way at least in cellular models is through exosome release (Emmanouilidou et al., 2010; Fussi et al., 2018). This inherent property to seed aggregation from one site to another may therefore underlie the pathogenesis of α-synucleinopathies.

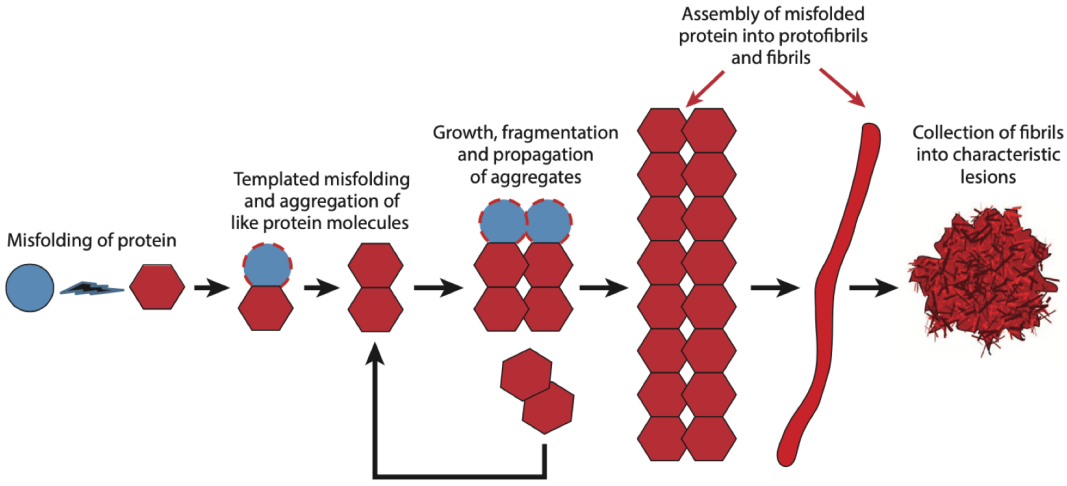


Figure 1.4 Templated aggregation and propagation of α-synuclein in related disorders

A schematic diagram depicting the cascade of pathological events beginning from the misfolding of pathogenic α-synuclein seeds to the formation of characteristic fibrillar lesions. The formation of pathogenic seeds is a rare and energetically unfavourable process, which depends on the exposure of backbone amide groups and enhanced protein concentrations. Once a seed has formed, as a result of yet unknown disease mechanisms, individual α-synuclein molecules are able to undergo conformational templating and join growing aggregates. The snowball effect of α-synuclein seeded aggregation recruits endogenous monomeric α-synuclein. Fragmentation of already existing agggregates generates new seeds, propagating disease to neighboring cells. Filamentous fibrils represent the endpoint of the aggregation cascade and accumulate into characteristic lesions. Image adapted from (Walker & Jucker, 2015).

Support to the hypothesis of seeded aggregation emerged from the discovery of Lewy pathology in therapeutically implanted neural grafts in the striata of patients with severe Parkinson's disease (Kordower, Chu, Hauser, Freeman, & Olanow, 2008; J.-Y. Li et al., 2008; W. Li et al., 2016). To validate this phenomenon, initial grafting studies have modelled seeded aggregation in cultured cells and in animals via the addition of α-synuclein assemblies either synthetically produced or derived from human brains (Desplats et al., 2011; Luk et al., 2009). Subsequent experiments in rodents have demonstrated that striatal and intramuscular injection of proteopathic assemblies induced Lewy pathology-like inclusions in parallel with neurodegeneration, providing evidence that α-synuclein inclusions have deleterious consequences (Luk et al., 2012; Mougenot et al., 2012; Sacino et al., 2014; Volpicelli-Daley et al., 2011). Similar phenotypes were also observed in non-human primate models of seeded aggregation (Arotcarena et al., 2020; Chu et al., 2019; Recasens et al., 2014).

Although the evidence mentioned above strongly contends that α-synuclein possesses prion properties, unlike 'authentic prions,' pathogenic α-synuclein assemblies have not been shown to transmit between individuals (Aguzzi & Lakkaraju, 2016; Tamgüney & Korczyn, 2018). A pertinent question is, therefore, how endogenous α-synuclein monomer becomes misfolded and transformed into an infectious species.

Firstly, α-synuclein has a persisting tendency to aggregate via its polypeptide backbone—thus, α-synuclein expression must be maintained within a highly controlled physiological range to maintain its solubility. Indeed, aggregated α-synuclein has been shown to be targeted and degraded by several proteostatic defence mechanisms, including molecular chaperones, the ubiquitin proteasome system and the lysosome (Vilchez, Saez, & Dillin, 2014). These machineries may become compromised under disease conditions (*SNCA* gene mutations or multiplications) or with increasing age, ultimately increasing the probability of intracellular α-synuclein aggregation.

Secondly, the physicochemical properties of α-synuclein make it capable of accumulating and binding to certain membrane structures (M. B. Jensen et al., 2011; Kubo et al., 2005; Pranke et al., 2011). These membrane interactions are enriched with α-helical α-synuclein assemblies, which may be the starting point of toxicity where α-synuclein becomes aberrantly folded. Preventing the misfolding and accumulation of α-synuclein into oligomeric complexes is mainly achieved by masking its central NAC region (61-95 aa), which contains an aggregation-prone hydrophobic sequence (Peelaerts, Bousset, Baekelandt, & Melki, 2018). Several lines of evidence have demonstrated that the NAC domain is shielded from the solvent, even when α-synuclein is in its native disordered state (Cox, Carver, & Ecroyd, 2014; Hartl, Bracher, & Hayer-Hartl, 2011). Here, the interaction between α-synuclein and dynamically shifting membranes at lipid surfaces may contribute to misfolding via a brief exposure to hydrophobic residue patches (Jao, Der-Sarkissian, Chen, & Langen, 2004; Trexler & Rhoades, 2009; Ulmer, Bax, Cole, & Nussbaum, 2005). In line with this hypothesis, deletion of key residues in the NAC domain (66-74 aa, 71-82 aa), abolished the aggregation potential of α-synuclein (Du et al., 2003; Giasson, Murray, Trojanowski, & Lee, 2001). Thirdly, variations in solution conditions and pH, such as in lysosomes, have also been shown to foster a permissive environment for the formation of α-synuclein aggregates (Breydo, Wu, & Uversky, 2012; Buell et al., 2014; Galvagnion et al., 2015).

Collectively, the pleomorphic nature of α-synuclein and the absence of an objective standard by which to describe α-synuclein assemblies, renders the labelling of oligomeric and fibrillar structures as arbitrary. Structural and functional aspects of α-synuclein assembly need to be fully characterised in order to understand their role in the disease process. Findings from such studies will inform future models on how to evaluate disease-relevant phenotypes.

1.4 Stem cell modelling of α-synuclein aggregation

iPSCs generated from patients harbouring Parkinson's disease-causing genes (e.g. *SNCA*) are playing an increasingly important role in disease-relevant experimental systems (Soldner & Jaenisch, 2018). Stem cell modelling offers the advantage of generating human neurons in a genetically and pharmacologically exploitable platform, however, their application to investigate adult-onset disease remains challenging (Goedert et al., 2017). Thus, early pathological changes can be investigated in such systems. iPSC-derived neurons enable the study of specific phenotypes directly from individuals with distinct genetic backgrounds. Interestingly, findings from these studies highlight shared pathogenic mechanisms from Parkinson's disease-causing genes (Figure 1.5), which may inform future work in understanding sporadic forms of disease.

To date, iPSC-derived dopaminergic neurons have been used to interrogate cellular phenotypes from Parkinson's disease-causing genes and the putative molecular mechanisms underlying these phenotypes (Tanudjojo et al., 2021). Dopaminergic neurons predominantly exhibited perturbations in organelle homeostasis including, endoplasmic reticulum stress, impairments in protein trafficking and degradation, mitochondrial dysfunction, and oxidative stress—alterations in calcium homeostasis have also been described (Caiazza, Lang, & Wade-Martins, 2020; Outeiro, Heutink, Bezard, & Cenci, 2021).

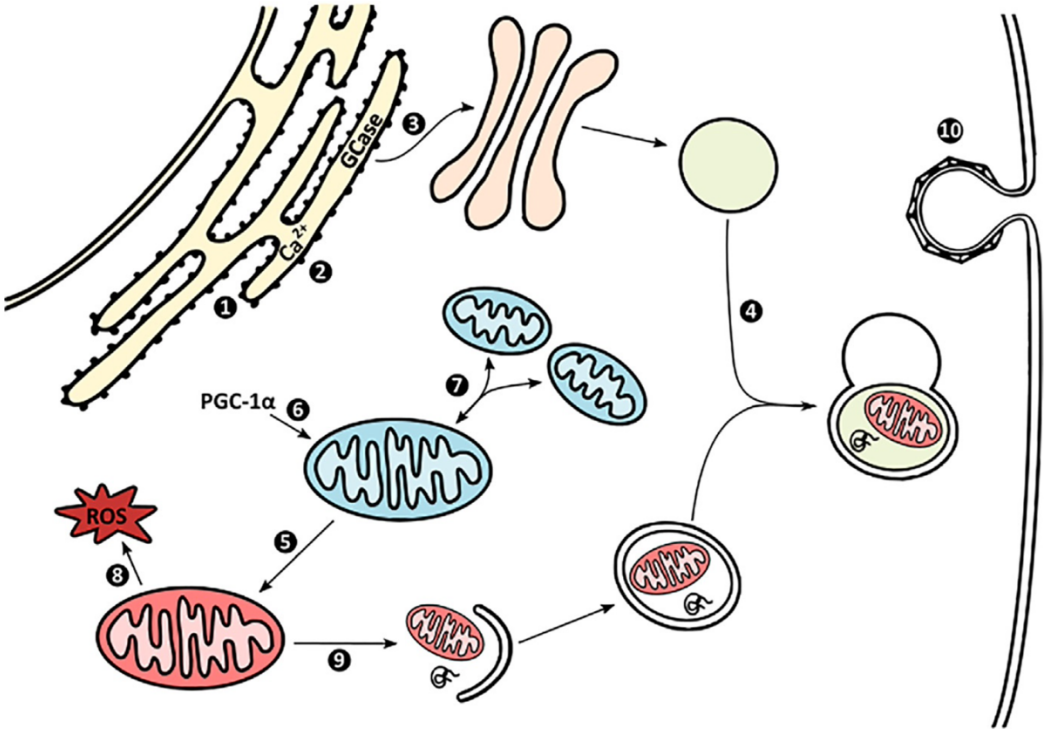


Figure 1.5 Major ranked phenotypes from iPSC-derived dopaminergic neurons from Parkinson's disease patients

(1) The accumulation of misfolded α-synuclein intracellularly triggers the unfolded protein response, which is mediated by the endoplasmic reticulum. The endoplasmic stress response can be assesed by measuring levels of mediator componenents (such as, binding immunoglobulin, protein disulfide isomerase, inositol-reuiring transmembrane kinase/endoribonuclease 1α, phospho-protein kinase-like endoplasmic reticulum kinase, phospho-eukaryotic initiation factor 2, spliced X-box binding protein 1, endoplasmic reticulum oxireductin 1, FK506-binding protein 9), or the accumulation of misfolded proteins within the endoplasmic reticulum (such as glucerebrosidase). The endoplasmic reticulum stress response is consistently activated in iPSC-dervied dopaminergic neurons from *SNCA* triplication and *GBA1* patients. (2) The endoplasmic reticulum is the major storage compartment for calcium in a cell and its calcium levels are altrered in dopaminergic neurons harbouring the *L444P GBA1* and *G2019S LRRK2* mutants. (3) The accumulation of immature lysosomal hydrolytic enzymes (e.g. glucerebrosidase) in the endoplasmic reticulum occurs in *SNCA* triplication neurons. (4) Lysosomal dysfunction was detected in *SNCA* and *GBA* mutant dopaminergic neurons. (5) Mitochondrial function is severely affected in Parkinson's disease. Specifically, components of the electron transport chain are impaired in neurons derived from *SNCA, GBA1, LRRK2,* and *PINK1* mutants. (6) Levels of peroxisome proliferator-activated receptor gamma coactivator 1α, one of the critical factors in mitochondrial biogenesis, are altered in *SNCA* triplication dopaminergic neurons. (7) *SNCA* dopaminergic neurons also exhibit impaired mitochondrial fusion and fission. (8) Enhanced reactive oxygen species burden was detected in *SNCA, PINK1,* and *PRKN* neurons. (9) Autophagic and mitophagic degradative processes were found to be dysfunctional in *SNCA, GBA1, LRRK2,* and *PRKN* doapminergic neurons. (10) Lastly, *LRRK2* dopaminergic neurons exhibited impaired clathrin-mediated endocytosis. Diagram adapted from (Caiazza et al., 2020).

The endoplasmic reticulum responds to the presence of misfolded and aggregated protein via the unfolded protein response, which induces an overall decrease in protein translation and an increase in particular chaperone and endoplasmic reticulum-associated degradation proteins (Smith, Ploegh, & Weissman, 2011). iPSC-derived dopaminergic neurons bearing the *GBA1* mutant *N370S* and *SNCA* p.A53T and triplication mutants displayed increased levels of endoplasmic stress markers, such as Hsp70 chaperone, binding immunoglobulin, and stress sensor, inositol requiring enzyme 1 (C. Y. Chung et al., 2013; H. J. Fernandes et al., 2016; Heman-Ackah et al., 2017; Zambon et al., 2019). *SNCA* triplication dopaminergic neurons also exhibited defects in the trafficking of lysosomal hydrolases from the endoplasmic reticulum to the Golgi apparatus resulting in the aberrant accumulation of immature endoplasmic enzymes, lysosomal dysregulation, and consequently α-synuclein accumulation, in a pathogenic feedforward loop (Mazzulli, Zunke, Isacson, Studer, & Krainc, 2016). Similarly, *G2019S* and *R1441C LRRK2* mutant dopaminergic neurons were deficient in clathrin-mediated endocytosis (Connor-Robson et al., 2019).

Deficits in mitochondrial function and turnover have been extensively studied in Parkinson's disease models (C. Y. Chung et al., 2013; Schöndorf et al., 2018; Zambon et al., 2019). *SNCA* p.A53T and triplication dopaminergic neurons consistently display decreased levels of basal respiration, ATP production, and maximal mitochondrial respiration compared to controls (Paillusson et al., 2017; Ryan et al., 2013). In the presence of seeded aggregation, mitochondrial function is even more compromised (Tanudjojo et al., 2021). It was also shown that oligomeric α-synuclein selectively induces oxidation of the ATP synthase β-subunit in *SNCA* triplication cortical neurons (Ludtmann et al., 2018). α-Synuclein pathology may also induce dysregulations in mitochondrial biogenesis and degradation in *PRKN, SNCA* p.A53T, and *G2019S LRRK2* mutant dopaminergic neurons (Hsieh et al., 2016;

Shaltouki, Hsieh, Kim, & Wang, 2018; Suzuki et al., 2017). Moreover, impaired mitochondrial motility followed by synaptic degeneration has been described in cortical neurons harbouring *SNCA* duplication (Prots et al., 2018). Additionally, nitration of microtubules was shown to block axonal mitochondrial transport in *SNCA* p.A53T dopaminergic neurons (Stykel et al., 2018). Mitochondria are also the principal source of reactive oxygen species and α-synuclein is believed to interact with mitochondria (K.-J. Lin et al., 2019). Accordingly, increased levels of reactive oxygen species, nitrosative stress, and induction of antioxidant genes (catalase, heme oxygenase) were detected in *SNCA* p.A53T and triplication dopaminergic neurons (Byers et al., 2011; Flierl et al., 2014; Ryan et al., 2013).

Mitochondrial and endoplasmic reticulum dysfunction are linked to altered calcium homeostasis (Brini, Ottolini, Calì, & Carafoli, 2013). Calcium has additional roles in synaptic release and plasticity in neurons (Mateos-Aparicio & Rodríguez-Moreno, 2020). *SNCA* triplication dopaminergic neurons exhibited abnormal calcium signalling in the presence of physiological concentrations of glutamate and dopamine—this response was found to be caused by the aberrant incorporation of α-synuclein oligomers in membranes leading to impaired membrane conductance and increased calcium influx (Angelova et al., 2020). More recently, stem cell models of Parkinson's disease have shown that aggregated α-synuclein promotes cell death by inducing lipid peroxidation (Angelova et al., 2020; Ludtmann et al., 2018). Interestingly, inhibition of lipid peroxidation abolished the interaction between α-synuclein and membranes, and normalised calcium influx, suggesting a role for α-synuclein-induced neuronal death via the peroxidation of polyunsaturated fatty acids (Angelova et al., 2020).

It is important to consider that some of the literature described above have modelled Parkinson's disease in cortical and dopaminergic neurons interchangeably.

In this context, the selective vulnerability of dopaminergic neurons versus other neuronal subtypes, such as cortical neurons, was evaluated in a comparative study using *SNCA* duplication stem cells (Brazdis et al., 2020). Here, differentiated dopaminergic neurons displayed increased α-synuclein pathology (insolubility and phosphorylation) and elevated levels of reactive oxygen species and protein nitration compared to cortical neurons—which culminated to the reduced survival of *SNCA* duplication neurons. Similar experiments in *SNCA* triplication neurons could generate even larger effect sizes compared to duplication neurons. These findings validate in a stem cell model, the selective vulnerability of dopaminergic neurons as seen in the substantia nigra of patient brains.

Stem cell modelling of Parkinson's disease is a powerful tool to screen the efficacy of potentially therapeutic agents. The success of translational experiments is dependent on standardised objective and reproducible readouts, which are currently sparse in iPSC-derived neurons. For example, cysteamine, an antioxidant compound used to treat cystinosis, was demonstrated to be neuroprotective in *SNCA* triplication dopaminergic neurons challenged with 6-oxidopamine (Siddu et al., 2020). In this study like in several others, neuronal viability was measured solely by quantifying neurite outgrowth length, as a measure of neurodegeneration (L. Lin et al., 2016; Luo et al., 2020; Oliveira et al., 2015). In another study which assessed the effect of α-synuclein on lipid homeostasis, *SNCA* triplication neurons exposed to oleic acid were shown to exhibit increased toxicity, based on a resazurin to resorufin conversion assay (Fanning et al., 2019). Quantification of neurofilament light chain is an additional marker of disease in neuronal cultures, however, it is not specific to neurotoxicity as remodelling of axons also triggers the release of neurofilament light chain (Barth et al., 2021; Donath et al., 2021). Lastly, cell death measurements generated either by manual counting of fragmented nuclei or propidium iodide uptake have been used,

however these are not suitable for high-throughput studies (Luo et al., 2020; Tanudjojo et al., 2021). It is evident that sensitive assays which can effectively measure neuronal viability is an unmet need in the stem cell field of neurodegeneration. Validating preclinical findings is indispensable towards the common goal of translating putative targets into clinical trial endpoints. Therefore, future studies employing iPSC-derived neurons would benefit from novel strategies to assess viability and in the meantime, rely on findings which corroborate results from multiple assays.

1.5 Aims and objectives

The lack of human model systems has been a longstanding limitation in the study of the pathogenesis of Parkinson's disease, especially in the context of α-synuclein aggregation. Previous research investigated the propagation of α-synuclein pathology in *in vitro* and *in vivo* animal and human models, but not in stem cell-derived neurons. Therefore, the focus of my doctoral studies was to delineate aggregate-induced disease mechanisms in iPSC-derived human dopaminergic neurons. I sought to create a reductionist system and explore dysregulated pathways with a view to identify targets for therapies.

The objectives of this dissertation were to:

1. Generate and characterise a robust model of α-synuclein seeded aggregation in Parkinson's disease patient iPSC-derived dopaminergic neurons harbouring *SNCA* mutations or multiplications.
2. Assess the functional effects of different fibrillar α-synuclein conformations on iPSC-derived dopaminergic neurons.
3. Evaluate the role of α-synuclein-interacting proteins, identified by protein biotinylation, on aggregation and aggregate-induced neurodegeneration.

Chapter 2

Materials and Methods

2.1 Cell culture

2.1.1 iPSC culture conditions

Stem cells were expanded and cultured on 1% Geltrex-coated (Gibco) six-well plates and supplemented daily with 2 mL/well of mTeSR1 (Stemcell). Stem cells were dissociated using Versene (0.48 mM EDTA, Gibco) according to manufacturer's instructions. iPSCs were passaged at approximately 75% confluency. Cells were washed once with pre-warmed phosphate buffer saline (PBS, Gibco) and 1 mL of Versene (Gibco) was added to each well of a six-well plate. Cells were then incubated for 5-10 min at 37°C. Cells were visualised underneath a light microscope to confirm dissociation. Following the incubation period, Versene was aspirated from the wells without dislodging the attached cell layer. 1 mL of mTeSR1 (Stemcell) was then added to each well and, using a 1 mL pipette tip, iPSCs were gently dissociated from the well. Cells in suspension were gently pipetted up and down to generate a homogenous suspension comprising of small clusters of cells. From this resuspension, iPSCs were passaged at the appropriate cell dilution in the presence of stem cell-specific anti-apoptotic factor, Y-27632 dihydrochloride (10 μM ROCKi, Bio-techne).

iPSC stocks were cryopreserved in a serum free medium, mFreSR-S (Stemcell), according to manufacturer's instructions. mFreSR-S (Stemcell) was stored and used at 4°C. Cells were dissociated using Versene (Gibco) as described above and resuspended gently in 1 mL of mFreSR-S (Stemcell) per well of a six-well plate. Resuspended cells were transferred into a 1.5 mL cryovial (Nunc, Thermo Scientific) then stored at -80 °C in a pre-refrigerated freezing container (Mr. Frosty, Nalgene). 24 h later, cryovials were moved to from -80 °C to liquid nitrogen storage.

2.1.2 Generation of human iPSC-derived midbrain dopaminergic neurons

Dopaminergic neurons were derived from human iPSC lines using previously published protocols (Jonikas et al., 2018; Kriks et al., 2011). Stem cell lines used were characterised previously and, in this study, Table 2.1 (Dafinca et al., 2016; H. J. Fernandes et al., 2016; Haenseler et al., 2017; Handel et al., 2016; Tanudjojo et al., 2021). Reprogramming of patient and fibroblasts to iPSCs was performed by Dr. Sally Cowley.

ID	Diagnosis	*SNCA* genotype	Sex	Biopsy age (years)	Original ID	Reprogramming method	iPSC clone characterisation	GEO
HC-1	healthy control	WT/WT	female	67	AH017-7	Cytotune1	Handel et al., 2016 doi:10.1093/hmg/ddv637	GSE69302
HC-2	healthy control	WT/WT	female	49	OX3-9	Cytotune1	Dafinca et al., 2016 doi:10.1002/stem.2388	GSE64584
HC-3	healthy control	WT/WT	male	67	SFC840-03-03	Cytotune1	Fernandes et al., 2016 doi:10.1016/j.stemcr.2016.01.013	GSE53426
SNCA^{A53T}-1	PD	A53T/WT	female	51	SFC828-03-09	Cytotune1	Haenseler et al., 2017 doi:10.1016/j.stemcr.2017.05.017	GSE89886
SNCA^{A53T}-2	PD	A53T/WT	male	46	SFC829-03-06	Cytotune1	Haenseler et al., 2017 doi:10.1016/j.stemcr.2017.05.017	GSE89886
SNCA^{TRIP}-1	PD	Triplication/ WT	female	55	SFC831-03-01	Cytotune1	Haenseler et al., 2017 doi:10.1016/j.stemcr.2017.05.017	GSE89886
SNCA^{TRIP}-2	PD	Triplication/ WT	female	55	SFC831-03-03	Cytotune1	Haenseler et al., 2017 doi:10.1016/j.stemcr.2017.05.017	GSE89886
SNCA^{TRIP}-3	PD	Triplication/ WT	female	55	SFC831-03-05	Cytotune1	Haenseler et al., 2017 doi:10.1016/j.stemcr.2017.05.017	GSE89886
SNCA^{TRIP}-4	PD	Triplication/ WT	female	55	ND34391G	Cytotune1	Heman-Ackah et al., 2017 doi:10.1093/hmg/ddx331	GSE89886
SNCA^{ISOTRIP}	PD	Isogenic WT/WT	female	55	Clone 1-13	Cytotune1	Heman-Ackah et al., 2017 doi:10.1093/hmg/ddx331	GSE89886

Table 2.1 iPSC clones used in this study

Each clone was differentiated at least three times.

iPSCs were plated onto 1% Geltrex-coated six-well plates (500 000 cells/well) and expanded in 2 mL/well of mTeSR1. This protocol does not require any passaging steps during the course of differentiation. Cells were cultured in a monolayer and replated as dopaminergic neurons at the final stage of the differentiation process. Differentiating cells were subjected to daily media changes (4 mL/well). Once iPSCs were above 90% confluent and acquired the characteristic stem cell morphology, differentiation was initiated by adding day *in vitro* (DIV) 0 media containing dual SMAD inhibitors, 2 μM A83-01 (Bio-techne) and 100 nM LDN-193189 (Sigma) in knockout serum replacement medium (KSR) comprised of KO-DMEM (Gibco), 15% KO serum replacement (Gibco), 2 mM L-glutamine (Gibco), 2 mM non-essential amino acids (Gibco), and 10 μM β-mercaptoethanol (Gibco). Floor plate induction occurred through DIV1-4 media, which contained 2 μM A83-01 (Bio-techne), 100 nM LDN-193189 (Sigma), 300 ng/mL sonic hedgehog (SHH) C25II (Bio-techne), 2 μM purmorphamine (Bio-techne) and 200 ng/mL fibroblast growth factor 8a (FGF8a, Bio-techne) in KSR media. To further promote floor plate induction and midbrain specification though WNT activation and GSK-3 inhibition, 3 μM CHIR-99021 (Bio-techne) was added from DIV3-12.

After DIV5, differentiating stem cells progress towards a neural progenitor cell lineage (Kriks et al., 2011). Therefore, KSR medium was gradually shifted to an N2-based neuronal medium containing neurobasal without phenol red (Gibco), 0.5X N2 supplement (Gibco), 0.5X B-27 supplement without vitamin A (Gibco) and 2 mM L-glutamine. DIV7-10 media contained 100 nm LDN-193189 and 3 μM CHIR-99021 in KSR medium mixed with gradually increasing proportions of N2-based neuronal medium.

Specification towards midbrain dopaminergic neurons begins after DIV10. DIV11-20 medium contained 20 ng/mL brain-derived neurotrophic factor neurotrophic

factor (BDNF, Peprotech), 20 ng/mL glia-derived neurotrophic factor neurotrophic factor (GDNF, Peprotech), 1 ng/mL transforming growth factor beta 3 (TGFβ3, Peprotech), 10 μM DAPT (Bio-techne), 200 μM ascorbic acid (AA, Sigma), 500 μM dibutyryl cyclic adenosine monophosphate (db-cAMP, Sigma) in neuronal differentiation media composed of neurobasal without phenol red, 1X B-27 supplement without phenol red and 2 mM L-glutamine. 1 μg/mL of laminin (Sigma) was added from DIV17-25. When axonal projections become visible within the differentiating monolayer, usually between DIV20-25, cells were replated onto 1% Geltrex-coated assay plates or 0.1% poly-l-ornithine and 1% Geltrex-coated assay coverslips. Cells were dissociated by incubating 1 mL of pre-warmed Accutase (Gibco) to one well of a six-well plate for 10 min followed by gentle resuspension using a p1000 pipette. Neurons were maintained in neuronal differentiation media containing the aforementioned small molecules (BDNF, GDNF, TGFβ3, DAPT, AA, db-cAMP in neurobasal supplement with B-27 and L-glutamine).

48 h after replating, neurons were treated with anti-mitotic agent Mitomycin C (MMC, Sigma). Media on culture plates was aspirated and replaced with 1 μg/mL MMC in medium containing neurobasal without phenol red, 1X B-27 Supplement without vitamin A and 2 mM L-glutamine for 90 min. Media containing MMC was then removed and neurons were washed once with prewarmed neurobasal. Neurons were subsequently maintained through half media changes bi-weekly with neuronal differentiation medium until analysis timepoints were reached.

2.1.3 Addition of exogenous α-synuclein fibrils in dopaminergic neurons

Human dopaminergic neurons were treated with either *de novo* generated α-synuclein polymorphs (fibrils and ribbons) or patient brain-amplified fibrils (3 cases of PD and 5 cases of MSA). α-Synuclein assemblies were kindly provided and characterised by Ronald Melki's group at various molar concentrations. These α-synuclein seeds were pre-sonicated prior to delivery. Assemblies were diluted at the appropriate concentration in neuronal differentiation medium (BDNF, GDNF, TGFβ3, DAPT, AA, db-cAMP in neurobasal supplement with B-27 and L-glutamine) and simply added neurons in a full media change.

2.1.4 HEK293 culture conditions

HEK293 cells (ATCC CRL-1573) were cultured in DMEM/F-12 (Gibco) supplemented with 10% fetal bovine serum (FBS, Sigma) and 100 µg/mL penicillin and 100 µg/mL streptomycin (Sigma), at 37 degrees Celsius and 5% carbon dioxide. HEK293 cells were dissociated using TrypLE Express Enzyme (Gibco) according to manufacturer's instructions.

The generation of single-cell clones used in the biotin ligase/protein interactome assay was performed by Dr. Samiha Shaikh, a post-doctoral researcher in our group. HEK293 cells were transiently transfected with BioID tagged α-synuclein (termed α-Syn-BirA*) using Lipofectamine 2000 (Invitrogen) and clonal lines were selected with 300 µg/mL G418 (Gibco). For SILAC labelling of the single cell clone, stably expressing wild-type α-Syn-BirA*, HEK cells were cultured for 10 doublings to fully incorporate the stable isotopes, in media containing either R0K0 (L-arginine 'light', L-lysine 'light'), R6K4 (L-arginine 'medium, L-lysine 'medium') or R10K8 (L-arginine 'heavy, L-lysine 'heavy') media (Gemini biosciences), supplemented with 10% dialysed FBS (10 k molecular weight cut-off, DC Biosciences), and 100 µg/mL penicillin and 100 µg/mL streptomycin. For single guide RNA (sgRNA) knockdown experiments, a clonal HEK cell line stably expressing wild-type α-synuclein tagged to Venus and Cas9 were used.

2.2 Live cell assays

2.2.1 Measurement of mitochondrial respiration

Oxygen consumption rates (OCR) were measured using the Seahorse XFe96 analyser (Seahorse Bioscience) in cells plated on XFe96 plates at a density of 50 000 cells/well. The Seahorse XF Mitostress Test kit (Seahorse Bioscience) was used to monitor OCR under aggregation conditions (Figure 2.1). Mitochondrial respiration or OCR was measured at baseline followed by sequential injection of ATP synthase inhibitor oligomycin (3 μM), mitochondrial uncoupler FCCP (1.25 μM) and respiratory chain inhibitors rotenone (0.5 μM) and antimycin A (0.5 μM). OCR values recorded at baseline and following the addition of the FCCP and rotenone/antimycin A were used to calculate three readouts: (i) basal respiration, (ii) ATP production and (iii) maximal respiration. Basal respiration was defined as the OCR at baseline in the absence of any treatments, demonstrating the oxygen consumption required to meet the cellular ATP demand resulting from mitochondrial proton leak. The decrease in OCR after injection of oligomycin was used to calculate ATP production, as the portion of basal respiration that was utilised to drive ATP production by the mitochondria. Maximal respiration was defined as the maximal OCR values attained following the addition of uncoupler FCCP, which mimics an artificial energy demand by stimulating the respiratory complex to operate a maximum capacity. This process triggers the rapid oxidation of substrates such as sugars, amino acids, and fats. Concentrations of oligomycin, FCCP and rotenone/antimycin A were carefully optimised for iPSC-derived dopaminergic neurons in our group with the help of Dr. Christos Zois (Jonikas et al., 2018). Results were normalised to total cell numbers using nucleic dye CyQuant (Invitrogen).

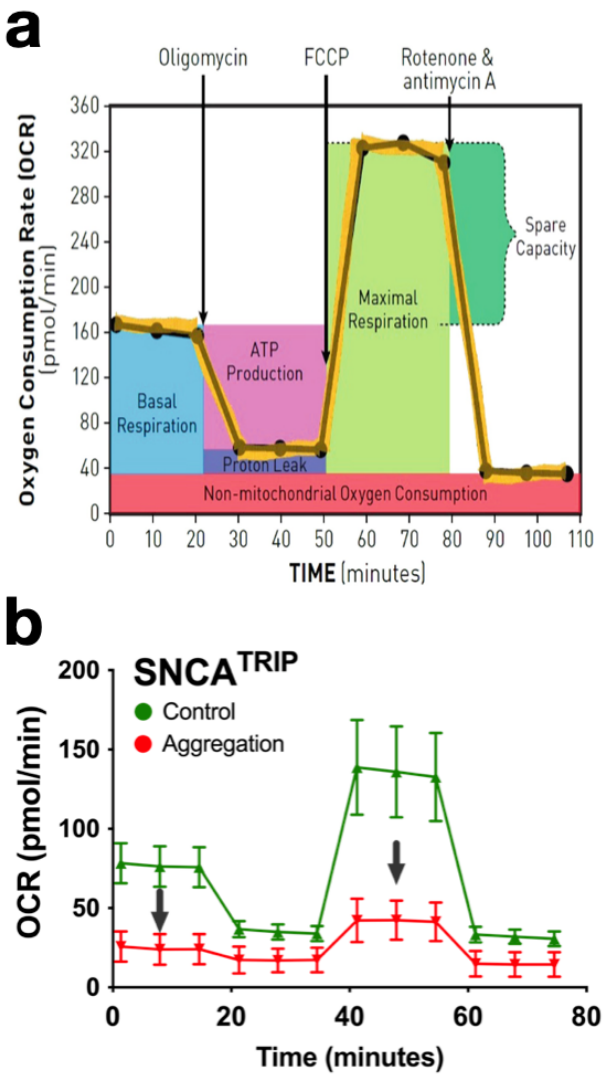


Figure 2.1 Agilent Seahorse XF Cell Mito Stress Test used to quantify oxygen consumption rate under aggregation conditions

a, Oligomycin (3 μM) inhibits ATP synthase (complex V from the electron transport chain and is injected first after basal measurements, resulting in a reduction in mitochondrial respiration or oxygen consumption rate (OCR). The decrease in OCR is associated with cellular ATP production. FCCP is an uncoupling agent which collapses the proton gradient thereby disrupting the mitochondrial membrane potential. FCCP (1.25 μM) is injected after oligomycin and as a result, electron flow through the electron transport chain is uninhibited leading to maximal oxygen consumption by complex IV. The third and final injection consists of a mixture of rotenone (0.5 μM) and antimycin A (0.5 μM), which inhibit complex I and III, respectively. The combination of rotenone and antimycin A arrests mitochondrial respiration. **b,** Representative assay demonstrating the effect of α-synuclein fibril-induced aggregation (1 μM) in reducing OCR (black arrows) in $SNCA^{TRIP}$ dopaminergic neurons.

2.3 Biochemical techniques

2.3.1 List of antibodies

Antibody	Supplier	Host	Function
anti-phospho S129 α-synuclein clone EP1536Y	Abcam, ab51253	rabbit monoclonal	ICC (1:1000), WB (1:2000)
anti-tyrosine hydroxylase clone LNC1	Millipore, MAB318	mouse monoclonal	ICC (1:250)
anti-βIII tubulin/TUJ1	Biolegend, MMS-435P	mouse monoclonal	ICC (1:1500)
anti-MAP2	Abcam, ab5392	chicken polyclonal	ICC (1:2000)
anti-SQSTM1/p62 clone 2C11	Abcam, ab56416	mouse monoclonal	ICC (1:1000)
anti-α-synuclein/Syn-1 clone 42	BD Biosciences, 610787	mouse monoclonal	WB (1:1000)
anti-β-actin	Abcam, ab8826	mouse monoclonal	WB (1:10 000)
anti-TOM20	Santa Cruz, FL-145	rabbit polyclonal	WB (1:1000)
Total OXPHOS rodent antibody cocktail	Abcam, ab110413	mouse monoclonal	WB (1:1000)
anti-PARK7/DJ-1	Abcam, ab18257	rabbit polyclonal	WB (1:2000)
anti-GLO1	Abcam, ab129124	mouse monoclonal	WB (1:2000)
anti-Advanced Glycated End-products (AGE)	Millipore, AB9890	goat polyclonal	WB (1:1000)
anti-Myc 9E10	Santa Cruz, SC-40	mouse monoclonal	IP (10 µg)
Alexa Fluor 594-labelled anti-rabbit IgG H&L	Abcam, ab150080	goat	ICC (1:1500)
Alexa Fluor 488-labelled anti-mouse IgG H&L	Abcam, ab150113	goat	ICC (1:1500)
Alexa Fluor 488-labelled anti-chicken IgY H&L	Abcam, ab150169	goat	ICC (1:1500)
HRP-labelled anti-rabbit IgG H&L	Thermo Fisher, 31460	goat	WB (1:5000)
HRP-labelled anti-mouse IgG H&L	Thermo Fisher, 31430	goat	WB (1:5000)
HRP-labelled anti-goat IgG H&L	Thermo Fisher, 31402	rabbit	WB (1:5000)
DyLight 680-conjugate anti-mouse IgG H&L	Cell Signalling, 5470	N/A	WB (1:5000)
DyLight 800-conjugate anti-rabbit IgG H&L	Cell Signalling, 5151	N/A	WB (1:5000)

Table 2.2 List of primary and secondary antibodies used in this study

ICC, immunocytochemistry. WB, western blotting. IP, immunoprecipitation.

2.3.2 Immunofluorescence staining

iPSC-derived dopaminergic and HEK293 cells were fixed with 4% paraformaldehyde (VWR) in PBS (Gibco), permeabilised in 0.1% Triton-X-100 (Sigma) followed by blocking in 3% bovine serum albumin (BSA, Sigma) in PBST (0.1% Tween-20, Sigma). Fixed, permeabilised, and blocked cells were then incubated with primary antibodies overnight at 4°C with agitation and fluorescently labelled secondary antibodies for 45 min at room temperature. Cells were washed three times in PBST for 5 min. Images were obtained using Zeiss LSM 710 confocal microscope (Carl Zeiss AG, Oberkochen, Germany). For markers of dopaminergic neurons, 10 images at 40X magnification were analysed for each marker per differentiation per line—at least 500 cells per condition were quantified. To measure aggregate length, a single image (63X) consisting of between 500 to 2000 events was obtained per timepoint per differentiation using confocal microscopy. Aggregate length was quantified in these images using the FIJI ImageJ (v2.1.1/1.53c) ridge detection plugin (v1.4.0) with the following parameters: 'optional_parameters': line width (3.5), high contrast (230), low contrast (50); 'mandatory_parameters': sigma (1.00), lower threshold (1.10), upper threshold (7.99). For nuclear fragmentation, 5 to 50 DAPI images (40X) were acquired per timepoint per differentiation using immunofluorescence microscopy and in total at least 300 cells were counted per clone per condition. Nuclear fragmentation counts were blinded and quantified manually on FIJI ImageJ (v2.1.1/1.53c).

2.3.3 Immunoblotting and immunoprecipitation

Immunoblotting for iPSC-derived dopaminergic neurons and HEK293 cells was performed using standard protocols after lysis in ice-cold RIPA Extraction Buffer (Thermo Scientific) supplemented with 100 mM *N*-Ethylmaleimide (NEM, Sigma), 100 mM phenylmethylsulphonyl fluoride (PMSF, Sigma), and 1X protease and 1X phosphatase inhibitor cocktails (Sigma). Lysates were homogenised by vortexing for 1 min three times and agitation for 30 min at 4°C followed by centrifugation for 5 min at 21 000 g at 4°C. If lysates remained highly viscous, a battery-operated pestle motor mixer (Argos Technologies) was used for 1 min on ice.

Protein concentrations were normalised using the BCA assay (Thermo Scientific) as per manufacturer's instructions. Samples were mixed with Laemmli buffer (NuPAGE LDS Sample Buffer 4X, Invitrogen) supplemented with 500 mm dithiothreitol (DTT, NuPAGE Sample Reducing Agent 10X, Invitrogen) and heated for 10 min at 75°C. Samples were heated at 75°C and not boiled (95-100°C) in order to preserve the integrity of phosphate groups and prevent any artificial modifications during sample processing (Ariesandi, Chang, Chen, & Chen, 2013; Giehm, Lorenzen, & Otzen, 2011; Miranda et al., 2013). Samples were separated by 4-12% SDS/PAGE (NuPAGE Novex Bis-Tris Gels, Invitrogen) and electrotransferred onto 0.2 µM nitrocellulose membranes (Invitrogen). Membranes were fixed in 0.4% PFA (VWR) for 20 min before blocking in either 5% powdered milk (Sigma) in PBST or 5% bovine serum albumin (BSA, Sigma) in PBST. Membranes were probed with primary antibodies overnight at 4 °C in blocking buffer and subsequently in secondary antibody for 60 min at room temperature also in blocking buffer. Blots were scanned using a ChemiDoc Imager (Bio-Rad) and band intensity was quantified using FIJI ImageJ (v2.1.1/1.53c).

For the detection of phosphorylated α-synuclein on serine 129 in α-synuclein fibril-induced aggregates from iPSC-derived dopaminergic and HEK293 cells were lysed in ice-cold RIPA Extraction Buffer (Thermo Scientific) as described above. After homogenisation of samples, lysates were fractionated either by ultracentrifugation for 2 h at 100 000 g at 4ºC for dopaminergic neurons or by benchtop centrifugation for 2 h at 21 000 g at 4ºC for HEK293 cells. Endogenously generated aggregates are not soluble in 0.1% SDS, therefore, fractionation isolates the protein soluble fraction (supernatant) from the insoluble fraction (pellet). To resolubilise the pellet, the insoluble fraction was then subjected to sonication (two cycles at 30% amplitude 1 sec on, 1 sec off for 30 s). for 1 min on ice in 2% SDS RIPA supplemented with NEM, PMSF and protease and phosphatase inhibitors as described above.

Immunoprecipitation to confirm the interaction between α-synuclein and DJ-1 was performed by Dr. Samiha Shaikh. Clonal HEK293 cell lines expressing BioID tagged α-synuclein (termed α-Syn-BirA*) were transfected to overexpress DJ-1 tagged with myc. Biotinylated proteins were detected with HRP-conjugated streptavidin.

2.3.4 Time-resolved FRET

Anti-oligomeric α-synuclein and anti-phosphorylated serine 129 α-synuclein kits were purchased from Cisbio (Perkin Elmer, Waltham, MA USA) and used according to manufacturer's instructions. Initial optimisation experiments were extensively carried out to determine the dynamic range of the assay in lysates from iPSC-derived dopaminergic neurons. Specific to this assay, neurons were replated in 1% Geltrex-coated 96-well plates at a density of 70 000 cells/well and matured to DIV45, the time of α-synuclein fibril addition. Neurons were subsequently assayed at timepoints ranging from 1 to 4 weeks post-seeding. Neurons were lysed in proprietary Cisbio lysis buffer and homogenised on a shaker at room temperature for 1 h followed by snap freezing at -80°C for 30 min to ensure complete lysis. HTRF 96-well microplates (Cisbio) were used to measure levels of either oligomeric α-synuclein or phosphorylated (S129) α-synuclein. Each assay reaction (total volume 20 µL) consisted of mixing 16 µL of diluted neuronal lysate with 2 µL d2 (acceptor)-tagged antibody and 2 µL Tb-Cryptate (donor)-tagged antibody. Samples and fluorophores were mixed and incubated for 24 h (oligomeric α-synuclein) or 1 h (pS129 α-synuclein).

In this assay, α-synuclein was detected in a sandwich format using two different and specific monoclonal antibodies (Figure 2.2). Each antibody is covalently linked to an acceptor and donor fluorophore, which when in close proximity fluoresces through Fluorescence Resonance Energy Transfer (FRET). In this assay, FRET technology was combined with a time-resolved measurement of fluorescence (homology time resolved fluorescence, HTRF), which introduces a time delay between 50-150 µseconds immediately after the system excitation and fluorescence reading. This time delay eliminates non-specific and short-lived emissions (background: compounds, proteins, medium), which overall increases the sensitivity and specificity of the assay. HTRF systems are characterised by the Förster radius, the distance at

which FRET efficient is 50 %. In this assay the Förster radius lies between 70 to 90 Angstroms.

Samples were excited at 340 nm and emission values were measured at 620 nm and 665 nm using a CLARIOstar Plus (BMG Labtech, Ortenberg, Germany). FRET signal is proportional to the number of antigen-antibody complexes and therefore α-synuclein (oligomeric or S129) concentration. Data were normalised to total protein concentration as determined using a BCA assay (Thermo Scientific). FRET signal intensity was analysed by calculating fold change values based on the background-subtracted ratio of 665/620 nm.

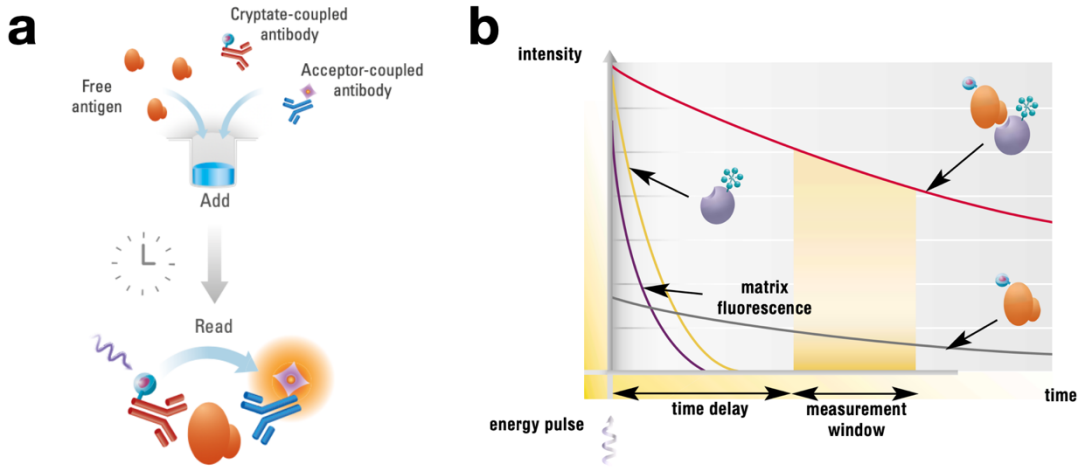


Figure 2.2 Homology time resolved fluorescence Cisbio kit

a, Antibodies conjugated to an acceptor and donor are mixed with cellular lysates. In the presence of the antigen in question, close proximity of the dyes followed by excitation of the donor results in fluorescence of the acceptor at a specific wavelength. **b,** Homology time resolved fluorescence records fluorescent signal after a time delay to reduce signal arising from non-specific agents. The energy emitted from the excitation source is immediately followed by a time delay, allowing interfering short-lived fluorescence to decay.

2.3.5 siRNA treatment

Small interfering RNAs (siRNAs) are inhibitory antisense oligonucleotides used to inhibit/knockdown gene expression (B. Hu et al., 2020). iPSC-derived dopaminergic neurons were treated with DJ-1 targeting Accell siRNA (Dharmacon) according to manufacturer's instructions. Lyophilised siRNA was reconstituted to a stock concentration of 40 µM using 5X siRNA buffer (Dharmacon) diluted to 1X in RNAse-free water (Dharmacon). Freshly diluted siRNA stock solutions were placed on an orbital shaker for 90 min at room temperature to ensure an efficient resuspension.

Human dopaminergic neurons were treated with two pulses of DJ-1 targeting siRNA at DIV41 (four days prior to the addition of exogenous fibrils on DIV45) and DIV51 (six days following the addition of exogenous fibrils). siRNA experiments were performed in a 96-well plate format and supplemented with 100 µL of neuronal growth media and DJ-1 siRNA at a final concentration of 1 µM. Neurons were incubated with DJ-1 siRNA for 96 h, which was followed either by treatment with α-synuclein fibrils or by a full media change.

2.3.6 Enzyme-linked immunosorbent assay for DJ-1

Knockout and knockdown of DJ-1 protein levels were confirmed by DJ-1 enzyme-linked immunosorbent assay (Bio-Techne) according to manufacturer's instructions.

This assay was performed in a 96-well plate format. Each well was coated with 100 µL of diluted capture antibody in PBS (Sigma) overnight at room temperature. Wells were washed twice with 400 µL of PBST (Sigma) and blocked with 1% BSA (Sigma) in PBST (Sigma) for 90 min at room temperature. Levels of total cellular protein was measured using the BCA Protein assay (Thermo Scientific). The optimal protein concentration for this assay was determined to be between 1000-2000 pg/mL. 100 µL of normalised protein lysates or standard were added in 1% BSA in PBST and incubated for 120 min at room temperature. Wells were then washed twice with PBST and sandwiched with 100 µL of detection antibody for another 120 min. 100 µL of Streptavidin-HRP was added to each well and incubated for 20 min at room temperature followed by the addition of 100 µL of substrate solution, containing the chromophore. After incubation with the substrate solution for 20 min at room temperature, 50 µL of stop solution was added and optical density was determined using a microplate reader (CLARIOstar, BMG Labtech, Germany) set to 450 nm with a wavelength correction set to 540 nm.

2.3.7 Neurofilament light chain immunoassay

Levels of neurofilament light chain (NfL) in the conditioned media of cultured human dopaminergic neurons were quantified by Single Molecule Array (Simoa) technology as described previously (Barth et al., 2021). This work was performed in collaboration with Dr. Melanie Barth and Dr. Gaye Tanriöver from Mathias Jucker's laboratory. iPSC-derived dopaminergic neurons were cultured in 12-well plates and supplemented with 500 µL of neuronal growth media across all conditions. Culture medium from neurons exposed to various α-synuclein assemblies at DIV60, 2-weeks post-seeding, was collected, aliquoted, and stored at -80 degrees Celsius. NfL concentrations were determined using the highly sensitive Simoa NF-Light Advantage Kit (Quanterix) according to manufacturer's instructions. Samples were pre-diluted (1:10 and 1:50) in NF-Light sample diluent (Quanterix) and measured using Simoa HD-1 Analyzer (Quanterix, USA). Internal reference samples were used in each assay and the detection limit of NfL was 0.038 pg/mL.

2.4 Molecular Biology techniques

2.4.1 Table of primers and sgRNAs

Description	Forward sequence	Reverse sequence
SNCA	5'-TGTAGGCTCCAAAACCAAGG-3'	5'-GGGGCTCCTTCTTCATTCTT-3'
GAPDH	5'-TGGAAGGACTCATGACCACAG-3'	5'-CAGTGGGGACACGGAAGG-3'
ACTB	5'-CTTCCTGGGCATGGAGTC-3'	5'-GCTCAGGAGGAGCAATGATCT-3'
DJ-1(*PARK7*), sgRNA1 used in HEK cell line	5'-CTGCACAGATGGCGGCTATC-3'	
DJ-1(*PARK7*), sgRNA2 used in HEK cell line	5'-TATGATGTGGTGGTTCTACC-3'	
GLO-1, sgRNA1 used in HEK cell line	5'-TCGTCCGTGAGGCCGCCGGA-3'	
GLO-1, sgRNA2 used in HEK cell line	5'-GCAGACCATGCTACGAGTGA-3'	
non-target control, sgRNA1 used in HEK cell line	5'-GGTATTCCGAAGTCCTCCGC-3'	
non-target control, sgRNA2 used in HEK cell line	5'-GGATACCTGGGCCGACTTTC-3'	
DJ-1 Exon2 for detection assay, DA, Product: 531 bp (WT) or 362 bp (KO) used in iPSC cell line	5'-CCTCATTATGTTTTCATCT CAGAGC-3'	5'-TGGGTCTGAAGGAAATATGGCA-3'
DJ-1 Exon2 for absence assay, AA, product: 464bp (WT) or no band (KO) used in iPSC cell line	5'-CGAGGACTGCCTCAACCAG-3'	5'-CTTGTCTGCCAAGAACCCCT-3'
DJ-1 Exon2 sequencing used in iPSC cell line	5'-TGGGTCTGAAGGAAATATGGCA-3'	
DJ-1 Exon4 for detection assay, DA, Product: 431 bp (WT) or 341 bp (KO) used in iPSC cell line	5'-CAGCGTGGACATCCTT GCAT-3'	5'-CACAGCCTCCTCCCGAAA-3'
DJ-1 Exon4 for absence assay. AA, Product: 284 bp (WT) or no product (KO) used in iPSC cell line	5'-TACTCTGCAGCGTGGACATC-3'	5'-TGTGCGCCCAGATTACCTC-3'
DJ-1 Exon4 sequencing used in iPSC cell line	5'-TGCACAGTTGAAATGAAATG-3'	
DJ-1, sgRNA1 targeting exon2 used in iPSC cell line	5'-TCATCCCTGTAGATGTCATGAGG-3'	
DJ-1, sgRNA2 targeting exon2 used in iPSC cell line	5'-CCACTGCTCACATTTAACGCTTG-3'	
DJ-1, sgRNA1 targeting exon4 used in iPSC cell line	5'-GTTACAGGGACCATATGATGTGG-3'	
DJ-1, sgRNA2 targeting exon4 used in iPSC cell line	5'-CCTCAA TAAAGCTGGGGGGGGGG-3'	

Table 2.3 List of primers and sgRNAs used in this study

2.4.2 Relative gene expression

Total RNA was isolated using the RNeasy Kit (Qiagen) according to manufacturer's instructions. Extracted total RNA was eluted in RNAse-free water and quality controlled using a spectrophotometer (NanoDrop 2000c, Thermo Scientific). 1 µg of cDNA was synthesised with random hexamers using the QuantiTect Reverse Transcription Kit (Qiagen). To quantify relative *SNCA* mRNA levels, real-time quantitative PCR was performed using Roche LightCycler 480 II Instrument and its associated software. Each reaction was carried out in a total volume of 10 µL in a 384-well plate, consisting of 5 ng of cDNA, LightCycler 480 SYBR Green I Master (Roche), and 1 µM of both forward and reverse primers. Data were normalised to two housekeeping genes, *GAPDH* and *ACTB*. All primer sequences used in this study are listed in Table 2.3. Primers were designed using Real-time PCR Primer and Probes Design Tool (GenScript). The GenBank accession number for genes of interest were first acquired from Ensembl genome browser. The accession numbers were entered into the Real-time PCR Primer and Probes Design Tool (GenScript) and primers crossing exon junctions were selected, the following parameters were used: PCR amplicon size range, 50-200; primer melting point minimum, 52°C, maximum, 56°C, maximum, 60°C. Roche LightCycler 96 System was used to calculate crossing threshold (Ct) values and relative gene expression was subsequently calculated using the delta delta Ct method.

2.4.3 CRISPR/Cas9 knockout in HEK293 cells

CRISPR/Cas9 knockout of DJ-1 and GLO-1 in HEK 293 cells overexpressing venus-tagged wilt-type human α-synuclein was performed by Dr. Samiha Shaikh. Two sgRNAs per target were designed using the online tool (http://crispor.tefor.net/) and cloned into a lentivirus backbone. All sgRNA sequences are shown in Table 2.3. To generate the virus, HEK293T cells were transfected with the appropriate plasmids. After 6 h, media was changed and harvested a further 48 h later. HEK293 WT α-syn-venus Cas9 cells were plated at a density of 3.5 x 10^5/ well. 48 h later, cells were transduced with 200 µl of conditioned viral media. 24 h later, media were replaced and a further 24 h later, cells were selected with 1.5 µg/ml puromycin for 3 days. Cells were then replated for immunofluorescence, immunoblotting or RNA extraction.

2.4.4 CRISPR/Cas9 modification in iPSC lines

The generation of the isogenic line for $SNCA^{TRIP}$ was described in detail previously and was kindly donated by Dr. Sabrina Heman-Ackah and Dr. Carlo Rinaldi (Heman-Ackah et al., 2017). In brief, Cas9 nickase sgRNAs were designed to target *SNCA* exon 4 and applied to the ND34391G iPSC line (obtained from the Coriell Institute, distributed through the NINDS Fibroblasts and iPSCs Collection). After clonal expansion of Cas9 nickase-transfected iPSCs, four clones were identified as variants by high resolution melt analysis and one clone was confirmed by sequencing as a double knockout. The double knockout clone (i.e. deletion of the two SNCA gene copies) was sequenced for off-target effects and quality controlled (Heman-Ackah et al., 2017). α-Synuclein mRNA and protein levels in the isogenic iPSC line were tested and shown to be reduced to levels comparable to the healthy control iPSC line (Heman-Ackah et al., 2017). In this context, isogenic refers to the fact that the parental *SNCA* triplication iPSC line and the double knockout clone possess identical genetic background, which includes overexpression of the other genes in the triplication locus, and selective reduction of *SNCA* gene dosage to achieve normal expression levels.

$SNCA^{TRIP/DJ\text{-}1\ KO}$ iPSC cell lines were generated at Bioneer AS (Denmark) using our $SNCA^{TRIP}$ line. To knockout DJ-1, the $SNCA^{TRIP}$ iPSC clone SFC831-03-03 was nucleofected with the CRISPR complexes formed by the two sgRNAs targeting either exon 2 or exon 4 and the HiFi Cas9 protein. For exon 2, two sgRNAs were designed targeting exon 2 and the downstream intron in order to remove a part of the gene causing a deletion of 169 base pairs. For exon 4, two sgRNAs were designed targeting exon 4 and the downstream intron causing a deletion of 90 base pairs. Single guide RNAs for genome editing were dissolved in DNAse and RNAse free buffer to a concentration of 100 mM. One µL of each sgRNA was mixed with 2 µL of HiFi Cas9 protein (IDT, #1081067) to form the active CRISPR/Cas9 complex. iPSCs were

cultured in 6 well plates coated with Matrigel (Corning Bioscience) in E8 medium until they reached a density of 70 – 90%. iPSCs were detached using Accutase (Gibco) and a total of 1.5 x 10^6 cells were co-nucleofected with the CRISPR/Cas9 complex. For the nucleofection, the P3 Primary Cell Kit (Lonza) was used and run with the program CA167. iPSCs were subsequently transferred back to a Matrigel-coated 100 mm dish in E8 medium supplemented with 1:200 diluted Revita cell supplement (Gibco). After one week, 96 colonies from each nucleofection were picked and analysed using PCR for either exon 2 or exon 4. The deletions were confirmed by two primer pairs, one pair placed around the deleted part and the other pair consisting of one primer within the deleted part and one outside of it. After single cell plating, three clones (two with exon 2 deletion and one with exon 4 deletion) were expanded and confirmed by sequencing of the targeted region 9. Their identity in relation to the original $SNCA^{TRIP}$ clone was also confirmed by short tandem repeat analysis. DJ-1 knockout was confirmed by enzyme-linked immunosorbent assay (Figure 5.18) and immunoblotting (Figure 5.19). Primer and sgRNA sequences are shown in Table 2.3.

2.5 Transcriptome analysis

RNA sequencing was performed in the Wellcome Centre for Human Genetics (Oxford, UK) with Dr. Theodosios Kyriakou. Transcriptomic analysis was performed by collaborators Dr. Devika Agarwal and Dr. David Sims.

2.5.1 Bulk RNA sequencing

Bulk RNA-Seq was performed to assess response to aggregation induced by *de novo* or brain-amplified α-synuclein assemblies under different experimental conditions: subtoxic aggregation using 0.1 μM α-synuclein seeds in $SNCA^{TRIP}$ or HC iPSC-derived neurons (*n*=24) or at two different timepoints (week 1 and week 2) using 1 μM α-synuclein seeds in $SNCA^{TRIP}$ iPSC-derived neurons (*n*=24). RNA samples were prepared using standard poly-A enrichment, 250-300 bp insert cDNA library was prepared with the NEB Next® Ultra™ RNA Library Prep Kit and sequenced on Illumina NovaSeq 6000 (S4) using 150 bp paired-end reads. Sequencing resulted in approximately 40 million reads per sample. RNA-Seq data are available at GEO under accession numbers GSE149632 and GSE171999.

2.5.2 Human substantia nigra transcriptomic cell-type atlas

Filtered substantia nigra single nuclei count data with cell type annotations for 7 post-mortem individuals was downloaded from the Broad Institute Single Cell Portal [https://singlecell.broadinstitute.org/single_cell]. The count matrices for all individuals were merged to result in 40,453 SN single nuclei with 24 cell types encompassing all known resident cell classes as identified previously in the literature (Welch et al., 2019). For the purpose of cell type deconvolution analysis in this study, these cell types were merged into eight major subtypes: astrocytes, dopaminergic neurons, endothelial, excitatory and inhibitory neurons, microglia, oligodendrocytes and oligodendrocyte progenitor cells.

2.5.3 Cell-type deconvolution of bulk RNA sequencing samples

Cell-type composition of the bulk RNA-Seq samples was characterized using MuSiC (X. Wang, Park, Susztak, Zhang, & Li, 2019), a cross-subject method that utilizes only the consistently expressed genes across multiple cells by up-weighting genes with low cross-subject variance (informative genes) and down-weighing genes with high cross-subject variance (non-informative genes). Additionally, we accounted for a potential bias based on differing cell type numbers across the cell types in the reference single cell atlas by randomly down sampling the eight major resident cell types to the same number (n=50) 100 times and then estimating the cell type composition of the bulk samples and averaging the proportions across the bootstraps to obtain the final cell-type estimates.

2.5.4 Analysis of RNA sequencing data

Kallisto (v0.46.2) (Bray, Pimentel, Melsted, & Pachter, 2016) was used to estimate abundance for Ensembl (release 88) protein-coding genes from RNA-Seq reads. Count data was imported into R (v4.0.3) using Tximport (v1.18.0) and genes with less than 10 reads across the 6 samples used in the comparison were filtered out. Differential gene expression was performed in DESeq2 (v1.30.0) (Love, Huber, & Anders, 2014) using the Wald test with an FDR threshold of 0.05 and a log2 fold-change threshold of 0.25. Gene Set Enrichment Analysis (GSEA) was performed using the Fgsea package (v1.16.0) (Sergushichev, 2016) in R (v4.0.3) with KEGG pathways. Genes were ranked for GSEA using the Wald statistic and Fgsea (v.1.16.0) was run with 1000 permutations. Principal Component Analysis and all plotting was performed in R (v4.0.3).

2.6 Interactome analysis

α-Synuclein interactors were investigated in HEK293 cells using the BioID2 system (D. I. Kim et al., 2016) by Dr. Samiha Shaikh. Mass spectrometry and the subsequent analysis was performed at the Target Discovery Institute by Dr. Roman Fishcer.

2.6.1 Affinity capture of biotinylated proteins

A C-terminal BioID2 tagged α-synuclein construct was generated by introducing full-length α-synuclein cDNA (ENST00000336904.7) into the MCS-BioID2-HA vector cloning vector (Addgene) using the restriction enzyme sites NheI and Kpn2I (Thermo Scientific). SILAC labelled HEK293 cells were plated in 6-well plates at a concentration of 9.8 x 10^5/ well. 48 h after plating, fibrils were added to SILAC labelled cells. R0K0 cells were treated with *de novo* generated α-synuclein fibrils, R6K4 cells were treated with PD-amplified fibrils and R10K8 cells were treated with MSA-amplified fibrils at a final concentration of 1 μM. 3 h after seeding, appropriate media containing biotin was added to all cells at a final concentration of 3.1 μM. After 24 h, media was replaced supplemented with biotin. A further 24 h later, cells were harvested in cell lysis buffer (50 mM Tris (Sigma), pH 7.4, 500 mM NaCl (Sigma), 0.4% SDS (Sigma), 5 mM EDTA (Sigma), 1 mM DTT (Sigma), and 1x protease inhibitor (Roche) or fixed in 4% PFA for immunofluorescence. Triton-X-100 (Sigma) was added to protein lysates to a final concentration of 2%. Cell lysates were sonicated for two cycles at 30% amplitude 1 sec on, 1 sec off for 30 s and centrifuged at 21 000 *g.* The supernatant was stored and the pellet (insoluble fraction) was resuspended in lysis buffer containing 2% SDS and sonicated for one sonication cycle, before centrifugation at 21 000 *g*. The supernatant was then pooled with previous lysate. Levels of total cellular protein was measured using the BCA Protein assay (Thermo Scientific). 1 mg of total protein from each of the three different experimental treatment groups R0K0, R6K4 and R10K8 were combined and incubated overnight on 300 μl of Myone streptavidin C1 beads (Thermo Scientific)

with constant rotation at 4°C. Beads were collected using a magnetic separation stand and were washed sequentially with wash buffer 1 (2% SDS), wash buffer 2 (0.1% deoxycholic acid, 1% Triton-X-100, 1mM EDTA, 500 mM NaCl, 50 mM HEPES (Gibco) pH 7.5 and finally wash buffer 3 (0.1% deoxycholic acid (Sigma), 0.5% NP-40 (Sigma), 1mM EDTA, 250 mM LiCl (Sigma), 10 mM Tris.Cl pH7.4). Beads were finally washed with 50 mM Tris.Cl pH 7.4 and resuspended with 1.5 ml of 50 mM Tris.Cl. 15% of the resuspended beads was saved for further analysis by immunoblotting and the remaining 85% was used for mass spectrometry. Beads were spun for 5 min at 2000 g for 5 min to collect beads and supernatant was removed.

2.6.2 Mass spectrometry and analysis

Beads were spun down and resuspended in 150 µL trypsin buffer (Promega). Samples were reduced using 10 µL of DTT (Sgima) reducing agent at a final concentration of 10mM and incubated for 45 min at room temperature. Samples were then alkylated with iodoacetamide at a final concentration of 40 mM and incubated for 45 min at room temperature. SMART Digest Trypsin (Thermo Scientific) was added in a 1:50 ratio with respect to total protein content and samples were digested at 70 degrees Celsius for 1 h. Samples were analysed on a nLC-MS/MS system consisting of an Orbitrap Fusion Lumos and Dionex Ultimate 3000 (Thermo Scientific). Peptides were separated on an Easyspray column (50cm) with a gradient of 2-35% ACN in 5% DMSO in 0.1% Formic Acid over 60 minutes. MS1 spectra were acquired with a resolution of 120k and an AGC target of 4E5. MS2 spectra were acquired in the linear ion trap after HCD fragmentation at 28% normalized collision energy for up to 35 ms and an AGC target of 4E3. Selected precursors masses were excluded for 60 sec. Data analysis was performed in Maxquant (v1.6.2.3) (Tyanova, Temu, & Cox, 2016) using SILAC settings (R0K0, R6K4 and R10K8). Peptide precursor ion abundance was used to compare the volume under the chromatographic signal of each peptide detected for a protein. Peptide signals were then summarised into ratios for each protein across the different conditions, yielding a fold change value. Specifically, the ratio of MSA- or PD- amplified to *de novo* fibrils was first calculated and then converted to log2 followed by statistical analysis within the biological replicates to yield fold changes and multiple testing corrected *p*-values. Carbamidomethylation (Cys) was a fixed modification and Oxidation (Met), Phosphorylation (Ser, Thr, Tyr) and protein N-terminal Acetylation were set a variable. Searches were performed with a mass tolerance of 10 ppm for precursors and 0.5 Da for fragments. Swissprot/Trembl FASTA file was used as database. Protein and peptide FDR were set to 1% with Match between Runs option

enabled. The mass spectrometry proteomics data have been deposited to the ProteomeXchange Consortium via the PRIDE partner repository with the dataset identifier PXD024198.

2.7 Generation of α-synuclein polymorphs

De novo generated and patient brain-amplified α-synuclein fibrils were produced and extensively characterised by Dr. Alexis Fenyi, Dr. Luc Bousset, and Dr. Ronald Melki. All α-synuclein fibrils were kindly donated for the purpose of this study as part of a collaboration within the IMPRiND Consortium.

2.7.1 α-Synuclein purification and assembly in fibrillar polymorphs

Recombinant human wild-type α-synuclein was expressed in E. coli BL21 DE3 CodonPlus cells (Stratagene) and purified as described previously (Ghee, Melki, Michot, & Mallet, 2005). It was next assembled for 7 days into the fibrillar polymorphs "fibrils" and "ribbons" as described (Bousset et al., 2013). The nature of α-synuclein fibrillar polymorphs was assessed by Transmission Electron Microscopy (TEM) after adsorption of the fibrils onto carbon-coated 200 mesh grids and negative staining with 1% uranyl acetate using a Jeol 1400 transmission electron microscope. The images were recorded with a Gatan Orius CCD camera (Gatan, Pleasanton, CA, USA). The resulting α-synuclein fibrillar polymorphs were fragmented by sonication for 20 min in 2 mL Eppendorf tubes in a Vial Tweeter powered by an ultrasonic processor UIS250v (250 W, 2.4 kHz; Hielscher Ultrasonic, Teltow, Germany) to generate fibrillar particles that are suitable for endocytosis, with an average size of 60 nm, as assessed by TEM analysis. Their proteinase K proteolytic patterns were assessed by SDS-PAGE analysis after staining with Coomassie blue. To this end, *de novo* generated α-synuclein fibrillar polymorph (1.4 mg/mL) in 150 mM KCl (Sigma), 50mM Tris-HCl (Sigma), pH 7.5 were treated at 37 degrees Celsius by Proteinase K (3.8 µg/ml) (Roche). Aliquots were removed at different time intervals following addition of the protease and transferred into Eppendorf tubes maintained at 90 degrees Celsius containing sample buffer (50mM Tris-HCl, pH 6.8, 4% SDS (Sigma), 2% beta-mercaptoethanol (Gibco), 12%

glycerol (Sigma) and 0.01% bromophenol blue (Sigma)) to immediately arrest cleavage. The tubes were incubated for 5 min at 90 degrees Celsius prior to SDS-PAGE (15%) analysis.

2.7.2 Patient brain homogenate preparation and quantification of pathogenic α-synuclein assemblies

Frozen brain tissues provided by the Oxford Brain Bank were weighed prior to the addition of protein misfolding cyclic amplification (PMCA) buffer (150mM KCl (Sigma), 50mM Tris-HCl (Sigma) pH7.5) in order to obtain a final homogenate of 20% (weight:volume). The homogenization was performed by sonication using the SFX 150 Cell Disruptor sonicator with a 3.17 mm microtip probe (Branson) for 1 minute, with 10 second pulses followed by 10 second pauses in a biosafety level 3 environment (BSL-3). The homogenates were aliquoted and immediately frozen in liquid nitrogen before storage at -80°C. All contaminated surfaces were cleaned with SDS (Alexis Fenyi et al., 2019a). Pathogenic α-synuclein was quantified using both a filter retardation assay and immunoblotting and a HTRF assay. The brain homogenates (0.5 mg) were immobilized on cellulose acetate membranes (0.2 µm pore size, Millipore) by filtration using a 48-slot slot-blot filtration apparatus (GE Healthcare). The membranes were blocked in 5% dried skimmed milk (Sigma) and probed with the anti α-synuclein antibody 4B12 (Biolegend, #807801) and anti P-S129 α-synuclein antibody 81A (Millipore, #MABN826). Following proteinase K digestion, neuronal lysates were immunoblotted with a mixture of ASyM (clone number 42, Agrisera, AS13 2719, residues 1-15), 4B12 (Biolegend, #807801, residues 103-108) and 10D2 (Merck, #MABN633, residues 118-127) and 10D2 (Merck, #MABN633, residues 118-127) antibodies to include multiple sites in α-synuclein's primary structure. Membranes were then incubated with HRP-conjugated goat anti-mouse IgG3 secondary antibody (Thermo Scientific, #M32707) for 1 h at room temperature. Proteins were visualized using ECL reagents (Pierce, USA).

Pathogenic phosphorylated α-synuclein was also quantified using an HTRF assay (Cisbio, #6FASYPEG) following manufacturer's instructions. Patients brains homogenates were diluted to 10% (weight:volume) in lysis buffer (Cisbio). 16µL of each

diluted brain homogenates were loaded into a 96 wells plate and mixed with 4 µL of HTRF donor and acceptor antibodies. Samples were incubated for 20 hours at room temperature. After incubation, FRET signal was measured upon excitation at 337 nm using a plate reader (CLARIOstar, BMG Labtech, Germany). FRET signal was recorded at 665nm and 620nm and analysed according to manufacturer's instructions.

2.7.2.1 Patient cases

Brain tissue homogenate from post-mortem brains with neuropathologically confirmed α-synucleinopathy, namely 3 cases from sporadic Parkinson's disease patients and 5 cases from multiple system atrophy patients. Of the MSA cases 4 had a predominantly Parkinsonian presentation and one case had a cerebellar presentation. Anterior cingulate was obtained from each Parkinson's disease case and corresponding controls. The cerebellum was used for each multiple system atrophy case and corresponding controls.

ID	Diagnosis	Sex	Age at death (years)	Braak staging	Original ID
PD1	sporadic PD	male	76	6	NP17
PD2	sporadic PD	female	70	2	NP112
PD3	sporadic PD	male	80	6	NP133
MSA1	MSA-P	male	71	n/a	PD080
MSA2	MSA-C	male	64	n/a	PD505
MSA3	MSA-P	male	46	n/a	PD515
MSA4	MSA-P	male	86	n/a	PD043
MSA5	MSA-P	female	67	n/a	PD821

Table 2.4 Post-mortem brain tissues used in this study

Each case was extensively characterised neuropathologically including staining for other proteinopathies. Parkinson's disease cases were sporadic without any familial cases and obtained from the anterior cingulate. Multiple system atrophy cases were obtained from the cerebellum. MSA-P, multiple system atrophy-parkinsonian type; MSA-C, multiple system atrophy-cerebellar type.

2.7.3 Amplification of pathogenic α-synuclein in patient brain homogenates by protein misfolding cyclic amplification

All operations were performed to BSL-3 standards. PMCA was performed as previously described. Briefly, each patient brain homogenate (2%, weight:volume) in PMCA buffer (150 mM KCl, 50 mM Tris-HCl, pH 7.5) containing monomeric α-synuclein (100 μM) was split in 2 tubes of PCR strips (BIOplastics). PMCA amplification was performed in quadruplicates for each patient using the Q700 generator and a 431MPX horn (Qsonica, Thermo Scientific). The power of the horn was set to 30% of maximal amplitude. The amplification cycles consisted in 15 seconds of sonication and 5 minutes of elongation of the resulting assemblies at 31 degrees Celsius. Every hour, 5 μL were withdrawn from each tube and diluted in 300 μl of 10 μM of Thioflavin T (ThT). The amplification was monitored by measuring ThT fluorescence using a Cary Eclipse Fluorescence Spectrophotometer (Agilent) with fixed excitation and emission wavelength at 440 nm and 480 nm respectively. The time at which an aliquot from one amplification reaction was withdrawn for a subsequent reaction was defined as the time where ThT fluorescence increased for each amplification reactions performed with PD and MSA brain homogenates, and not in reactions containing control patients brain homogenates or monomeric α-synuclein alone. Cycle 2 and 3 were performed following the same protocol using 2% of the preceding cycle reaction as seeds for PD cases, 5% for MSA cases. The amounts of brain homogenates and PMCA amplified assemblies used in each amplification reaction were defined through an optimization study aimed at maintaining high stringency by minimizing the *de novo* aggregation of α-synuclein under the same experimental conditions. The time at which an aliquot from one amplification reaction was withdrawn for a subsequent amplification reaction was also defined through an optimization study aimed at avoiding the formation of fibrillar α-synuclein assemblies *de novo*. The PMCA reactions products resulting from the 3rd

amplification cycle were spun for 30 minutes at 50,000*g*, the amount of monomeric α-synuclein in the supernatant was assessed spectrophotometrically and the pelleted assemblies were resuspended in phosphate-buffered saline buffer and their shape was assessed by TEM. All resuspended assemblies, at a final concentration of 100 μM α-synuclein, were fragmented by sonication for 20 min in 2 mL Eppendorf tubes in a Vial Tweeter powered by an ultrasonic processor UIS250v (250 W, 2.4 kHz; Hielscher Ultrasonic), aliquoted, flash frozen in liquid nitrogen and stored at -80°C until they were added to cell cultures. Their size was measured in order to validate that their length (60 to 100nm) was similar to that of *de novo* generated fibrils and ribbons and their limited proteolytic fingerprints analysed as described for α-synuclein fibrillar polymorphs generated *de novo*.

2.8 Statistical analysis

All statistical analyses were performed using GraphPad Prism 9 (Graphpad Software Inc., CA USA). All data were examined for normality and statistical tests were chosen accordingly. For normally distributed data, a one-way ANOVA was used followed by Tukey's multiple comparison test. For non-normally distributed data, the Kruskal-Wallis test was used followed by Dunn's multiple comparison test. A two-sided unpaired Student's *t*-test was used where indicated when two conditions were compared. The null hypothesis was rejected at a significance level of p=0.05. For experiments involving iPSC lines, *n* biological replicates were defined as differentiations performed at least one cell-split apart and each clone was differentiated at least three times.

2.9 Ethical approval

Ethical approval was obtained from the Oxford C REC Ethics Committee (No. 15/SC/0639) for the use of human tissue.

Chapter 3

Modelling α-synuclein seeded aggregation in human iPSC-derived dopaminergic neurons with recombinant fibrils

3.1 Introduction

3.1.1 Stem cell modelling of Parkinson's disease

Progress in cellular reprogramming and induced pluripotent stem cell technologies have led to the development of disease models that utilise patient-derived brain cells (Parr, Yamanaka, & Saito, 2017; Yamanaka, 2012). This opportunity to culture patient cell lines *in vitro* has subsequently given rise to novel ways in which the pathomechanisms of genetically linked diseases can be studied. The ability to exploit stem cell pluripotency offers much potential to investigate disease phenotypes in specific cell types and puts a large emphasis on the development and optimisation of differentiation protocols. Presently, over 385 neuronal lines from Parkinson's patients have been generated across 67 independent studies since 2011, demonstrating the breadth of data originating from stem cell research (Tran, Anastacio, & Bardy, 2020).

The lack of disease-modifying therapies in neurodegeneration is the direct result of multiple failed clinical trials (Seppi et al., 2019; Tolosa et al., 2020). In particular, the pathogenesis of Parkinson's disease is incompletely understood, and its diagnosis relies primarily on clinical manifestations occurring long after cellular pathology (Del Tredici & Braak, 2020). Additionally, biomarkers are lacking at all stages of disease and heterogeneity between patients is substantially high (Espay et al., 2020). Taken together, these challenges represent the bottleneck of preclinical translational research that stem cell studies aim to overcome. Stem cell-derived neurons exhibit

certain degenerative phenotypes which to some extent recapitulate previously identified post-mortem and biopsy samples (Haston & Finkbeiner, 2016). They obviate discrepancies in cross-species data from animal models, offer a full human genome and are ethically discreet unlike embryonic stem cells. Despite relevant concerns with end-product maturation, stem cell-derived neurons provide, to date, the closest representation of 'patient brains in a dish' (Soldner & Jaenisch, 2018). Ultimately, stem cell-derived neurons will find their greatest purpose in firstly, the discovery of druggable therapeutic targets, and secondly, in high-throughput screening assays of such drugs.

Selective degeneration of dopaminergic neurons in the substantia nigra and the presence of Lewy pathology occurring throughout the brain are two cardinal features in Parkinson's disease (Goedert et al., 2017). Progressive degeneration is accompanied by the presence of, and likewise believed to be caused by the formation of filamentous and misfolded α-synuclein aggregates that accumulate intracellularly into Lewy bodies and Lewy neurites (Del Tredici & Braak, 2012a; Luk et al., 2012). These α-synuclein species propagate through conformational templating or seeded aggregation and are thought to cause toxicity and neuronal death (Lashuel et al., 2013). I therefore sought to establish a robust model of α-synuclein seeded aggregation in a completely human system with induced pluripotent stem cell (iPSC)-derived dopaminergic neurons, which has not been established previously in models of Parkinson's disease. Furthermore, based on previous models using immortalised cell lines and primary cultures, I modelled seeded aggregation using exogenously added α-synuclein fibrils that were generated *de novo* (Luk et al., 2009; Volpicelli-Daley, Luk, & Lee, 2014) or amplified in the presence of human brain homogenate. Similar experimental procedures have been developed and were brought to a high-throughput system in models of Alzheimer's disease investigating the seeded aggregation of tau

(Medda et al., 2016; Oakley et al., 2021). Therefore, my overall objective was to faithfully model α-synuclein aggregation in stem cell-derived neurons. Such a model could decipher disease mechanisms in a reductionist manner, requiring a relatively pure population of dopaminergic neurons and α-synuclein fibrils that have been highly characterised.

3.1.2 Differentiation of dopaminergic neurons

Numerous protocols describing the differentiation of midbrain dopaminergic neurons have been developed in the past fifteen years (Arenas, Denham, & Villaescusa, 2015). Candidate cell sources include (i) foetal neural stem cells or progenitor cells, (ii) human embryonic stem cells derived from blastocysts, (iii) human induced pluripotent stem cells derived from fibroblasts, or (iv) direct reprogramming of fibroblasts into neurons (Berry, Smith, Young, & Mack, 2018; Traxler, Edenhofer, & Mertens, 2019). All these methods have successfully generated neurons that share dopaminergic identity, however only a subset of them have generated neurons that share the accurate morphology, expression of markers and electrophysiological functionality (Arenas et al., 2015).

Human midbrain dopaminergic neurons are anatomically present in three distinct nuclei: (i) the substantia nigra pars compacta (SNpc, A9 group), (ii) the ventral tegmental area (VTA, A10 group) and (iii) the retrorubral field (RrF, A8 group) (Dunnett, Bentivoglio, Bjorklund, & Hokfelt, 2005). Although core molecules involved in the synthesis of dopamine are shared across subtypes (e.g. tyrosine hydroxylase (TH) and dopa decarboxylase (DDC)), the heterogeneity between each subtype can be distinguished at a molecular level (Poulin et al., 2018). To improve models of Parkinson's disease, it is vital that stem cells differentiate into dopaminergic neurons from selectively vulnerable regions such as the SNpc, rather than the VTA, a region which is remarkably spared in diseased patients (Brichta & Greengard, 2014). For example, neurons from the SNpc primarily express aldehyde dehydrogenase 1 family member A1 (Aldh1a1) and G-protein-regulated inward-rectifier potassium channel 2 (Girk2), whereas neurons from the VTA express calcium-binding proteins calbindin 1 and 2 (Cal1 and Cal2) and cholecystokinin (Cck) (Veenvliet et al., 2013). Interestingly, previous studies in mice demonstrated that the conditional deletion of FOXA1/2 showed

a reduction of Girk2-positive neurons in the SNpc that was not observed in the VTA (Stott et al., 2013). Moreover, the deletion of Sox6 resulted in the loss of TH-positive and Aldh1a1-positive neurons in the SNpc whilst conversely increasing TH-positive and calbindin-positive neurons in the VTA (Panman et al., 2014). Therefore, by examining subtype-specific markers, we may conclude that FOXA1/2 and Sox6 are mainly involved in the specification towards SNpc neurons. It is likely that additional marker genes are involved in subtype specification, however these studies illustrate the importance of using the correct markers to define subtypes when differentiating stem cells into dopaminergic neurons.

More recent studies aimed towards distinguishing distinct populations of dopaminergic neurons have relied on data generated from RNA sequencing (Kamath et al., 2021). Specifically, transcriptomic analysis in the substantia nigra of human patients revealed further subtypes within nigral tissues, leading to question whether any of these additional subtypes in the substantia nigra are more susceptible to neurodegeneration. By studying patient brains at single cell resolution, one study identified 10 subtypes within the substantia nigra, including one subtype marked by the gene AGTR1, which was highly vulnerable to neurodegeneration (Kamath et al., 2021). The AGTR1 subtype was also enriched for the expression of risk genes associated with Parkinson's disease, suggesting that multiple risk loci may act within substantia nigra subtypes to influence neurodegeneration. Future research into the transcriptional characterisation of differentially vulnerable dopaminergic neurons will therefore inform *in vitro* models of Parkinson's disease and enable mechanistic studies into potential pathways of neurodegeneration.

Human induced pluripotent stem cells are most reliable due to their reprogramming efficiency and their capacity to self-renew. A more stringent temporal implementation of morphogenetic signals was a key step towards the development of improved differentiation protocols. The goal for correct specification of dopaminergic

neurons includes firstly a high percentage of TH-positive cells and secondly the co-expression of transcription factors FOXA2 and LMX1A, which drive dopaminergic neurogenesis (Arenas et al., 2015). Earlier studies discovered that dual SMAD inhibition, of bone morphogenetic protein (BMP), TGF-β, activin and nodal signalling at the start of differentiation, increased neural induction and eliminated the use of feeder layers (Chambers et al., 2009). Subsequently, it was found that higher concentrations of sonic hedgehog (SHH) and fibroblast growth factor 8a (FGF8a) during neural induction was required for specification towards the floor plate (Metzakopian et al., 2012). However, midbrain specification was not achieved until the addition of a GSK3β inhibitor, CHIR 99021, which activated WNT/β-catenin signalling, an essential pathway in the development of dopaminergic neurons (Kriks et al., 2011). This was first demonstrated by the work of Lorenz Studer, a pioneer in the field of stem cell differentiations, where CHIR 99021 was shown to be a key ingredient in the generation of correctly specified induced pluripotent stem cell-derived dopaminergic neurons.

Characterisation of the cultures from Studer's group revealed consistent results—the neurons generated possessed multiple dopaminergic markers and exhibited biochemical and electrophysiological properties of mature neurons (Kriks et al., 2011). Comparatively, cells differentiated from Studer's protocol produced the highest proportion of dopaminergic markers, including 75% TH-positive neurons and 80% FOXA2-positive neurons, which were also co-localising with LMX1A (Figure 3.1). Transcript analysis of dopaminergic markers in cultured cells also yielded novel results, revealing upregulated transcripts (*TFF3, EBF1/3 and TTR*) matching those detected human nigral samples. Lastly, cultured neurons survived transplantation in rodent models, whilst retaining marker expression, not forming overgrowths, and rescuing phenotypes in a battery of motor and behavioural tests. In summary, an understanding

of the precise effect of signalling molecules has led to the refinement of current protocols, to achieve cells that are transplant-grade and of the correct subtype.

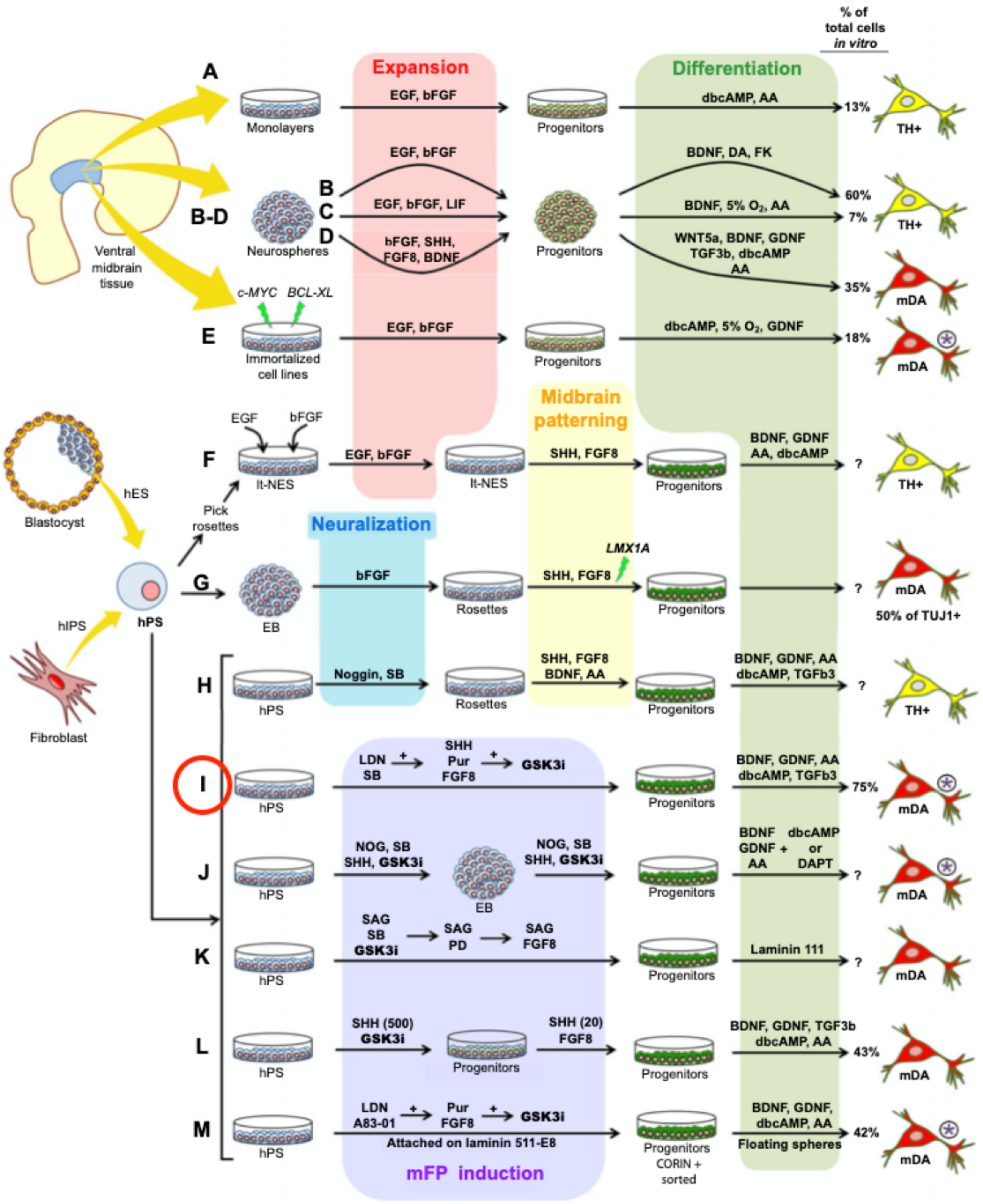


Figure 3.1 Protocols for the differentiation of human stem cells and pluripotent stem cells into midbrain dopaminergic neurons

Human foetal ventral midbrain tissue has been used for the differentiation of dopaminergic progenitors into tyrosine hydroxylate (TH)-positive neurons (yellow) or correctly specified dopaminergic neurons (red). Differentiation protocols have cultured cells in monolayers (A), neurospheres (B-D) or immortalised cell lines (E). Additionally, human pluripotent stem cells derived from blastocysts (ESCs) or reprogrammed fibroblasts (iPSCs) have been used to culture long-term neuroepithelial stem cells (lt-NES) (F), embryoid bodies (G), or for direct reprogramming into dopaminergic neurons (H-M). Red circle (I) indicates the protocol used in this study. Green lightning (E, G) indicates overexpression of indicated factors. Circled asterisk (*) indicates cells that were functional in animal models. References: A (Sánchez-Pernaute, Studer, Bankiewicz, Major, & McKay, 2001), B (Riaz, Jauniaux, Stern, & Bradford, 2002), C (Maciaczyk, Singec, Maciaczyk, & Nikkhah, 2008), D (Ribeiro et al., 2013), E (Courtois et al., 2010), F (Falk et al., 2012), G (Friling et al., 2009), H (Chambers et al., 2009), I (Kriks et al., 2011), J (Kirkeby et al., 2012), K (Denham et al., 2012), L (Xi et al., 2012), M (Doi et al., 2014). Image adapted from Arenas et al. (2015).

3.1.3 α-Synuclein seeded aggregation and phosphorylation on serine 129

The precise function of α-synuclein remains to be elucidated, however its most pertinent role revolves around the modulation of membrane binding and vesicular trafficking (Burré, 2015). Knockout studies suggest that although synucleins may not be essential for survival, they may be an important factor in the homeostatic maintenance of neurons under stress conditions, caused either by ageing or through cellular damage (Chandra et al., 2004; Greten-Harrison et al., 2010).

In contrast to physiological α-synuclein, fibrillar α-synuclein which accumulates in Lewy pathology is detergent-insoluble and resistant to proteinase activity (Campbell et al., 2000; Masuda-Suzukake et al., 2014). Pathogenic α-synuclein is misfolded in β sheets and adopts multiple oligomeric conformations, hence its label as a protein-chameleon (Drescher, Huber, & Subramaniam, 2012; Uversky, 2003). Lewy pathology is present in 2-5% of neurons in diseased brains and its most reliable pathomarker is hyperphosphorylation on α-synuclein serine 129 (pSYN), which is present in over 90% of aggregated α-synuclein (Anderson et al., 2006; Fujiwara et al., 2002). A fraction of α-synuclein in Lewy inclusions is also ubiquitinated (Tofaris et al., 2003). It has been suggested that the formation of α-synuclein aggregates is a neuroprotective mechanism aimed at demobilising toxic oligomers (Bendor et al., 2013). However, despite challenges in identifying the most neurotoxic α-synuclein species in Lewy pathology, α-synuclein fibrils are unlikely to be benign.

Whether phosphorylation on serine 129 inhibits or exacerbates α-synuclein pathology remains an area of debate. Unlike the core NAC region, the coiled C-terminus of α-synuclein is not involved in its fibrillation and contains the majority of post-translational modification sites including, phosphorylation (Y125, S129, Y133, Y136), truncation (D115, D119, P120, E130, and D135), ubiquitination (K96), and transglutaminase cross-linking (Q109) (Hoyer, Cherny, Subramaniam, & Jovin, 2004;

Oueslati, 2016; Oueslati et al., 2010). Phosphorylation on serine 129 has been implicated in several molecular pathways, such as the inhibition of α-synuclein membrane binding, increased dopamine uptake through modulating the activity of α-synuclein at the synapse, the disruption of bivalent metal ion binding sites (e.g. Fe^{2+} and Pb^{2+} on residue D119), and an increased turnover/clearance rate via targeted autophagic degradation (Fiske et al., 2011; Hara et al., 2013; Kuwahara, Tonegawa, Ito, Mitani, & Iwatsubo, 2012; Machiya et al., 2010; Nübling et al., 2014). These findings strongly suggest that phosphorylation may alter the conformation of α-synuclein, and hence its functional properties. Indeed, a proteomic study comparing physiological and phosphorylated α-synuclein identified that the wild-type α-synuclein interactome consisted of predominantly mitochondrial components, whereas phosphorylated α-synuclein interacted aberrantly with cytoskeletal and synaptic proteins (McFarland, Ellis, Markey, & Nussbaum, 2008). Phosphorylated α-synuclein has also been shown in the rodent brain to preferentially interact with Rab GTPase 8a (Rab8a), a guanine nucleotide-binding protein that regulates vesicle trafficking (Yin et al., 2014). Intriguingly, overexpression of Rab8a increased intracellular α-synuclein accumulation but decreased α-synuclein-induced toxicity.

Exploring the relative effects of phosphorylated α-synuclein *in vivo* has yielded contrasting results. α-Synuclein is constitutively phosphorylated on serine 129 by several kinases, such as G-protein coupled receptor kinases (GRKs) or polo-like kinases (PLKs) (Oueslati, 2016). In a *Drosophila* and rodent parkinsonian models, overexpression of GRKs (GRK2 and GRK6) resulted in increased levels of phosphorylated α-synuclein and enhanced cell loss (L. Chen & Feany, 2005; Sato et al., 2011). In contrast, overexpression of PLK2 in the rat midbrain was found to increase phosphorylated α-synuclein, but significantly reduced α-synuclein-induced dopaminergic neuronal death (Oueslati, Schneider, Aebischer, & Lashuel, 2013; Salvi

et al., 2012). Here, PLK2-induced phosphorylation was shown to increase α-synuclein clearance via autophagic degradation and hence, believed to be neuroprotective by reducing α-synuclein abundance. The discrepant phenotypes observed between PLK-mediated versus GLK-mediated phosphorylation suggest that the functional effect of α-synuclein phosphorylation is governed, to some extent, by the kinase responsible for its phosphorylation. Therefore, it is plausible that the activity of different kinases contributes to α-synuclein pathology in Parkinson's disease.

The majority of studies to date modelling seeded aggregation have utilised α-synuclein seeds (i) isolated from diseased tissue and (ii) synthetically pre-formed from recombinant α-synuclein. Synthetic α-synuclein fibrils are, therefore, a valuable tool to study the pathogenesis α-synucleinopathies. Fibrils can be generated *de novo* by self-aggregating recombinant α-synuclein or alternatively, patient-derived seeds may be amplified with recombinant α-synuclein (Bousset et al., 2013; Conway et al., 2000; A. Fenyi et al., 2021; Soto & Pritzkow, 2018). The potential to produce distinct α-synuclein conformers raises the question if subtle ultrastructural differences between α-synuclein seeds confer different seeding propensities and toxicities. Indeed, two *de novo* assemblies have been characterised and named based on morphology: fibrils and ribbons (Bousset et al., 2013). Striatal injection into the rat revealed that ribbons induced pSYN but did not lead to neurodegeneration in contrast to fibrils (Peelaerts et al., 2015). Whether such strains exist in human brain is currently unknown and untested but could explain the diverse phenomenology and severity in α-synucleinopathies (i.e. PD, DLB and MSA). It is therefore possible that the pathogenesis of α-synucleinopathies depends on cellular environment and α-synuclein assembly type generated.

3.1.4 Assay workflow: α-synuclein seeded aggregation in patient-derived dopaminergic neurons

By combining induced pluripotent stem cell-derived human dopaminergic neurons and *de novo* generated α-synuclein fibrils, I established one of the first models of seeded aggregation in human dopaminergic neurons (Figure 3.2). I cultured neurons until days *in vitro* (DIV) 45, at which point α-synuclein fibrils were exogenously added. Neurons were characterised from healthy control and patients with familial Parkinson's disease ($SNCA^{A53T}$ and $SNCA^{TRIP}$). I quantified levels of pSYN as the main pathological marker of aggregation at several timepoints following the addition of fibrils.

The objectives of this chapter were to:

1. Generate iPSC-derived neurons expressing dopaminergic markers
2. Assess the effect of α-synuclein fibrils on pSYN levels in dopaminergic neurons
3. Compare the seeding propensity between control, $SNCA^{A53T}$ and $SNCA^{TRIP}$ dopaminergic neurons
4. Determine the effects of fibril concentration and timeline of aggregate formation
5. Measure *SNCA* transcription in response to aggregation
6. Ask whether the conformation of seeds influences intraneuronal aggregation using two distinct polymorphs terms fibrils or ribbons.

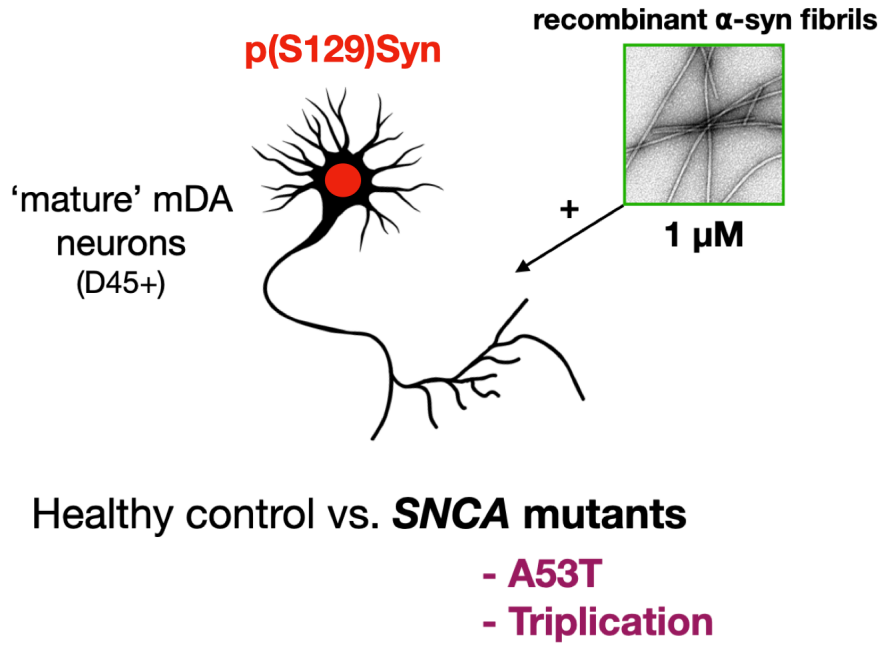


Figure 3.2 Modelling α-synuclein aggregation in human iPSC-derived dopaminergic neurons

iPSCs derived from healthy controls and patients harbouring SNCA mutations, including the A53T missense and triplication mutations were differentiated into midbrain dopaminergic neurons. Neurons were matured and exposed to 1 µM synthetic α-synuclein fibrils at days in vitro 45 and assayed at 2 and 4 weeks after. Pathological serine 129 phosphorylation on α-synuclein was used as the main marker for endogenously generated aggregates.

3.2 Results

3.2.1 Dopaminergic markers in human iPSC-derived neurons

3.2.1.1 Stem cell identifications

Induced pluripotent stem cell lines used in this study have been characterised and validated for pluripotency in previous studies as referenced in the Methods and Materials (Table 2.1).

3.2.1.2 Quantitation of dopaminergic and neuronal markers: tyrosine hydroxylase and beta-3 tubulin

To model seeded aggregation, my first aim was to generate induced pluripotent stem cell-derived dopaminergic neurons that expressed the correct markers. Several studies have previously published modified versions of Studer's protocol, including our group. The modifications include replacing one of the dual SMAD inhibitors (SB431542 10 μM to A83-01 2 μM; a more potent TGFβ inhibitor) and further increasing levels of SHH (100 ng/mL to 300 ng/mL) and FGF8a (100 ng/mL to 200 ng/mL). These changes yielded a greater proportion of TH-positive neurons from 60% in the published studies (Arenas et al., 2015) to 76% whilst maintaining key electrophysiological properties (Jonikas et al., 2018; Tanudjojo et al., 2021). Differentiating stem cells were subject to daily media replacement and were exposed to a combination of small molecules to generate neural progenitor cells by day 10, by inducing floor plate specification, and dopaminergic neurons by day 20, by a series of neural growth factors (Figure 3.3).

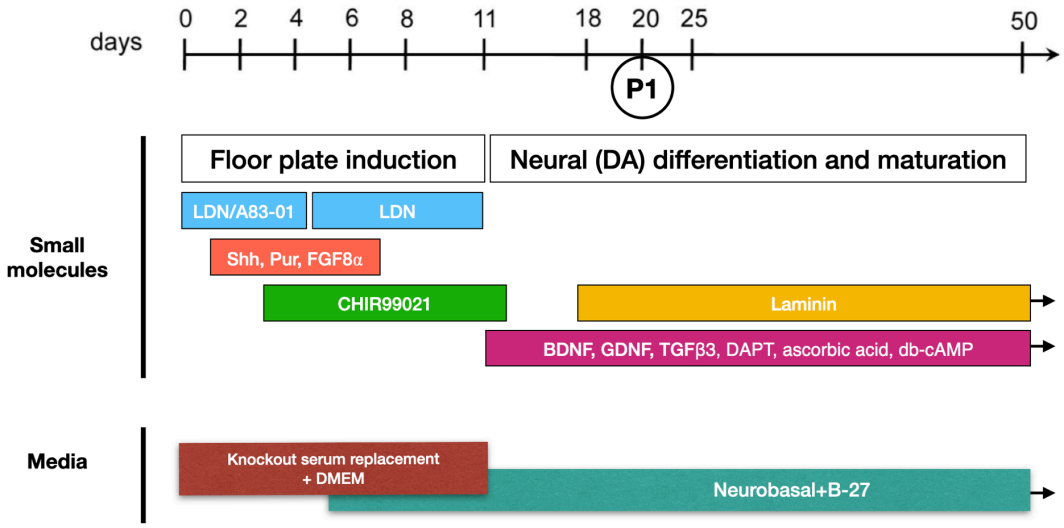


Figure 3.3 Differentiation protocol for generation of dopaminergic neurons from iPSCs

Dopaminergic neurons were generated using a protocol adapted from Kriks et al. (2011). iPSCs were exposed to a series of small molecules in a two-stage process requiring firstly, the induction of the floor plate and secondly, neuralisation into dopaminergic neurons. Stem cells were differentiated in a monolayer with daily media changes up to day 20. Cells were replated at day 20 and treated with mitomycin-C on day 23 to prevent the proliferation of non-neuronal mitotic cells. Neurons were matured until day 45 before being assayed.

Stem cells were differentiated when confluent and maintained as a monolayer from DIV0 up to DIV20 (Figure 3.4a). By DIV20, neural projections were visible in the gaps that formed within the monolayer, which is an indicator that the cells were ready to be dissociated. One day following re-plating on DIV21, the neurons began to form shorter projections (Figure 3.4b top). And by DIV35, neuronal projections formed a complex network (Figure 3.4b bottom).

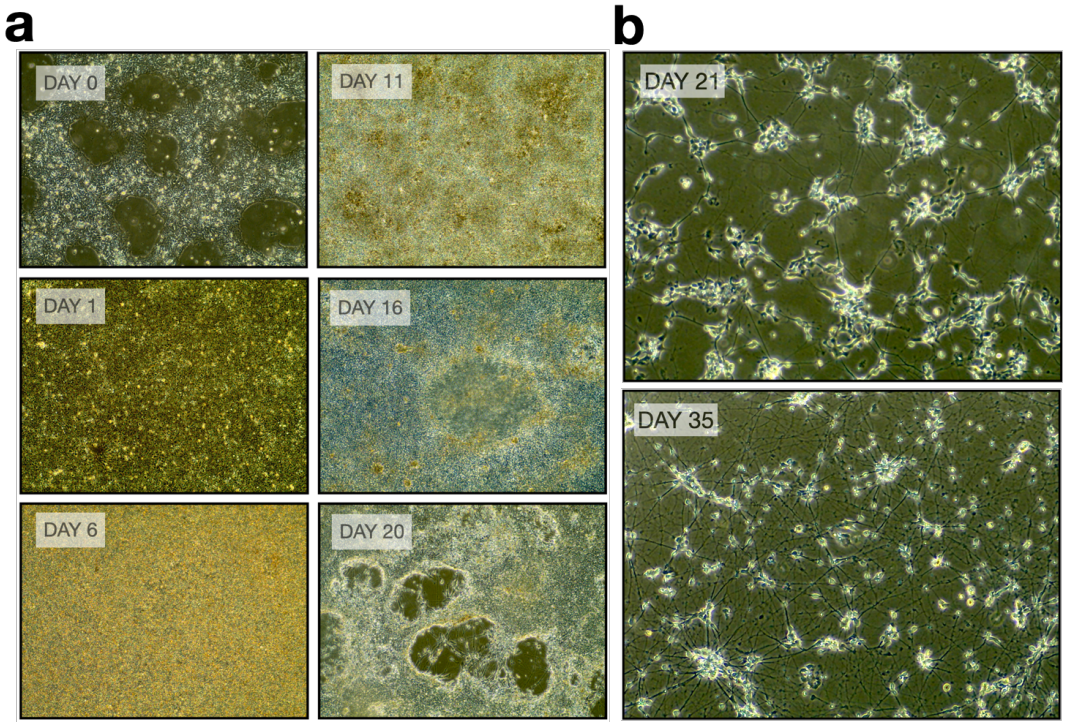


Figure 3.4 Image journal of differentiating iPSCs from day 0 to day 35

a, iPSCs were differentiated in a monolayer when cells were above 90% confluent. As observed using brightfield microscopy, the surface morphology of differentiating stem cells remained consistent until day 10. By day 11, ridges begin to form on the surface and remain until day 16/17. By day 20, neuronal projections become visible within gaps that have formed in the monolayer. This indicates that the neurons are ready to be dissociated and re-plated. **b,** After re-plating on day 21, some projections are visible and by day 35 axonal projections have fully extended and formed a network of neurons. Brightfield images taken on 10X lense, no size bar available.

I confirmed by immunofluorescence at DIV60 that in all cell lines used, dopaminergic neurons co-expressed TH and pan-neuronal marker β-3 tubulin (TUJ1). The average differentiation efficiency across all cell lines was similar with 76% expressing TH and 93% expressing TUJ1 (Figure 3.5). I also confirmed that all cell lines expressed dendritic marker, microtubule associated protein 2 (MAP2) (Figure 3.5).

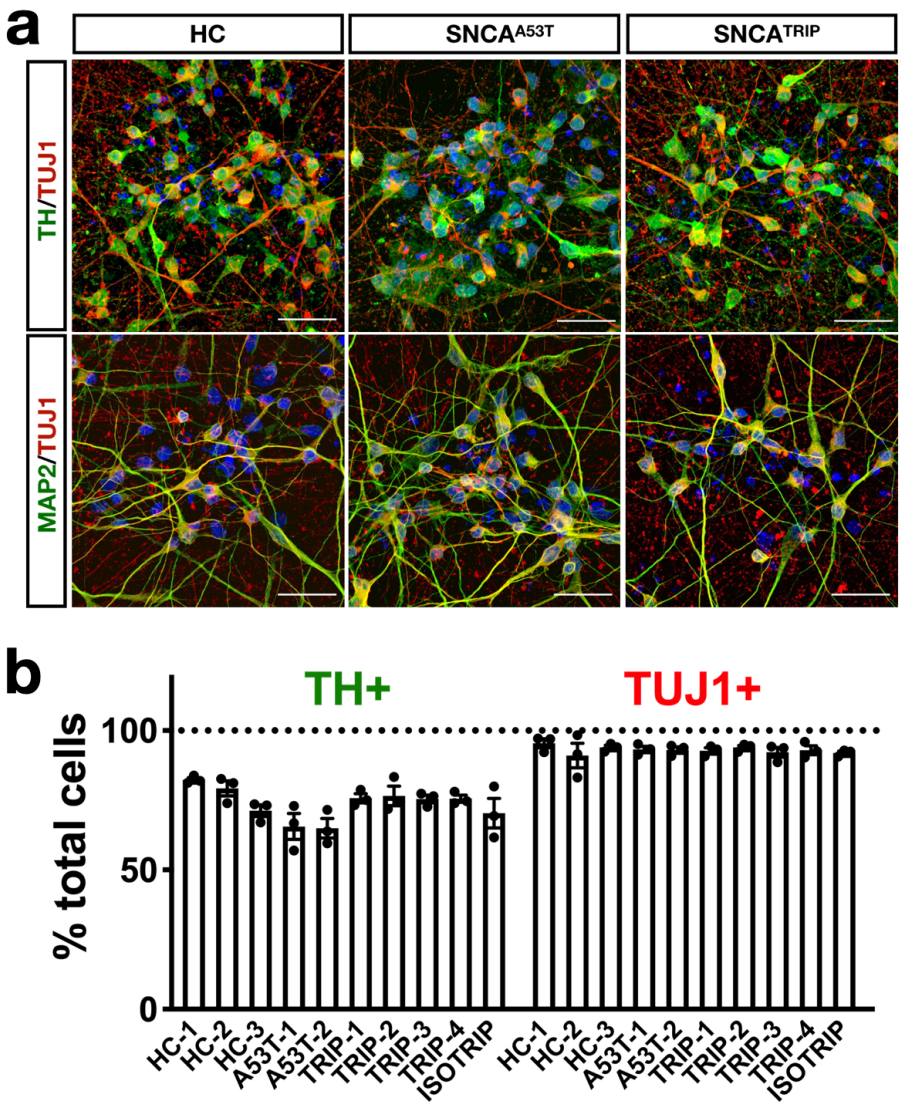


Figure 3.5 Characterisation of human iPSC-derived dopaminergic neurons

a, Representative confocal images of control and patient-derived dopaminergic neurons were positive for and co-localised with dopaminergic marker tyrosine hydroxylase (TH), dendritic marker MAP2, and β-3 tubulin (TUJ1). **b,** Quantification of markers revealed 76% TH-positive neurons and 93% TUJ1-positive neurons across all cell lines. Dopaminergic markers were quantifiied by blinded manual counting. Each dot corresponds to one clone differentiated once and data are mean±s.e.m from n=3 differentiations per clone.

To further confirm the identity of the cells using multiple markers we analysed the whole cell transcriptome using bulk RNA-Seq. Cell-type deconvolution was performed by our collaborators Dr. Devika Agarwal and Dr. David Sims comparing the neurons I generated to a multi-subject human single-cell atlas of the SNpc using the MuSiC method. Cell-type composition of the bulk RNA-Seq samples from two independent experiments was estimated across multiple bootstraps and identified 60-70% dopaminergic neurons in accordance with the immunostaining data (Figure 3.6).

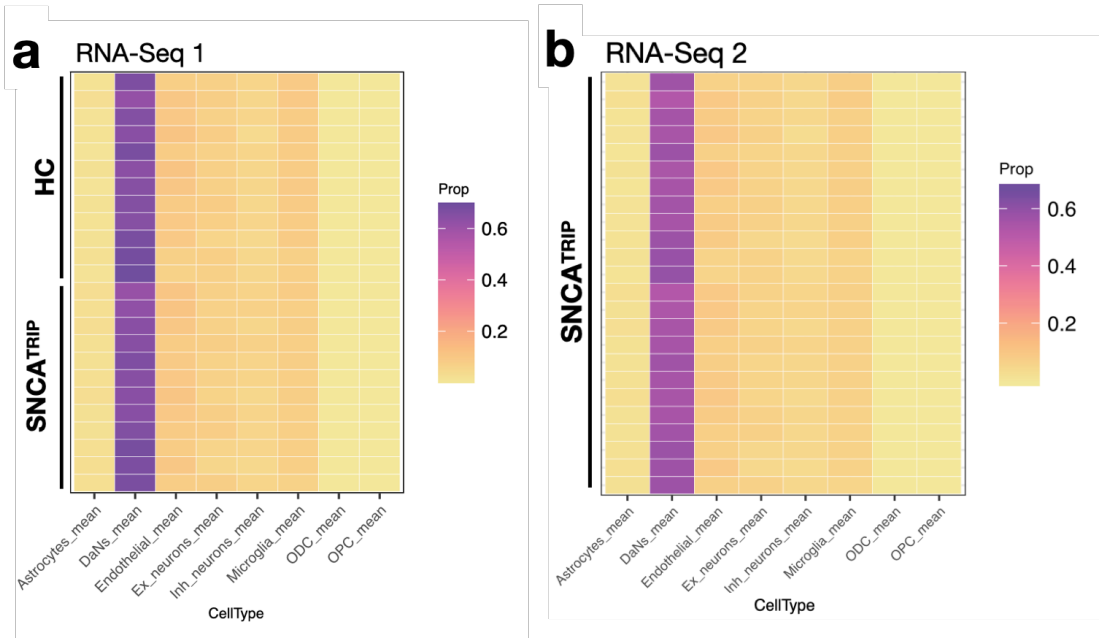


Figure 3.6 Dopaminergic neuron identity by bulk RNA-Seq

Transcriptomic analysis in two bulk RNA-Seq experiments demonstrated that 60-70% of neurons were dopaminergic when compared to a multi-subject human single cell atlas of the substantia nigra. **a,** Transcriptomic analysis was performed in healthy control (3 age-matched individuals, n=4 per clone) and $SNCA^{TRIP}$ (3 clones from one patient, n=4 per clone) followed by **b,** in $SNCA^{TRIP}$ lines only (3 clones from one patient, n=8 per clone).

3.2.2 Addition of exogenous α-synuclein fibrils induced the accumulation of pSYN in dopaminergic neurons

To assess whether the addition of exogenous *de novo* generated fibrils seed the aggregation of endogenous α-synuclein, I visualised the localisation of pSYN-positive inclusions through confocal microscopy and measured levels of pSYN by immunoblotting.

Addition of exogenous fibrils triggered pSYN-positive inclusions in dopaminergic neurons. The accumulation of pSYN was observed in both healthy control and $SNCA^{TRIP}$ dopaminergic neurons, with a more pronounced effect seen in triplication neurons (Figure 3.7a). The morphologies of pSYN-positive inclusions were reminiscent of Lewy neurites and Lewy bodies. They were either located in axons as neuritic inclusions or in the soma as speckled dots and inclusion bodies (Figure 3.7b). Some of the pSYN-positive inclusions co-localised with aggresomal marker p62 (Figure 3.7b), which is another marker detected in a proportion of Lewy bodies.

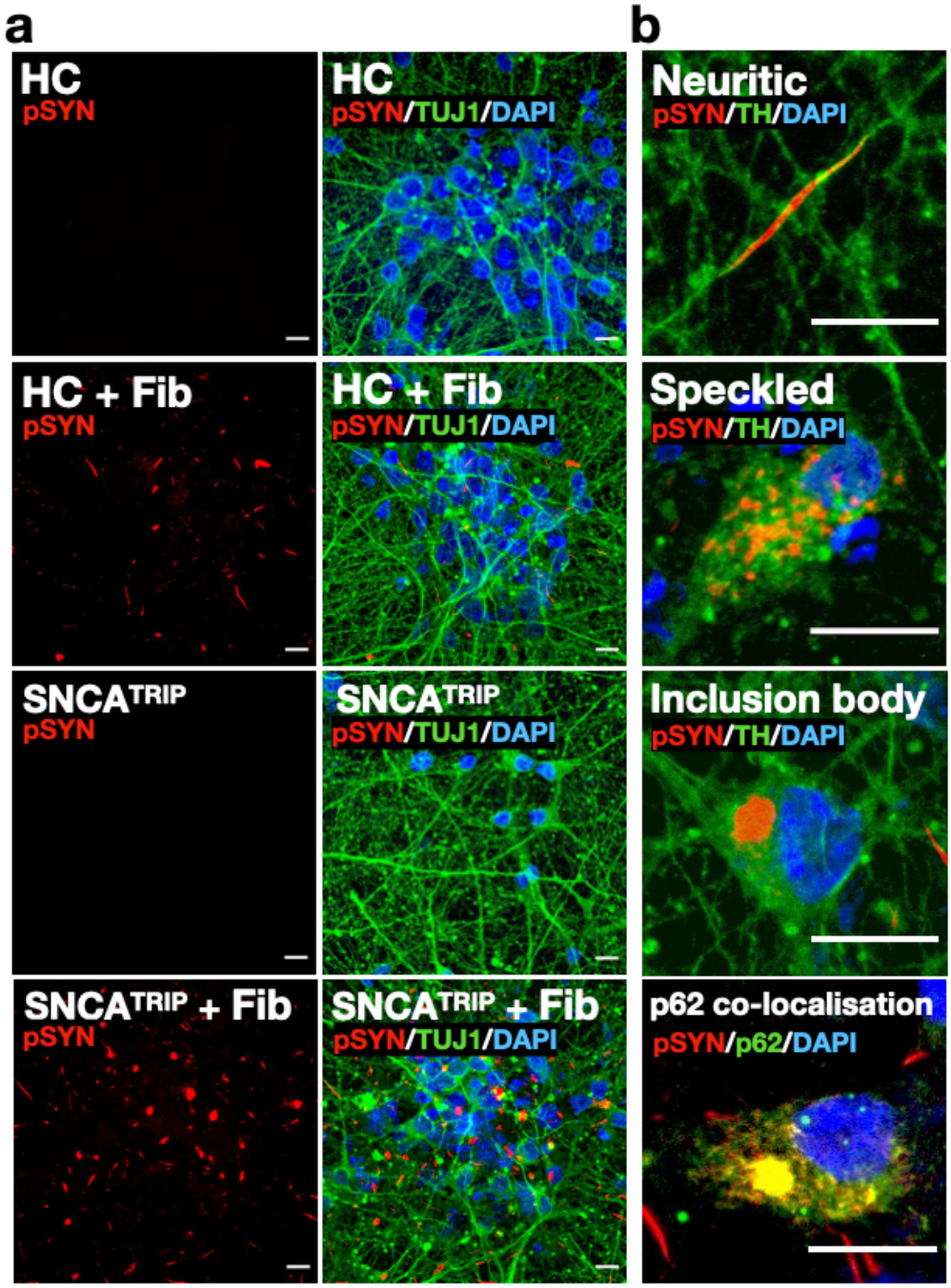


Figure 3.7 Representative confocal images of pSYN inclusions in human iPSC-derived dopaminergic neurons

a, Addition of exogenous α-synuclein fibrils seeded the aggregation of endogenous α-synuclein as evident by pSYN immunoreactivity in red. pSYN accumulation was observed in both healthy control and SNCA^{TRIP} dopaminergic neurons, with the latter demonstrating increased pSYN-positive inclusions. **b,** pSYN-positive aggregates adopted Lewy pathology-like morphologies and were localised in axons (neuritic) or the soma (speckled and inclusion body). pSYN-positive aggregates also co-localised with aggresomal marker p62. HC, healthy control; SNCA^{TRIP}, α-synuclein triplication; Fib, *de novo* α-synuclein fibrils; pSYN, α-synuclein phosphorylated on serine 129; TUJ1, β-3 tubulin; TH, tyrosine hydroxylase. Scale bar: 10 μm.

I then sought to optimise the concentration of α-synuclein fibrils required to generate detectable levels of pSYN. I added increasing concentrations of α-synuclein fibrils (0, 0.1, 1, 2 μM) to healthy control dopaminergic neurons at DIV45 and quantified levels of pSYN in the RIPA-insoluble fraction 2 weeks post-seeding (Figure 3.8). I found that pSYN levels increased in a dose-dependent with increasing concentrations of exogenously fibrils. No pSYN was detected without fibril treatment at the timepoints tested. Although fibrils at 2 μM generated the strongest effect, fibrils at 1 μM induced pSYN levels that were readily detectable. Therefore, I opted to continue experimenting using fibrils at 1 μM to maximise the use of resources.

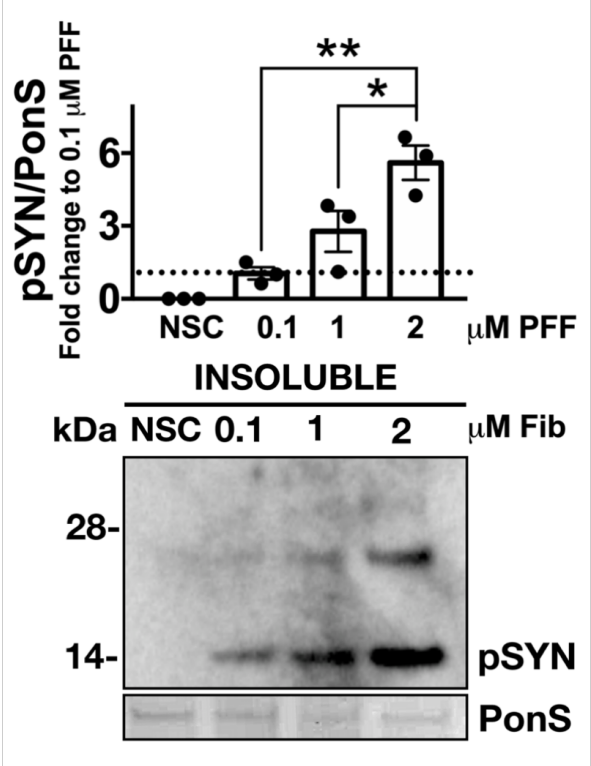


Figure 3.8 RIPA-insoluble fractions from seeded neuronal lysates were immunoreactive for pSYN by immunoblotting

Healthy control neurons were exposed to increasing concentrations of α-synuclein fibrils at DIV45 and assayed two weeks post-treatment. Neuronal lysates were ultracentrifuged at 100 000 g, and the 0.1% SDS RIPA-insoluble fraction was re-solubilised in 2% SDS RIPA. By immunoblotting, increasing concentrations of fibrils resulted in a dose-dependent response in pSYN signal. A final concentration of 1 μM was selected to be used in future experiments. NSC, non-seeded control, non-treated control. Each dot corresponds to one clone differentiated once and data are mean±s.e.m from n=3 differentiations per clone. *P<0.05,**P<0.01 by one-way ANOVA followed by Tukey's multiple comparison test.

To confirm that pSYN signal corresponded to aggregated α-synuclein, I performed cell fractionation and examined the detergent-insoluble 100,000 *g* pellet. I found that pSYN is detected almost exclusively in the insoluble fraction (97%) compared to the soluble fraction (Figure 3.9) indicating that it reflects aggregated α-synuclein.

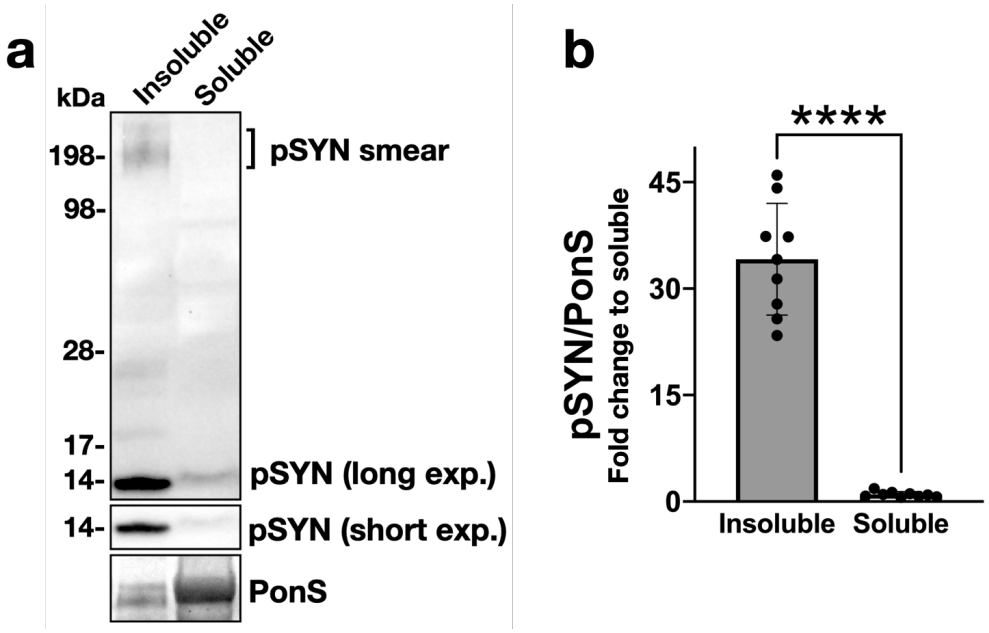


Figure 3.9 Phosphorylated α-synuclein in RIPA-insoluble fraction

a, iPSC-derived dopaminergic neurons from $SNCA^{TRIP}$ were seeded with de novo fibrils (1 μM) and lysed in 0.1% SDS RIPA buffer. Neuronal lysates were fractionated into soluble and insoluble fractions following 100 000 g centrifugation. Immunoblotting revealed that pSYN was almost exclusively found in the RIPA-insoluble fraction. Also observed in the insoluble fraction was pSYN-positive higher molecular weight smear at 198 kDa. The immunoblot is representative of three independent experiments. **b,** Quantification of immunoblots demonstrated that 97% of pSYN is present in the RIPA- insoluble fraction. Each dot corresponds to one clone differentiated once and data are mean±s.e.m from 3 differentiations per clone. For panel **b,** n=9, ****P<0.0001, by two-sided unpaired Student's t-test.

As a further control to validate that pSYN signal arises from intraneuronal α-synuclein and not phosphorylation of exogenous seeds, I tested the effects of *de novo* fibrils generated from human recombinant α-synuclein with the serine 129 to alanine (S129A) mutation that cannot be phosphorylated. I compared the addition of S129A mutant fibrils to previously used recombinant α-synuclein fibrils and demonstrated that both were equally potent in inducing pSYN (Figure 3.10). Wild-type and mutant fibrils exhibited similar results in two cell models, HEK cells overexpressing Venus-tagged α-synuclein and induced pluripotent stem cell-derived dopaminergic neurons. S129A mutant fibrils were characterised previously and kindly donated by Ronald Melki's group (Shrivastava et al., 2020).

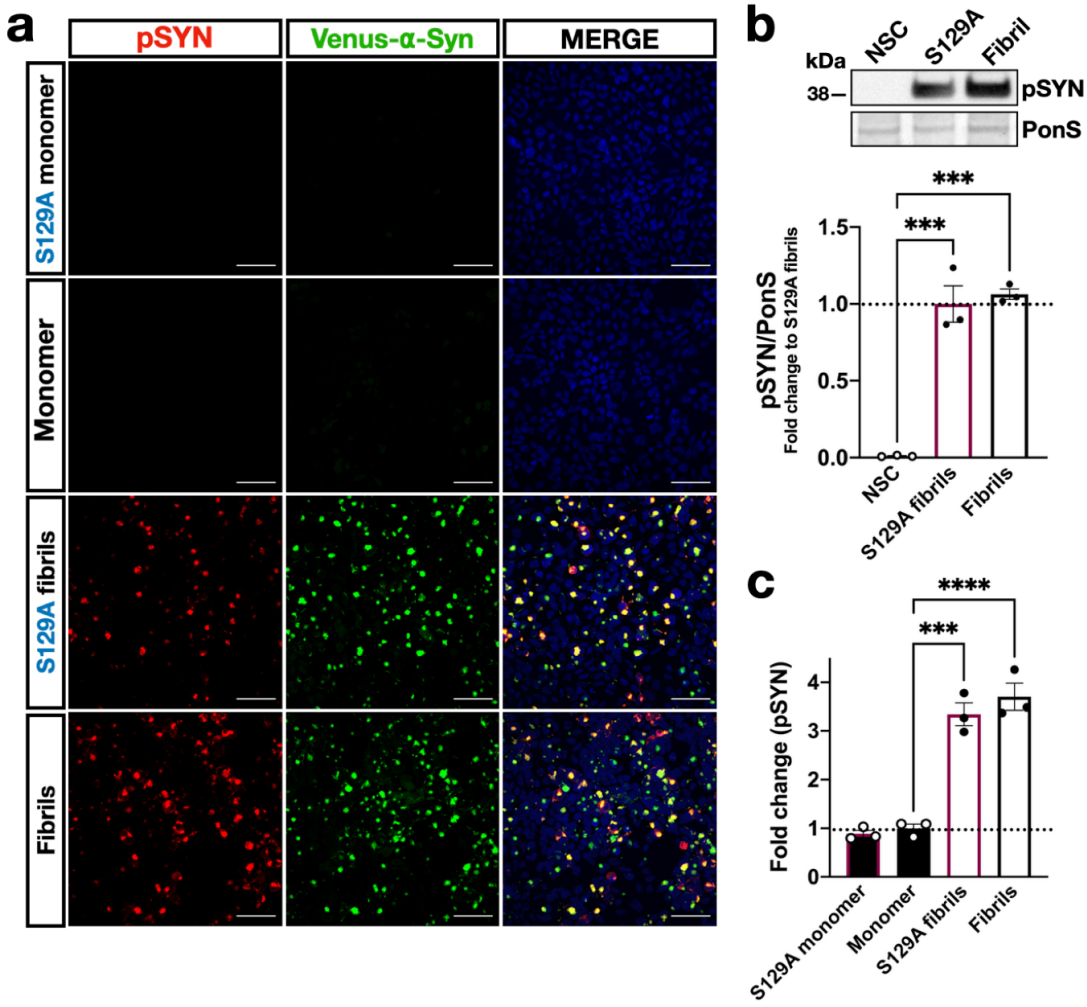


Figure 3.10 S129A mutant *de novo* fibrils induce p-S129 α-synuclein-positive inclusions

a, Confocal images of HEK 293 cells over expressing α-synuclein- Venus treated with S129A mutant human recombinant α-synuclein monomer (1 μM), wildtype human recombinant α-synuclein monomer (1 μM), S129A mutant de novo fibrils (1 μM), and wildtype de novo fibrils (1 μM). S129A mutant fibrils seed p-S129 α-synuclein (pSYN) and Venus positive inclusions similarly to wildtype de novo fibrils. Images are representative of three independent experiments. Scale bar: 50 μm. **b,** Immunoblotting analysis of HEK 293 cells expressing α-synuclein-Venus demonstrated that S129A mutant and wildtype de novo fibrils both seeded aggregates with similar levels of pSYN. Representative immunoblot with quantification from n=3 independent experiments. **c,** iPSC-derived dopaminergic neurons from SNCA^{TRIP} were exposed to either S129A mutant or wildtype monomers or fibrils and analysed through a time resolved fluorescence assay (HTRF) specific to pSYN. S129A mutant fibrils induced similar pSYN levels compared to wildtype de novo fibrils. Each dot in panel **c** corresponds to one clone differentiated once (n=3). NSC, non-seeded control, non-treated control. Data are shown as mean±s.e.m. In panels **b** and **c,** ***P<0.001,****P<0.0001 by one-way ANOVA followed by Tukey's multiple comparison test.

3.2.3 SNCA^{TRIP} dopaminergic neurons exhibit the highest burden of pSYN-positive inclusions

Familial cases are caused by mutations in the α-synuclein gene (e.g. SNCA^{A53T}) or by gene multiplications (e.g. SNCA^{TRIP}). Therefore, I sought to assess the effect of these mutant backgrounds on aggregation propensity by studying iPSC-derived dopaminergic neurons derived from patients with SNCA^{A53T} or SNCA^{TRIP}. α-Synuclein fibrils were added to culture media in a single treatment to dopaminergic neurons at DIV45 and assayed 2 weeks post-seeding. Using a homology time resolved FRET assay specific to pSYN, aggregation was highest in SNCA^{TRIP} lines followed by SNCA^{A53T} and healthy control, when corrected to their non-seeded control (Figure 3.11a). At the timepoints tested (DIV45), there was no detectable aggregation prior to seeding based on pSYN or oligomeric α-synuclein FRET signal across all these lines (Figure 3.11b/c). Therefore, in the absence of spontaneous aggregation, these results show that p.A53T mutation or increased wild-type protein levels promote seeded aggregation in human neurons with the latter having the strongest effect. To further develop this model of seeded aggregation, I exclusively used healthy control and SNCA^{TRIP} lines for subsequent experiments.

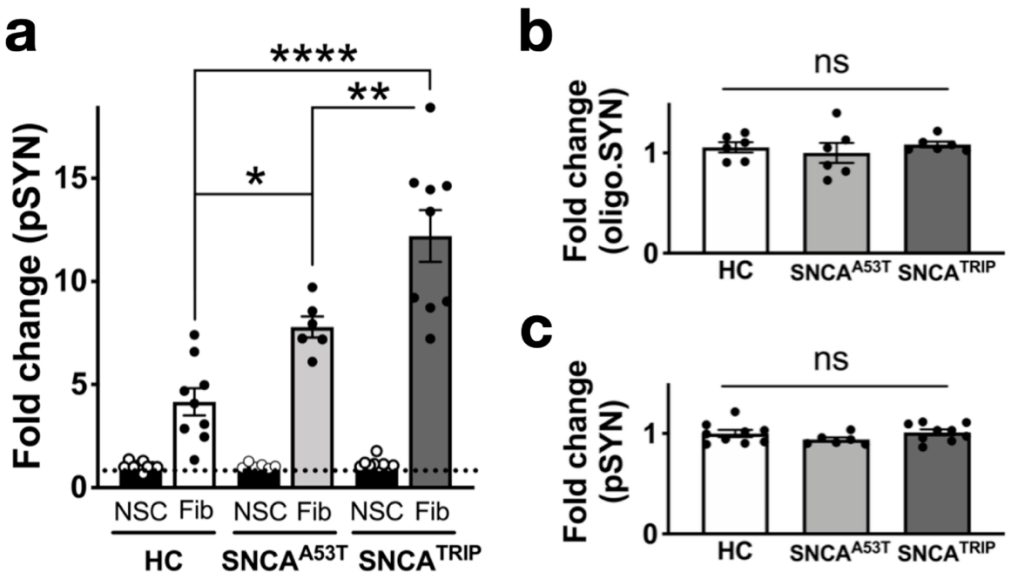


Figure 3.11 Seeded aggregation in healthy controls, SNCA^{A53T} and SNCA^{TRIP} iPSC-derived dopaminergic neurons

a, Dopaminergic neurons harbouring either the missense A53T mutation (SNCA^{A53T}) or SNCA gene triplication (SNCA^{TRIP}) had increased levels of pSYN compared to healthy controls 2 weeks post seeding (1 μM), with SNCA^{TRIP} neurons exhibiting the highest burden of seeded aggregates as quantified by HTRF (n=9 for healthy control, n=9 for SNCA^{TRIP}, n=6 for SNCA^{A53T}). **b,** No aggregation was detected in iPSC-derived dopaminergic neurons without seeding. Using time resolved FRET specific to oligomeric α-synuclein, no aggregation was detected in healthy controls, SNCA^{A53T} and SNCA^{TRIP} prior to seeding at DIV45. **c,** No pSYN was detected under the same basal conditions in healthy controls, SNCA^{A53T} and SNCA^{TRIP}. n=9 for healthy control, n=9 for SNCA^{TRIP}, n=6 for SNCA^{A53T}. NSC, non-seeded control, non-treated control. Each dot in panels **a,b,c,** corresponds to one clone differentiated once. Data are shown as mean±s.e.m. In panels **a,b,c,** ns: non-significant *P<0.05,**P<0.01,****P<0.0001 by one-way ANOVA followed by Tukey's multiple comparison test.

3.2.4 α-Synuclein fibrils induce a time and dose-dependent increase in pSYN accumulation in dopaminergic neurons

Parkinson's disease is a slowly progressive disorder. I therefore investigated the evolution of aggregates with time in culture by comparing healthy control to $SNCA^{TRIP}$ lines. Dopaminergic neurons were treated with increasing concentrations of *de novo* fibrils (0.01, 0.1, 1 μM) and assayed over several weekly timepoints (weeks 1-4). The formation of pSYN aggregates in dopaminergic neurons was detectable at 1 week, increasing further by 4 weeks post-seeding (Figure 3.12a). Moreover, at each timepoint tested, $SNCA^{TRIP}$ neurons demonstrated higher levels of seeded aggregation compared to healthy controls, recapitulating previous findings.

The time- and dose-dependent increase of pSYN after a single treatment with *de novo* fibrils was reminiscent of intraneuronal templating of available α-synuclein monomer. Interestingly, these findings correlated with the progressively increased expression of α-synuclein with time in culture. By immunoblot analysis, $SNCA^{TRIP}$ lines exhibited on average 2.5-fold increase in endogenous α-synuclein monomer compared to healthy control neurons at all timepoints tested (Figure 3.12b).

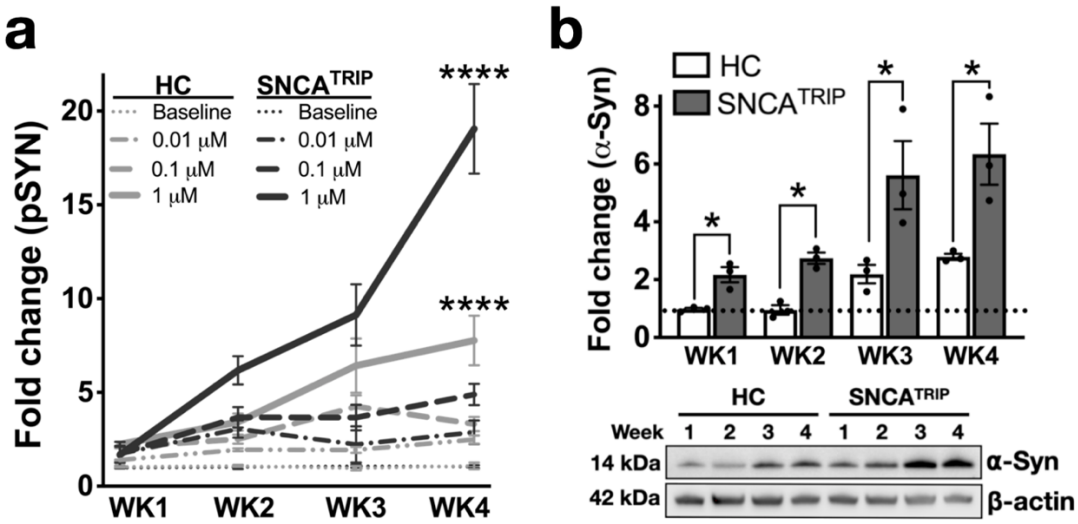


Figure 3.12 A single exposure to α-synuclein fibrils induce a dose and time-dependent response in healthy controls and SNCA^{TRIP} iPSC-derived dopaminergic neurons

a, A single exposure to α-synuclein fibrils on DIV45 at an increasing dose (baseline, 0.01, 0.1, 1 μM) induced a dose and time-dependent increase in pSYN signal as quantified by homology time resolved fluorescence (n=9 for SNCA^{TRIP} and n=5 for healthy control). pSyn levels were quantified at weeks 1 to 4. At each timepoint and with each concentration tested, SNCA^{TRIP} neurons consistently demonstrated a higher propensity to seeded aggregation compared to controls. **b,** Endogenous α-synuclein expression in dopaminergic neurons also increased over time in culture. Across timepoints, α-synuclein levels at baseline was increased by 2.5-fold in SNCA^{TRIP} neurons compared to healthy control as assessed by immunoblotting (n=3). Each dot in panels **b** corresponds to one clone differentiated once. Data are shown as mean±s.e.m. In panels **a,b,** *P<0.05, ****P<0.0001 by one-way ANOVA followed by Tukey's multiple comparison test.

3.2.5 α-Synuclein fibril-induced aggregation upregulates SNCA mRNA in dopaminergic neurons

α-Synuclein transcript levels were shown to be elevated in some but not all studies which used post-mortem brain tissue from patients with sporadic forms of Parkinson's disease (Tagliafierro & Chiba-Falek, 2016). Therefore, I assessed *SNCA* mRNA levels in patient-derived dopaminergic neurons following α-synuclein aggregation. To this end, I performed quantitative real-time PCR comparing baseline and 2 weeks post-seeding in healthy control and $SNCA^{TRIP}$ neurons (Figure 3.13a). I found that *SNCA* mRNA was significantly increased in both control and triplication neurons upon seeded aggregation with *de novo* α-synuclein fibrils. This finding suggests that sequestration of α-synuclein monomer into aggregates leads to the compensatory upregulation of *SNCA* (Figure 3.13b). In these experiments I have also confirmed that at baseline $SNCA^{TRIP}$ neurons expressed approximately 2-fold increased levels of *SNCA* mRNA compared to healthy controls.

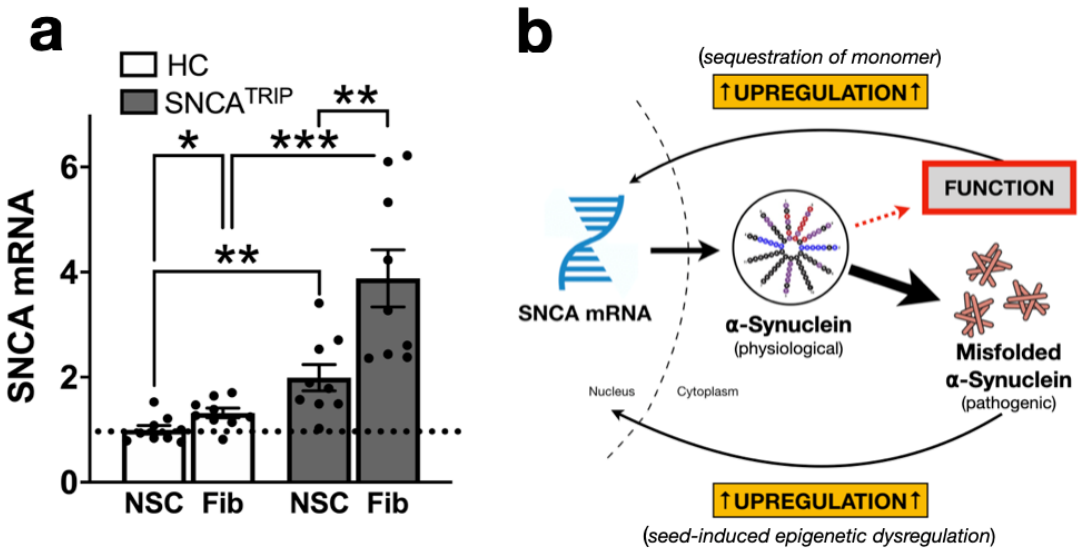


Figure 3.13 α-Synuclein aggregation upregulates *SNCA* mRNA in iPSC-derived dopaminergic neurons

a, Upregulation of *SNCA* mRNA was triggered by α-synuclein fibril treatment (1 μM) 2 weeks post-seeding at DIV45 in both healthy controls (n=9) and SNCA^{TRIP} (n=9) neurons. The induction of *SNCA* mRNA was more pronounced in SNCA^{TRIP} neurons compared to control. *SNCA* mRNA was also 1.9-fold higher in SNCA^{TRIP} neurons compared to control, corroborating previous findings (Singleton et al., 2003). **b,** *SNCA* mRNA upregulation may be triggered either as (i) a compensatory mechanism resulting from physiological α-synuclein being recruited to aggregates or (ii) through the direct interaction of pathological seeds with cellular signalling pathways. NSC, non-seeded control, non-treated control. Each dot in panel **a** corresponds to one clone differentiated once. Data are shown as mean±s.e.m. In panel **a,** *P<0.05, **P<0.01, ***P<0.01 ****P<0.0001 by two-sided unpaired Student's t-test.

3.2.6 The conformation of α-synuclein polymorphs influences aggregation

The discovery that *de novo* generated α-synuclein fibrils could adopt distinct conformations introduced the concept that α-synuclein strains may account for differences in the pathogenesis of Parkinson's disease (Bousset et al., 2013). Self-aggregating human recombinant α-synuclein in a buffer comprised of lower salt concentrations versus physiological salt concentrations gives rise to structurally distinct polymorphs based on limited proteolysis and electron microscopy (Figure 3.14a). For example, transmission electron microscopy revealed that these α-synuclein conformers possessed a cylindrical aspect when obtained under physiological conditions and a ribbon-like aspect (flat and twisted), when obtained under lower salt conditions (Figure 3.14b).

To assess whether α-synuclein structure can influence the extent of aggregation, I compared the seeding propensity of fibrils to ribbons in human dopaminergic neurons. Fibrils and ribbons were exogenously added to healthy control and $SNCA^{TRIP}$ neurons and pSYN levels were quantified at 2 and 4-weeks post-seeding. At each timepoint, I found that α-synuclein ribbons yielded significantly higher levels of pSYN compared to fibrils in both healthy control and triplication neurons (Figure 3.14c/d). These results corroborated previous findings in iPSC-derived cortical neurons (Gribaudo et al., 2019a) and in primary cultures (Peelaerts et al., 2015), suggesting that α-synuclein strains can determine the propensity to recruit endogenous α-synuclein and accelerate the formation of pSYN-positive inclusions in human dopaminergic neurons.

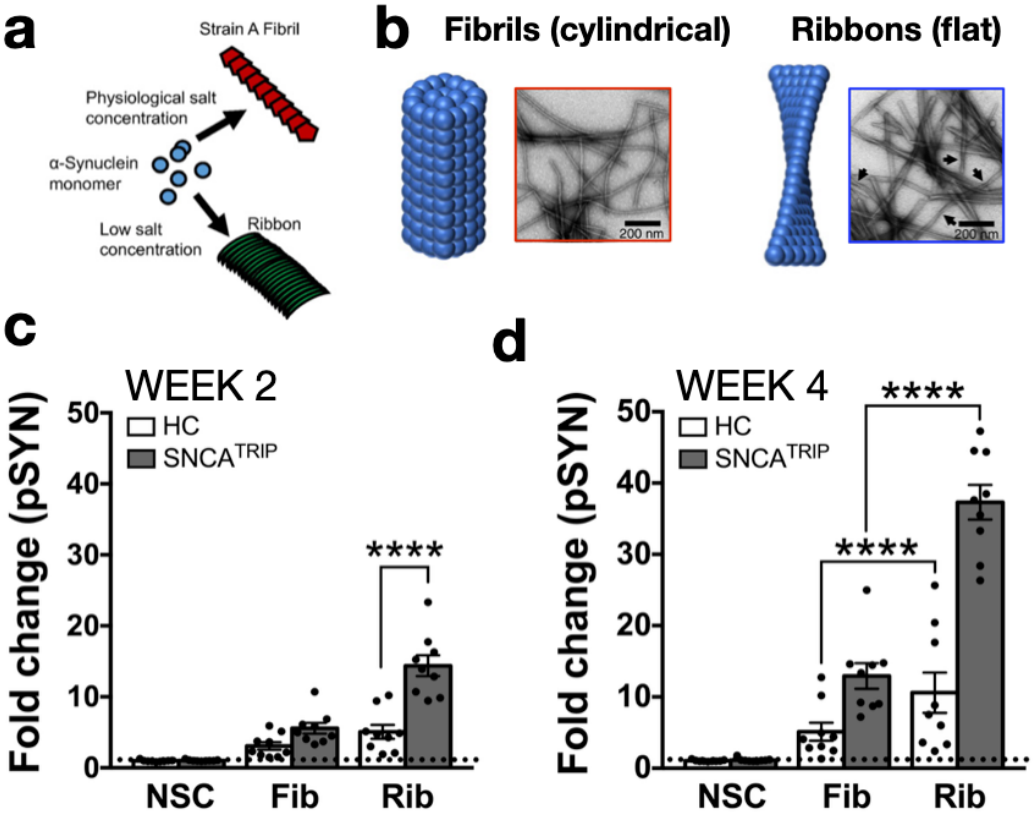


Figure 3.14 α-Synuclein ribbons exhibited higher seeding propensity than fibrils

a, Synthetic fibrils are generated *de novo* by self-aggregating human recombinant α-synuclein in physiological salt concentrations. Conversely, ribbons are generated through the same process, however, in the presence of low salt concentrations beneath physiological levels (Bousset et al., 2013; Peng, Gathagan, & Lee, 2018). **b,** The difference in salt concentrations yielded synthetic α-synuclein 'seeds' that were conformationally distinct. Electron microscopy revealed that the ultrastructure of α-synuclein fibrils were cylindrical, whereas ribbons were flat (Bousset et al., 2013). **c,** α-Synuclein ribbons (1 μM) induced higher levels of pSyn accumulation compared to fibrils (1 μM) in both healthy control (n=9) and SNCA^{TRIP} (n=9) dopaminergic neurons at two weeks post-seeding and at **d,** 4 weeks post-seeding. NSC, non-seeded control, non-treated control. Each dot in panels **c, b,** corresponds to one clone differentiated once. Data are shown as mean±s.e.m. In panels **a,b,** ****P<0.0001 by one-way ANOVA followed by Tukey's multiple comparison test.

3.3 Discussion

Modelling Parkinson's disease using iPSC-derived dopaminergic neurons has become a prominent tool to investigate disease mechanisms and subsequently perform high throughput assays for targeted drug discovery. Moreover, the ability to study patient-derived neurons has proven essential towards improving disease-relevance in models. Taking advantage of stem cell differentiation technology, I generated and characterised a robust model of α-synuclein seeded aggregation in human dopaminergic neurons, which recapitulated key disease features (Tanudjojo et al., 2021). Patient and control stem cells alike readily differentiated into dopaminergic neurons co-expressing markers TH (76%), TUJ1 (93%) and MAP2 (not quantified, Figure 3.5). α-Synuclein fibril-induced aggregates in dopaminergic neurons were insoluble in RIPA buffer and immunoreactive to pSYN. $SNCA^{TRIP}$ dopaminergic neurons demonstrated the highest propensity to seeded aggregation compared to $SNCA^{A53T}$ and control neurons, respectively (Figure 3.8). Dopaminergic neurons also demonstrated a dose and time-dependent response in α-synuclein aggregation after a single exposure to fibrils (Figure 3.12). In the presence of aggregation, *SNCA* mRNA was upregulated (Figure 3.13). Lastly, α-synuclein ribbons induce significantly more pSYN-positive aggregates in dopaminergic neurons compared to α-synuclein fibrils (Figure 3.14). Taken together, these data demonstrate that α-synuclein seeded aggregation can be modelled in iPSC-derived dopaminergic neurons via the addition of exogenous fibrils and the quantification of pSYN.

Midbrain dopaminergic neurons are not a homogenous group—for instance, the substantia nigra is selectively vulnerable in Parkinson's disease but not the VTA (Anderegg, Poulin, & Awatramani, 2015). Indeed, multiple single cell studies have identified several subtypes, therefore stressing the importance of modelling the correct cell type of interest (Fiorenzano, Sozzi, Parmar, & Storm, 2021; Kamath et al., 2021). I

have demonstrated that, in contrast to other published protocols yielding approximately 50% TH-positive cells, fine-tuning the concentration of a few small molecules in a modified protocol from Kriks et al., (2011) was able to generate a purer population of dopaminergic neurons with 76% TH-positive cells (Jonikas et al., 2018). Since 2011, studies have built upon the previously published protocol by Kriks et al. to increase the purity of TH-positive neurons and to reduce the number of cells expressing off-target markers. By adjusting cell density during differentiation and controlling the timepoints for small molecule exposure, one study generated 90% TH-positive neurons, that co-expressed with multiple dopaminergic markers, FOXA2, NURR1, DAT1, PITX3, GIRK2 and VMAT2 (Luo et al., 2020). Moreover, another study recently demonstrated that a biphasic or two-step activation of WNT signalling with small molecule CHIR 99021 significantly minimized the number of diencephalic, hindbrain and non-neuronal contaminants in culture (T. W. Kim et al., 2021). Instead of a one-step treatment with CHIR 99021 at 3 μM, the two-step approach mimics more closely the developmental pattern and introduces CHIR at a lower concentration (0.7 μM) followed by a higher concentration (3 μM). These findings illustrate how novel modifications to an already functional protocol can ameliorate reprogramming efficiency, which may be considered for the optimisation of future experiments.

One challenge in modelling Parkinson's' disease and more broadly neurodegeneration, is obtaining tissue samples that reflect the age and maturity of patients (Mehta et al., 2018). Converting cells to a pluripotent state has been shown to erase the epigenome and alter age-related phenotypes which may be relevant to disease progression (Huh et al., 2016). Developments in this field have enabled somatic cells, such as fibroblasts, to be differentiated directly into induced neurons (iN) (Vierbuchen et al., 2010). iNs have been used to model late-onset neurodegenerative diseases, however these protocols are still in their infancy as they often lack the co-

expression of core neuronal subtype markers and exhibit poor survivability (Abernathy et al., 2017; Carter, Halmai, & Fink, 2020; Mollinari et al., 2018). Alternatively, several groups have also attempted to artificially age neurons *in vitro*, for example via telomerase manipulation (Pardo Muñoz et al., 2017; Vera, Bosco, & Studer, 2016).

Given the multitude of reprogramming techniques available, it has become increasingly clear that extensive characterisation is necessary to determine the identity of neurons that have been subjected to the differentiation process. Whole transcriptome analysis by RNA-Seq revealed that, in my hands, iPSC-derived dopaminergic neurons displayed 60-70% homology compared to a multi-subject human single cell atlas of the subtstantia nigra. These results strongly suggest that within 60-70% of the neuronal population generated, correct subtype specification (midbrain A9) has been achieved (Figure 3.5 and Figure 3.6). Other cell signatures detected in my cultures included astrocytes (2%), inhibitory (5%) and excitatory neurons (6%), microglia (10%), and endothelial cells (9%). These off-target effects are inherent to all differentiation protocols—however, as previously described, manipulating the dosage and timing of small molecules, or adjusting cell density based on differentiation stage may ultimately increase the purity of cultured iPSC-derived dopaminergic neurons. Evidently, neurons do not exist in isolation but in a complex architecture comprising diverse neuronal subtypes with adjacent non-neuronal cells, namely astrocytes and microglia (Lake et al., 2016). The role of these non-neuronal cells residing in the brain is an emerging area in the context of neurodegeneration and our lab is currently exploring this in neuronal-microglial co-cultures (Schmidt et al., 2021; Sergi et al., 2021). However, in this study, my aim was to investigate the effect of exogenous α-synuclein fibrils on iPSC-derived dopaminergic neurons. I sought to model seeded aggregation in a reductionist manner with a view to identify cell-autonomous modifiers that are discussed in Chapter 5.

Importantly, the pSYN-positive and p62-positive aggregate morphology (neuritic, speckled, inclusion body, Figure 3.7) in iPSC-derived dopaminergic neurons were reminiscent of Lewy bodies and neurites in the human brain. In addition to being immunoreactive to pSYN, Lewy bodies were shown by super-resolution microscopy to be a crowded environment of membranes, including vesicular structures and dysmorphic organelles (Moors et al., 2018; Shahmoradian et al., 2019). It remains unclear if pSYN accumulation *in vitro* shares the same composition as Lewy pathology—iPSC-derived dopaminergic neurons are assayed in a shorter period at a maximum of 4 weeks post-seeding (DIV73) and do not possess any crosstalk between cell types as a homogenous population. In particular, one study demonstrated that the formation of Lewy pathology, in primary hippocampal neurons, was an interplay between α-synuclein fibrillization, post-translational modifications and interactions between α-synuclein aggregates and membranous organelles: mitochondria, autophagosome, endolysosome (Mahul-Mellier et al., 2020). Here, the process of inclusion formation, rather than α-synuclein fibrillization alone, was shown to be deleterious to neurons. A series of viability assays reported that the maturation of α-synuclein fibrils into larger aggregates was accompanied by mitochondrial and synaptic dysfunctions. In principle, it is likely that converging mechanisms and phenotypes may also be occurring in my stem cell model.

The modelling of α-synuclein seeded aggregation in iPSC-derived neurons relies on the addition of exogenous α-synuclein fibrils to trigger endogenously generated intracellular aggregates. Fibril concentration was optimised by adding increasing concentrations of fibrils ranging from 0, 0.01, 0.1, 1, up to 2 μM (Figure 3.8 and Figure 3.12a), and quantifying levels of pSYN at several timepoints from 1 week to 4 weeks post-seeding (Figure 3.12a). Through biochemical assays including immunoblotting and FRET signal, I observed that using 1 μM of α-synuclein fibrils

resulted in highly detectable levels of α-synuclein aggregation within the timeframe where stem cell-derived neurons remained viable *in vitro.* In my hands, iPSC-derived dopaminergic neurons reached senescence beyond DIV80 or 'what would be' 5 weeks post-seeding.

Indeed, the concentration of α-synuclein fibrils used in the current seeding assay (1 μM or 13.3 μg/mL) are supraphysiological compared to levels of α-synuclein detected in human subjects, which are typically quantified in the pg/mL or ng/mL range (Chang, Yang, Yang, Chang, & Wu, 2020; Farotti, Paolini Paoletti, Simoni, & Parnetti, 2020; Parnetti et al., 2014; Takahiko Tokuda et al., 2006). Studies investigating α-synuclein as a diagnostic biomarker have aimed to identify differences in circulating α-synuclein concentrations between Parkinson's disease patients and controls, such as healthy individuals or patients with other non-parkinsonian neurological disorders (Grey et al., 2015). In the cerebrospinal fluid, total α-synuclein was consistently shown to be lower in Parkinson's disease patients (36.5 ng/mL; interquartile range (IQR): 25.8-49.6 ng/mL) compared to controls (22.15 ng/mL; IQR: 11.86-38.64 ng/mL) (Paleologou et al., 2009; Parnetti et al., 2014; T Tokuda et al., 2010). Conversely, detection of oligomeric and phosphorylated forms of α-synuclein in the cerebrospinal fluid, which are considered pathogenic species, were found to be elevated in Parkinson's disease patients (oligomeric: 116 pg/mL, IQR: 76-170 pg/mL; phosphorylated on serine 129: 18.6 pg/mL, IQR: 15.7-23.3 pg/mL) compared to controls (oligomeric: 57 pg/mL, IQR: 36-106.5 pg/mL; phosphorylated on serine 129: 13.7 pg/mL, IQR: 9.2-18.5 pg/mL) (Majbour et al., 2016).

In contrast to the cerebrospinal fluid, peripheral total α-synuclein quantified from plasma and serum revealed increased levels in Parkinson's disease patients compared to controls in the pg/mL range. (Bougea et al., 2019; Chang et al., 2020). Consistent with this trend, plasma exosomes containing total α-synuclein was also

shown to be increased in Parkinson's disease patients compared to controls at overall lower concentrations in the fg/mL range (C.-C. Chung, Chan, Chen, Hung, & Hong, 2021). Moreover, the presence of oligomeric and phosphorylated forms of total α-synuclein have also been reported in plasma and serum samples of diseased patients and are currently under further investigation as peripheral biomarkers of Parkinson's disease (Zheng et al., 2021).

The seeding propensity in $SNCA^{TRIP}$ dopaminergic neurons was increased compared $SNCA^{A53T}$ neurons, suggesting that endogenous levels of α-synuclein monomer plays a more significant role than the A53T mutation in the context of seeded aggregation (Figure 3.12a). Consistent with these findings is the enhanced clinical severity in patients harbouring the SNCA triplication mutation, who typically present with early onset symptoms at 35 years of age as opposed to 60-70 years of age in individuals harboring the A53T mutant (Polymeropoulos et al., 1997; Singleton et al., 2003). With a single exposure to α-synuclein fibrils, diseased neurons displayed a dose and time-dependent increase in pSYN accumulation, which reflects the progressive nature of Parkinson's disease. Additionally, I demonstrated that, at baseline in the absence of any treatments, monomeric α-synuclein levels increased over time in culture in dopaminergic neurons (Figure 3.12b). A previous study also reported increasing α-synuclein levels with age in nigral tissues from primate models, suggesting a link between age-related stress and the role for α-synuclein (Chu & Kordower, 2007). As *in vitro* neurons exist outside of a physiological system, the observed increase in α-synuclein levels may be related to increased maturation and/or cellular stress.

Interestingly, I found that seeded aggregation in human dopaminergic neurons led to an upregulation of SNCA mRNA which was most prominent $SNCA^{TRIP}$ neurons (Figure 3.13). Increased *SNCA* mRNA has been reported in the midbrain and in

individually microdissected dopaminergic neurons of the substantia nigra from Parkinson's disease brains (Chiba-Falek, Lopez, & Nussbaum, 2006; Gründemann, Schlaudraff, Haeckel, & Liss, 2008). In addition, analysis of *SNCA* mRNA in the human temporal cortex in Parkinson's disease and dementia with Lewy bodies also demonstrated a correlation between the number of α-synuclein immunoreactive Lewy bodies and the abundance of *SNCA* mRNA expression (Rockenstein et al., 2001). These data suggest that the extent of SNCA expression is a key determinant of aggregation.

Although the molecular basis of this finding remains unknown and may involve epigenetic or microRNA dysregulation, it suggests that neurons with the highest level of SNCA expression are prone to intracellular amplification of aggregates due to feedback upregulation of α-synuclein monomer (Desplats et al., 2011; Miñones-Moyano et al., 2011). α-Synuclein has been shown to bind its own mRNA to regulate translation, therefore it is likely that misfolded or aggregated α-synuclein does not bind its own mRNA and consequently abolishes this inhibitory feedback loop (Zanzoni et al., 2013). Alternatively, pathological α-synuclein seeds may either directly interfere with transcriptional pathways or indirectly activate certain cytotoxic pathways (Guhathakurta, Bok, Evangelista, & Kim, 2017; Tagliafierro & Chiba-Falek, 2016).

MicroRNAs 34b/c, which influence mitochondrial function, were found to be down-regulated in the substantia nigra amongst other regions in Parkinson's disease patients with Lewy pathology (Miñones-Moyano et al., 2011). MicroRNAs 34b/c also targeted the 3'-UTR and repressed SNCA expression (Villar-Menéndez et al., 2014). Therefore, aggregation may be associated with the downregulation of microRNAs (e.g. 34b/c) that contribute to SNCA overexpression in vulnerable regions of diseased brains. Furthermore, α-synuclein aggregation may induce chromatin remodelling, promoting further transcription of SNCA. For example, DNA hypomethylation was widely detected

in the substantia nigra of PD and DLB patients (Jowaed, Schmitt, Kaut, & Wüllner, 2010; Matsumoto et al., 2010). SNCA expression is dependent on intron 1 methylation, hence inhibition of methylation in this region would result in increased *SNCA* gene expression. Interestingly, α-synuclein was shown to sequester DNA methyltransferase 1 (DNMT1) away from the nucleus to cytoplasmic aggregates in Parkinson's disease brains and mouse models alike (Desplats et al., 2011). Sequestration of DNMT1 provides a putative mechanism whereby other proteins can attach onto α-synuclein aggregates—subsequently increasing SNCA mRNA and ultimately leading to neurodegeneration.

MPTP injection in the substantia nigra of rats locally increased α-synuclein expression by activating NF-ϰB which in turn increased histone H3 acetylation at the promoter site of SNCA (P. Liu et al., 2014). Here, elevated α-synuclein levels was triggered in response to the activation of an inflammatory pathway following a chemical insult. Hence, it may also be likely that α-synuclein seeds may influence similar pathways in the context of aggregation. Moreover, exposure to other cellular stressors such as dopamine (Gómez-Santos et al., 2003), interleukin 1-β (Tanji et al., 2001), lipopolysaccharide (Tanji et al., 2002), nerve growth factor (Lee Clough & Stefanis, 2007), basic fibroblast growth factor (Rideout, Dietrich, Savalle, Dauer, & Stefanis, 2003) and serum deprivation (Ostrerova et al., 1999) have been shown to up-regulate SNCA, suggesting that α-synuclein may initially undertake a neuroprotective role when cells are challenged. Intracellular aggregation of α-synuclein is well known to cause multiple deficits, such as oxidative stress and the unfolded protein response—all of which may, in a vicious cycle, contribute to the overexpression of SNCA.

Lastly, α-synuclein ribbons seeded aggregation to a much larger extent compared to fibrils (Figure 3.14). Similar to recently discovered characteristics in tau pathology, the observed differences in seeding propensity between fibrils and ribbons

suggests that conformationally distinct α-synuclein assemblies may also confer different toxicities (Dujardin et al., 2018). Phenotypic differences have been reported previously, describing higher cytotoxic effects with α-synuclein fibrils and in contrast, higher seeding propensity with ribbons (Bousset et al., 2013; Gribaudo et al., 2019b; Peelaerts et al., 2015). These data suggest that aggregate burden does not necessarily correlate with disease burden. Rather, that α-synuclein conformation is the more plausible determinant of toxicity.

As we know through electron microscopy that ribbons are structurally distinct compared to *de novo* α-synuclein fibrils (Bousset et al., 2013), increased seeded aggregation in the presence of α-synuclein ribbons suggests differences in the manner in which dopaminergic neurons process such assemblies. Therefore, exposure to α-synuclein ribbons and the resulting increase in aggregation may also be explained by differences in intracellular kinetic factors, such as enhanced endosomal uptake rate, decreased degradation rate, or lastly, increased fibril fragmentation rate—which may ultimately increase the number of templating events in a cell and promote the cell to cell transfer of α-synuclein seeds (Sang et al., 2021).

Chapter 4

Modifiers of α-synuclein seeded aggregation and toxicity in iPSC-derived dopaminergic neurons

4.1 Introduction

4.1.1 α-Synuclein strains in α-synucleinopathies

α-Synuclein has been referred to as a protein chameleon in the literature, due to its intrinsic quality for conformational plasticity (Drescher et al., 2012; Silva, Breydo, & Uversky, 2013; Uversky, 2003). The deleterious aggregation of α-synuclein is invariably associated with a group of neurodegenerative diseases now termed α-synucleinopathies (Spillantini & Goedert, 2000). These disorders include Parkinson's disease, Dementia with Lewy bodies, multiple system atrophy and in rarer cases pure autonomic failure and neurodegeneration with brain iron accumulation. α-Synucleinopathic patients display distinct clinical presentations whilst also exhibiting differences in the intracellular localisation and pattern of α-synuclein deposition (Coon & Singer, 2020). For example, in Parkinson's disease, α-synuclein aggregates in neuronal Lewy inclusions whereas in multiple system atrophy, α-synuclein accumulates in oligodendrocytes in the form of glial cytoplasmic inclusions (Valera & Masliah, 2018). Although Parkinson's disease is slowly progressing and disabling, multiple system atrophy is life-limiting with an average prognosis of 7 years from the time of diagnosis (Wenning, Colosimo, Geser, & Poewe, 2004). This heterogeneity between α-synucleinopathies may be explained through the existence of conformationally distinct α-synuclein 'strains' (Holec & Woerman, 2021).

The concept of strains in infectious proteins first appeared following the discovery that scrapie prions isolated from different tissues possessed different

molecular profiles (Bessen & Marsh, 1992). Further characterisation of these scrapie agents demonstrated that they were indeed associated to specific disease phenotypes, validating the presence of strains in prion infectivity (Telling et al., 1996). As α-synuclein behaves similarly to prion proteins, the strain hypothesis in α-synucleinopathies and more broadly aggregation-associated neurodegeneration has also now begun to emerge (Peelaerts et al., 2018). Multiple *in vitro* studies have demonstrated that α-synuclein conformers can be distinguished through biochemical and functional assays (Bousset et al., 2013; Candelise et al., 2019; C. Kim et al., 2016; Peng, Gathagan, Covell, et al., 2018; Pieri, Madiona, & Melki, 2016; Van der Perren et al., 2020). Moreover, α-synuclein strains exhibited differential toxicities when tested in rodent models, causing varying degrees of aggregation and neurodegeneration (Guo et al., 2013; Peelaerts et al., 2015; Pieri et al., 2016).

The notion that differences in aggregate localisation may be caused by α-synuclein strain-dependent phenotypes was first shown in a rat model using synthetic fibrils (Peelaerts et al., 2015). Here, although *de novo* generated fibrils and ribbons both induced the accumulation of pSYN, α-synuclein aggregates were differentially localised in oligodendroglial cells, demonstrating that conformation-specific behaviours can be reproduced in a physiological system. To investigate whether aggregates from Lewy pathology and glial cytoplasmic inclusions represent different strains, sarkosyl-insoluble α-synuclein was isolated from patient brains and subjected to a battery of tests (Peng, Gathagan, Covell, et al., 2018), including limited proteolysis and differential antibody immunoreactivity, revealing a unique pattern for each isolated strain. Peng et al. (2018) further assessed the effect of adding back these isolated α-synuclein seeds *in vivo* in mice modified to express α-synuclein in oligodendrocytes. Interestingly, injection of pathogenic α-synuclein from Lewy bodies induced aggregates reminiscent of glial cytoplasmic inclusions in oligodendrocytes—

suggesting that the cellular environment rather than the α-synuclein seed is the determining factor in the generation of pathological strains. Further investigations using fluorescent probes, nuclear magnetic resonance, and especially cryogenic electron microscopy (cryo-EM) elucidated the conformational differences between Parkinson's disease and multiple system atrophy strains (Burger, Fenyi, Bousset, Stahlberg, & Melki, 2021; Shahnawaz et al., 2020; Strohäker et al., 2019). With the advent of cryo-EM technology, subtle nuances in α-synuclein fibrillar polymorphs have now become detectable as described below in Figure 4.1.

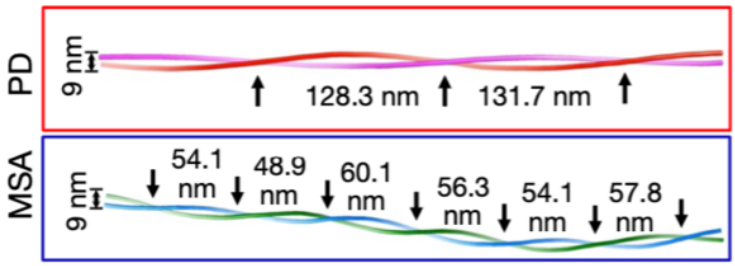


Figure 4.1 Structural differences between brain-amplified α-synuclein fibrils from Parkinson's disease and multiple system atrophy patient

Three-dimensional helical models from cryogenic electron microscopy displaying periodic twisting of α-synuclein filaments. Black arrows indicate twist localisation. Periodic spacing (nm) in PD-amplified α-synuclein fibrils was longer/wider compared to MSA-amplified fibrils (Shahnawaz et al., 2020).

In addition to these basic investigations, the clinical heterogeneity within α-synucleinopathies (e.g. Parkinson's disease, mild-motor predominant, intermediate, diffuse malignant; multiple system atrophy, parkinsonian-type or cerebellar-type) may also hint towards the existence of disease subtypes. Several α-synuclein strain subtypes have been identified in Parkinson's disease and visualised through conformation-specific antibodies (Henderson et al., 2020). These strains may also target distinct brain regions or different cell types (A. Lau et al., 2020). Furthermore, α-synuclein strains in the human brain may also exist as an ensemble or cloud of distinct yet disease-specific conformational states, similar to what has been suggested previously for prion strains (Collinge & Clarke, 2007). The prion cloud model for α-synuclein proposes that seeded amyloid aggregates may form a wide range oligomeric or fibrillar structures, potentially generating few dominant conformers and several non-dominant conformers (Hoppe, Uzunoğlu, & Nussbaum-Krammer, 2021). Interestingly, in the case where dominant conformers were to decrease in proportion, for example as a result of its targeted degradation, non-dominant conformers may possibly become more prominent and further induce neurotoxicity.

The application of α-synuclein seeds amplified from post-mortem brains, in contrast to the use of *de novo* generated fibrils, increases the disease relevance of currently used human models (Tanudjojo et al., 2021). Similar to the pathogenesis of prion proteins, α-synuclein strain *infectivity* largely depends on two factors, firstly, the structural properties of α-synuclein fibrils and secondly, the genetic background of the host cell (Peelaerts et al., 2018). It remains to be discovered at present, precisely which α-synuclein strain is the most toxic species in Parkinson's disease. Based on our current understanding, strain-induced toxicity may arise from the interplay between misfolded α-synuclein seed, endogenous α-synuclein, and cellular microenvironment, which may all create conformation-specific interactomes. An important unanswered

question is which protein interactions form a permissive milieu that mechanistically link strain propagation to neurodegeneration.

4.1.2 Brain-amplified fibrils by protein misfolding cyclic amplification

Limited accessibility to α-synuclein seeds isolated directly from diseased brains presents a challenge to their use in models of seeded aggregation (Jung et al., 2017). In addition, aggregate isolation from post-mortem brains may not be representative of the actual seed or seed diversity present under physiological conditions. To circumvent these obstacles, a technique termed protein misfolding cyclic amplification (PMCA), originally used to study transmissible spongiform encephalopathies (Soto, Saborio, & Anderes, 2002), was re-purposed to amplify α-synuclein seeds from brain-derived material (Herva et al., 2014; Jung et al., 2017). Since its inception, PMCA has led to the fast amplification of seeds whilst also serving as a diagnostic tool for α-synucleinopathies (Castilla et al., 2006; Alexis Fenyi et al., 2019b; Kang et al., 2019; Singer et al., 2020).

The technique of PMCA shares the same principle with DNA amplification by polymerase chain reaction (Saborio, Permanne, & Soto, 2001; Soto et al., 2002). PMCA is defined as a cyclic process which dramatically accelerates the rate of conformational templating (Figure 4.2). Minute quantities of α-synuclein seeds are amplified by templating human recombinant α-synuclein monomer (Figure 4.2a). Templated seeds then undergo sonication to multiply the number of templating growth sites, which are then used for further amplification of batches of monomeric α-synuclein (Figure 4.2b).

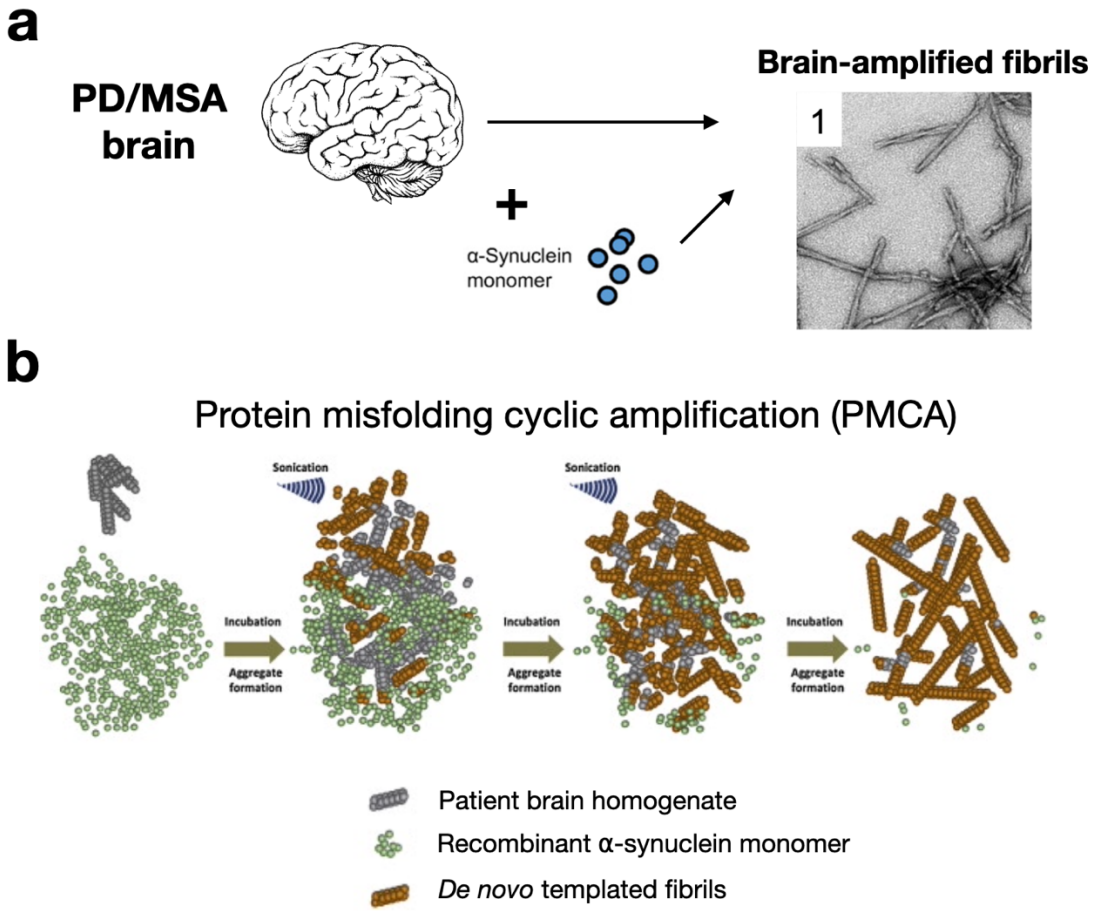


Figure 4.2 Amplification of α-synuclein from diseased brain homogenates

a, Human brain homogenate was isolated from post-mortem patients with Parkinson's disease and multiple system atrophy. Human recombinant α-synuclein was *de novo* aggregated in the presence of post-mortem brain homogenates to created brain-amplified fibrils. **b,** Generation of brain-amplified fibrils was performed using a methodology termed protein misfolding cyclic amplification (PMCA). A small amount of patient brain homogenate (reaction template) was added and mixed with a large amount of recombinant α-synuclein monomer (reaction substrate) and incubated at 37 degrees Celsius with constant agitation. In between incubation cycles, fibrils were sonicated to fractionate newly generated aggregates into smaller seeds. Repeating cycles of incubation and sonication results in the exponential amplification of seeds initially present in brain homogenates (Saá & Cervenakova, 2015).

PMCA also has an application as a highly sensitive assay in the diagnosis of Parkinson's disease and multiple system atrophy (Kang et al., 2019; Singer et al., 2020). PMCA assay conditions have successfully amplified α-synuclein seeds *in vitro* from substantially low volumes, therefore tissue biopsies may be used as a disease biomarker which in some cases may also detect early-stage patients (Groveman et al., 2018; Shahnawaz et al., 2017). The detection of pathological α-synuclein seeds in human tissues (e.g. cerebrospinal fluid, blood, gastrointestine) represents on average a detection sensitivity over 90% and specificity over 95% (Shahnawaz et al., 2017). Amyloidogenic proteins in tissue biopsies usually become detectable by Thioflavin T fluorescence after the second or third cycle of amplification and disease-specific strains are characterised by their kinetics as determined by α-synuclein polymerization levels (Singer et al., 2020).

Additionally, it is important to distinguish α-synuclein strains isolated directly from human brains to α-synuclein assemblies that were derived by PMCA. For purposes of clarity in this body of work, I will define α-synuclein 'strains' as fibrillar α-synuclein species which are directly related to the human brain. In contrast, PMCA involves a process which synthetically templates authentic human α-synuclein strains with recombinant α-synuclein. Amplifying such species *ex vivo* introduces two additional non-physiological variables, which are (i) mechanical agitation to induce aggregation and (ii) templating with recombinant α-synuclein protein in a salt buffer. Hence, PMCA-derived fibrils hereafter will be termed as 'brain-amplified α-synuclein assemblies.'

4.1.3 Dysregulated cellular pathways associated with α-synuclein pathology

There is currently an incomplete understanding of how selective vulnerability in cell types or neuroanatomical region functions in the context of seeded aggregation (Blauwendraat et al., 2020; Henderson, Cornblath, et al., 2019). To this end, genome-wide transcriptomic analyses have been performed in Parkinson's disease (Nido et al., 2020) and multiple system atrophy (Mills, Ward, Kim, Halliday, & Janitz, 2016) brains from post-mortem patients. Whole transcriptome analysis by RNA sequencing in over 60 original studies revealed that Parkinson's disease brains converge on previously reported signatures including mitochondrial function, vesicle trafficking, synaptic transmission, and immune responses (Borrageiro, Haylett, Seedat, Kuivaniemi, & Bardien, 2018; Zambon et al., 2019). Since then, more recent refinements in the RNA extraction and processing protocols (e.g. ribosomal RNA depletion) aimed at reducing RNA degradation alongside correcting for cell type composition have improved the deciphering of transcriptomic signals from the human brain (Nido et al., 2020). For example, Nido et al. analysed prefrontal cortex tissues from Parkinson's disease patients and found that including the classically defined metabolic, vesicular, and inflammatory phenotypes, pathways related to the endoplasmic reticulum, lipid oxidation, and the unfolded protein response were highest in gene expression signatures. Corroborating these findings, isogenically corrected SNCA triplication iPSC-derived cortical neuron transcripts also showcased a phenotype in the unfolded protein response (Heman-Ackah et al., 2017). In contrast, much fewer studies were performed in brain tissues from multiple system atrophy, yet, similar genes were enriched also in the frontal gyrus such as, vesicle-mediated transport, synaptic transmission, and those involving membranous organelles: endoplasmic reticulum, Golgi apparatus (B. J. Chen et al., 2016; Mills et al., 2016).

Interestingly, gene expression profiling of patient brains from Parkinson's disease and multiple system atrophy both displayed enrichment of long intervening non-coding RNAs (lincRNAs), which remodel chromatin and have diverse functions in RNA stabilisation, transcription regulation and enhancer activity (Mills et al., 2016; Theo et al., 2017). For instance, lincRNA-p21 has been shown in a mouse and neuroblastoma model to sequester microRNA-1277-5 leading to increased expression of α-synuclein—which in turn decreased viability and activated apoptosis (X. Xu et al., 2018). Similarly in primary hippocampal slices, differential α-synuclein expression was found to contribute to the selective vulnerability of cells in response to fibril addition (Luna et al., 2018). These studies strongly implicate the role of endogenous monomeric α-synuclein levels in the pathogenesis of Parkinson's disease brains, linking increased expression levels to cell death. This hypothesis is likely true in a human system as it has already been shown in an *in vivo* murine model, i.e. that patterns of α-synuclein pathology are dependent on anatomical connectivity and regional α-synuclein expression (Henderson, Cornblath, et al., 2019).

4.1.4 Assay workflow: phenotypic characterisation of patient brain-amplified α-synuclein fibrillar assemblies

In the previous Chapter, I established and characterised a model of α-synuclein seeded aggregation in patient iPSC-derived dopaminergic neurons using *de novo* fibrils. To further improve the disease relevance of my model, I sought to investigate the effects of brain-amplified α-synuclein fibrillar assemblies on healthy control and $SNCA^{TRIP}$ dopaminergic neurons. pSYN-positive aggregates triggered by patient brain-amplified fibrils were phenotypically characterised based morphology and neurotoxicity. Subsequently, whole transcriptome analysis was performed on neurons exposed to *de novo* and brain-amplified assemblies to explore the molecular drivers of toxicity in my model.

The objectives of this chapter were to:

1. Characterise PMCA-amplified α-synuclein assemblies derived from patient brain homogenates
2. Assess the effect of patient brain-amplified fibrils on pSYN accumulation
3. Assess the effect of patient brain-amplified fibrils on neuronal viability
4. Investigate differential gene expression in the presence of brain-amplified α-synuclein assembly-induced aggregation
5. Evaluate the effect of isogenic correction of *SNCA* triplication on pSYN accumulation and viability

4.2 Results

4.2.1 Amplification and characterisation of pathogenic α-synuclein from Parkinson's disease and multiple system atrophy patients

4.2.1.1 Characterisation of patient brain-amplified α-synuclein fibrillar assemblies

To investigate the effects of α-synuclein assemblies from Parkinson's disease and multiple system atrophy, synthetic descendants of aggregated α-synuclein in human brain homogenate were generated using protein misfolding cyclic amplification. Patient-brain amplified fibrils were generated and characterised by Ronald Melki and his group as part of a collaboration within the IMPRiND Consortium.

Isolated brain homogenates were initially characterised by quantifying the levels of pathological α-synuclein present in each case. The amount of total α-synuclein and pSYN were quantified by filter retention and homology time resolved fluorescence (HTRF). These measurements showed that first, the total amount of α-synuclein was slightly lower in multiple system atrophy brain homogenates (Figure 4.3a). Secondly, the amount of pSYN was similar in control and Parkinson's disease patient brain homogenates and significantly higher in homogenates from multiple system atrophy brains (Figure 4.3b). As expected, the amount of pathogenic, phosphorylated α-synuclein, varied significantly from one patient to another and was 5-12-fold higher in diseased patient homogenates compared to similar homogenates from control patients (Figure 4.3c).

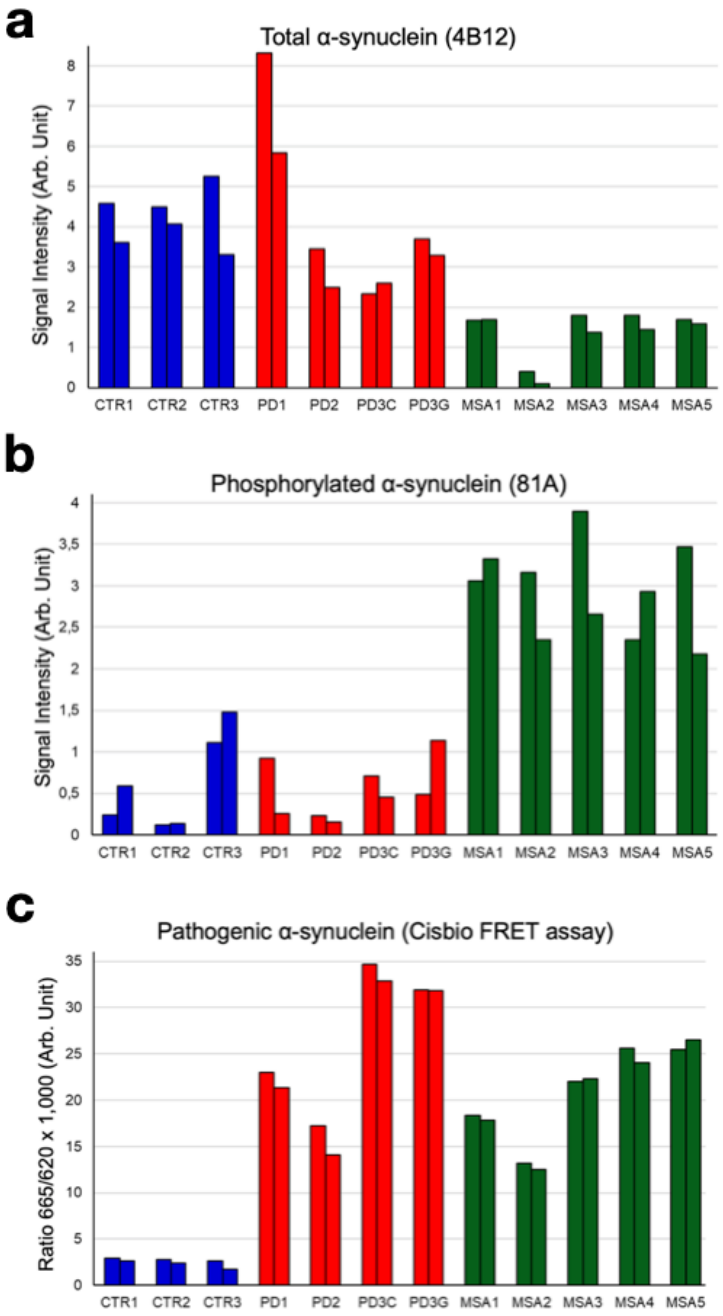


Figure 4.3 Quantification of pathogenic α-synuclein aggregates in patient brains

Brain tissues from three PD (cingulate cortex (C) and temporal gyrus (G)), five MSA (cerebellum) as well as 3 age-matched healthy control patients were obtained at autopsy and processed into total brain homogenates. **a** and **b**, The amount of pathogenic, aggregated α-synuclein in the different brain homogenates was determined using a filter retardation assay (*n*=3). 50 µl of brain homogenates (1% in PBS, weight:volume), equivalent to 0.5 mg of brain homogenate, were filtered on cellulose acetate membranes and probed with **a**, 4B12 (total α-synuclein) or **b**, 81A (phosphorylated α-synuclein) antibodies. **c**, The amount of pathogenic, phosphorylated, α-synuclein in PD and MSA brain homogenates (10% in PBS, weight:volume) was also quantified using homology time resolved fluorescence (*n*=3). The data for each patient are means of the recorded signal±s.e.m (*n*=2). Data in this figure was generated by Dr. Alexis Fenyi and Dr. Luc Bousset from Ronald Melki's group.

4.2.1.2 Protein misfolding cyclic amplification of α-synuclein assemblies

Brain homogenates were blindly subjected to three cycles of amplification in Ronald Melki's laboratory by means of protein misfolding cyclic amplification. Amplification steps were performed in an iterative manner to avoid *de novo* assembly of monomeric α-synuclein into fibrils within the experimental timeframe, ensuring that α-synuclein seeds generated in each amplification step were derived from brain homogenates. The assembly of α-synuclein into oligomers was monitored by fluorescence through thioflavin T binding (ThT). At the 400 min timepoint, when ThT signal was detectable in the patient brain homogenate samples but not in controls, an aliquot from the first amplification cycle was transferred and diluted in the presence of monomeric α-synuclein and assembly was further monitored by ThT signal. From the first cycle of amplification, samples were diluted 20-fold for MSA cases and corresponding controls and 50-fold for PD cases and corresponding controls. Aliquots were added to 100 μM monomeric α-synuclein in PMCA assembly buffer. Two additional amplification cycles were performed by diluting the assemblies generated at the end of cycle 2 and 3 in PMCA buffer containing monomeric α-synuclein (cycle 2 durations: 4 h for controls PD and MSA cases; cycle 3 durations: 3 h for PD and 6 h for MSA and corresponding controls).

Brain homogenates from 3 Parkinson's disease and 5 multiple system atrophy patients but not the control samples exhibited seeding propensity after amplification cycles (Figure 4.4a). The resulting α-synuclein assemblies were imaged by transmission electron microscopy (TEM), which demonstrated that the resulting assemblies were fibrillar in nature (Figure 4.4b). PD- and MSA-amplified fibrils both exhibited a twisted shape when compared to *de novo* generated α-synuclein fibrils.

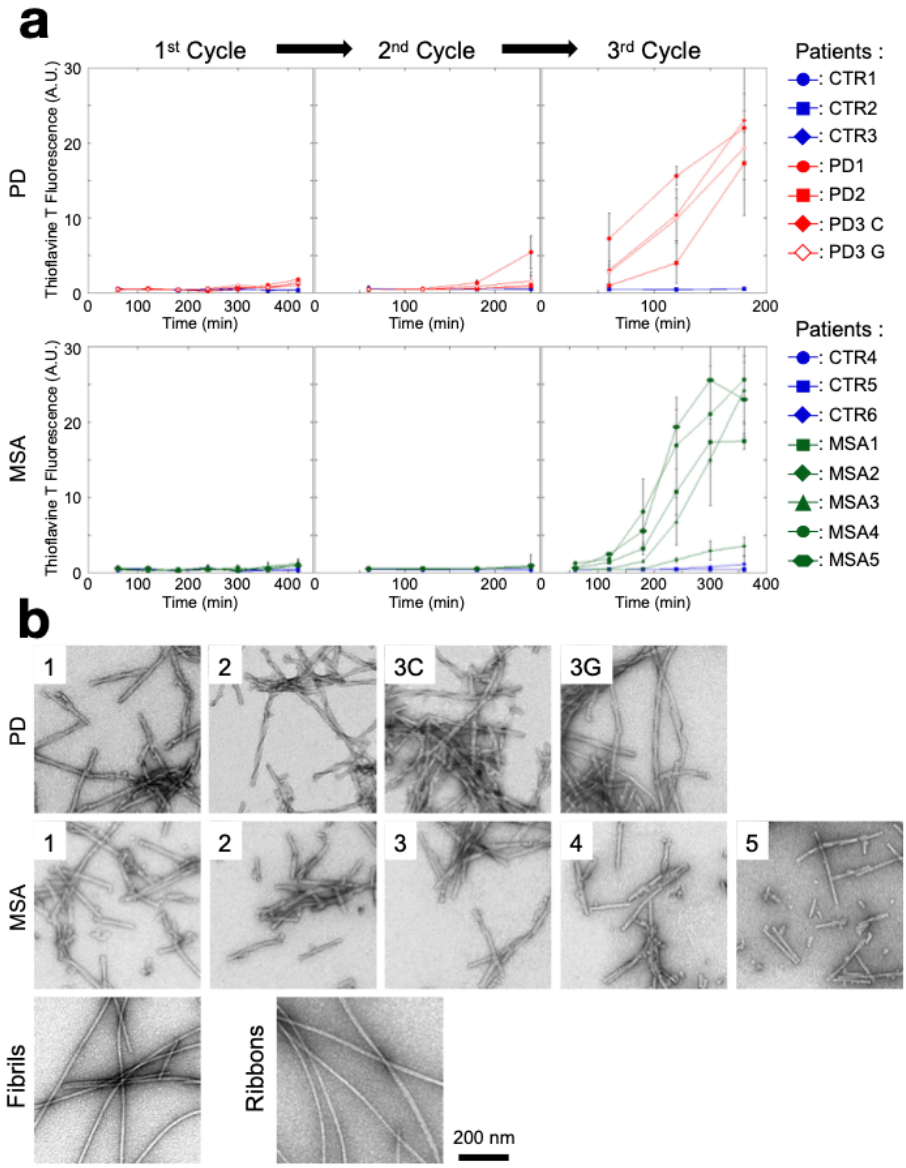


Figure 4.4 Three cycle amplification of pathogenic α-synuclein seeds and electron micrographs of resulting assemblies

a, Protein misfolding cyclic amplification (PMCA) was performed on Parkinson's disease (PD, top panels in red and corresponding controls in blue) and multiple system atrophy (MSA, bottom panels in green and corresponding controls in blue) brain homogenates. Three cycle amplifications were required to generate templated fibrils, as quantified by Thioflavin T fluorescence. Patient brain homogenates (2% weight:volume) was added in the first cycle in PMCA buffer (150 mM KCl, 50 mM Tris-HCl, pH 7.5) containing recombinant α-synuclein monomer (100 μM). The following amplification cycles were seeded by 2% or 5% (volume:volume) of preceding amplification cycles. The total mass of brain homogenate and PMCA-amplified assemblies used in each amplification reaction were previously defined following optimisation studies aimed at minimising *de novo* aggregation of α-synuclein. The duration of each cycle was also previously optimised. Each curve represents an average of n=4 replicates ± std.dev. **b,** Electron micrographs of fibrillar α-synuclein assemblies obtained after the third amplification cycle from each of the three PD cases and five MSA cases, and fibrils and ribbons. For PD3, the temporal gyrus (PD 3G) and cingulate cortex (PD 3C) were examined. Scale bar: 200 nm. Data in this figure was generated by Dr. Alexis Fenyi and Dr. Luc Bousset from Ronald Melki's group.

Resulting α-synuclein assemblies were additionally finger-printed by SDS-PAGE after limited proteolysis with Proteinase K. PD- and MSA-amplified α-synuclein fibrils revealed distinct limited proteinase K (3.8 μg/mL) digestion patterns when assayed at 1-, 5-, 15-, 30-, and 60-min (Figure 4.5a). Proteolytic patterns from PD-amplified fibrils yielded profiles dominated by three discrete bands, unlike fibrils amplified with MSA homogenate. Quantification of the intensity of the band with the lowest molecular weight (arrowhead in Figure 4.5a) that was common between the two profiles, demonstrated that, consistent in all cases, PD-amplified fibrils were more resistant to proteolysis compared to MSA-amplified fibrils (Figure 4.5b).

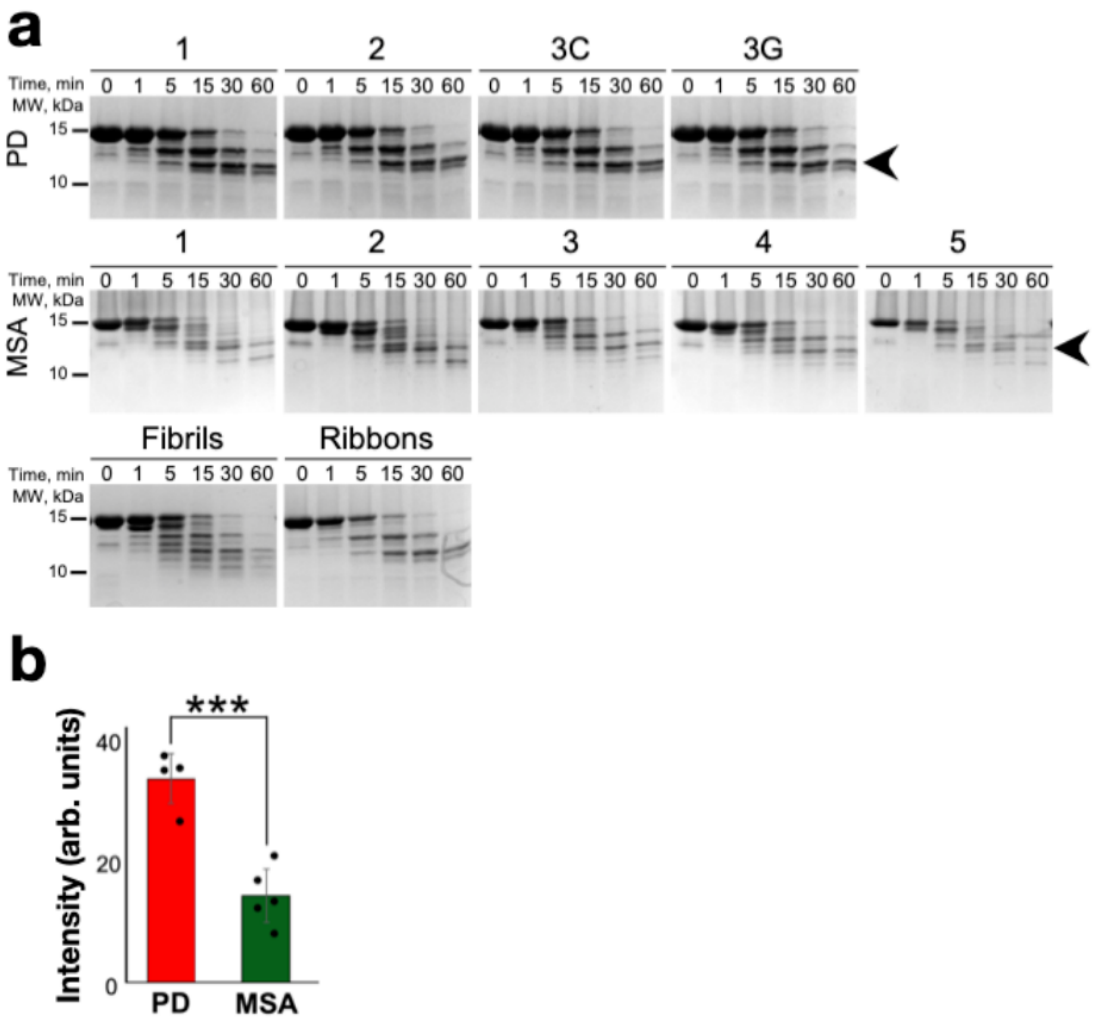


Figure 4.5 Limited proteolytic patterns of PMCA-amplified α-synuclein assemblies

a, Limited proteolysis was performed on PMCA-amplified PD and MSA fibrils, *de novo* fibrils, and ribbons. Samples were collected after the third amplification cycle and mixed with proteinase K (3.8 μg/mL) and assayed at 1-, 5-, 15-, 30-, and 60-min. SDS-PAGE analysis was performed, and gels were stained with Coomassie blue. **b,** The intensity of the proteolytic band generated at 15 min and indicated by the arrowhead was normalised to that of α-synuclein at time 0 for each PD (red, *n*=4) and MSA (green, *n*=5) patient sample. PD-amplified assemblies exhibited higher resistance to proteolysis compared to MSA-amplified assemblies. In panel **b,** data are mean±s.e.m, ****P*<0.001, by two-sided unpaired Student's t-test. Data in this figure was generated by Dr. Alexis Fenyi and Dr. Luc Bousset from Ronald Melki's group.

4.2.2 Brain-amplified α-synuclein assemblies cause progressive degeneration of iPSC-derived dopaminergic neurons

Until recently, mainly *de novo* α-synuclein fibrils have been used to model seeded aggregation *in vitro* and *in vivo* (Peelaerts & Baekelandt, 2016; Wong & Krainc, 2017). Therefore, I sought to investigate the effects of brain-amplified fibrils with the aim of producing a more disease-relevant model. To this end, I investigated the effects of recombinant α-synuclein fibrils assembled *de novo* or amplified in the presence of Parkinson's disease (*n*=3) or multiple system atrophy (*n*=5) brain homogenates.

4.2.2.1 Brain-amplified α-synuclein assemblies share similar seeding potency compared to α-synuclein fibrils in dopaminergic neurons

Individual brain-amplified α-synuclein assemblies were tested at two concentrations (0.1 μM and 1 μM) in three clonal lines from $SNCA^{TRIP}$ or three healthy control lines, each independently differentiated three times. I found that PD-amplified or MSA-amplified fibrils had similar seeding potencies compared to *de novo* α-synuclein fibrils at 2 weeks post-seeding as measured by pSYN accumulation (Figure 4.6).

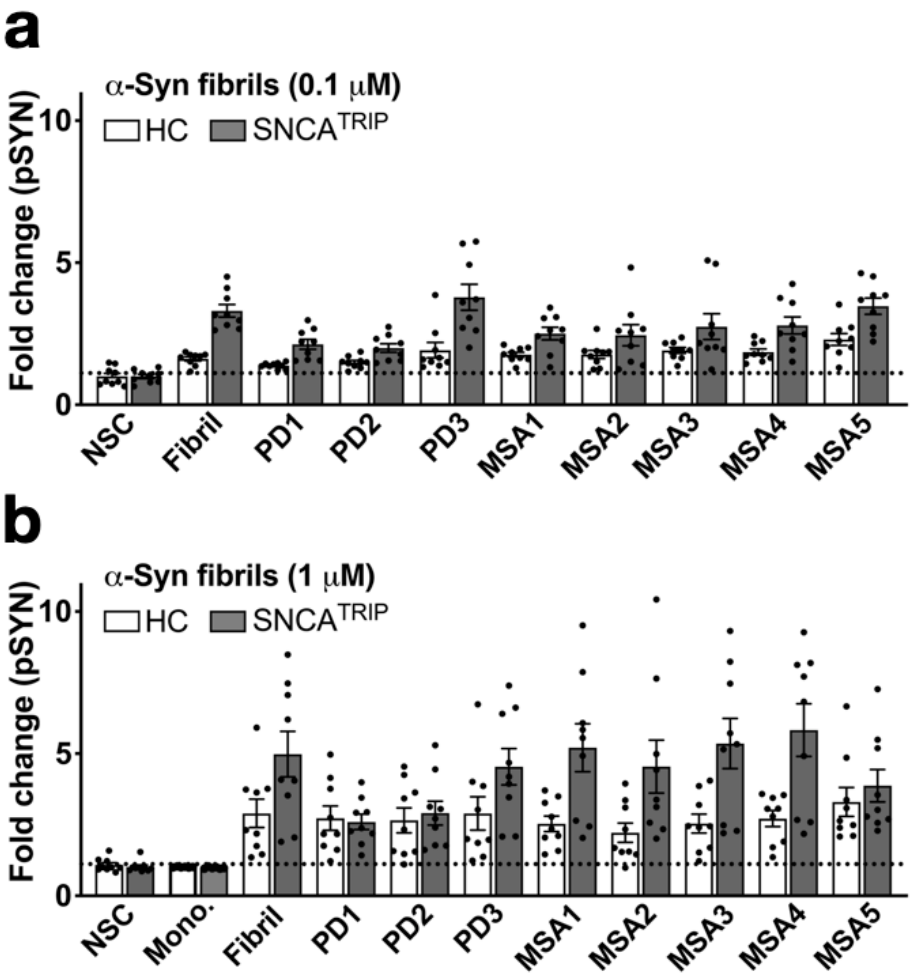


Figure 4.6 Aggregation propensity of *de novo* and brain-amplified α-synuclein fibrils

Similar levels of pSYN were detected by homology time resolved fluorescence in neuronal lysates seeded with **a,** 0.1 μM or **b,** 1 μM fibrils when comparing *de novo* fibrils to each case of PD- or MSA-amplified assemblies (n=9 for **a** and **b**). NSC, non-seeded control, non-treated control. Each dot corresponds to one clone differentiated once and data are mean±s.e.m.

4.2.2.2 Brain-amplified α-synuclein assemblies exhibit morphologically distinct pSYN-positive aggregates

As each assembly preparation had similar TEM characteristics (Figure 4.4 and Figure 4.5) and seeding propensity (Figure 4.6), I analysed blindly the effect of pooled PD-derived and pooled MSA-derived assemblies on $SNCA^{TRIP}$ and healthy control dopaminergic neurons. PD-derived assemblies were pooled by mixing fibrils from the three Parkinson's disease cases (PD1-3, Table 2.4 and Figure 4.6) into a single mixture, similarly, MSA-derived assemblies were pooled by mixing the five multiple system atrophy cases (MSA1-5, Table 2.4 and Figure 4.6). Pooled PD- and MSA-amplified assemblies were used hereafter, unless otherwise specified. Despite brain-amplified assemblies sharing similar seeding potencies, when assessed morphologically, I observed that pSYN-positive aggregates in $SNCA^{TRIP}$ dopaminergic neurons differed depending on the type of α-synuclein assembly used (Figure 4.7a). Specifically, MSA-amplified fibrils triggered the formation of short neuritic and speckled inclusions, whereas PD-amplified fibrils induced the formation of longer neuritic aggregates. *De novo* generated fibrils induced inclusions with an intermediate morphology. Aggregate morphology was quantified by total length (nm) using Fiji ImageJ (Ridge Detection plugin) in three $SNCA^{TRIP}$ clones each differentiated three times (Figure 4.7b).

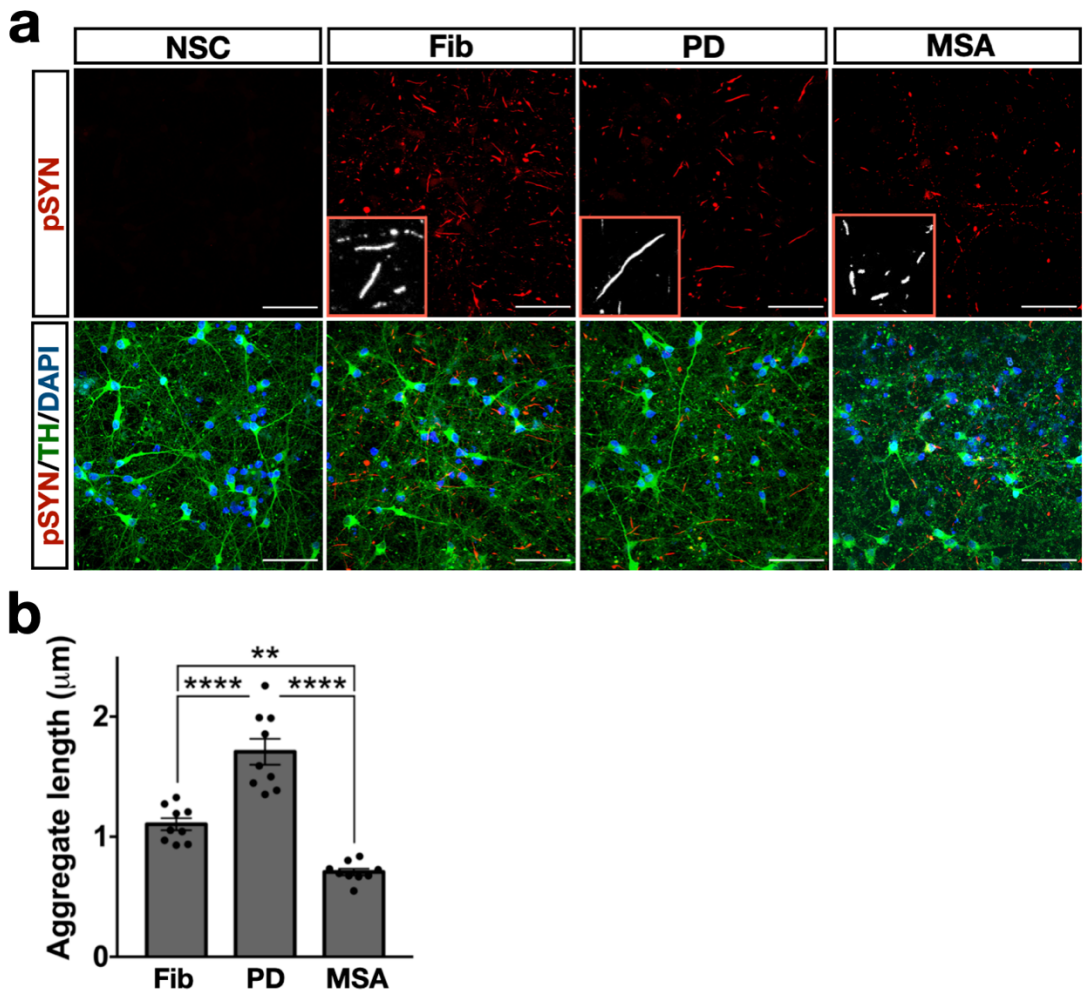


Figure 4.7 De novo and brain-amplified α-synuclein fibrils induce distinct pSYN-positive aggregates in SNCA^{TRIP} dopaminergic neurons

a, Representative confocal images of SNCA^{TRIP} dopaminergic neurons treated with *de novo* and patient brain-amplified fibrils (1 μM). pSYN (red, top), tyrosine hydroxylase (TH, green, bottom). Images are representative of three independent differentiations (scale bar: 50 μm). pSYN positive-aggregates induced by MSA-amplified fibrils were shorter and more speckled, whereas pSYN-positive aggregates induced by PD-amplified fibrils were neuritic and longer in length compared to ones induced by *de novo*-generated fibrils (n=9). NSC, non-seeded control, non-treated control. **b,** Aggregate lengths generated from each condition was quantified by image analysis software FIJI (Ridge Detection plugin). Each dot corresponds to one clone differentiated once and data are shown as mean±s.e.m. In panel **b,** ***P<0.001,****P<0.0001 by one-way ANOVA followed by Tukey's multiple comparison test.

Aggregate morphologies were also assessed in healthy control neurons. In particular, control neurons exposed MSA-amplified fibrils exhibited a similar pattern to SNCA^{TRIP} neurons, inducing pSYN-positive aggregates that were shorter and more speckled (Figure 4.8).

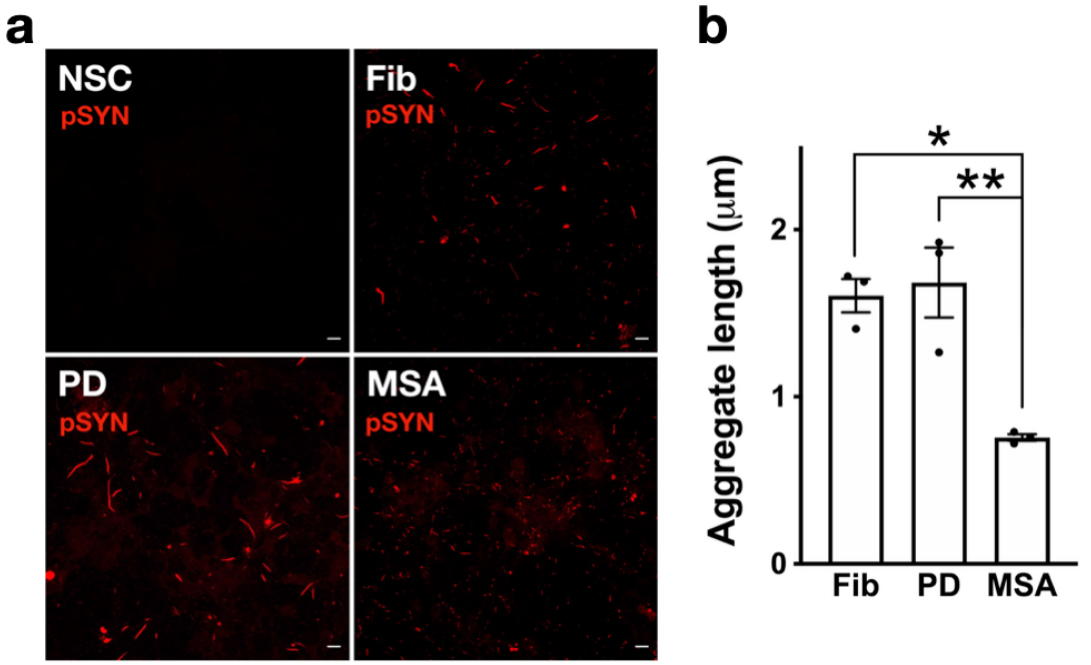


Figure 4.8 *De novo* and brain-amplified α-synuclein fibrils induce distinct pSYN-positive aggregates in healthy control dopaminergic neurons

a, Representative confocal images of healthy control dopaminergic neurons treated with *de novo* and patient brain-amplified fibrils (1 μM). Similar to the phenotypes described in SNCA^{TRIP} dopaminergic neurons, pSYN positive-aggregates induced by MSA-amplified fibrils were also shorter and more speckled. **b,** Aggregate lengths generated from each condition was quantified by image analysis software FIJI (Ridge Detection plugin). Each dot corresponds to one clone differentiated once and data are shown as mean±s.e.m. In panel **b,** $^{*}P<0.05$, $^{**}P<0.01$ by one-way ANOVA followed by Tukey's multiple comparison test.

To ensure that these patterns did not arise from the length of the exogenous fibrils, all assemblies were imaged by TEM to assess their length. Electron micrographs of the α-synuclein assemblies used in this study, both *de novo* generated and brain-amplified assemblies included, revealed seeds of similar lengths (60-100 nm) across all conditions (Figure 4.9). These results suggest that the morphological differences observed in pSYN-positive inclusions (Figure 4.6 and Figure 4.7) were structural differences between α-synuclein assemblies.

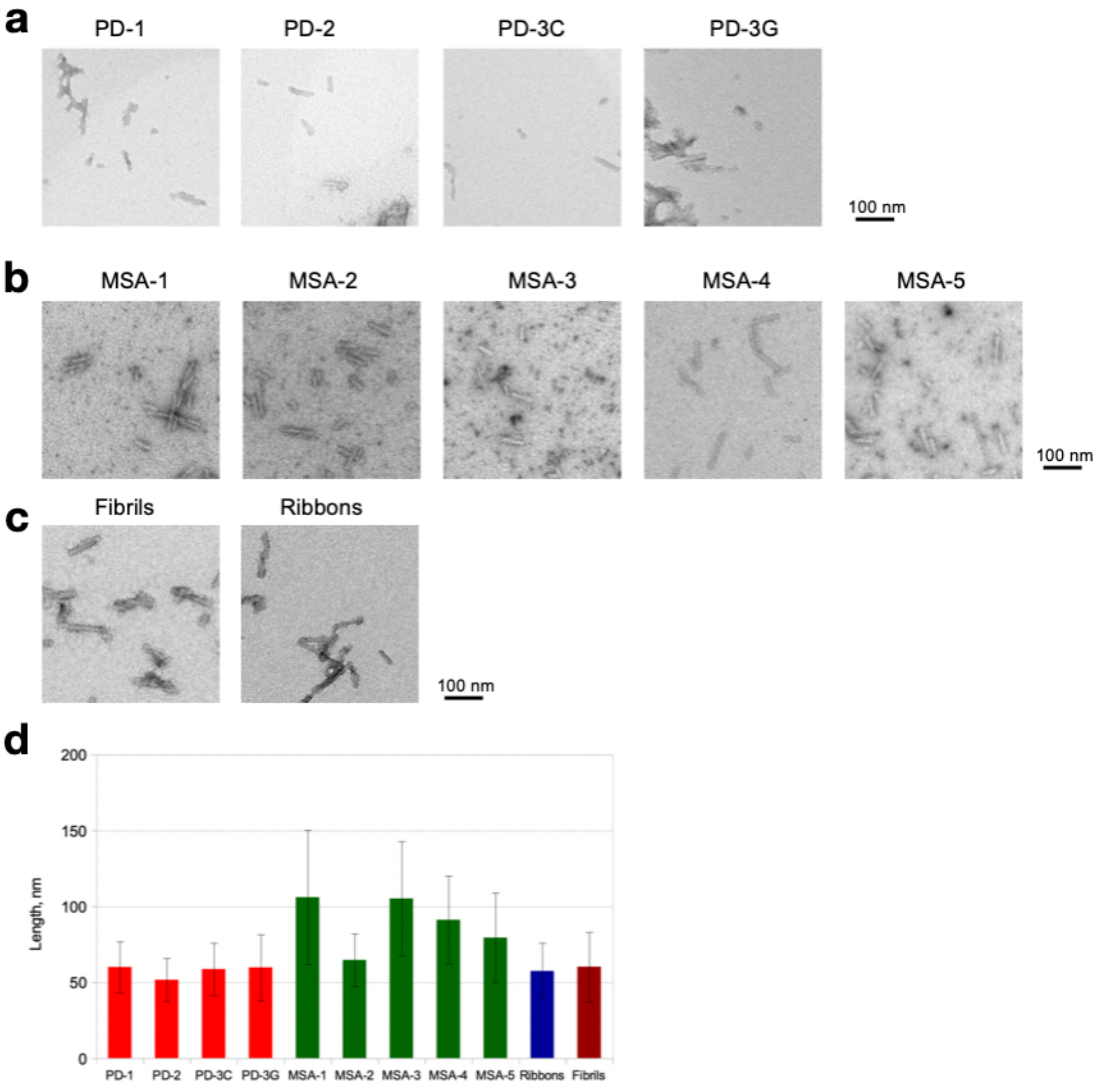


Figure 4.9 Electron microscopy measurements of *de novo* generated fibrils and brain-amplified assemblies after sonication

α-Synuclein assemblies were sonicated under strictly controlled conditions and assessed for filament length. **a**, PD- amplified **b**, MSA-amplified and **c**, *de novo* generated (fibrils and ribbons) assemblies had overall similar lengths (Scale bar: 100 nm). In panels **a-c**, each TEM image is representative of one independent fibril preparation (n=4 for PD; n=5 for MSA; scale bar: 100 nm). **d**, The average length of all sonicated fibrils used for seeding was 60 nm. PD-1 (n=102 fibrils), PD-2 (n=115 fibrils), PD-3C (n=100 fibrils), PD-3G (n=92 fibrils), MSA-1(n=115 fibrils), MSA-2(n=105 fibrils), MSA-3(n=102 fibrils), MSA-4(n=110 fibrils), MSA-5 (n=102 fibrils), Fibrils (n=116 fibrils), Ribbons (n=104 fibrils). Data are mean±std.dev. Data in this figure was generated by Dr. Alexis Fenyi and Dr. Luc Bousset from Ronald Melki's group.

To confirm that α-synuclein assemblies templated their conformation onto endogenous monomeric α-synuclein, proteinaceous aggregates were isolated from seeded neuronal lysates and tested for limited proteolysis. Endogenously generated aggregates were isolated from seeded neuronal lysates by ultracentrifugation at 100 000 g and probed for α-synuclein through immunoblotting. A cocktail of three α-synuclein antibodies were used, ASyM (AA1-15), 4B12 (AA103-108), 10D2 (AA118-127), which were specific to the N- and C-terminals of α-synuclein (Landureau, Redeker, Bellande, Eyquem, & Melki, 2021). Limited proteolysis with increasing concentrations of Proteinase K (0, 0.01, 0.1, 1 µg/mL) after 1 h revealed that endogenously generated aggregates shared a similar proteolytic pattern (Figure 4.10a) compared to α-synuclein conformers newly assembled through protein misfolding cyclic amplification (Figure 4.5). Aggregates found in seeded neuronal lysates from PD-amplified fibrils displayed stronger resistance to Proteinase K digestion compared to aggregates induced by MSA-amplified fibrils (Figure 4.10b).

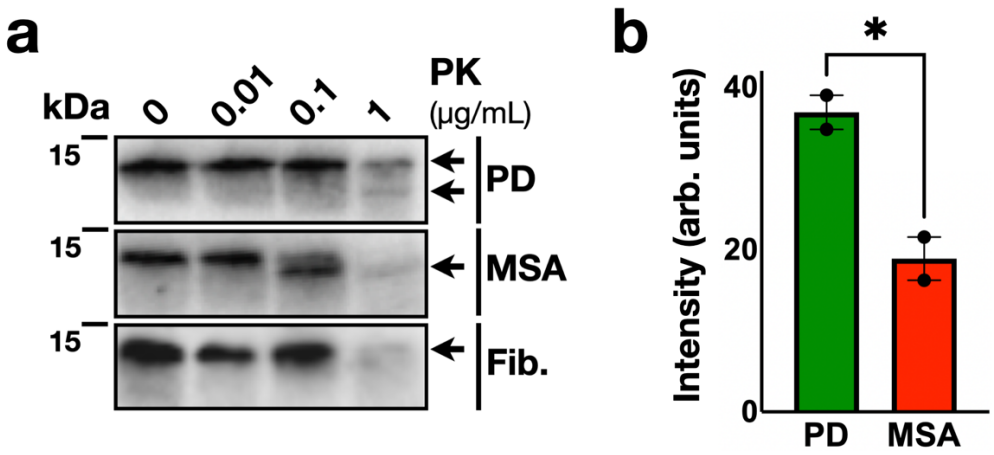


Figure 4.10 Limited proteolytic patterns of α-synuclein assembly-induced aggregates from iPSC-derived dopaminergic neurons

a, Proteinase K digestion (1 h) of seeded neuronal lysates ($SNCA^{TRIP}$) followed by immunoblotting with a combination of anti-α-synuclein antibodies (ASyM, 4B12, 10D2) revealed distinct fragments and resistance to proteolysis in PD-seeded versus MSA-seeded neuronal aggregates (immunoblot representative of $n=2$ independent experiments. **b,** Endogenously generated neuronal aggregates demonstrated similar proteolytic patterns to α-synuclein assemblies characterised in Figure 4.5, PD-seeded aggregates (1 µM) exhibited higher resistance to proteolysis compared to MSA-seeded aggregates (1 µM). In panel **b,** data are mean±s.e.m, $^{*}P<0.05$, by two-sided unpaired Student's t-test. Data in this figure was generated by Dr. Alexis Fenyi and Dr. Luc Bousset from Ronald Melki's group.

4.2.3 Brain-amplified α-synuclein assemblies are neurotoxic in SNCA^{TRIP} dopaminergic neurons

I then sought to investigate the effect of distinct α-synuclein assemblies on neuronal viability. Multiple studies have demonstrated through biochemical and cellular assays that α-synuclein assemblies displayed toxicity to various extents in rodent models (Bousset et al., 2013; Peelaerts et al., 2018; Shahnawaz et al., 2020; Soto & Pritzkow, 2018), but not in human stem cell-derived dopaminergic neurons. I observed that in SNCA^{TRIP} dopaminergic neurons, pSYN-positive aggregates triggered by PD-amplified (1 μM) or MSA-amplified (1 μM) fibrils caused the loss of neuronal axonal integrity as evidenced by tyrosine hydroxylase (Figure 4.7a) and TUJ1 immunostaining (Figure 4.11a), which was accompanied by progressively increased nuclear fragmentation (Figure 4.11b/c). Nuclear fragmentation at 2 weeks post-seeding resulted in approximately 30% loss of viable neurons as assess by nuclear fragmentation in both healthy control and SNCA^{TRIP} dopaminergic neurons (Figure 4.11b). This phenotype further progressed by 3 weeks post-seeding only in SNCA^{TRIP} neurons seeded with PD-amplified fibrils (60% death) and MSA-amplified fibrils (80% death; Figure 4.11c). Interestingly, at 3 weeks post-seeding, the progressive decline in neuronal viability was not observed in healthy control dopaminergic neurons (Figure 4.11c). Overall, MSA-amplified fibrils were more neurotoxic compared to PD-amplified fibrils.

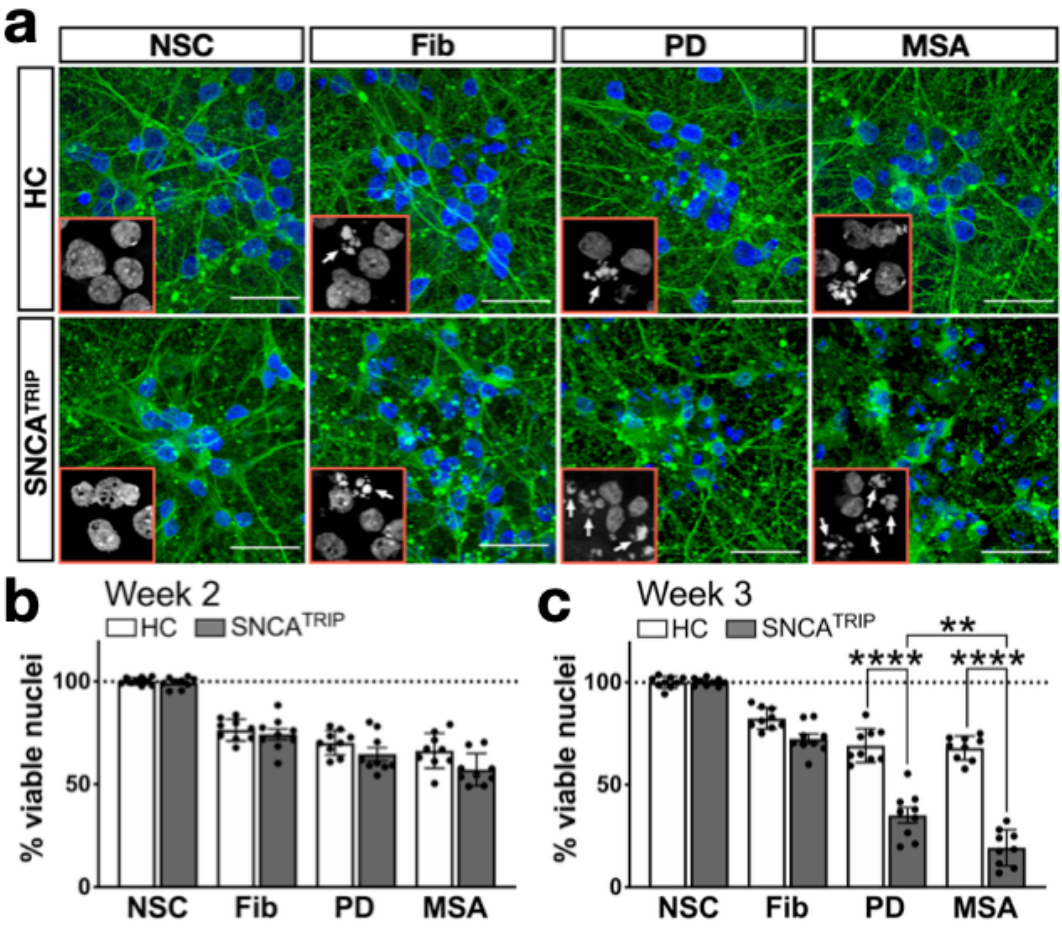


Figure 4.11 Progressive neurodegeneration in PD- and MSA-seeded SNCA^{TRIP} dopaminergic neurons

a, Representative confocal images from three independent differentiations depicting nuclear fragmentation (DAPI) and axonal degeneration (TUJ1), which were especially prominent in SNCA^{TRIP} dopaminergic neurons treated with PD- and MSA-amplified fibrils (1 μM). Healthy control (top) and SNCATRIP (bottom) lines were treated with *de novo* fibrils, PD- or MSA-amplified fibrils (scale bar: 30 μm). **b,** Viability was similar across conditions in healthy control (n=9) and SNCA^{TRIP} (n=9) neurons at 2 weeks post-seeding. **c,** Increased nuclear fragmentation was detected in SNCA^{TRIP} dopaminergic neurons exposed to MSA-amplified fibrils followed by PD-amplified fibrils at 3 weeks post-seeding (n=9). Healthy control lines did not exhibit a similarly progressive phenotype (n=9). NSC, non-seeded control, non-treated control. Each dot corresponds to one clone differentiated once and data are shown as mean±s.e.m. In panels **b,c,** $^{**}P<0.01$,$^{****}P<0.0001$ by one-way ANOVA followed by Tukey's multiple comparison test.

To exclude the effects of contaminants from brain homogenates, I tested blindly each individual (not pooled) brain-amplified batch against its corresponding brain homogenate that was used for amplification to its final dilution (PD cases, *n*=3; MSA cases, *n*=5). Control homogenates and corresponding brain-amplified assemblies were tested in parallel at 3 weeks post-seeding on a single $SNCA^{TRIP}$ clone that was differentiated three times (Figure 4.12). These results confirmed that neuronal death was caused by brain-amplified α-synuclein assemblies and not contaminants within the brain homogenates used to generate and amplify fibrils. Additionally, monomeric α-synuclein had no effect on neuronal viability. Consistent with the finding that pooled MSA-amplified assemblies were more neurotoxic compared to pooled PD-amplified assemblies (Figure 4.11), the mean viability of $SNCA^{TRIP}$ dopaminergic neurons exposed to each individual brain-amplified MSA assembly (average of 5 cases: 54.18% viable cells ±3.91% s.e.m.) was also significantly decreased (p=0.03) compared to individually tested PD-amplified assemblies (average of 3 cases: 62.10% viable cells ±2.78% s.e.m., Figure 4.12).

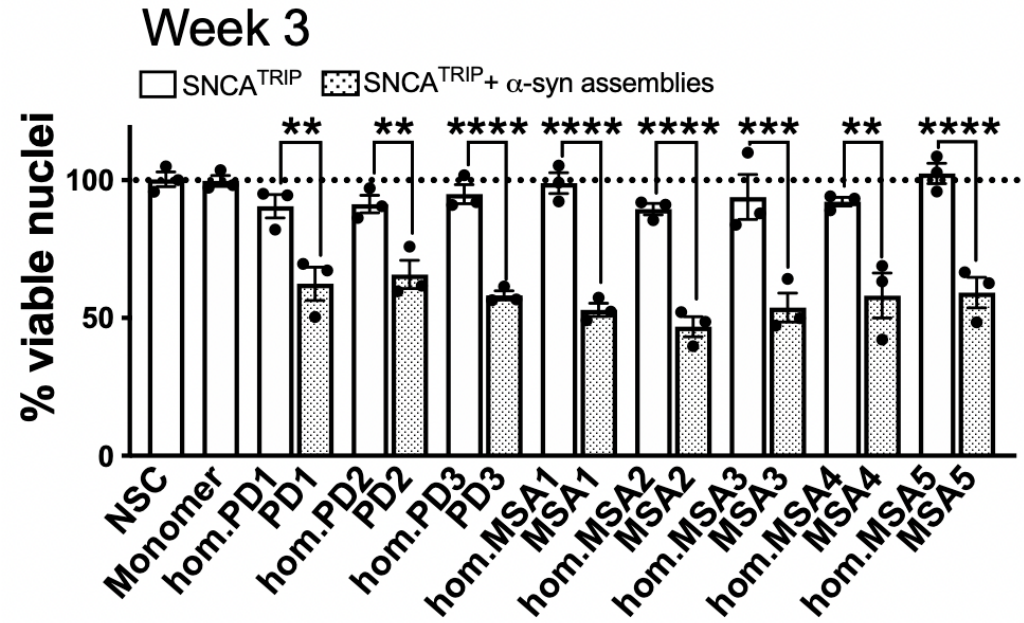


Figure 4.12 α-Synuclein monomer and homogenates from each PD and MSA case did not cause toxicity in contrast to corresponding amplified α-synuclein assemblies in SNCA^{TRIP} dopaminergic neurons

To exclude the effects of contaminants in patient brain homogenates, homogenate from each brain-amplified batch was tested blindly against its corresponding brain homogenate used for amplification. Brain homogenates from each case (1 μM) had no effect on viability, whereas each individual brain-amplified case (1 μM) from 3 PD and 5 MSA cases were neurotoxic at 3 weeks post-seeding (n=3). Monomeric α-synuclein (1 μM) had no effect on viability. NSC, non-seeded control, non-treated control. Each dot corresponds to one clone differentiated once and data are shown as mean±s.e.m. **P<0.01,,***P<0.001, ****P<0.0001 by one-way ANOVA followed by Tukey's multiple comparison test.

To further assess the toxic phenotype observed in dopaminergic neurons treated with patient brain-amplified α-synuclein assemblies, levels of neurofilament light chain (NfL) were measured in the conditioned media of neurons exposed to various α-synuclein assemblies. Detection of NfL in the blood and cerebrospinal fluid has been established as diagnostic marker in patients suffering from neurodegeneration (Bacioglu et al., 2016; Byrne et al., 2017; Mattsson, Andreasson, Zetterberg, Blennow, & Initiative, 2017)—and more recently in an *in vitro* model of α-synuclein seeded aggregation (Barth et al., 2021). NfL measurements were performed using the highly sensitive Single Molecule Array (Simoa) technology by Dr. Melanie Barth and Dr. Gaye Tanriöver from Mathias Jucker's group as a collaboration within the IMPRiND Consortium. We found that at two weeks post-seeding, NfL release in the conditioned medium was highest in $SNCA^{TRIP}$ dopaminergic neurons treated with MSA-amplified α-synuclein fibrils (1 µM, Figure 4.13b), whilst no differences between treatment groups were detected in healthy control neurons (Figure 4.13a). Interestingly, although not statistically significant, both healthy control and patient neurons exposed to *de novo* generated fibrils exhibited reduced mean differences in levels of NfL compared to treatments with brain-amplified assemblies. I have shown that *de novo* generated fibrils induce slight deficits in cell viability (Figure 4.11), therefore the discrepancy in NfL release could reflect differences in neuronal remodelling processes occurring in neurons specifically exposed to *de novo* fibrils (Reinert et al., 2020; Zucchi et al., 2020).

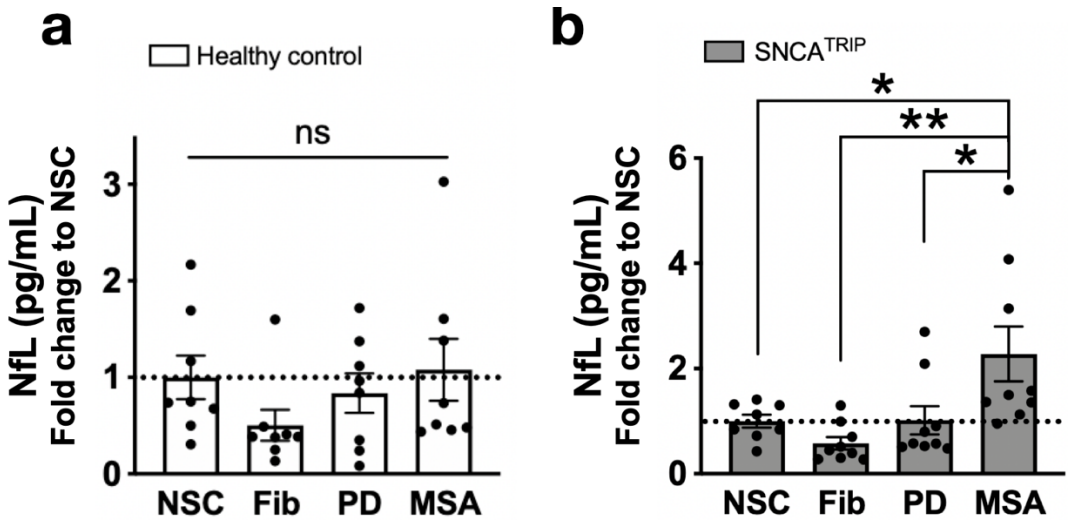


Figure 4.13 Neurofilament light chain release in dopaminergic neurons exposed to *de novo* and patient brain-amplified α-synuclein fibrils

a, Healthy control (*n*=9) and **b,** SNCA^{TRIP} (*n*=9) dopaminergic neurons were exposed to *de novo* and patient brain-amplified α-synuclein fibrils at DIV45 and neurofilament light chain (NfL) release was quantified in conditioned media using Single Molecule Array (Simoa) technology at two weeks post-seeding. Conditioned medium from MSA-amplified fibril-treated SNCA^{TRIP} neurons exhibited the highest amounts of NfL release compared to neurons exposed to PD-amplified fibrils or *de novo* fibrils. NSC, non-seeded control, non-treated control. Each dot corresponds to one clone differentiated once and data are shown as mean±s.e.m. $^{\#}$P=0.06, **P*<0.05,***P*<0.01, by one-way ANOVA followed by Tukey's multiple comparison test. Data in this figure was generated by Dr. Melanie Barth and Dr. Gaye Tanriöver from Matthias Jucker's group.

Collectively, these data demonstrate in human dopaminergic neurons, that brain-amplified fibrils generate distinct patterns of pSYN-positive aggregation and proteotoxicity—supporting the existence of heterogenous α-synuclein strains within α-synucleinopathies that reflects disease severity in Parkinson's disease and multiple system atrophy.

4.2.4 α-Synuclein monomer levels is a critical determinant of assembly-induced toxicity in iPSC-derived dopaminergic neurons

4.2.4.1 Whole transcriptome analysis under seeded aggregation in iPSC-derived dopaminergic neurons

To further investigate molecular drivers of α-synuclein assembly-induced neuronal death, whole transcriptome analysis by bulk RNA-Seq was performed in iPSC-derived dopaminergic neurons under seeded aggregation. $SNCA^{TRIP}$ neurons were analysed at 1- and 2-weeks post-seeding with *de novo* generated fibrils (1 μM), pooled PD-amplified (1 μM) and pooled MSA-amplified fibrils (1 μM). The 1-week timepoint was selected as this was earliest timepoint at which a consistent pSYN signal was detected by homology time resolved fluorescence (Figure 3.12a). The 2-week timepoint was selected as this was when endogenous aggregation of pSYN was more prominent while neuronal loss remained minimal and similar across all conditions previously tested (Figure 4.6b and Figure 4.11b). Bioinformatic analysis was performed by collaborators, Dr. Devika Agarwal and Dr. David Sims. Principle component analysis (PCA) on the 1000 most variable protein-coding genes illustrated that samples segregated based on timepoint (1 or 2 weeks) and clustered based on the presence of aggregation irrespective of the α-synuclein used (Figure 4.14).

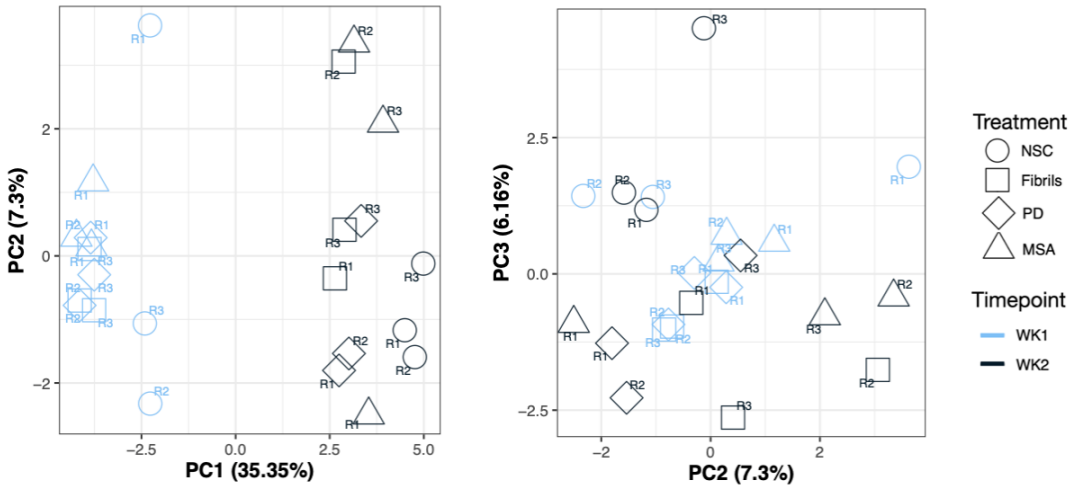


Figure 4.14 Principal component analysis on the 1000 most variable protein-coding genes by bulk RNA-Seq in seeded neurons vs non-seeded controls

Principle component analysis showed that samples clustered by time (week 1 vs. week 2) and treatment (aggregation vs. baseline) but not by α-synuclein assembly used (fibril concentration: 1 μM; *n*=3 per condition per timepoint). Data in this figure was analysed by Dr. Devika Agarwal and Dr. David Sims.

Based on the separation patterns described in the PCA plots, all aggregation conditions were pooled and differential gene expression tool, DESeq2, was used to identify significant differences between aggregation and baseline conditions at each timepoint. At 1-week post-seeding, a total of 11 genes were upregulated and 6 genes were downregulated in $SNCA^{TRIP}$ dopaminergic neurons (Figure 4.15). At 2-weeks post-seeding, a total of 19 genes were upregulated and 37 genes were downregulated in $SNCA^{TRIP}$ dopaminergic neurons (Figure 4.15). The low number of hits in this experiment may be attributed to a high variability present between iPSC clonal lines.

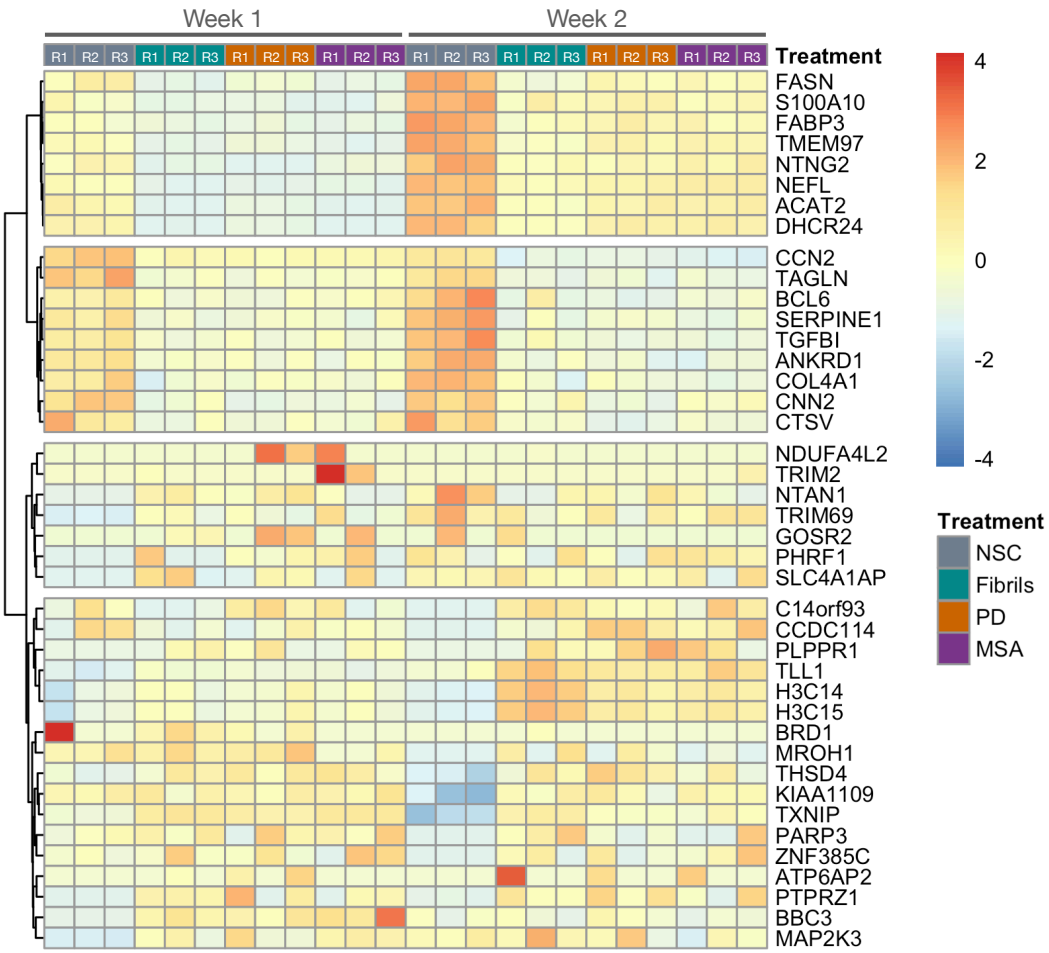


Figure 4.15 Differential gene expression by bulk RNA-Seq in seeded neurons vs. non-seeded controls

Heatmap of top 15 up and down differentially expressed genes at week 1 and week 2 post-seeding (1 μM), with scaled rlog transformed values across samples for each gene represented by colours on the corresponding row (*n*=3 per condition per timepoint). RNA-Seq data were deposited in GEO under accession number GSE171999. Data in this figure was analysed by Dr. Devika Agarwal and Dr. David Sims.

Moreover, to identify putative intracellular responses to α-synuclein aggregation, Gene Set Enrichment Analysis (GSEA) using Gene Ontology (GO) was performed. Several PD-relevant pathways related to organelle homeostasis were enriched in the top 20 GO terms at 1- and 2-weeks post-seeding, however, the gene expression patterns associated with these terms did not reach statistical significance (p=0.05) with α-synuclein fibril addition (Figure 4.16). Notable week 1 GO terms included the Unfolded Protein Response and endoplasmic reticulum stress, endosomal and endosome to Golgi transport, and multivesicular sorting pathways (Figure 4.16, top). Week 2 GO terms included pathways such as, protein folding, membrane proteolysis, mitochondrial membrane protein insertion, organelle fusion and apoptosis (Figure 4.16, bottom).

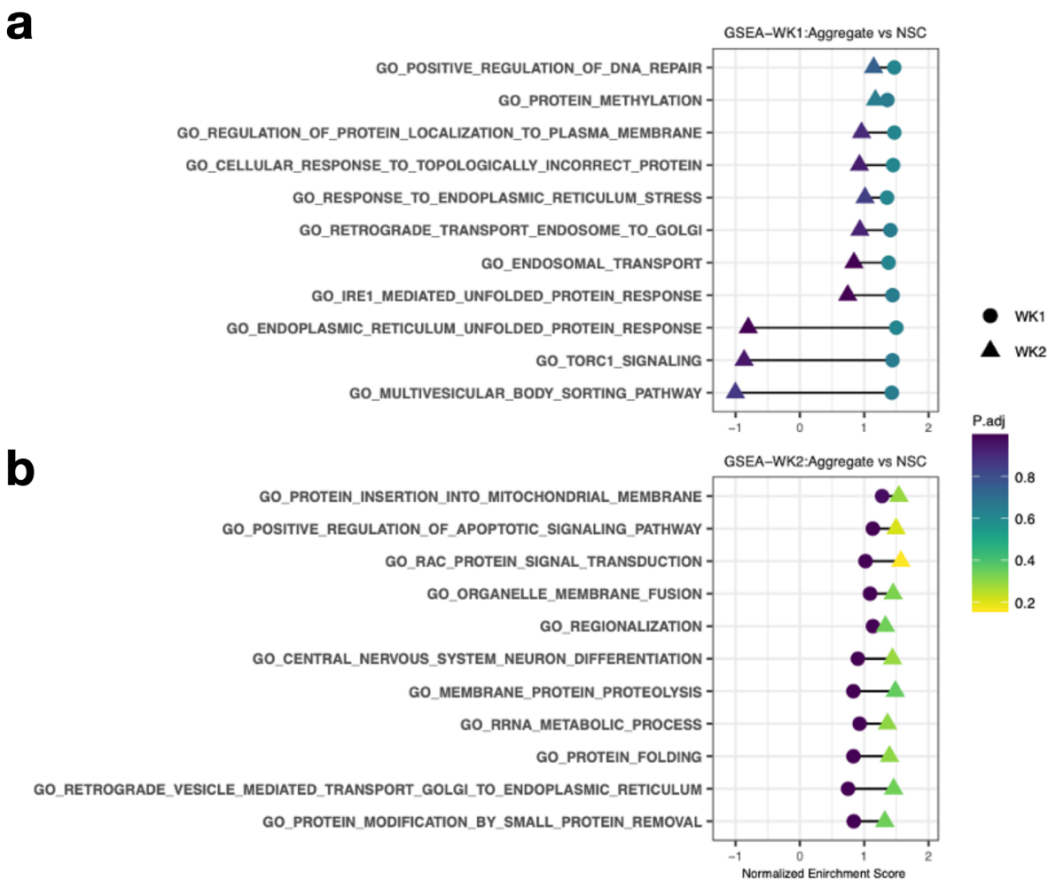


Figure 4.16 Gene set enrichment analysis by bulk RNA-Seq in seeded neurons vs. non-seeded neurons

Top 20 Gene Ontology (GO) terms identified using Gene Set Enrichment Analysis (GSEA) were enriched in biologically relevant pathways that differed at week 1 from week 2 suggesting a progressive impact of aggregation on organelle homeostasis (fibril concentration, 1 μM). Specifically, among the top 20 GO terms, Unfolded Protein Response and endoplasmic reticulum stress, endosomal and endosome to Golgi transport were up regulated at **a,** week 1 (*n*=3 per condition per timepoint) whereas protein folding, membrane proteolysis, mitochondrial membrane protein insertion, organelle fusion and apoptosis were detected in **b,** week 2 (*n*=3 per condition per timepoint). RNA-Seq data were deposited in GEO under accession number GSE171999. Data in this figure was analysed by Dr. Devika Agarwal and Dr. David Sims.

4.2.5 α-Synuclein fibril-induced aggregation impairs mitochondrial function in iPSC-derived dopaminergic neurons

I proceeded to functionally assess the impact of α-synuclein aggregation on one of the organelles identified by RNA-Seq (Figure 4.16), focusing on mitochondrial respiration. Extracellular flux analysis of oxygen consumption rates (OCR) was performed at 2 weeks post-seeding with *de novo* generated fibrils (1 μM), pooled PD-amplified (1 μM) and pooled MSA-amplified fibrils (1 μM). Exposure to each type of α-synuclein assembly led to a significant deficit in mitochondrial respiration which was similar across all assemblies used when corrected for total cell number in healthy control (Figure 4.17a) and $SNCA^{TRIP}$ dopaminergic neurons alike (Figure 4.17b). Of note, the effect size triggered by α-synuclein assemblies on mitochondrial respiration was greater in healthy controls compared to $SNCA^{TRIP}$ neurons (Figure 4.17). This result may be explained by differences in baseline OCR rates between healthy controls (200-400 pmol/min) and $SNCA^{TRIP}$ neurons (100-200 pmol/min). Baseline OCR rates in healthy control and patient lines were quantified in Chapter 5 (Figure 5.20). The significantly lower baseline OCR in $SNCA^{TRIP}$ neurons suggests that mitochondrial respiration is already impaired, therefore, reducing the dynamic range of the assay in these cells. It is also likely that lower OCR rates in $SNCA^{TRIP}$ neurons may be near the limit of detection and thus be less sensitive to changes in OCR resulting from fibril-induced mitochondrial impairments.

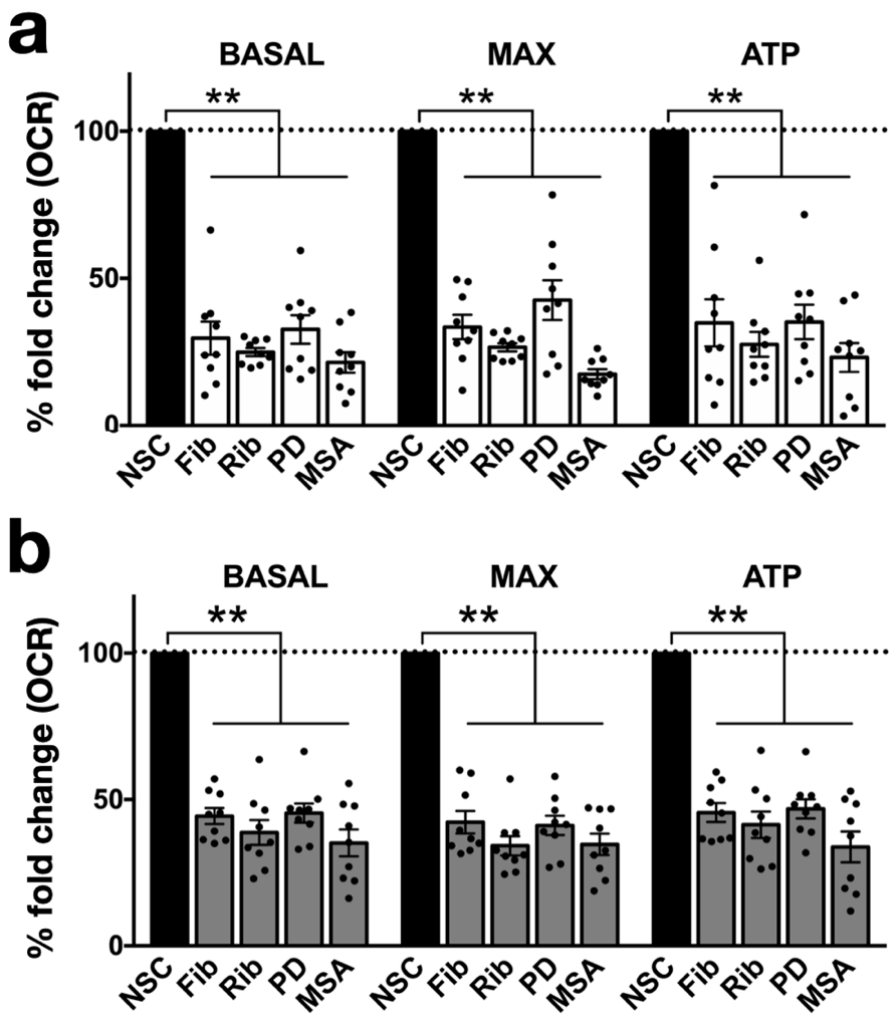


Figure 4.17 De novo fibrils and patient brain-amplified assembly disrupt mitochondrial respiration

De novo fibrils, ribbons, or brain-amplified fibrils (1 μM) similarly reduced oxygen consumption rate (OCR), maximal respiration and ATP production measured at 2 weeks post-seeding in both **a,** healthy control (n=9) and **b,** $SNCA^{TRIP}$ dopaminergic neurons (n=9). NSC, non-seeded control, non-treated control. Each dot corresponds to one clone differentiated once. Data are shown as mean±s.e.m. $^{**}P<0.01$ by one-way ANOVA followed by Tukey's multiple comparison test.

The reduction in mitochondrial respiration observed across all conditions as a result of α-synuclein fibril-induced aggregation was not associated with the loss of mitochondrial mass as demonstrated by immunoblotting of mitochondrial marker, TOM20 relative to β-actin (Figure 4.18). Furthermore, no differences were detected in components of the respiratory complex, using an antibody cocktail specific to the five subunits of the electron transport chain (Figure 4.18).

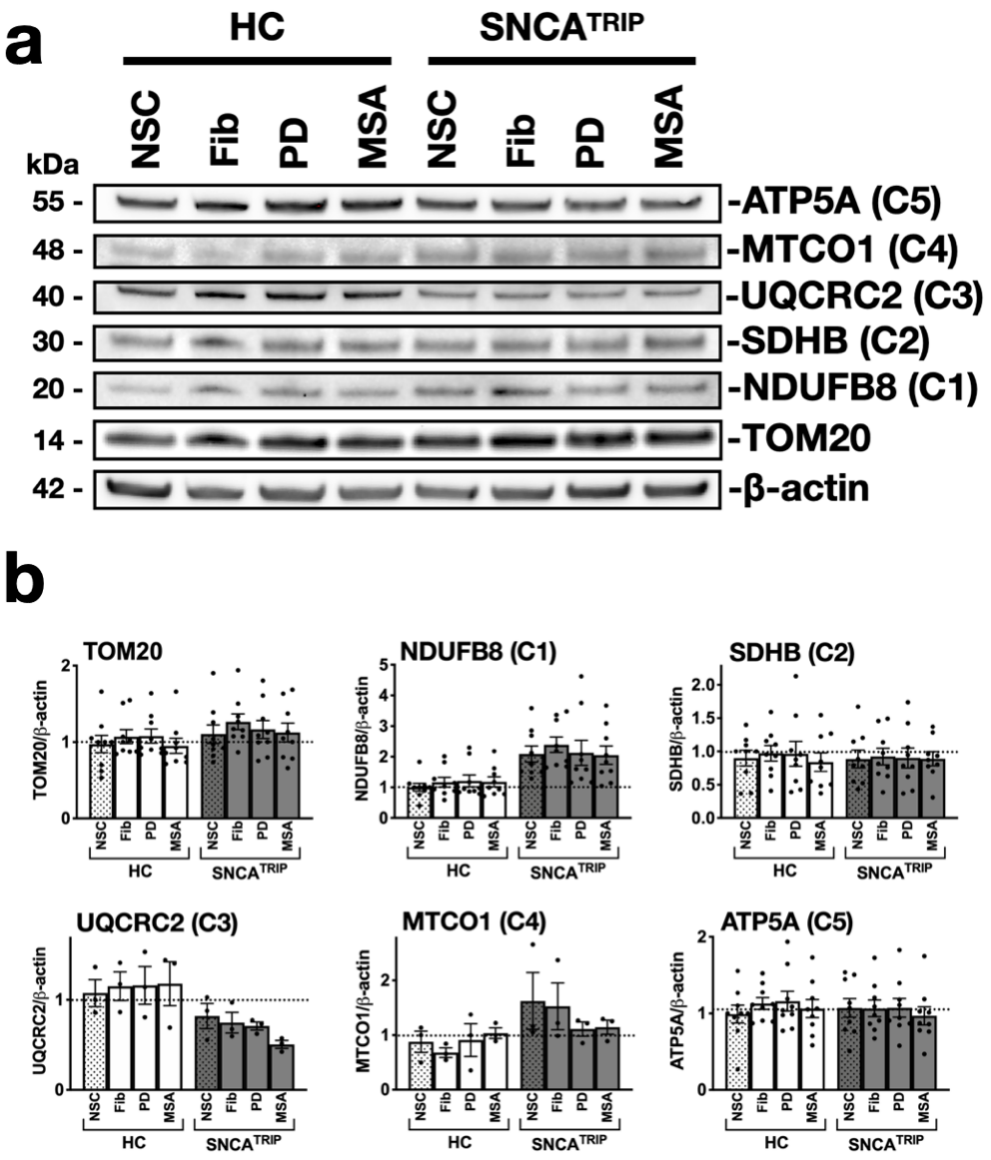


Figure 4.18 Assessment of mitochondrial function and OXPHOS complex proteins in response to treatment with *de novo* or brain-amplified α-synuclein fibrils

a, Representative immunoblots from three independent experiments showing no difference in respiratory complex components or levels of mitochondrial mass marker, TOM20, normalised to β-actin were detected in neuronal lysates 2 weeks post-seeding (1 μM). **b,** Quantification of corresponding immunoblots. NSC, non-seeded control, non-treated control. Each dot corresponds to one clone differentiated once. Data are shown as mean±s.e.m. Statistical significance was calculated by one-way ANOVA followed by Tukey's multiple comparison test.

Therefore, although oxidative phosphorylation was reduced under aggregation conditions, these results did not correlate with the extent of subsequent neuronal death observed in $SNCA^{TRIP}$ dopaminergic neurons treated with patient brain-amplified fibrils. In addition to the absence of any differential deficit observed in oxidative phosphorylation, no transcriptome pathway was identified by bulk RNA-Seq even at subtoxic levels of aggregation induced by 0.1 μM α-synuclein fibrils (Figure 4.19). Exposure to 0.1 μM α-synuclein fibrils triggered readily detectable levels of pSYN through homology time resolved fluorescence (Figure 3.12) but did not influence mitochondrial respiration in healthy control (Figure 4.19a) and $SNCA^{TRIP}$ (Figure 4.19b) dopaminergic neurons 2 weeks post-seeding. Likewise at 2 weeks post-seeding (0.1 μM), whole transcriptome analysis in healthy control (n=3) and $SNCA^{TRIP}$ (n=3) neurons did not reveal any significant pathways. Rather, PCA on the 1000 most variable genes showed that these samples clustered by genomic background rather than treatment type: non-seeded control versus α-synuclein fibril-induced aggregation (Figure 4.19c).

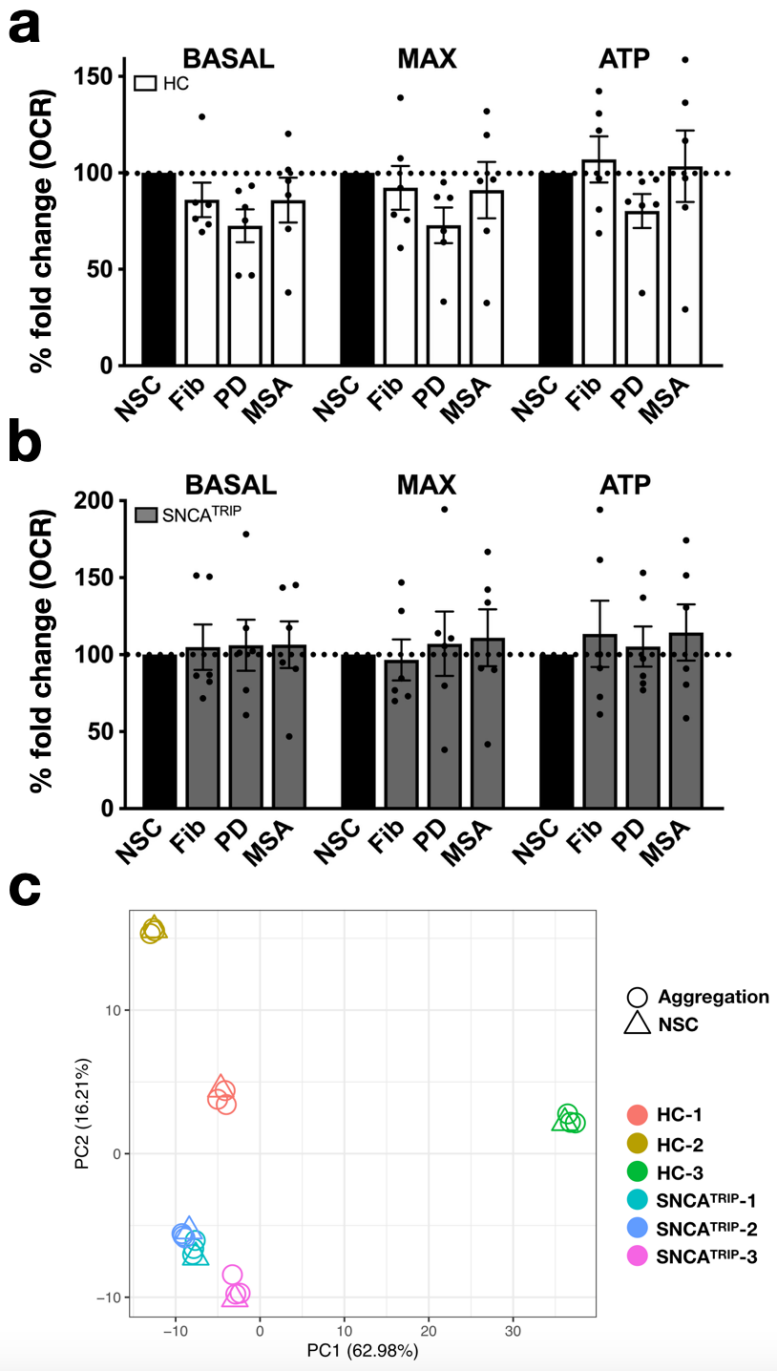


Figure 4.19 Characterisation of aggregation in iPSC-derived dopaminergic neurons treated with 0.1 µM fibrils

Seeded aggregation with either *de novo* generated or brain-amplified fibrils at 0.1 µM did not cause any overt deficit in OCR, maximal respiration and ATP production in **a,** healthy control (*n*=6) or **b,** SNCA^{TRIP} neurons (*n*=6). **c**, Principle component analysis (PCA) on the 1000 most variable protein-coding genes in samples seeded with 0.1 µM seeds (*de novo* fibrils, PD- or MSA-amplified fibrils) clustered by genomic background rather than treatment type (NSC vs. aggregation). NSC, non-seeded control, non-treated control. For panels **a** and **b,** each dot corresponds to one clone differentiated once and data are mean±s.e.m. Statistical significance was calculated by one-way ANOVA followed by Tukey's multiple comparison test. RNA-Seq data in panel **c** were deposited in GEO under accession number GSE149632. Data in panel **c** was analysed by Dr. Devika Agarwal and Dr. David Sims.

4.2.6 Isogenic correction of α-synuclein levels reduces neurodegeneration

To investigate the relevance of α-synuclein levels and exclude genomic background confounders, I assessed the effect of fibril treatment on a different pair of isogenic $SNCA^{TRIP}$ clones characterised previously (Heman-Ackah et al., 2017). In healthy persons, 2 copies of SNCA are present (Figure 4.20a), however patients harbouring the triplication mutation possess 4 copies of SNCA (Figure 4.20b). Isogenic correction of the triplication locus required excision of the two aberrant SNCA copies on one of the alleles (red box, Figure 4.20b). Isogenic correction of α-synuclein levels was sufficient to reduce aggregation (Figure 4.20c) and reverse neuronal death (Figure 4.19d). Exposure to 1 μM *de novo* generated α-synuclein fibrils revealed that isogenic correction in $SNCA^{TRIP}$ ($SNCA^{ISOTRIP}$) resulted in decreased pSYN accumulation to levels comparable with healthy control dopaminergic neurons at 2 weeks post-seeding (Figure 4.6b). Furthermore, $SNCA^{ISOTRIP}$ neurons did not exhibit the same vulnerability to PD- and MSA-amplified α-synuclein fibrils found in $SNCA^{TRIP}$ neurons. Exposure to 1 μM *de novo* generated, and patient brain-amplified fibrils did not induce progressive neuronal loss in $SNCA^{ISOTRIP}$ neurons at 3 weeks post-seeding compared to in $SNCA^{TRIP}$ neurons. Therefore, a 2.5-fold increase in endogenous monomeric α-synuclein levels in $SNCA^{TRIP}$ neurons was sufficient to account for their differential vulnerability—most likely due to a critical burden of proteotoxic conformers being reached.

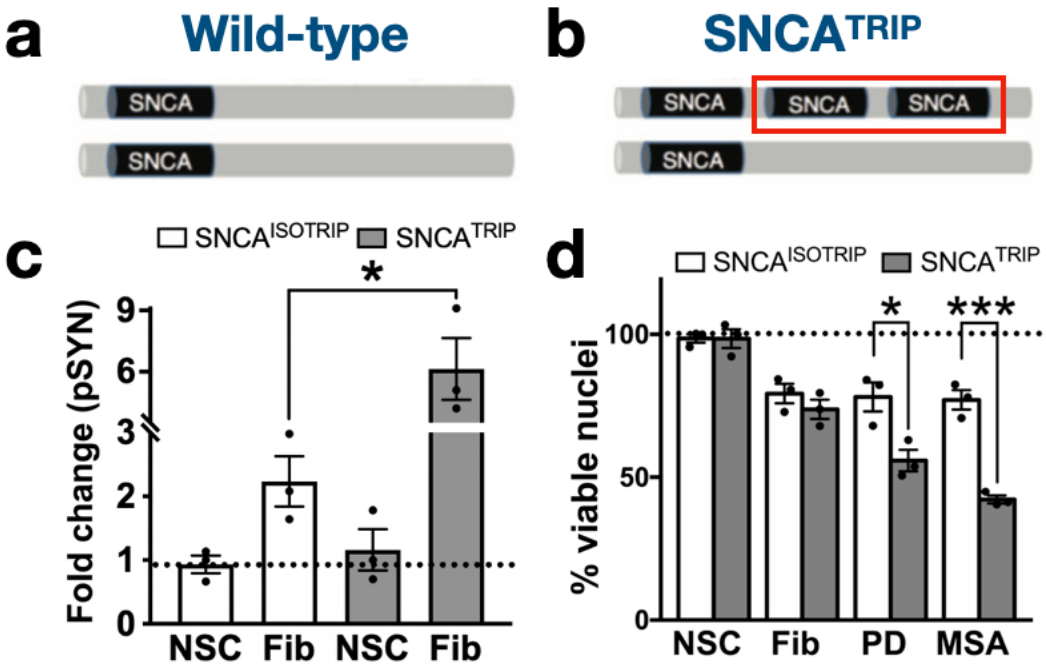


Figure 4.20 α-Synuclein expression is a critical determinant of assembly-induced toxicity

a, Schematic representation of wild-type or physiological α-synuclein with 2 allelic copies of SNCA and **b,** α-synuclein triplication with 4 allelic copies. An isogenic control line was generated from an α-synuclein triplication clone ($SNCA^{ISOTRIP}$) by collaborators (Heman-Ackah et al., 2017). To engineer the $SNCA^{ISOTRIP}$ line, CRISPR/Cas9 was used to excise the 2 extra SNCA copies residing in the triplication zone and to subsequently normalise α-synuclein levels. **c,** α-Synuclein fibril-induced aggregation (1 μM) was partially rescued through isogenic correction as assessed by homology time resolved fluorescence specific to pSYN. $SNCA^{ISOTRIP}$ neurons (n=3) accumulated significantly less pSYN compared to its corresponding $SNCA^{TRIP}$ line (n=3) 2 weeks post-seeding. **d,** Nuclear fragmentation in $SNCA^{TRIP}$ dopaminergic neurons (n=3) 3 weeks post-seeding (1 μM) was also rescued by isogenic correction of SNCA expression (1 μM). NSC, non-seeded control, non-treated control. Each dot corresponds to one clone differentiated once. Data are shown as mean±s.e.m. *P<0.05, ***P<0.001 by one-way ANOVA followed by Tukey's multiple comparison test.

4.3 Discussion

PMCA is an established technique that offers the ability to study phenotypes that arise uniquely from conformationally distinct α-synuclein strains, as their amplification is performed in the absence of potential contaminants or post-translational modifications inherent to studies on tissue extracts (Alexis Fenyi et al., 2019b; Saborio et al., 2001; Strohäker et al., 2019; Van der Perren et al., 2020). In collaboration with Ronald Melki's group, we showed that α-synuclein assemblies amplified in the presence of human brain homogenate generated ThT-positive seeds that were of fibrillar nature as seen in electron micrographs (Figure 4.4). PD- and MSA-amplified assemblies adopted a twisted shape and exhibited distinct limited proteinase K digestion patterns compared to *de novo* generated fibrils (Figure 4.5), suggesting that amplified fibrils indeed represent conformational strains and can be discriminated as described in the literature (Shahnawaz et al., 2020).

However, the full extent to which fibrils amplified with brain homogenate resemble those found within the brain requires the resolution of their cryo-EM structures. Recently, the cryo-EM structures of fibrils amplified in the presence of sarkosyl-extracted α-synuclein seeds from multiple system atrophy brain homogenates, were found to display some level of heterogeneity between the amplified product and starting material (Lövestam et al., 2020). This result suggests that multiple factors which are yet unknown, contribute to α-synuclein conformation. It is also likely that the use of detergents such as sarkosyl may have interfered with relevant factors required for faithful amplification. In contrast, PMCA α-synuclein assemblies used in this study were directly amplified from brain homogenates in the absence of any detergent or potential ligands. In one study, sarkosyl-extracted aggregates from post-mortem brains revealed that α-synuclein in glial cytoplasmic inclusions was more resistant to proteolysis compared to α-synuclein found in Lewy

bodies (Peng, Gathagan, Covell, et al., 2018), however, we found the reverse to be true in samples processed without detergents (Figure 4.5). Unlike protocols which depend on detergent-based protein enrichment, PMCA has been shown to faithfully reproduce α-synuclein folds based on electron micrographs and proteolytic patterns (Burger et al., 2021). We have shown that amplified α-synuclein isolated from Parkinson's disease brains are more resistant to proteolysis compared to fibrils amplified from multiple system atrophy brains (Figure 4.5). Likewise, we found these proteolytic patterns to be matching in RIPA-insoluble fractions from neuronal lysates seeded with brain-amplified α-synuclein assemblies (Figure 4.10), which confirms a degree of congruity between α-synuclein in PMCA fibrils and in intracellular aggregates.

Importantly, I demonstrated that α-synuclein assemblies amplified in the presence of human brain homogenate exert distinct patterns of intraneuronal aggregation and neurotoxicity, causing the death of human neurons with increased α-synuclein levels—in a manner that reflects disease severity in Parkinson's disease and multiple system atrophy patients. Brain-amplified fibrils induced similar levels of pSYN accumulation compared to *de novo* generated fibrils (Figure 4.6), yet brain-amplified fibrils, and MSA-amplified assemblies in particular, were significantly more neurotoxic (Figure 4.11 and Figure 4.13). These data suggest that the death of neurons may be caused, at least partly, by the differential toxicity of brain-amplified α-synuclein assemblies. And that MSA-amplified fibrils do indeed represent a distinct strain compared to PD-amplified fibrils (Prusiner et al., 2015). Previous studies also reported differential cytotoxicities by using brain-amplified assemblies in immortalised cell lines and primary cultures, but not in human neurons (Peng, Gathagan, Covell, et al., 2018; Shahnawaz et al., 2020).

It remains an open question whether oligomeric or filamentous α-synuclein strains in Parkinson's disease patients consists of a single species or of an ensemble

of conformationally distinct α-synuclein conformers. The ultrastructure of glial cytoplasmic inclusions found in multiple system atrophy brains was recently resolved by cryo-EM and shown to consist of two types of filaments (Schweighauser et al., 2020). Thus, it is plausible that several strain 'subtypes' within Parkinson's disease brains also exist. In experiments where I sought to assess the effects of PD- and MSA-amplified assemblies on neuronal viability (Figure 4.11), α-synuclein assemblies from individual cases were pooled based on disease type (PD, 3 cases; MSA, 5 cases). When tested individually, each α-synuclein assembly triggered relatively equal levels of aggregation as assessed by pSYN signal (Figure 4.6), therefore providing the rationale to pool disease-specific assemblies in subsequent functional assays. Importantly, the three PD cases tested displayed similar levels of neurotoxicity compared to each other—likewise, the five MSA cases tested also exhibited similar neurotoxicities (Figure 4.12). By analysing the effects of pooled α-synuclein assemblies, the data generated provide an insight into the average effect of PD- and MSA-amplified assemblies.

Human $SNCA^{TRIP}$ dopaminergic neurons but not healthy control neurons exhibited progressive degeneration in response to brain-amplified fibrils (Figure 4.11). In my hands, $SNCA^{TRIP}$ dopaminergic neurons expressed approximately 2.5-fold more α-synuclein compared to controls (Figure 3.12). The enhanced expression of α-synuclein in triplication neurons may have contributed to their accelerated cell death in response to brain-amplified assemblies, which concurs with results from animal models demonstrating that α-synuclein expression is linked with selective vulnerability in neurons (Courte et al., 2020; Henderson, Cornblath, et al., 2019; Luna et al., 2018). Therefore, I infer that in human dopaminergic neurons, the presence of toxic α-synuclein assemblies combined with increased endogenous monomeric α-synuclein levels both act as fundamental players in neurodegeneration.

α-Synuclein is intrinsically prone to aggregate and is highly expressed in the brain, likely through its functional properties in neurons (Monsellier & Chiti, 2007; Oosawa & Asakura, 1975; Tartaglia, Pechmann, Dobson, & Vendruscolo, 2007). Conformational α-synuclein strains may exist in a state of equilibrium and oligomerise in a stochastic fashion throughout the course of one's life—thus having a persisting tendency to form aggregates (Peelaerts et al., 2018). Nonetheless, accumulation of α-synuclein is a rare occurrence in healthy brains and incidental Lewy pathology is believed to represent prodromal stages of Parkinsonism (Frigerio et al., 2011). Under physiological conditions, the expression levels of α-synuclein and its oligomerisation are maintained within a safe range through a host of proteins which target aggregation and modulate degradation (Dobson, 1999; Knowles, Vendruscolo, & Dobson, 2014). Proteostasis is maintained by the ubiquitin proteasome system, molecular chaperones, and autophagosome-lysosomes that selectively degrade and clear misfolded α-synuclein (Vilchez et al., 2014). These systems comprise a cell's natural defence against protein aggregation, however, in disease (*SNCA* mutations; missense mutations: $SNCA^{A53T}$, $SNCA^{E46K}$ and gene multiplications: duplication, triplication), ageing or environmental stressors, proteostatic balance is disrupted and the efficiency of cellular defensive mechanisms is reduced. These factors in turn promote pathology through the formation of aggregates whose growth rate outbalances their clearance rate.

Using a stem cell line isogenically corrected for $SNCA^{TRIP}$ (Heman-Ackah et al., 2017), I demonstrated that reduced expression of α-synuclein was sufficient to rescue the aggregation and neurodegenerative phenotype observed in $SNCA^{TRIP}$ dopaminergic neurons (Figure 4.20), normalising pSYN accumulation and nuclear fragmentation to levels comparable with healthy control neurons. Differential toxicity was observed in neurons exposed to PD- and MSA-amplified assemblies at 3 weeks

post-seeding in all SNCA^{TRIP} lines, a timepoint where no differential effect was detected in healthy control or isogenic lines. This finding reinforces the notion that levels of endogenous α-synuclein, by significantly increasing the aggregation potential in individual neurons, is a major driver behind strain-induced toxicity. However, it is possible that differential toxicities could also be detectable at a later timepoint beyond 3 weeks in control neurons. Further characterisation of brain-amplified fibrils in various cell lines from α-synucleinopathic patients, to assess survival, may reveal additional factors that render neurons susceptible to death.

α-Synuclein strains have been shown to target distinct brain regions and cell types (A. Lau et al., 2020). In this study, I modelled seeded aggregation of α-synuclein in a reductionist manner by solely culturing human dopaminergic neurons (Tanudjojo et al., 2021). Future studies may attempt to reproduce the phenotypes observed in dopaminergic neurons but in other cell types such as cortical or motor neurons. More recently, human midbrain organoids have become available and provide an additional model to study α-synuclein aggregation (Jo et al., 2021; M.-H. Lee et al., 2021). As cellular environment impacts strain conformation (Peng, Gathagan, Covell, et al., 2018), *in vitro* studies modelling seeded aggregation in a co-culture system consisting of neurons, astrocytes, and glia also provide a valuable platform to investigate mechanisms underlying cell to cell interactions (Fernandes, Chutna, Chu, Conde, & Outeiro, 2016). For example, one study demonstrated that exposure to monomeric α-synuclein disrupted the integrity of the blood-brain barrier in rat brain endothelial cells co-cultured with rat pericytes (Dohgu et al., 2019). Here, Dohgu et al. (2019) showed the interaction between α-synuclein and pericytes impaired endothelial permeability through the release of inflammatory compounds. Neuroinflammation in Parkinson's disease and more broadly neurodegeneration has been modelled extensively; and the crosstalk between microglia and astrocytes in a co-culture system has been reported

to contribute towards the degradation of aggregate-prone proteins such as α-synuclein and amyloid-β (Rostami et al., 2021). Together with DPhil candidate Antigoni Katsikoudi from our lab, we developed a more complex model of seeded aggregation by co-culturing iPSC-derived dopaminergic neurons with iPSC-derived microglia. Our preliminary data revealed that aggregation triggered by *de novo* generated fibrils was significantly reduced in the presence of healthy control microglia compared to $SNCA^{TRIP}$ dopaminergic neurons alone. Upon further characterisation of this model, future studies would benefit from investigating the effect of patient brain-amplified fibrils on disease phenotypes in these co-cultures—with the aim of understanding mechanisms of neuroprotection and equally, neurodegeneration.

How PD- and MSA-amplified α-synuclein assemblies cause neuronal death is not fully understood and research in this area is in its early stages (Delenclos et al., 2019). Whole transcriptome analysis of α-synuclein aggregation in human iPSC-derived dopaminergic neurons identified dysregulated pathways that were specific to timepoints at 1-week and 2-weeks post-seeding (Figure 4.16). However, due to a substantially high degree of variability between cell lines used, including clonal lines, the total number of significant hits generated was lower than expected. Furthermore, increased variability may account for the fact that our RNA-sequencing data was unable to replicate the finding that *SNCA* mRNA was upregulated upon seeded aggregation. Under the current experimental conditions (n=3), the results from our power calculations determined that a total sample size of 12 independent biological repeats was necessary to generate meaningful hits with a p value cut-off of 0.05 (Abrams, Johnson, Huang, Payne, & Coombes, 2019). The additional 9 independent repeats are currently underway. Principle component analysis in the 1000 most variable protein-coding genes likewise revealed that samples clustered based on timepoint (1-week or 2-weeks post-seeding) and treatment (baseline vs. aggregation)

but was not able to discriminate the type of α-synuclein assembly used (Figure 4.13). Therefore, subsequent pathway analysis was performed by comparing non-seeded controls to aggregation conditions, pooling the data from *de novo* generated fibrils and PD- and MSA-amplified assemblies.

Consistent with previous research, gene ontology terms in seeded dopaminergic neurons revealed dysregulated pathways which recapitulate events in the aggregation cascade (Borrageiro et al., 2018). Upon addition of exogenous α-synuclein fibrils, impaired endosomal and autophagosome function has been reported in primary cultures and is considered to be an early effect of aggregation (Volpicelli-Daley, Gamble, et al., 2014). α-Synuclein is found within endosomes and has also been shown to interact with numerous factors involved in the intracellular trafficking of vesicles such as early endosomes or multivesicular bodies (T. Hasegawa et al., 2011; Tofaris et al., 2017). In addition, α-synuclein modulates vesicle trafficking through its interaction with prenylated Rab acceptor protein 1 localised to the Golgi apparatus and late endosomes (H. J. Lee, Kang, Lee, & Im, 2011). α-Synuclein is also associated with members of the SNARE complex, which is required for membrane fusion events between late endosomes and lysosomes/autophagosomes and synaptic vesicle fusion (Burré, Sharma, & Südhof, 2014; Burré et al., 2010; Nichols & Pelham, 1998). In accordance with these findings, gene set enrichment analysis of dopaminergic neurons at 1-week post-seeding revealed aberrations in endosomal transport, endoplasmic reticulum stress, retrograde transport from the endosome to the Golgi apparatus, and the multivesicular body sorting pathway (Figure 4.16 top). We found additional defects in the unfolded protein response at 1-week post seeding which was specifically mediated by inositol-requiring enzyme 1 (IRE1), a key activator that propagates the unfolded protein response signal from the endoplasmic reticulum to the cytosol (Adams, Kopp, Larburu, Nowak, & Ali, 2019). This finding correlates

strongly with a previous study using the same model cell line ($SNCA^{TRIP}$ dopaminergic neurons), which identified an endoplasmic reticulum stress phenotype, marked by the induction of the IRE1α /X-box-binding protein 1(XBP1) pathway and culminating in terminal unfolded protein response activation (Heman-Ackah et al., 2017).

By 2-weeks post-seeding, gene expression patterns related to apoptotic signalling and organelle membrane dysfunction were identified (Figure 4.16b). Although gene expression associated with the above gene ontology terms at both timepoints did not reach statistical significance, this analysis describes the evolution of pathology induced by seeded aggregation in human dopaminergic neurons. α-Synuclein possesses a highly lipophilic element which enhances its interaction with membranes and may ultimately disrupt lipid bilayers (Fusco et al., 2017). Altogether, transcriptomic analysis of seeded dopaminergic neurons suggests that the toxic gain of function of aggregated α-synuclein is diverse and to some extent mediated by deleterious effects on organelle membrane function (Fusco et al., 2014; Shrivastava et al., 2015). Yet, strain-specific effects on molecular pathways remain unknown. To this end, I am currently optimising methods to explore the effects of α-synuclein aggregation in cultured neurons at single cell resolution.

Protein insertion into the mitochondrial membrane was another gene ontology term identified in seeded dopaminergic neurons (Figure 4.16 bottom). Mitochondrial impairment in Parkinson's disease has been ascribed to aberrant interactions between α-synuclein oligomers and oxidative phosphorylation or aggregate-induced mitochondrial fragmentation (Di Maio et al., 2016; Ludtmann et al., 2018; Valdinocci, Kovarova, Neuzil, & Pountney, 2021; Zambon et al., 2019). In agreement with such findings, I observed a significant reduction in metabolic activity in both healthy control and $SNCA^{TRIP}$ dopaminergic neurons upon seeded aggregation (Figure 4.17). This reduction in mitochondrial respiration was not linked, in my hands, with decreased

mitochondrial mass as assessed by translocase of outer membrane 20 (TOM20) or with components of the respiratory chain (Figure 4.18) suggesting a functional impairment which does not necessarily correlate with the degree of subsequent neuronal death induced by brain-amplified fibrils (Figure 4.11).

It has been established that distinct α-synuclein conformers represent disease-specific strains with differential neurotoxicities (Burger et al., 2021; Melki, 2015; Peng, Gathagan, & Lee, 2018; Shahnawaz et al., 2020). Therefore, subtle differences in α-synuclein structure dictates the functional characteristics of α-synuclein assemblies such as their tropism for distinct neuronal populations and pathogenicities—and in particular, the amino acid side chains that protrude on the surface of aggregated α-synuclein, define and modulate its intracellular interactome (Peelaerts et al., 2018).

Our current understanding of α-synuclein's interactome is in its nascent phase, whether in the cytosol or on organellar membranes. Nonetheless, one may consider that α-synuclein polymorphs are able to interact with coinciding but unique protein groups. These differential interactions have yet to be shown to underlie disease phenotypes in the clinical setting, however such processes can be studied experimentally. Fibrillar α-synuclein is known to cross-seed with tau and amyloid-β, two key pathogenic proteins in Alzheimer's disease (Wong & Krainc, 2017). In this example, for instance, fibrillar tau was shown to trigger α-synuclein aggregation in an *in vivo* mouse model, suggesting that aggregate-prone proteins share some degree of biophysical homology as they were able to cross-seed each other (Williams, Sorrentino, Weinrich, Giasson, & Chakrabarty, 2020). At a molecular level, α-synuclein has also been shown to interact with other proteins, such as the α3-subunit of Na+/K+-ATPase, which is sequestered in the presence of fibrils and oligomers leading to decreased sodium extrusion (Shrivastava et al., 2015). In addition to protein sequestration, the interaction between aggregated α-synuclein and potential protein partners may also

result in their loss of function or redistribution—all of which inhibits homeostasis and leads to cell death. Understanding the mechanism of action of α-synuclein strain-induced toxicity thus relies on exploring the interactome/proteome of α-synuclein under seeded aggregation conditions.

Chapter 5

Mechanisms of Parkinson's disease-associated α-synuclein strain toxicity

5.1 Introduction

5.1.1 α-Synuclein protein interactome through proximity labelling

α-Synucleinopathies present with distinct clinical phenotypes which may arise from the structural differences between α-synuclein assemblies as outlined in Chapter 4. We hypothesized that the conformational differences between these assemblies may define distinct pattern of protein interactions. Therefore, elucidation of the physical interactions between α-synuclein assemblies and the cellular proteome may provide essential clues as to which culprit proteins drive disease or conversely, which proteins counteract the deleterious effects of misfolded α-synuclein. To date, over 530 protein interactors have been discovered for various forms of α-synuclein (https://thebiogrid.org/112506/summary/homo-sapiens/snca.html) but this work has not been done for α-synuclein as it assembles inside cells .

Firstly, co-immunoprecipitation was used in conjunction with mass spectrometry to identify and compare protein interactions of phosphorylated (serine 129) versus physiological α-synuclein (McFarland et al., 2008). Here, immunoprecipitation of physiological α-synuclein pulled down complexes that were highly enriched for oxidative phosphorylation proteins whereas pathogenic and phosphorylated α-synuclein pulled down proteins involved in vesicular trafficking and cytoskeletal maintenance. Although co-immunoprecipitation offers an unbiased and high-throughput strategy for identifying protein-protein interactions, this strategy depends heavily on the optimisation of lysis buffers to preserve bonds between

interacting proteins whilst avoiding contaminants. Thus, only stable protein complexes may be recovered using standard co-immunoprecipitation techniques and often confounded by contaminants. More recently, to counter the disruption of protein interactions by lysis buffer detergents, one group developed a UV-dependent protein cross-linking technique to covalently bind oligomeric α-synuclein to its interacting partners (van Diggelen et al., 2020). Cross-linked interactions with oligomeric α-synuclein combined with mass spectrometry in these experiments were enriched for membrane proteins and in particular, the sodium-potassium pump, synaptobrevin-2B, and voltage-dependent anion channels.

Secondly, candidate-based experiments have also demonstrated that specific interactions with α-synuclein are required for specific biological functions. For example, knockout of SNARE chaperone cysteine-string protein-α in mice revealed an interaction between α-synuclein and the SNARE complex, such as synaptobrevin-2 and SNAP-25 (M. Sharma et al., 2012). Complementary α-synuclein knockout studies further reinforced α-synuclein's involvement in SNARE complex assembly during exocytosis (Burré et al., 2014; Burré et al., 2010)—and linked its function to several steps in vesicle trafficking, such as endocytosis (Vargas et al., 2014). Additional low-throughput interaction experiments, involving the reconstitution of protein complexes also demonstrated an interaction between α-synuclein and Parkinson's disease-associated proteins such as microtubule-associated protein tau (P. H. Jensen et al., 1999) and Parkin (P. Choi et al., 2001).

Lastly, interactome mapping of specific proteins by proximity labelling has emerged as a prominent biochemical tool to identify protein-protein interactions in live cells (Qin, Cho, Cavanagh, & Ting, 2021; Trinkle-Mulcahy, 2019). In contrast to affinity purification techniques, proximity labelling relies on the ability to tag neighbouring proteins with biotin—which are subsequently detected using streptavidin and

identified through mass spectrometry. Proximity labelling by biotinylation confers several advantages including (i) the possibility to capture weak or transient interactions that can be lost during the processing of samples, (ii) the applicability of biotinylation towards both soluble and insoluble proteins, and (iii) the extraordinarily strong affinity between biotin and streptavidin, which is resistant to detergents and denaturing conditions and allows for high-stringency extractions that overall reduce background contaminants (D. I. Kim & Roux, 2016; Rees, Li, Perrett, Lilley, & Jackson, 2015). At present, protein mapping based on generating reactive biotin derivatives has been performed using two functionally similar techniques: biotinylation identification (BioID) and ascorbate peroxidase (APEX) proximity labelling.

The first-generation approach towards BioID utilised an engineered biotin ligase (BirA*) derived from *Escherichia coli* with mutation R118G at the catalytic site, which destabilises activated biotin (bitinoyl-5'-AMP) and allows it to form covalent bonds with exposed lysine residues of proximal proteins (Roux, Kim, Raida, & Burke, 2012). Under these conditions, a bait protein fused to BirA* biotinylates neighbouring proteins within a 10 nm radius (D. I. Kim et al., 2014). BioID (35 kDa) consists of 321 amino acids and is slightly larger than green fluorescent protein, which in some instances prevented the efficient targeting of certain fusion proteins (D. S. Liu, Loh, Lam, White, & Ting, 2013). To circumvent this limitation, a novel and more efficient BioID2 (28 kDa) system was developed by substituting *Escherichia coli*-derived biotin ligase with the smallest known biotin ligase from the bacterium *Aquifex aeolicus* (D. I. Kim et al., 2016). Through its smaller size, BioID2 enables higher selectivity in the targeting of fusion proteins, necessitates lower levels of biotin supplementation, and enhances the labelling of proximal proteins (Han, Li, & Ting, 2018).

Application of the BioID system using α-synuclein as a bait has been recently performed in two studies (J.-Y. Lee et al., 2021; Popova et al., 2021). In the first study,

wild-type and SNCA^{A53T} α-synuclein interactors were compared in SH-SY5Y neuroblastoma cells (J.-Y. Lee et al., 2021). Wild-type α-synuclein was found to interact with cytoplasmic, mitochondrial, and nucleic proteins, whereas SNCA^{A53T} α-synuclein differentially interacted with plasma membrane and endoplasmic reticulum proteins. In particular, SNCA^{A53T} α-synuclein demonstrated a propensity for nuclear localisation, which in subsequent mechanistic experiments was shown to regulate transcriptional adapter 2-α and block downstream histone H3 acetylation. In the second study, a yeast model revealed that expression of both α-synuclein and phosphorylated α-synuclein on serine 129 reduced the abundance of proteasomal subunits (Popova et al., 2021). Here, biotin labelling demonstrated that phosphorylated α-synuclein was found in close proximity to proteasomal base subunit, regulatory particle AAA ATPase 2, suggesting a mechanism whereby pathogenic α-synuclein is targeted to and degraded via the proteasome.

Alternatively, APEX technology has also been used to resolve α-synuclein interactors in cell lines and neurons (C. Y. Chung et al., 2017; Follett et al., 2016; Sanz et al., 2019). APEX (27 kDa) catalyses the oxidation of biotin-phenol to the short-lived and highly reactive biotin-phenoxyl radical in the presence of hydrogen peroxide—the reaction between electron-rich amino acids and biotin-phenoxyl results in their biotinylation (Lam et al., 2015). Cells which express a bait protein fused to APEX are incubated in the presence of biotin phenol for 30 min and subsequently exposed to hydrogen peroxide for 60 sec to induce biotinylation, lending the advantage of increased speed of labelling (APEX, 1 min vs BioID, up to 24 h), which can be used to study dynamic processes in a temporally resolved manner (Nguyen, Kim, Doan, Lee, & Lee, 2019). Consistent with the literature, application of APEX technology in rat cortical neurons revealed that α-synuclein interacts primarily with biological processes involved in protein trafficking, endocytosis, vesicular transport, cytoskeletal

homeostasis and mRNA metabolism (C. Y. Chung et al., 2017). Altogether, proteins that emerge in common between α-synuclein interactome studies are likely to reflect true cellular events, either from direct or indirect events in α-synuclein toxicity.

5.1.2 The neuroprotective role of DJ-1

DJ-1 was originally discovered as a mitogen-dependent oncogene involved in the Ras signalling transduction pathway (Nagakubo et al., 1997)—and loss of function mutations in its coding gene, *PARK7*, were subsequently linked to early onset autosomal recessive Parkinson's disease (Bonifati, Rizzu, Van Baren, et al., 2003). DJ-1 is a small and ubiquitous protein (20 kDa), which senses oxidative stress through an essential cysteine residue within its active site and neutralises reactive oxygen species (Inden et al., 2006; Taira et al., 2004). DJ-1 exists as a homodimer primarily in the cytoplasm, and under conditions of stress in mitochondria and nuclei (Zhang et al., 2005).

Post-mortem studies have demonstrated that regions of Alzheimer's disease and Parkinson's disease brains with proteinaceous deposits exhibit elevated levels of oxidised DJ-1, which is considered to be neuroprotective (Bandopadhyay et al., 2004; J. Choi et al., 2006). Cysteine residue C106 in DJ-1 is key to its function in sensing oxidative stress (Kinumi, Kimata, Taira, Ariga, & Niki, 2004). Differential oxidization of C106 allows DJ-1 to respond accordingly to varying levels of oxidative stress; depending on the levels of free oxide radicals, DJ-1 becomes sequentially oxidized from its weakly activated reduced form, C106-SH, to its mildly active sulfenated form, C106-SOH, and to its highly active sulfinated form, C106-SO_2H (M. S. Choi et al., 2014). Excessive oxidative stress renders DJ-1 into its inactive form, C106-SO_3H—interestingly, inactive DJ-1 has been detected in sporadic Parkinson's disease cases, suggesting its relevance to the pathogenesis of both idiopathic and familial disease cases (Ariga et al., 2013).

In addition to its role in sensing oxidative stress and neutralising reactive oxygen species, DJ-1 has been shown to function as a molecular chaperone, a protease, a transcriptional regulator, an RNA-binding protein, a mitochondrial regulator,

an autophagy regulator and lastly, a glyoxalase (Dolgacheva, Berezhnov, Fedotova, Zinchenko, & Abramov, 2019). The most prominent roles that DJ-1 is involved in are outlined in Figure 5.1.

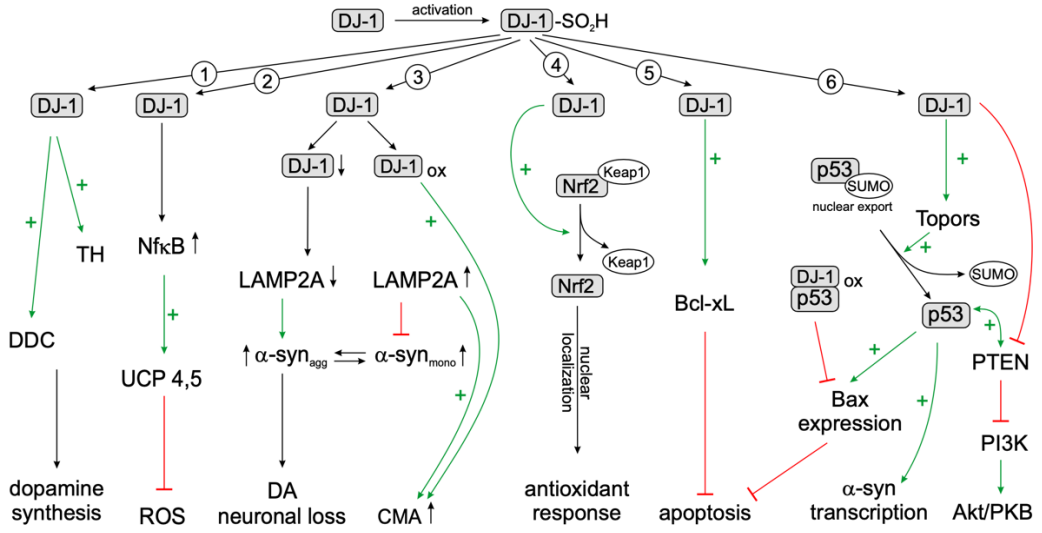


Figure 5.1 Cellular functions of DJ-1

1, DJ-1 upregulates dopamine synthesis by activating tyrosine hydroxylase (TH) and 4-dihydroxy-L-phenylalanine decarboxylase (DDC). **2,** DJ-1 translocates to the nucleus and transcriptionally activates NF-κB which in turn promote the expression of mitochondrial uncoupling proteins (UCP) that protect against reactive oxygen species (ROS). **3,** DJ-1 enhances α-synuclein clearance by activating chaperone mediated autophagy (CMA). **4,** DJ-1 contributes to the antioxidant response by activating nuclear receptor factor 2 (Nrf2). **5,** DJ-1 prevents apoptosis by upregulating B-cell lymphoma extra-large (Bcl-xL). **6,** DJ-1 positively regulates p53 via Topors-mediated SUMOylation. DJ-1 overexpression decreases Bax levels and inhibits apoptosis. DJ-1 inhibits phosphatase and tensin homolog (PTEN) which in turn activates the phosphoinositide 3-kinase/ protein kinase B (PI3K/PKB) pathway (Dolgacheva et al., 2019).

5.1.3 Glycating stress and its relevance in Parkinson's disease

Dicarbonyl stress, characterised by the unbalanced formation of α-oxoaldehyde metabolites has been associated with natural ageing and multiple diseases including tumour growth, diabetes, and importantly, neurodegeneration (Biosa et al., 2017). Glucose metabolism and lipid peroxidation generate carbonyl groups that are highly reactive towards proteins, nucleic acids, and lipids—such as, methylglyoxal (MGO). MGO preferentially targets lysine and arginine residues and forms cytotoxic advanced glycation end products (AGEs), which in turn promotes aggregation and decreases viability (Adrover et al., 2014; Kalapos, 1994; Lo, Westwood, McLellan, Selwood, & Thornalley, 1994; Taghavi, Habibi-Rezaei, Amani, Saboury, & Moosavi-Movahedi, 2017).

Cells have evolved to become highly adapted to respond to protein glycation. Their primary line of defence includes the activity of glyoxalase enzymes 1 and 2, which react directly with MGO and glyoxal (GO) and generate lactate or glycolate, respectively, in two steps using glutathione (GSH) in the first (Rabbani & Thornalley, 2015). Another protective mechanism against the accumulation of AGEs involves the activity of deglycating enzymes, which disrupt the glycation cascade through the removal of MGO and GO adducts from protein side chains (Wu & Monnier, 2003). It is noteworthy that glycation of proteins and oxidative stress are interlinked as multiple studies have shown that MGO causes the formation of reactive oxygen species whilst also significantly depleting GSH (Di Loreto et al., 2004; Di Loreto et al., 2008; Kikuchi et al., 1999; Shangari & O'Brien, 2004).

The consequences of protein glycation are more pronounced in the brain compared to other tissues and DJ-1 has been shown to possess both glyoxalase and deglycase activity (Bélanger et al., 2011; J.-y. Lee et al., 2012; Richarme et al., 2015). Glycation, as an inevitable age-related process, may therefore be involved in the

pathogenesis of Parkinson's disease. For example, data from mice which are fed a high glycaemic index diet, indicate that neurons from the substantia nigra are most vulnerable to stress and that the majority of MGO-affected proteins are localised in this region (Uchiki et al., 2012). Glucose is readily metabolised into reducing sugars that react covalently to proteins, generating AGEs that are ultimately deleterious to protein homeostasis (Miranda & Outeiro, 2010). Interestingly, diabetes, a systemic condition of defective glucose metabolism, has been identified as an important risk factor for Parkinson's disease (G. Hu, Jousilahti, Bidel, Antikainen, & Tuomilehto, 2007; Y. Sun et al., 2012; Vicente Miranda, El-Agnaf, & Outeiro, 2016)—and a drug used to treat diabetic patients, exenatide, was clinically proven to ameliorate symptoms in Parkinson's disease patients (Athauda et al., 2017; Foltynie & Aviles-Olmos, 2014). AGE levels are also significantly elevated in α-synucleinopathic brains (Dalfó et al., 2005). Moreover, AGEs were detected proximal to Lewy pathology, suggesting that carbonyl compounds may promote aggregation (Castellani, Smith, Richey, & Perry, 1996; Münch et al., 2000).

5.1.4 DJ-1 mutants in Parkinson's disease

A plethora of mutations in *PARK7* have been discovered since it was linked to Parkinson's disease in 2003 (Repici & Giorgini, 2019). Loss of function of DJ-1 was first found to be caused by a homozygous point mutation (L166P) in an Italian family and a 14 082 bp deletion in a Dutch family (Bonifati, Rizzu, Squitieri, et al., 2003). Loss of function of DJ-1 impairs multiple key cellular processes, for example the DJ-1 C106 mutant removes its oxidative stress sensor function and the DJ-1 L166P mutant interferes with signalling pathways by mislocalising to mitochondria and nuclei (Figure 5.2). In addition, several studies have investigated the effect of DJ-1 mutations on its three-dimensional structure (Görner et al., 2007; Malgieri & Eliezer, 2008; Ramsey & Giasson, 2010; Wilson, Collins, Hod, Ringe, & Petsko, 2003). This work revealed that while some DJ-1 mutants interfere with dimer formation, others do not, suggesting that DJ-1 mutants may contribute to disease via alternative mechanisms that are yet known.

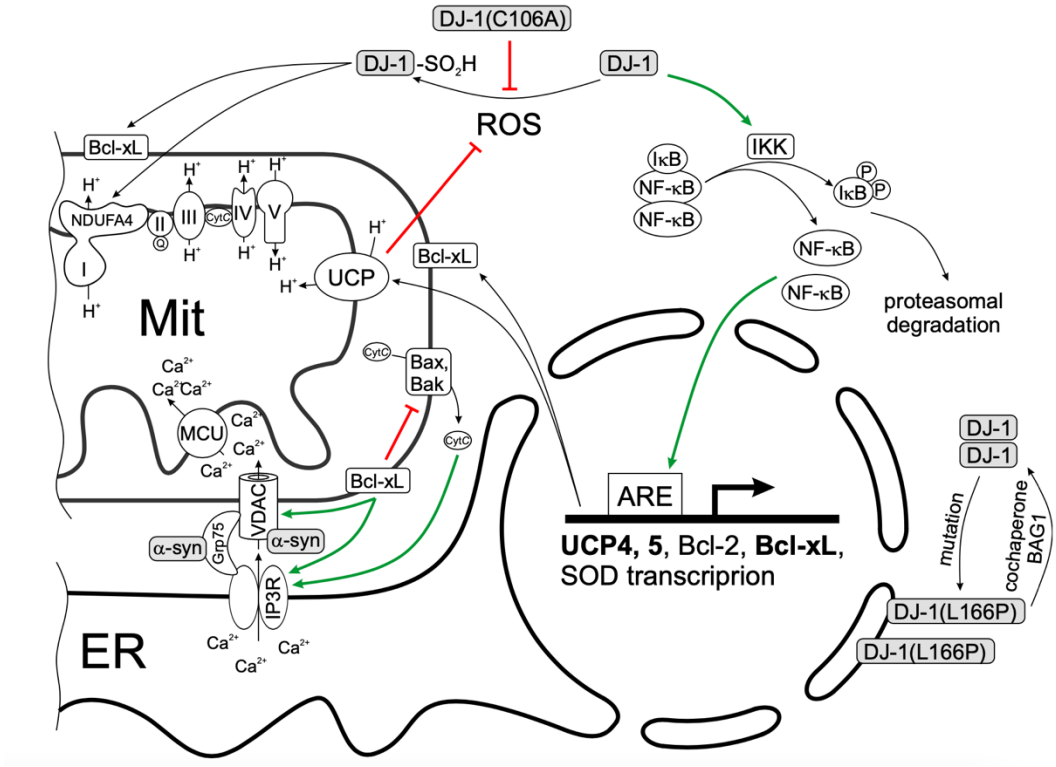


Figure 5.2 DJ-1 mutants disrupt its protective function against oxidative stress

Reactive oxygen species (ROS)-induced DJ-1 activation interacts with complex 1 from the electron transport chain and maintains its activity. DJ-1 negatively regulates the production of ROS and promotes the upregulation of uncoupling proteins through the NF-κB pathway, which ultimately decrease intracellular ROS levels. Bcl-xL inhibits apoptosis by mediating mitochondrial and reticular calcium through the activation of inositol trisphosphate receptor (IP3R) and voltage-dependent anion-selective channel (VDAC) within the mitochondrial associated membrane (MAM) complex. DJ-1 mutants interfere with its protective function. For example, the DJ-1 C106A mutant blocks its ROS-dependent activation and the DJ-1 L166P interrupts signaling pathways by mislocalising to mitochondria and nuclei (Dolgacheva et al., 2019).

To date, solely one post-mortem brain from a patient with DJ-1-linked (L172Q) Parkinson's disease has been shown to exhibit Lewy pathology, suggesting that DJ-1 mutations are causatively linked to α-synuclein pathology (Taipa et al., 2016). Furthermore, a genotype-phenotype relationship study, which focused on autosomal recessive forms of parkinsonism, Parkin, PINK1, and DJ-1, found that DJ-1 mutant carriers displayed the highest proportion (57%) of non-motor systems (Kasten et al., 2018). These findings strongly implicate DJ-1 in the pathogenesis of Parkinson's disease and in addition to characteristic motor symptoms, DJ-1 function is also related to non-motor aspects of symptomology.

Detection of oxidized forms of DJ-1 has been made possible via the development of novel antibodies (Yoshiro Saito et al., 2009). Oxidized or active forms of DJ-1 have been detected in Parkinson's disease brains with Lewy pathology, in particular in dopaminergic neurons of the substantia nigra, in astrocytes of the striatum, and in glia from regions in the central nervous system related to movement such as the inferior olivary nucleus and red nucleus (Yoshiro Saito, 2014). Increased glycating stress may be one contributor to increased levels of oxidized DJ-1 in the brain of Parkinson's disease patients (Guerrero, Vasudevaraju, Hegde, Britton, & Rao, 2013). Lewy pathology in these cases has been associated with the presence of AGEs, therefore the role of DJ-1 as a glyoxalase and importantly, a deglycase, indicates its relevance to α-synuclein aggregate formation. Indeed, several lines of evidence point towards the deglycase activity of DJ-1 in mitigating α-synuclein aggregation and toxicity in cell and animal models (N. Sharma, Rao, & Kalivendi, 2019; Shendelman, Jonason, Martinat, Leete, & Abeliovich, 2004; Sun, An, & Pu, 2012; W. Zhou et al., 2011; Zondler et al., 2014). DJ-1 was also shown to inhibit α-synuclein aggregation by regulating chaperone-mediated autophagy (C.-Y. Xu et al., 2017).

As DJ-1 counters oxidative stress and attenuates α-synuclein aggregation, it has garnered attention as a potential therapeutic target for Parkinson's disease. One approach involves increasing wild-type DJ-1 levels to obtain neuroprotection (Figure 5.3a). Increasing DJ-1 levels via viral transduction (HIV-TAT system) in cell lines or via intranigral injections in rodent models has proven to be efficacious in rescuing phenotypes not only in Parkinson's disease models but also in multiple system atrophy models (Gao et al., 2012; Glat, Ben-Zur, Barhum, & Offen, 2016; Inden et al., 2006; S.-Y. Sun et al., 2012). A second approach involves the identification of compounds that target DJ-1 and inhibit its excessive oxidation into an inactive state (C106-SO_3H; Figure 5.3b). By virtually screening brain penetrant compounds based on their crystal structure, one group has identified several molecules that were subsequently shown to be able to stabilize the oxidation state of cysteine 106 on DJ-1 and prevent its inactivation (Miyazaki et al., 2008). Trial of such compounds in rodent models yielded promising results and rescued the death of dopaminergic neurons from the substantia nigra whilst restoring locomotor function (Kitamura et al., 2011; Takahashi-Niki et al., 2015).

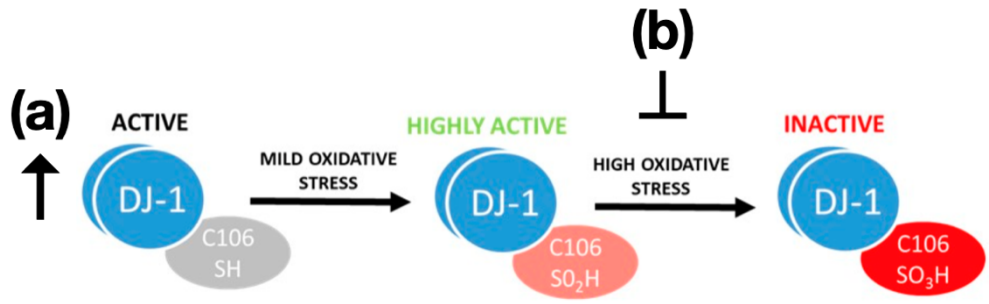


Figure 5.3 DJ-1 as a therapeutic target in Parkinson's disease

Compounds that target DJ-1 may either **a,** increase its basal activity or **b,** stabilise its active form to ultimately increase neuroprotection against oxidative stress (Repici & Giorgini, 2019).

5.1.5 Assay workflow: phenotypic characterisation of DJ-1 knockout under conditions of α-synuclein seeded aggregation

Through the use of biotin proximity labelling, we identified DJ-1 as a differentially interacting protein with α-synuclein between cells exposed to *de novo* generated fibrils versus brain-amplified fibrils. Ablation of DJ-1 in HEK293 cells and $SNCA^{TRIP}$ dopaminergic neurons increased levels of aggregation and increased the neurotoxicity of fibril-induced aggregates. Moreover, the presence of aggregation and DJ-1 knockout triggered the toxic accumulation of AGEs. α-Synuclein aggregates induced by *de novo* fibrils were also more ubiquitinated on K12 versus aggregates induced by brain-amplified fibrils.

The objectives of this chapter were to:

1. Identify differentially interacting proteins with α-synuclein under seeded aggregation conditions using BioID2
2. Validate the interaction of α-synuclein with DJ-1 by co-immunoprecipitation
3. Assess the effect of DJ-1 and GLO1 knockout in HEK293 cells expressing Venus-tagged α-synuclein
4. Quantify AGEs under α-synuclein seeded aggregation conditions and in the absence of DJ-1
5. Investigate whether ubiquitination of α-synuclein is affected by glycation
6. Assess the effect of MGO treatment in $SNCA^{TRIP}$ dopaminergic neurons under seeded aggregation conditions
7. Determine the effect of DJ-1 knockout in $SNCA^{TRIP}$ dopaminergic neurons under seeded aggregation conditions using CRISPR/Cas9.

5.2 Results

5.2.1 Differential protein interactome of *de novo* versus patient brain-amplified α-synuclein assemblies

Although a critical level of aggregation is necessary to cause cell death in neurons, the distinct effects of patient brain-amplified and *de novo* generated α-synuclein assemblies in $SNCA^{TRIP}$ dopaminergic neurons suggest additional mechanisms by which brain-amplified assemblies confer toxicity. One hypothesis is that toxicity may arise from differential aberrant strain interactions within the intracellular proteome—either by disrupting critical protein functions or by evading homeostatic defence systems.

Optimisation of α-synuclein protein interaction experiments *in vitro* were performed by Dr. Samiha Shaikh and the subsequent analysis mass spectrometry data analysis was performed by Dr. Roman Fischer.

5.2.1.1 Biotin ligase, BioID 2, proximity labelling of α-synuclein in HEK293 cells

To investigate such mechanisms in the context of intracellular α-synuclein aggregation, proximity-dependent biotin identification, BioID2, was used to uncover potential interacting proteins (Roux, Kim, Burke, & May, 2018). To this end, a HEK293 cell line stably expressing human wild-type α-synuclein fused to biotin ligase (BirA* isolated from *Escherichia coli*) was generated to label interacting proteins within a 10 nm radius of aggregated α-synuclein induced with the addition of *de novo* generated fibrils, PD-amplified fibrils, or MSA-amplified fibrils (Figure 5.4a). In control experiments, biotinylation of proteins co-localised with α-synuclein-BirA* aggregates that were also immunoreactive for phosphorylated α-synuclein at serine 129 (Figure 5.4b).

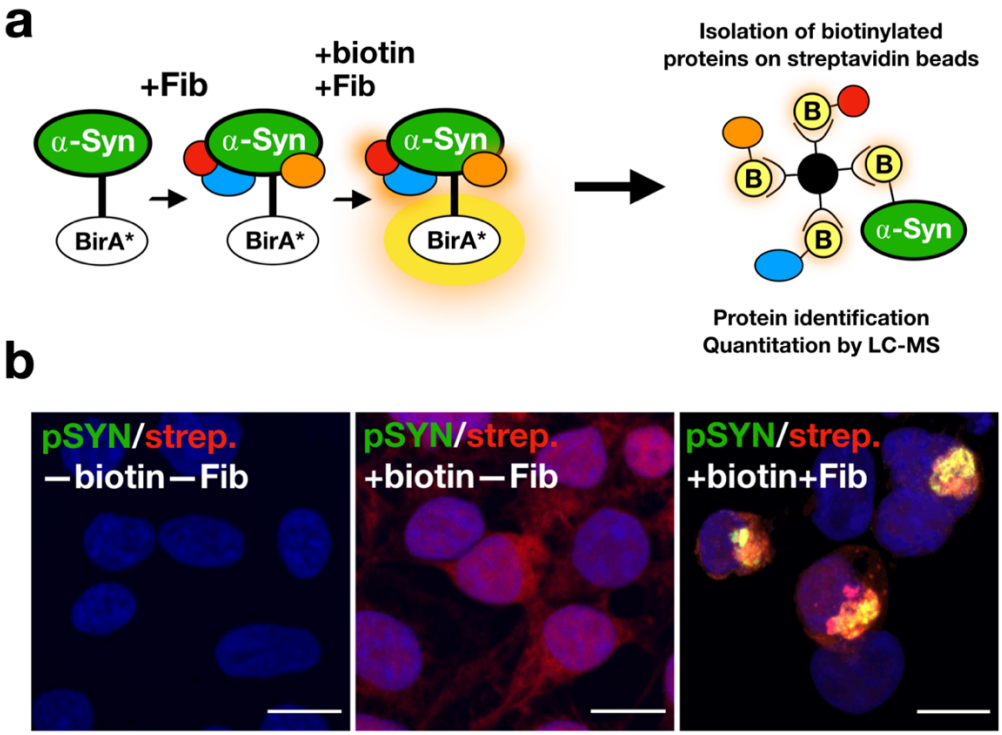


Figure 5.4 Biotin ligase (BioID) tagged α-synuclein (α-Syn-BirA*) in HEK293 cells

a, α-Syn-BirA* clonal cells were exposed to *de novo* generated α-synuclein fibrils followed by the addition of biotin, resulting in the biotinylation of proximal proteins (10 nm radius) to aggregated α-synuclein within cells. Biotinylated proteins were subsequently captured using streptavidin beads. **b,** Confocal images of HEK293 cells exposed to *de novo* α-synuclein fibrils (0.5 μM) and treated with biotin (3.1 μM) were immunolabelled for pSYN (green) and streptavidin (red) to identify biotinylated proteins. pSYN signal colocalised with streptavidin signal, showing that α-synuclein co-localises with biotinylated proteins.

A ratiometiric biotin ligase, BioID2, strategy with stable isotope labelling using amino acids in cell culture (SILAC) was employed to label samples in three distinct treatment groups: *de novo* generated α-synuclein fibrils, PD-amplified fibrils, and MSA-amplified fibrils (Figure 5.5). HEK293 cells expressing α-synuclein-BirA* were exposed to various α-synuclein assemblies, each labelled with a unique arginine (R) and lysine (K) isotope configuration including R0K0 for *de novo* fibril-treated cells, R6K4 for PD-amplified fibril-treated cells, and R10K8 for MSA-amplified fibril-treated cells (Figure 5.5b). α-Synuclein fibril assemblies (1 μM) and biotin (3.1 μM) were exogenously added onto cells and assayed after 48 h in order to capture the 'historical' cascade of protein interactions over the course of the intracellular accumulation and assembly of α-synuclein into aggregates caused by various assemblies. 48 h post-seeding is a timepoint which was previously optimised to generate highly detectable levels of aggregation without saturating potential differential effects between conditions in HEK and neuroblastoma cell lines overexpressing α-synuclein.

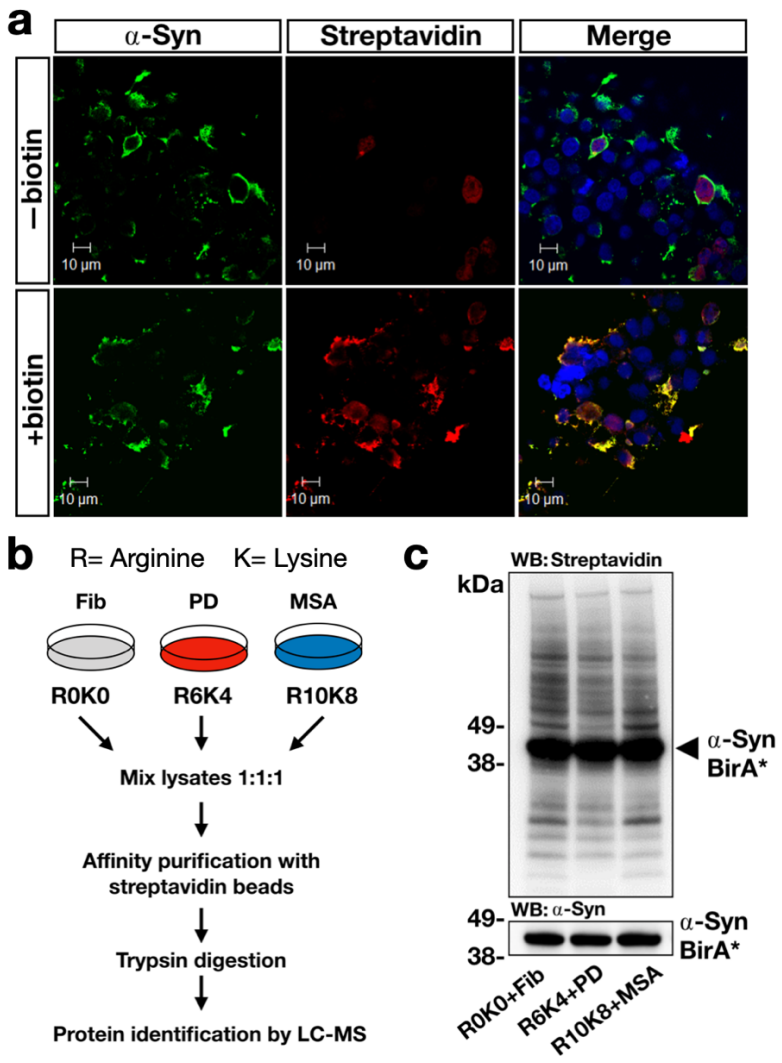


Figure 5.5 Confocal images of cells treated with biotin and biotinylation of SILAC labelled cells

a, Staining pattern of α-synuclein with streptavidin. Cells expressing α-Syn-BirA* were treated with biotin and stained with α-synuclein and streptavidin. In the presence of biotin, α-synuclein co-localised with biotinylated proteins. Images are representative of three independent experiments (scale bar: 10 µm). **b,** Summary of workflow: SILAC labelled cells were treated with *de novo* generated or brain amplified fibrils and biotin. 48 h post treatment, cells were lysed, immunoblotted and **c,** probed for streptavidin to test for equal biotinylation. The lysates were pooled together, and biotinylated proteins were isolated using streptavidin beads. The bound fraction was then subjected to trypsin digestion and further processed for mass spectrometry. Panel **c** is representative of two independent experiments. R= Arginine, K= Lysine. Data in this figure was generated by Dr. Samiha Shaikh.

5.2.1.2 Identification of α-synuclein interacting partner DJ-1 under seeded aggregation

Biotinylated proteins were immunoprecipitated with streptavidin-conjugated beads and subjected to mass spectrometry to identify the landscape of α-synuclein interactions during its assembly into aggregates. We found that 1,002 proteins interacted with α-synuclein in this model (Appendix). Clustering analysis identified 56 differentially interacting proteins when comparing treatments with *de novo* generated fibrils versus patient brain-amplified fibrils, which included the Parkinson's disease-associated protein DJ-1 (Figure 5.6 and Appendix). Label-free quantification of mass spectrometry data revealed that DJ-1 abundance was reduced in samples where α-synuclein was templated with pooled PD-amplified (3 cases) and pooled MSA-amplified (5 cases) fibrils compared to *de novo* generated fibrils. This finding suggests that DJ-1 interacts less with α-synuclein assemblies triggered with brain-amplified fibrils compared to those triggered with *de novo* fibrils.

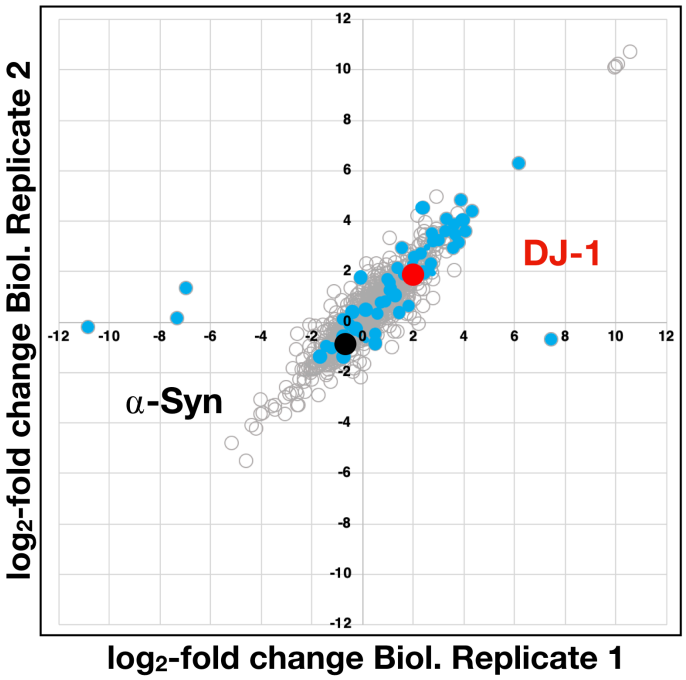


Figure 5.6 Mass spectrometry of biotinylated proteins under α-synuclein seeded aggregation

A total of 1002 proteins were identified using BioID2 α-Syn-BirA* (grey circles) under conditions of seeded aggregation. Biotinylated proteins from cells seeded with either *de novo* or patient brain-amplified fibrils identified 56 differentially interacting proteins (blue dots), including DJ-1 (red dot); α-synuclein is shown for comparison (black dot). Cells treated with *de novo* generated α-synuclein fibrils exhibited increased biotinylation or interaction with DJ-1 compared to cells treated with PD- or MSA-amplified fibrils. Data in this figure was analysed by Dr. Roman Fischer.

5.2.1.3 Validation of differential interaction between α-synuclein and DJ-1

The differential interaction between α-synuclein assemblies and DJ-1 was confirmed by immunoprecipitation (Figure 5.7). Consistent with results from mass spectrometry analysis, immunocapture of DJ-1 tagged to c-myc in seeded cells followed by immunoblotting with streptavidin demonstrated the enhanced interaction (approx. 1.5-fold increase) between intracellular α-synuclein assemblies and DJ-1 seeded with *de novo* fibrils compared to PD- and MSA-amplified fibrils. No differences in biotinylated DJ-1 between samples treated with PD- and MSA-amplified fibrils were detected.

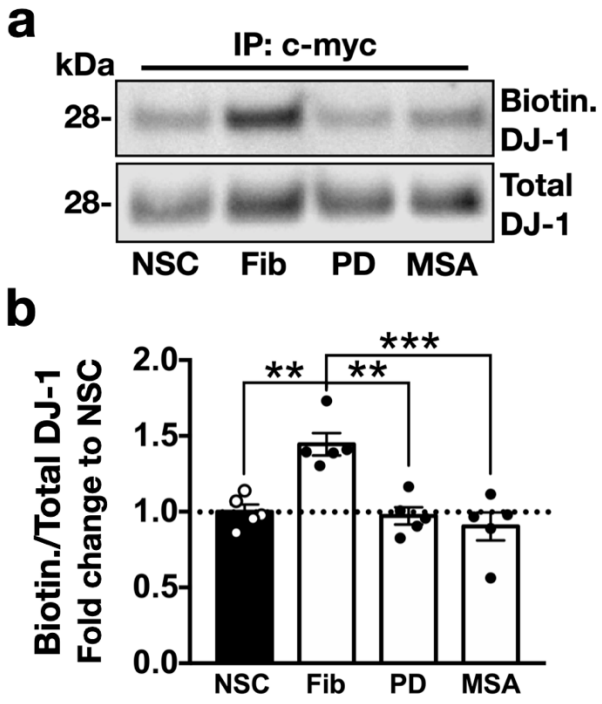


Figure 5.7 α-Synuclein interacts with DJ-1 in HEK293 cells expressing α-Syn-BirA*

a, DJ-1 immunocapture followed by streptavidin immunoblotting confirmed the enhanced interaction between intracellular α-synuclein assemblies and DJ-1 seeded with *de novo* generated fibrils compared to PD- and MSA-amplified fibrils. **b,** Cells exposed to *de novo* generated fibrils displayed approximately 1.5-fold increased interaction with α-synuclein compared to cells treated with patient brain-amplified fibrils (n=5). NSC, non-seeded control, non-treated control. Data are shown as mean±s.e.m. In panel **b,** $^{**}P<0.01$, $^{***}P<0.001$ by one-way ANOVA followed by Tukey's multiple comparison test. Data in this figure was generated by Dr. Samiha Shaikh.

5.2.2 DJ-1 knockout and GLO1 knockout in HEK293 cells under seeded aggregation

DJ-1 functions as a deglycase and mutations leading to the loss of function in its gene, *PARK7*, causes early-onset autosomal recessive Parkinson's disease with Lewy pathology (Bonifati, Rizzu, Van Baren, et al., 2003; Richarme et al., 2017; Taipa et al., 2016). Therefore, we sought to explore the impact of CRISPR/Cas9-mediated knockout of either DJ-1 or a related upstream protein acting in the same pathway, glyoxalase-1 (GLO1; Figure 5.8) on assembly-induced α-synuclein aggregation.

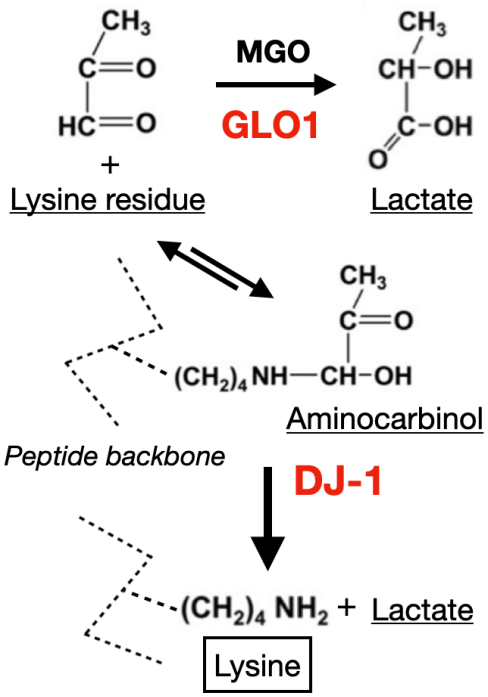


Figure 5.8 Pathway of methylglyoxal detoxification involving DJ-1 and GLO1

Glycation is a naturally occurring non-enzymatic covalent reaction between sugars and dicarbonyls (e.g., methylglyoxal, MGO) which leads to protein inactivation. MGO is spontaneously generated as a by-product from the glycolytic pathway and induces toxic protein modifications in the form of advanced glycation end products (AGEs). MGO is enzymatically detoxified by GLO1 into a less reactive substance, *d*-lactate. MGO also forms covalent adducts in the presence cysteines, arginines, and lysines, more specifically MGO forms hemithioacetals with cysteines and aminocarbinols with arginines and lysines. α-Synuclein does not contain any cysteine or arginine residues (https://www.uniprot.org/uniprot/P37840), therefore it may only form aminocarbinols. These aminocarbinols are further detoxified by DJ-1 into arginine/lysine and lactate—preventing the formation of AGEs (Richarme et al., 2015).

In these experiments, a clonal line stably expressing Cas9 and α-synuclein fused at the c-terminus to fluorescent Venus protein was generated using HEK293 cells. Venus protein was fused to the C-terminus of α-synuclein to limit potential interferences with its aggregation kinetics. For example, masking residues on the N-terminus (AA 1-60) and the central region of α-synuclein, also termed non-amyloid-β component (NAC; AA 61-95), have been shown to modify the aggregation propensity of α-synuclein (Näsström, Andersson, Lejon, & Karlsson, 2019; Stephens et al., 2020).

DJ-1 knockout and GLO1 knockout in HEK293 cells expressing Venus-α-synuclein were exposed to α-synuclein assemblies including *de novo* generated fibrils and PD- and MSA-fibrils. Firstly, I observed by immunofluorescence that the addition of exogenous fibrils in DJ-1 knockout cells increased aggregation as assessed by pSYN and Venus signal (Figure 5.9). Visually, the number of pSYN inclusions and Venus inclusions alike were significantly higher in DJ-1 knockout cells compared to their corresponding non-target control. I also demonstrated that pSYN inclusions co-localised with Venus-α-synuclein, confirming that Venus signal is representative of α-synuclein aggregation.

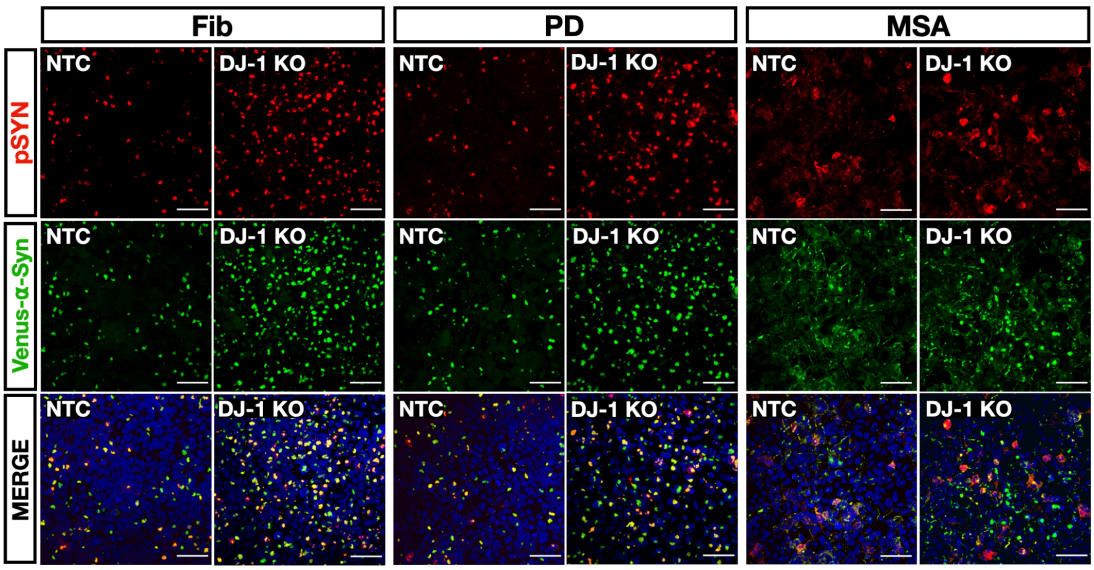


Figure 5.9 Confocal images of seeded aggregation in CRISPR/Cas9 knockout of DJ-1 in HEK293 cells expressing Venus-tagged α-synuclein

Representative confocal images of seeded aggregation in DJ-1 knockout HEK293 cells expressing Venus-α-synuclein. Addition of exogenous fibrils, irrespective of α-synuclein assembly, increased α-synuclein aggregation as visualised by pSYN (red) and Venus (green) signal. Images are representative of six independent experiments (scale bar: 30 μm).

Consistent with immunofluorescence findings, I demonstrated by immunoblotting that DJ-1 knockout and GLO1 knockout in HEK293 Venus-α-synuclein cells both increased levels of pSYN by approximately 2-fold upon exposure to each α-synuclein assembly (Figure 5.10). Increased aggregation under these conditions was also accompanied by cellular dysfunction as measured by lactate dehydrogenase (LDH) release in the conditioned media (Figure 5.10c/f).

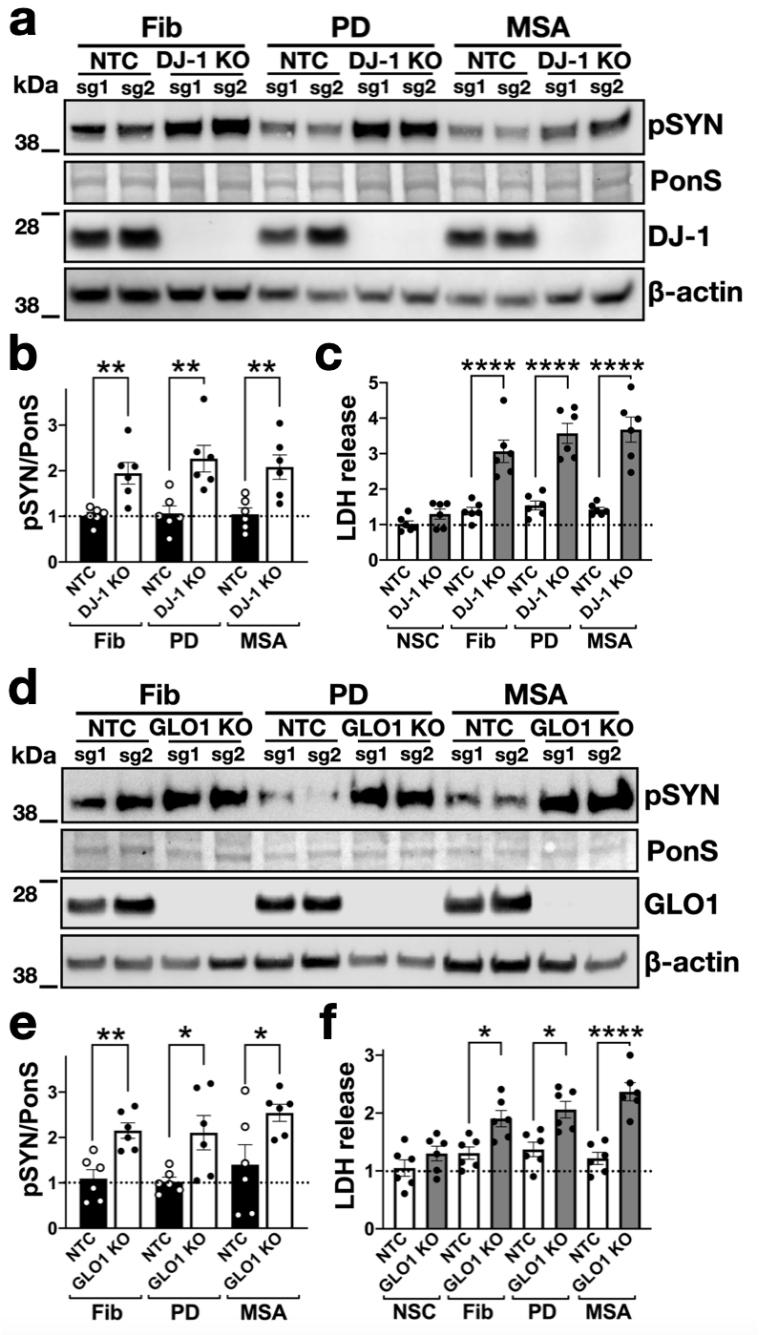


Figure 5.10 CRISPR/Cas9 knockout of DJ-1 and GLO1 in HEK293 cells expressing Venus-tagged α-synuclein

Seeded aggregation (0.5 μM, 48 h) with *de novo* generated fibrils and PD- and MSA-amplified fibrils unanimously increased levels of pSYN as assessed by immunoblotting in **a+b,** DJ-1 KO cells and likewise in **d+e,** GLO1 KO cells. Increased aggregation of α-synuclein was accompanied by increased release of lactate dehydrogenase (LDH) in both **c,** DJ-1 KO and **f,** GLO1 KO cells. Data in this figure is representative of six independent experiments. Molecular weight (MW) of pSYN: 14 kDa, MW of Venus: 26.8 kDa, MW of Venus-tagged α-synuclein: 40.8 kDa. NTC, non-target control. Data are shown as mean±s.e.m. In panels **b,c,e,f,** **P*<0.05 ***P*<0.01, *****P*<0.0001 by one-way ANOVA followed by Tukey's multiple comparison test.

5.2.3 Advanced glycation end products in HEK293 cells under seeded aggregation

Lewy pathology in Parkinson's disease has been previously associated with advanced glycation end products (AGEs), which have been shown to cross-link α-synuclein and accelerate α-synuclein aggregation (Y.-G. Choi & Lim, 2010; Münch et al., 2000; Shaikh & Nicholson, 2008). In particular, α-synuclein was found to be glycated and glycosylated in cell models and neurons, affecting its folding properties and toxicity (Guerrero et al., 2013). In line with these findings, we detected glycation of α-synuclein in fractionated cell lysates treated with *de novo* fibrils, PD-amplified fibrils, and MSA-amplified fibrils compared to non-seeded controls (Figure 5.11a). Importantly, I further observed that seeded DJ-1 knockout lysates exhibited increased levels of advanced glycation end products at the molecular weight corresponding to Venus-tagged α-synuclein compared to seeded controls as assessed by immunoblotting (Figure 5.11b/c).

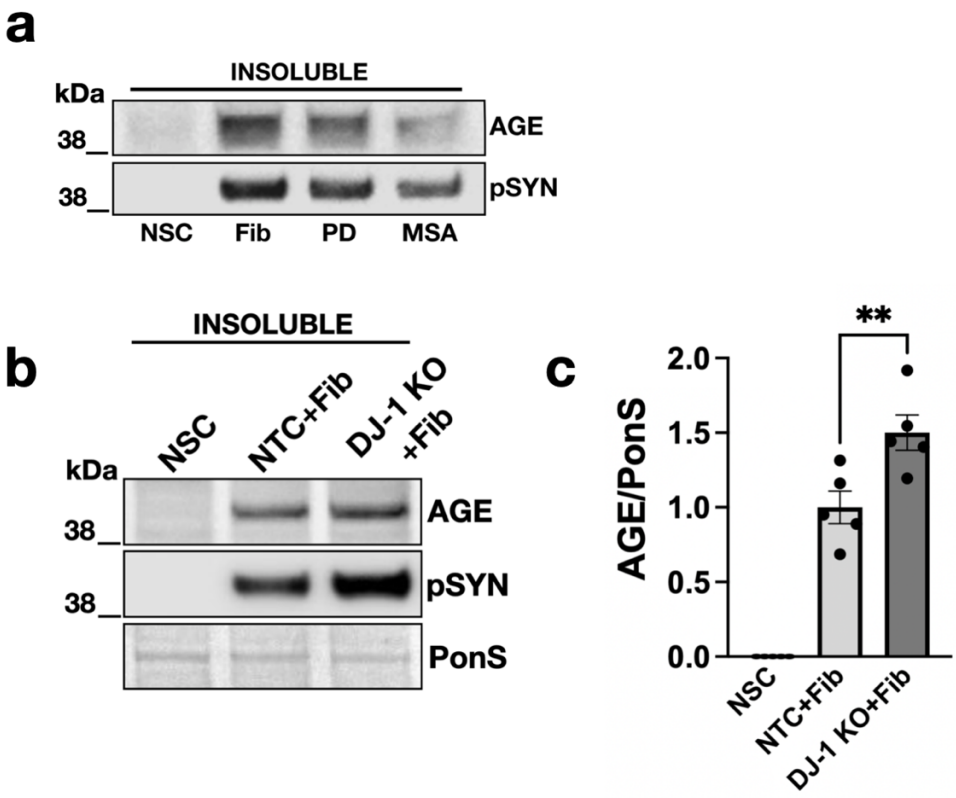


Figure 5.11 Seeded aggregation triggered advanced glycation end products in HEK293 cells

a, pSYN-positive aggregates isolated in the RIPA-insoluble fraction were immunoreactive for advanced glycation end products at the molecular weight of venus-tagged α-synuclein as assessed by immunoblotting (*n*=2 independent experiments). This signal was not observed in similarly processed non-seeded cell extracts **b,** *De novo* fibril addition (0.5 μM) in DJ-1 KO HEK293 cells expressing Venus-tagged α-synuclein induced increased levels of advanced glycation end products compared to seeded controls **c,** as quantified by immunoblotting. Molecular weight (MW) of pSYN: 14 kDa, MW of Venus: 26.8 kDa, MW of Venus-tagged α-synuclein: 40.8 kDa. NSC, non-seeded control, non-treated control.

5.2.4 Quantitation of α-synuclein K12 containing peptide with or without GlyGly modification

The N-terminus lysine (K) residues of native monomeric α-synuclein from K6-45 were shown to be the main sites for glycation in *in vitro* and *in vivo* brain models (Vicente Miranda et al., 2017). Incidentally, lysine residues on K12, K21, K45, K58, and K96 were previously identified in our group as sites of monomeric α-synuclein ubiquitination for lysosomal degradation (Tofaris et al., 2011). Hence, we searched our mass spectrometry results for differential ubiquitination by analysing proportions of glycine-glycine-lysine modified peptides on α-synuclein. Glycine-glycine-lysine modified peptides, which represent ubiquitin linkage sites, were discovered to be significantly more abundant on K12 in aggregated α-synuclein induced by *de novo* generated fibrils compared to those by patient brain-amplified fibrils from Parkinson's disease and multiple system atrophy (Figure 5.12). Given that the N-terminus of α-synuclein contains multiple principal sites for glycation, these findings suggest that glycation may block the ubiquitination of specific lysine residues, and indirectly increase the levels of aggregated α-synuclein through decreased degradation. For example, aggregates templated from brain-amplified conformers may evade DJ-1 interaction leading to more glycation on K12 preventing ubiquitination. This could explain the lower levels of glycine-glycine-lysine modified peptides on K12 compared to aggregates templated from *de novo* generated fibrils.

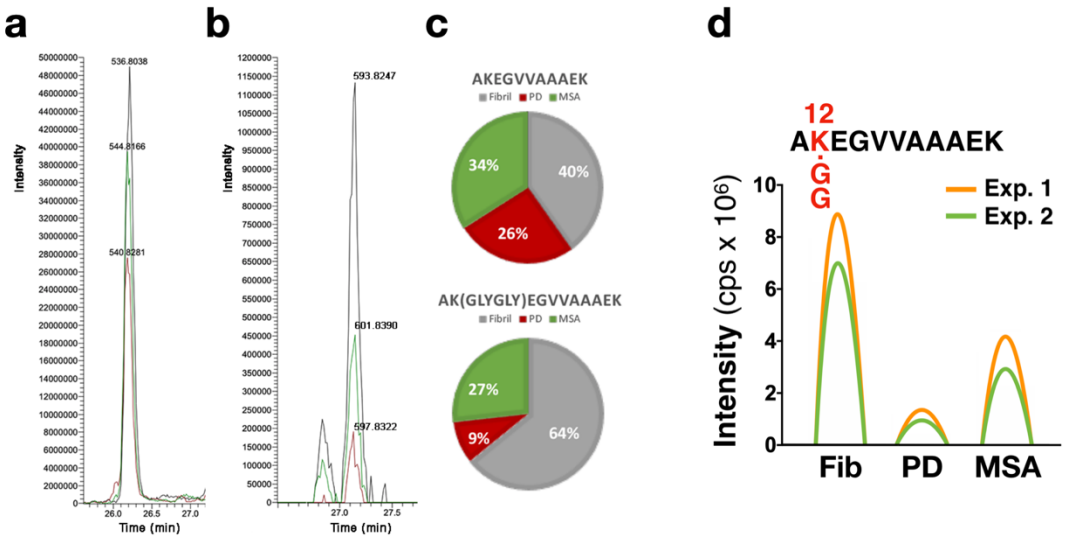


Figure 5.12 SILAC quantitation for K12 containing peptide with and without GlyGly modification

a, Extracted Ion Chromatograms for each monoisotopic SILAC precursor ion showed highest abundance of unmodified K12 peptide in cells seeded with *de novo* generated fibrils (SILAC light @ m/z 536.8), with similar but lower abundance in cells seeded with PD- (SILAC medium @ m/z 540.8) and MSA-amplified (SILAC heavy @ m/z 544.8) fibrils. **b,** The corresponding GlyGly modified version of the peptide was mostly detected in cells seeded with *de novo* generated fibrils (SILAC light @ m/z 593.8) and was much less abundant in cells seeded with PD (SILAC medium @ m/z 597.8) or MSA (SILAC heavy @ m/z 601.8) amplified fibrils. **c**, Relative abundance distribution of mass spectrometry detected signal derived from unmodified K12 peptide (upper) and GlyGly modified K12 peptide (lower). **d,** Illustrated chromatographs for each monoisotopic SILAC precursor ion demonstrating that samples treated with PD- and MSA- amplified fibrils had much lower amounts of K12 ubiquitinated α-synuclein than samples treated with *de novo* generated fibrils (*n*=2). The mass spectrometry data were deposited to the ProteomeXchange Consortium via the PRIDE partner repository with the dataset identifier PXD024198. Data in this figure was analysed by Dr. Roman Fischer.

5.2.5 Methylglyoxal treatment in iPSC-derived dopaminergic neurons under seeded aggregation

Detection of advanced glycation end-products in HEK293 cells treated with α-synuclein assemblies could potentially indicate that saturating the deglycase activity of DJ-1 via the addition of exogenous methylglyoxal (MGO) may exacerbate α-synuclein seeded aggregation and toxicity in iPSC-derived dopaminergic neurons. Accordingly, I found that two treatments of MGO (250 μM), given two weeks post-seeding with *de novo* generated fibrils, increased both aggregation (pSYN, Figure 5.13a) and fibril-induced neuronal death (nuclear fragmentation, Figure 5.13b).

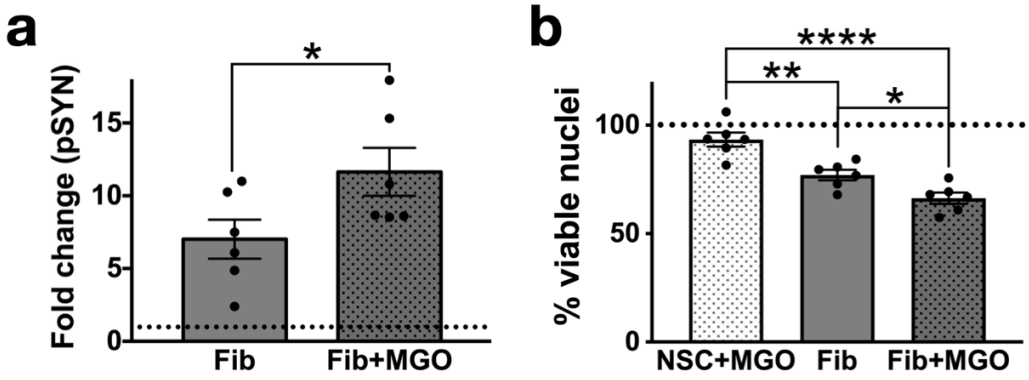


Figure 5.13 Methylglyoxal treatment exacerbates disease phenotypes in human SNCA^{TRIP} dopaminergic neurons

Dopamine neuron maintenance media was supplemented with two pulses of methylglyoxal (MGO, 250 μM) during the two weeks post-seeding with *de novo* generated -synuclein fibrils (1 μM). **a,** MGO increased fibril-induced aggregation as quantified by pSYN (n=6) and **b,** exposure to MGO increased fibril-induced death of dopaminergic neurons as measured by nuclear fragmentation (n=6). NSC, non-seeded control, non-treated control. Data are shown as mean±s.e.m. In panels **a,b,** *P<0.05 **P<0.01, ****P<0.0001 by one-way ANOVA followed by Tukey's multiple comparison test.

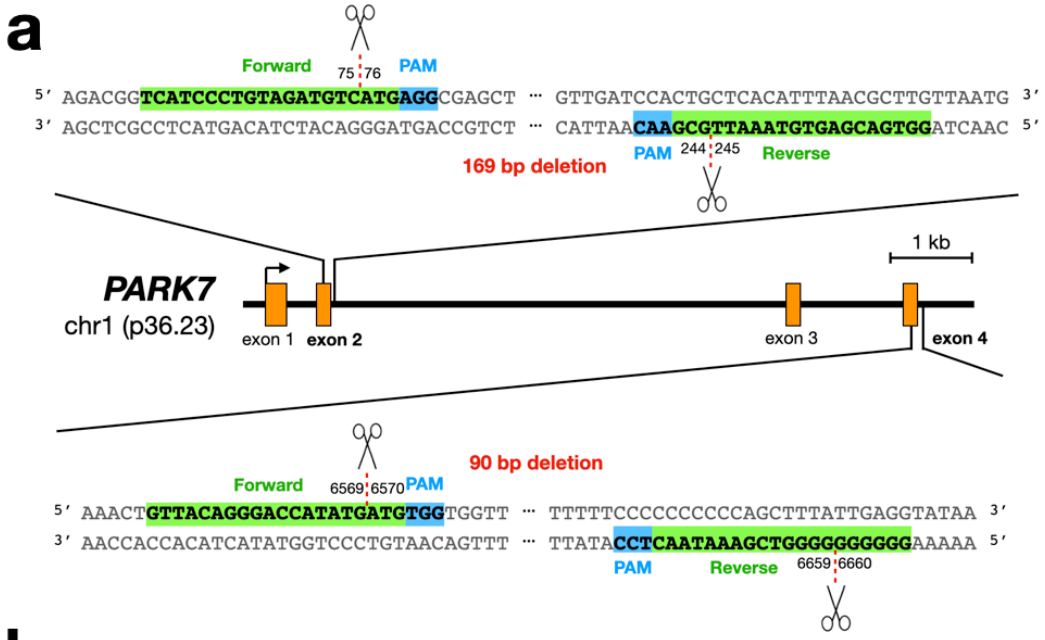
5.2.6 DJ-1 knockout in human iPSC-derived dopaminergic neurons exacerbates aggregate-induced toxicity

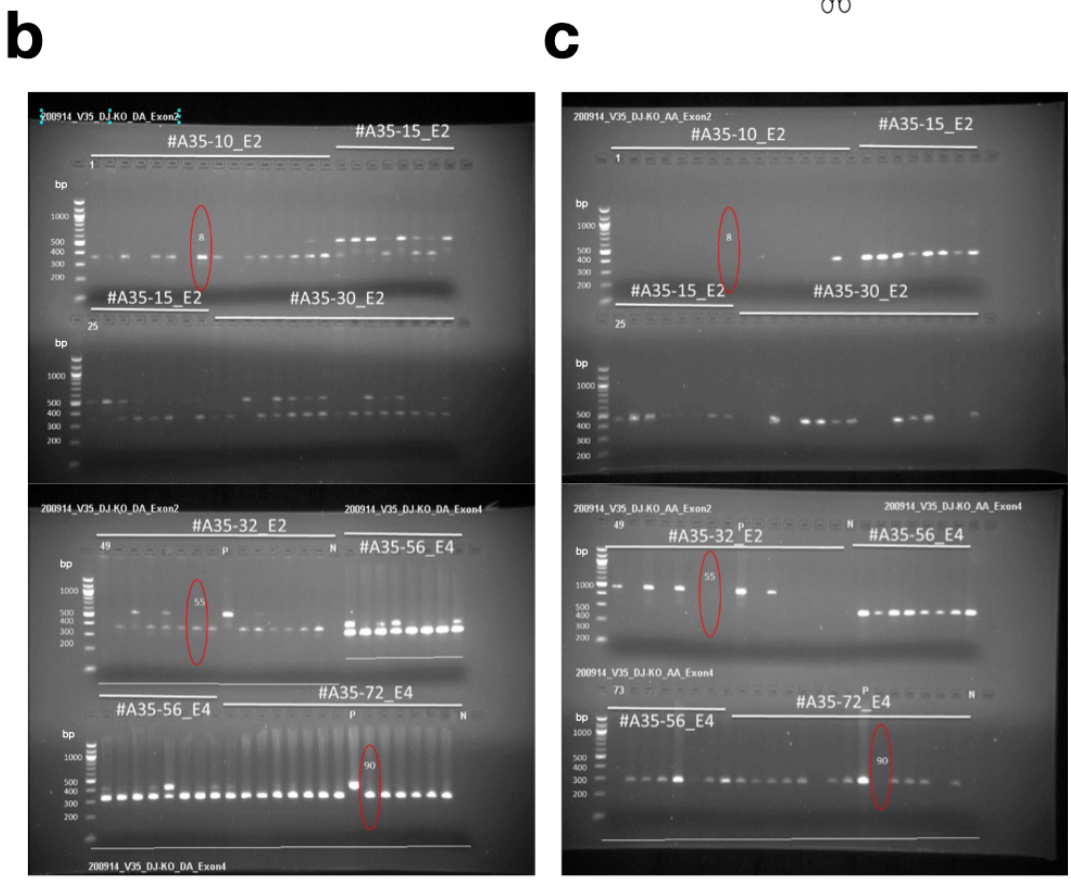
5.2.6.1 Generation of CRISPR/Cas9 knockout of DJ-1 in SNCA^{TRIP} stem cells

To further validate my findings in HEK293 cells, we generated DJ-1 knockout iPSC clones in our SNCA^{TRIP} line through Bioneer, Denmark. CRISPR/Cas9-mediated knockout of DJ-1 in our SNCA^{TRIP} line and the subsequent characterisation of the generated SNCA$^{TRIP/DJ\text{-}1\ KO}$ clones was performed by Dr. Benjamin Schmid at Bioneer. A total of three SNCA$^{TRIP/DJ\text{-}1\ KO}$ clones were generated (Figure 5.14). Two clones were generated with an exon 2 deletion and one clone was generated with an exon 4 deletion—clonal lines were selected based on polymerase chain reaction experiments confirming the absence of exons 2 and 4 (Figure 5.14b/c).

Figure 5.14 Generation of DJ-1 knockout clones in SNCA^{TRIP} iPSCs (*on next page*)

a, A total of 3 SNCA$^{TRIP/DJ\text{-}1\ KO}$ clones were generated by interrupting the translation of exon 2 (clone 1 and 2) and exon 4 (clone 3). SNCA^{TRIP} iPSCs were nucleofected with CRISPR complexes formed by two sgRNAs targeting either exon 2 or exon 4 of DJ-1 and the HiFi Cas9 protein. After one week, colonies from each nucleofection were picked and analysed by two primer pairs to identify knockout clones. One primer pair was placed around the deleted region and includes part of the neighbouring intronic region (detection assay; DA) whilst a separate primer pair was placed within the deleted region (absence assay; AA). Positive clones in the DA will have a shorter PCR product, whilst positive clones in the AA will have no product. Selected single cells were expanded and tested by DA and AA PCR for exon 2 and exon 4. **b,** For positive clones in the DA, bands at 362 bp (exon 2) or 341 bp (exon 4) were expected. Unwanted wild-type clones showed higher bands at 531 bp (exon 2) or 431 bp (exon 4). **c,** For positive clones in the AA, no bands were expected. Unwanted wild-type clones showed bands at 479 bp (exon 2) or 284 bp (exon 4). Panels **b** and **c** are representative of one PCR experiment per isolated clone. Data in panels **b** and **c** were generated by Dr. Benjamin Schmid.


a
Forward
75 76
PAM
5′ AGACGGTCATCCCTGTAGATGTCATGAGGCGAGCT ··· GTTGATCCACTGCTCACATTTAACGCTTGTTAATG 3′
3′ AGCTCGCCTCATGACATCTACAGGGATGACCGTCT ··· CATTAACAAGCGTTAAATGTGAGCAGTGGATCAAC 5′
169 bp deletion
PAM
244 245
Reverse
1 kb
PARK7
chr1 (p36.23)
exon 1
exon 2
exon 3
exon 4
90 bp deletion
Forward
6569 6570
PAM
5′ AAACTGTTACAGGGACCATATGATGTGGTGGTT ··· TTTTTCCCCCCCCCCAGCTTTATTGAGGTATAA 3′
3′ AACCACCACATCATATGGTCCCTGTAACAGTTT ··· TTATACCTCAATAAAGCTGGGGGGGGGGAAAAA 5′
PAM
Reverse
6659 6660


b
c
#A35-10_E2
#A35-15_E2
#A35-15_E2
#A35-30_E2
#A35-32_E2
#A35-56_E4
#A35-56_E4
#A35-72_E4

Selected DJ-1 knockout iPSC clones were subjected to Sanger DNA sequencing to validate the predicted deletions in DJ-1 (*PARK7*). DNA sequencing analysis revealed a deletion of 169 bp in exon 2 and the downstream intron in SNCA$^{TRIP/DJ\text{-}1\ KO}$ clones 1 and 2, and a deletion of 90 bp in exon 4 and the downstream intron in SNCA$^{TRIP/DJ\text{-}1\ KO}$ clone 3 (Figure 5.15).

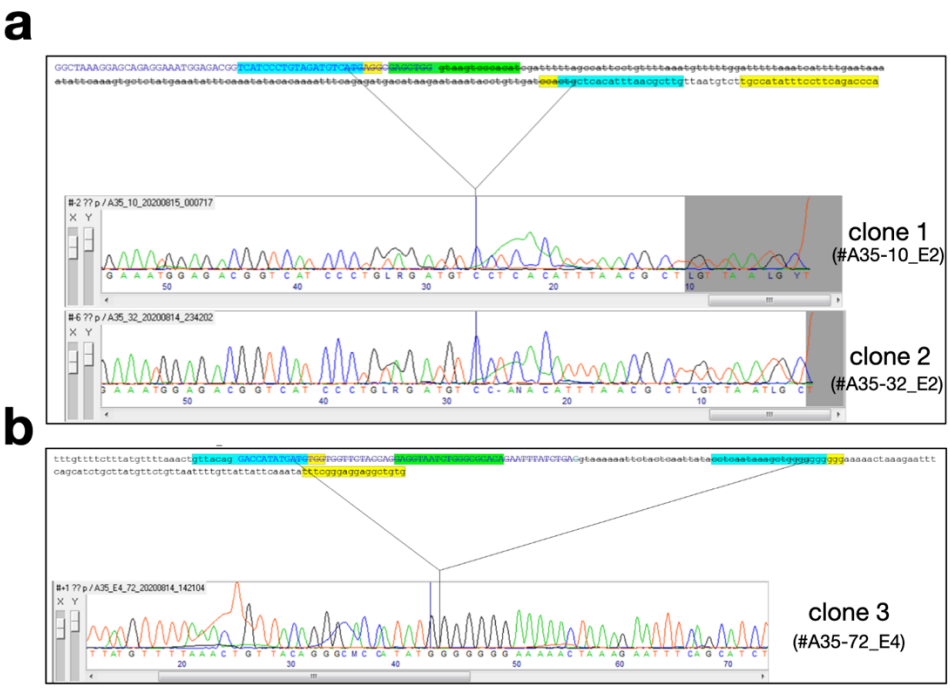


Figure 5.15 Validation of deletions in PARK7 (DJ-1) by Sanger sequencing

a, Sanger sequencing analysis of SNCA$^{TRIP/DJ\text{-}1\ KO}$ clone 1 (#A35-10_E2) and clone 2 (#A35-32_E2) confirmed a deletion of 169 bp at the indicated site. **b,** Sanger sequencing analysis of SNCA$^{TRIP/DJ\text{-}1\ KO}$ clone 3 (#A35-72_E4) confirmed a deletion of 90 bp at the indicated site. Data in this figure was generated by Dr. Benjamin Schmid.

Lastly, short tandem repeat analysis was performed to verify that iPSC SNCA$^{TRIP/DJ\text{-}1\ KO}$ clones shared the same identity as their SNCA^{TRIP} line of origin. The number of allelic repeats tested in each locus was identical between all lines tested, demonstrating that SNCA$^{TRIP/DJ\text{-}1\ KO}$ clones 1/2/3 were indeed derived from the parent SNCA^{TRIP} line (Figure 5.16).

SNCA$^{TRIP/DJ\text{-}1KO}$

	clone 1		clone 2		clone 3		**SNCA^{TRIP}**	
Marker	Allele 1	Allele 2	Allele 1	Allele 2	Allele 1	Allele 2	Allele 1	Allele 2
AMEL	X		X		X		X	
CSF1PO	12		12		12		12	
D13S317	9	11	9	11	9	11	9	11
D16S539	11	12	11	12	11	12	11	12
D18S51	13	22	13	22	13	22	13	22
D19S433	14		14		14		14	
D21S11	30	31,2	30	31,2	30	31,2	30	31.2
D2S1338	21	23	21	23	21	23	21	23
D3S1358	16	17	16	17	16	17	16	17
D5S818	11		11		11		11	
D7S820	9	11	9	11	9	11	9	11
D8S1179	13	14	13	14	13	14	13	14
FGA	20	23	20	23	20	23	20	23
TH01	7	9,3	7	9,3	7	9,3	7	9.3
TPOX	8	11	8	11	8	11	8	11
vWA	15	18	15	18	15	18	15	18

Figure 5.16 Short tandem repeat analysis of CRISPR/Cas9 DJ-1 knockout clones and their corresponding line of origin

The number of allelic repeats tested in each locus matched between all lines, confirming that SNCATRIP/DJ-1 KO clones 1/2/3 were derived from the parent SNCATRIP iPSC line. Data in this figure was generated by Dr. Benjamin Schmid.

Cultured iPSC SNCA$^{TRIP/DJ\text{-}1\ KO}$ clones 1/2/3 shared distinctive pluripotent stem cell morphologies, akin to their SNCA^{TRIP} line of origin (Figure 5.17a). These cells displayed large colonies with clear borders, containing small round cells with large nuclei and notable nucleoli (Amit & Itskovitz-Eldor, 2011). Furthermore, I confirmed the absence of DJ-1 in iPSC SNCA$^{TRIP/DJ\text{-}1\ KO}$ clones 1/2/3 by immunoblotting (Figure 5.17b).

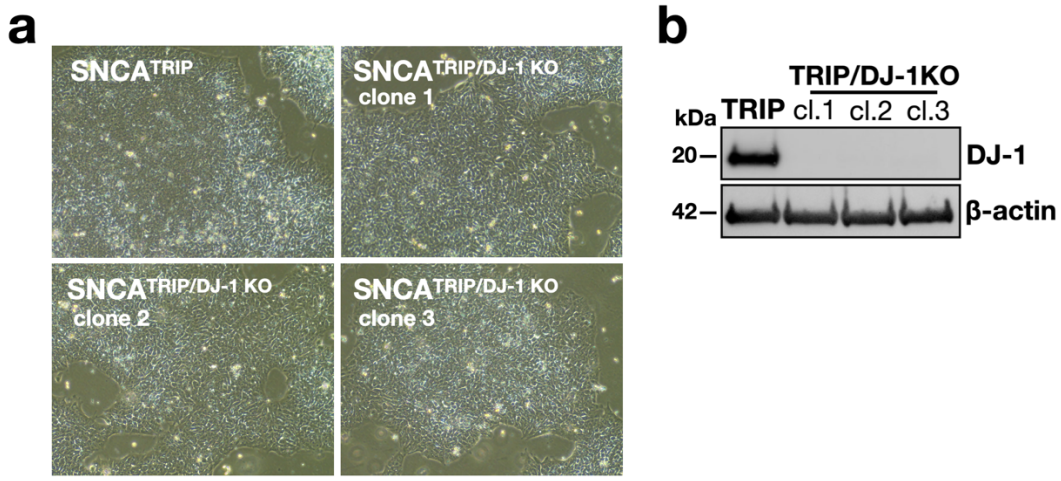


Figure 5.17 Loss of DJ-1 in selected iPSC clones

a, SNCA^{TRIP} and SNCA$^{TRIP/DJ\text{-}1\ KO}$ iPSCs shared distinctive pluripotent stem cell morphologies as small round cells with large nuclei. **b,** DJ-1 knockout was confirmed by immunoblotting in all SNCA$^{TRIP/DJ\text{-}1\ KO}$ iPSC clones (n=9 for SNCA$^{TRIP/DJ\text{-}1\ KO}$, n=3 for SNCA^{TRIP}). In panel **a**, brightfield images taken on 10X lense, no size bar available.

5.2.6.2 Characterisation of SNCA$^{TRIP/DJ\text{-}1\ KO}$ iPSC-derived dopaminergic neurons

I showed that each SNCA$^{TRIP/DJ\text{-}1\ KO}$ clone successfully differentiated into dopaminergic neurons to the same extent as the SNCA^{TRIP} line of origin (Figure 5.18a/b). I also confirmed further the knockout of DJ-1 in SNCA$^{TRIP/DJ\text{-}1\ KO}$ clones using a highly sensitive and DJ-1 specific enzyme linked immunosorbent assay (Figure 5.18c).

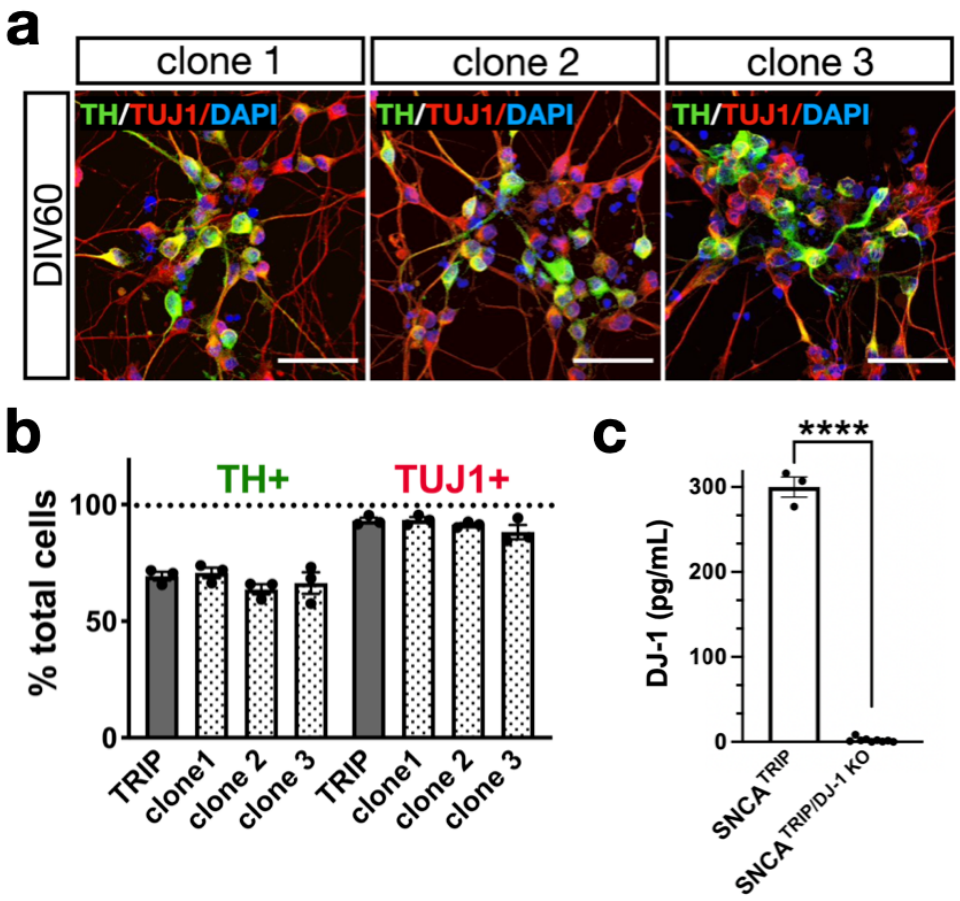


Figure 5.18 Characterisation of human SNCA$^{TRIP/DJ\text{-}1\ KO}$ dopaminergic neurons

a, SNCA$^{TRIP/DJ\text{-}1\ KO}$ iPSC lines differentiated into dopaminergic neurons. Images are representative of three independent differentiations (scale bar: 30 μm). **b,** Quantification of the percentage of TH- and TUJ1-positive in DJ-1 knockout clones was similar to their corresponding SNCA^{TRIP} iPSC line of origin (n=9 for SNCA$^{TRIP/DJ\text{-}1\ KO}$, n=3 for SNCA^{TRIP}). **c,** DJ-1 knockout was confirmed by enzyme-linked immunosorbent assay in dopaminergic neurons (n=9 for SNCA$^{TRIP/DJ\text{-}1\ KO}$, n=3 for SNCA^{TRIP}). Data are shown as mean±s.e.m. In panels **c,** ****P<0.0001 by two-sided unpaired Student's t-test.

DJ-1 knockout in mouse and human neurons has been shown to increase endogenous α-synuclein levels (Burbulla et al., 2017). At baseline, in human SNCA$^{TRIP/DJ\text{-}1\ KO}$ dopaminergic neurons, α-synuclein levels were similar at DIV30 (Figure 5.19a/b) compared to the SNCA^{TRIP} line of origin but increased in DJ-1 knockout clones with time in culture at DIV60 (Figure 5.19c/d).

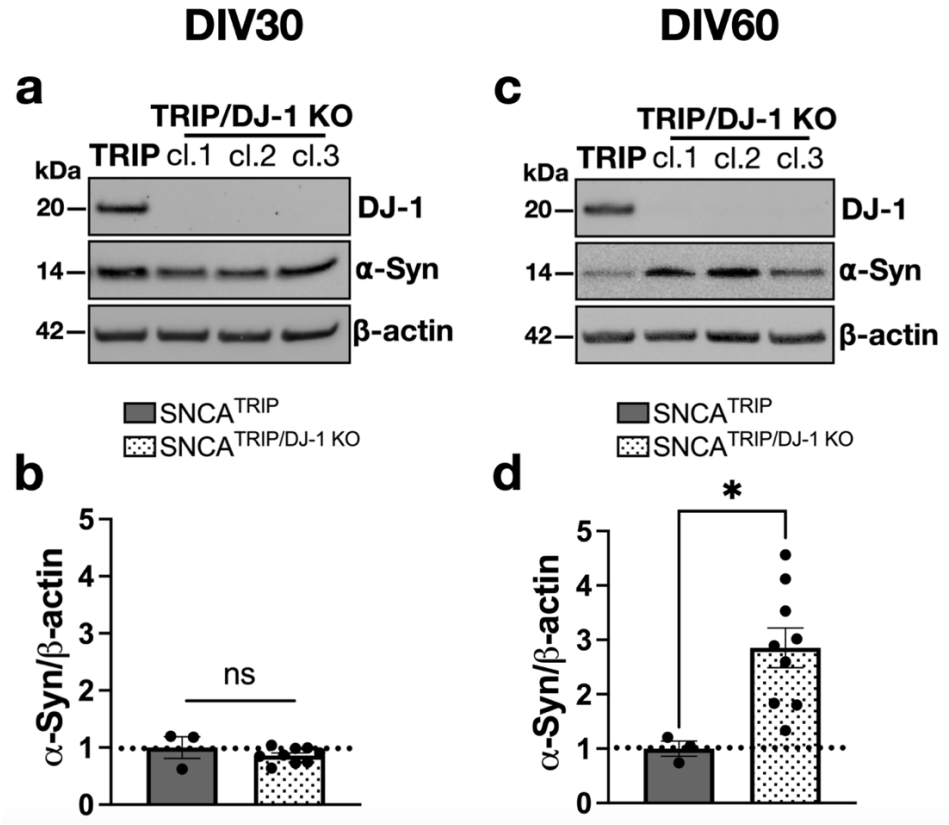


Figure 5.19 Baseline α-synuclein levels increased with time in culture in SNCA$^{TRIP/DJ\text{-}1KO}$ compared to SNCA^{TRIP} iPSC-derived dopaminergic neurons

a, Representative immunoblot for neuronal α-synuclein levels at DIV30 showed no difference between parental iPSC line SNCA^{TRIP} and SNCA$^{TRIP/DJ\text{-}1\ KO}$ lines. This was quantified in panel **b** (n=9 for SNCA$^{TRIP/DJ\text{-}1\ KO}$, n=3 for SNCA^{TRIP}). **c,** Representative immunoblot at DIV60 demonstrated increased α-synuclein levels in SNCA$^{TRIP/DJ\text{-}1\ KO}$ lines compared to SNCA^{TRIP}. This was quantified in panel **d** (n=9 for SNCA$^{TRIP/DJ\text{-}1\ KO}$, n=3 for SNCA^{TRIP}). Each dot represents one clone differentiated once and data are mean±s.e.m from 3 independent differentiations. In panel **d,** *P<0.01, by unpaired Student's t-test.

Additionally, I demonstrated that increased α-synuclein levels at baseline in SNCA$^{TRIP/DJ\text{-}1\ KO}$ dopaminergic neurons was associated with deficits in oxidative phosphorylation at DIV60 compared to healthy control and SNCA^{TRIP} neurons, respectively (Figure 5.20). These findings corroborate with previously published data, showing that the combined effect of elevated intracellular α-synuclein and absence of DJ-1 severely impairs mitochondrial function in neuroblastoma, primary neurons and stem cell-derived dopaminergic neurons (Burbulla et al., 2017; Y. Liu et al., 2019; N. Sharma et al., 2019).

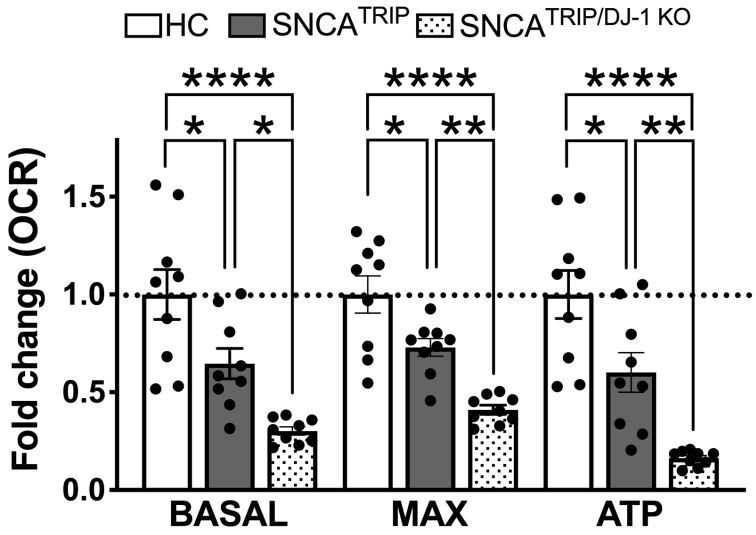


Figure 5.20 DJ-1 knockout in SNCA^{TRIP} dopaminergic neurons further impairs mitochondrial respiration

Reduced basal oxygen consumption rate (OCR), maximal respiration and ATP production was observed in SNCA$^{TRIP/DJ\text{-}1\ KO}$ neurons relative to SNCA^{TRIP} and healthy control lines at baseline on DIV60. Data are shown as mean±s.e.m. *P<0.05 **P<0.01, ****P<0.0001 by one-way ANOVA followed by Tukey's multiple comparison test.

5.2.6.3 Accelerated neurodegeneration in SNCA$^{TRIP/DJ\text{-}1\ KO}$ dopaminergic neurons under seeded aggregation

DJ-1 is primarily involved in a cell's antioxidant response but has also been known, in *in vitro* and *in vivo* models, to play a role in inhibiting α-synuclein aggregation, perhaps by promoting α-synuclein clearance through chaperone-mediated autophagy (C.-Y. Xu et al., 2017). In agreement with these findings and with our DJ-1 knockout experiments in seeded HEK293T cells (Figure 5.10), SNCA$^{TRIP/DJ\text{-}1\ KO}$ dopaminergic neurons also exhibited increased accumulation of pSYN in response to the addition of exogenous *de novo* generated and PD- and MSA-brain amplified fibrils (Figure 5.21a). Homozygous mutations in *PARK7* cause autosomal recessive Parkinson's disease through the loss-of-function of DJ-1 (Bonifati, Rizzu, Squitieri, et al., 2003). As ablation of DJ-1 overall potentiates seeded aggregation in neurons, I asked whether knockdown of DJ-1 also increases on seeded aggregation. Indeed, several compound heterozygous mutations in PARK7 were surprisingly discovered to be disease-causing (Hedrich et al., 2004). DJ-1 small interfering RNA-mediated knockdown achieved 54% and 61% protein reduction in healthy control and SNCA^{TRIP} dopaminergic neurons, respectively (Figure 5.21b). These experiments showed that knockdown of DJ-1 by 50% or more was sufficient to potentiate seeded aggregation in control and SNCA^{TRIP} neurons (Figure 5.21c).

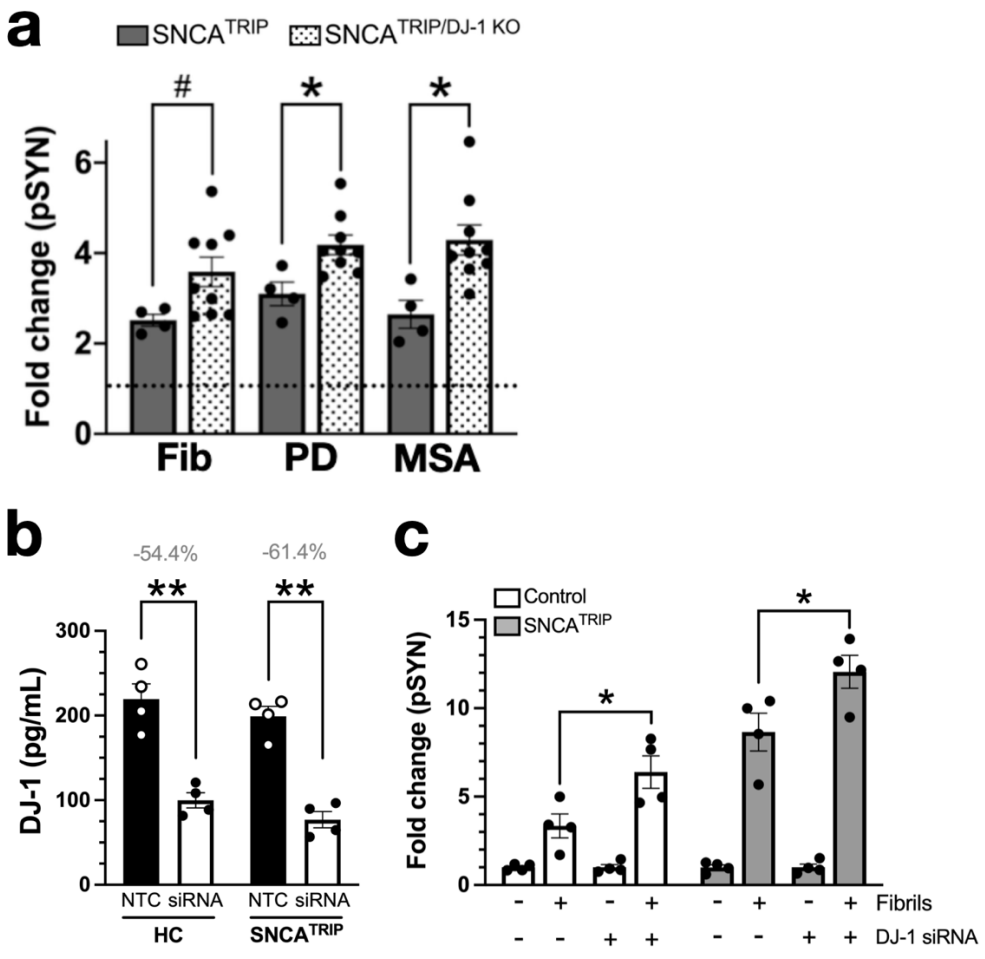


Figure 5.21 DJ-1 knockout in SNCA^{TRIP} dopaminergic neurons exacerbates seeded aggregation

a, Enhanced assembly-induced aggregation of pSYN was observed in surviving SNCA$^{TRIP/DJ\text{-}1\ KO}$ neurons at 2-weeks post-seeding (1 μM) as quantified by HTRF (n=9 for SNCA$^{TRIP/DJ\text{-}1\ KO}$, n=4 for SNCA^{TRIP}). **b,** DJ-1 targeting small interfering RNA (siRNA, 1 μM) treatment reduced DJ-1 levels by 54.4% in healthy control (n=3) and by 61.4% in SNCA^{TRIP} (n=3) dopaminergic neurons as assessed by enzyme-linked immunosorbent assay. **c,** DJ-1 knockdown increased α-synuclein fibril-induced (1 μM) aggregation of pSYN at two-weeks post-seeding in both healthy control (n=4) and SNCA^{TRIP} neurons (n=4) as quantified by HRTF. NTC, non-target control. Each dot corresponds to one clone differentiated once. Data are shown as mean±s.e.m. In panel **a,** $^{\#}P$=0.06, $^{*}P$<0.5 by one-way ANOVA followed by Tukey's multiple comparison test. In panels **b,c,** $^{*}P$<0.05 $^{**}P$<0.01, by two-sided unpaired Student's t-test.

In my earlier experiments, DJ-1 knockout in HEK293 cells expressing Venus fused to α-synuclein increased assembly-induced aggregation levels and was toxic to cells (Figure 5.10). Likewise, $SNCA^{TRIP}$ dopaminergic neurons lacking DJ-1 accumulated higher levels of aggregated α-synuclein (Figure 5.21). Therefore, I sought to investigate the role of DJ-1 on neuronal viability under conditions of pathogenic α-synuclein assembly. Upon seeded aggregation with *de novo* generated and patient brain-amplified assemblies, $SNCA^{TRIP/DJ\text{-}1\ KO}$ dopaminergic neurons exhibited accelerated cell death that was already detectable at 1-week post-seeding. At this timepoint, irrespective of the type of α-synuclein seed used, I observed that exposure to either *de novo* or brain-derived α-synuclein fibrils led to severe axonal degeneration in $SNCA^{TRIP/DJ\text{-}1\ KO}$ dopaminergic neurons (Figure 5.22a). Loss of axonal integrity in DJ-1 knockout neurons was concomitant with increased neuronal death as assessed by nuclear fragmentation (Figure 5.22b) and LDH release (Figure 5.22c).

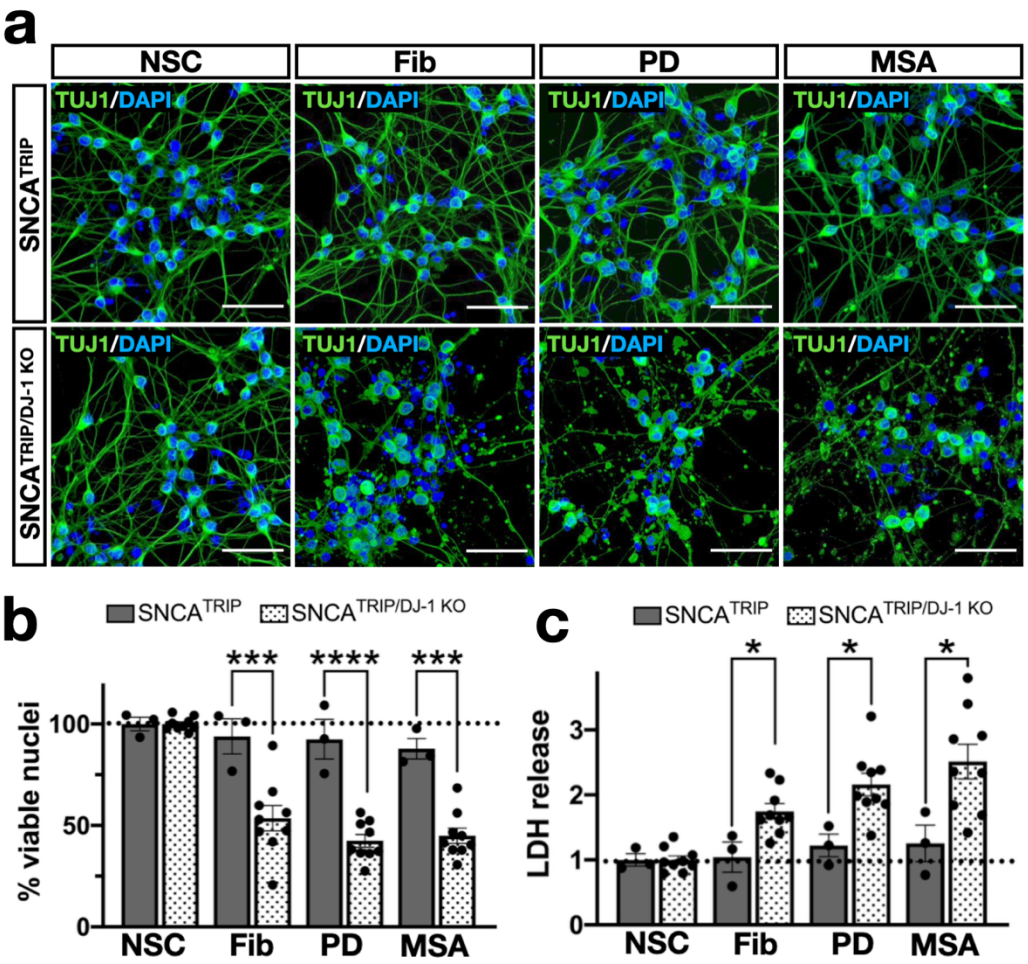


Figure 5.22 α-Synuclein seeded aggregation causes severe neurotoxicity in SNCA$^{TRIP/DJ\text{-}1\ KO}$ dopaminergic neurons

a, Accelerated neuronal death was detected at 1-week post-seeding in SNCA$^{TRIP/DJ\text{-}1\ KO}$ clones irrespective of the type of α-synuclein assembly used when compared to their corresponding SNCA^{TRIP} line of origin. Images are representative of three independent differentiations (scale bar: 30 μm). **b,** Quantification of nuclear fragmentation in the SNCA$^{TRIP/DJ\text{-}1\ KO}$ clones seeded with *de novo* generated fibrils (1 μM), PD-amplified fibrils (1 μM) or MSA-amplified fibrils (1 μM) at 1-week post-seeding (n=9 for SNCA$^{TRIP/DJ\text{-}1\ KO}$, n=3 for SNCA^{TRIP}). At the 1-week timepoint, dopaminergic neurons from the SNCA^{TRIP} line of origin did not exhibit a similarly severe phenotype until 3-weeks post-seeding. **c,** Increased lactate dehydrogenase (LDH) release was detected in SNCA$^{TRIP/DJ\text{-}1\ KO}$ neurons (n=9 for SNCA$^{TRIP/DJ\text{-}1\ KO}$, n=3 for SNCA^{TRIP}). NSC, non-seeded control, non-treated control. Each dot corresponds to one clone differentiated once. Data are shown as mean±s.e.m. *P<0.05 ***P<0.001, ****P<0.0001 by one-way ANOVA followed by Tukey's multiple comparison test.

Collectively, these results lend credence to the hypothesis that differential interactions of α-synuclein strains with the cellular proteome, as evidenced here by DJ-1, may modulate their pathogenic effects—whereas restricting such interactions (e.g. through CRISPR/Cas9-mediated knockout) impairs α-synuclein proteostasis and exacerbates aggregate-induced neuronal death.

5.3 Discussion

An important finding in my work is that assembly-induced toxicity may arise from altered interactions with the cellular proteome, as shown here for DJ-1 (Figure 5.6). It was first suggested through a series of α-synuclein fibrillation assays that DJ-1 inhibits the formation of α-synuclein oligomers *in vitro*, potentially through its function as a redox-sensitive chaperone (Martinat et al., 2004; Shendelman et al., 2004). Subsequent experiments revealed that the active sulfinated form of DJ-1, C106-SO_2H, was significantly more effective in inhibiting α-synuclein aggregation compared to its non-active sulfenated form, C106-SOH (W. Zhou, Zhu, Wilson, Petsko, & Fink, 2006). Here, further oxidation of DJ-1 to its inactive form resulted in the loss of its secondary structure and concurrently its ability to inhibit aggregation. More recently, DJ-1 was also shown to interact with monomeric and oligomeric α-synuclein, whereas DJ-1 mutants impaired these interactions (Zondler et al., 2014). Our biotinylation experiments demonstrated that DJ-1 interaction with intracellular α-synuclein assemblies was most pronounced when seeded with *de novo* generated fibrils versus brain-amplified fibrils, suggesting that strain-specific conformations may determine the strength of such interactions.

Loss of function mutations in DJ-1 cause early onset autosomal recessive Parkinson's disease with Lewy pathology (Taipa et al., 2016). Ablation of DJ-1 in my experiments increased levels of seeded aggregation and aggregate-induced toxicity in HEK293 cells (Figure 5.10) and iPSC-derived dopaminergic neurons (Figure 5.21). Beyond its chaperone activity, we hypothesised that the interaction between DJ-1 and α-synuclein or other proximal proteins during the aggregation cascade may serve a protective effect via deglycation (Richarme et al., 2017). Indeed, multiple epidemiological studies revealed that hyperglycaemic states including pre-existing diabetes mellitus or a high glycaemic index diet were significant risk factors for

developing Parkinson's disease, implicating enhanced glycation in the pathogenic cascade (Becker, Brobert, Johansson, Jick, & Meier, 2008; Cereda et al., 2011; Murakami et al., 2010). In addition, blood glucose levels were elevated in *SNCA* knockout mice, suggesting that α-synuclein negatively regulates glucose metabolism (Kurz et al., 2011). We found that aggregated α-synuclein was glycated in cells and that the presence of AGEs was more pronounced in seeded DJ-1 knockout cells (Figure 5.11). Furthermore, knockout of endogenous glyoxalase, GLO1, also increased α-synuclein aggregation (Figure 5.10). How glycation promotes neurodegeneration remains unclear and is likely multifactorial.

Post-translational modifications on α-synuclein and how they modulate aggregation propensity and neurotoxicity is an important area of research, as phosphorylation on serine 129 and modifications in other sites, were found to be disease-modifying in various models (Tenreiro, Eckermann, & Outeiro, 2014; Y. Wang et al., 2012). In the context of this Chapter, these post-translational modifications are suggested to act as pathological alterations which induce changes in protein structure and stability. A possible mechanism linking glycating stress to α-synuclein-induced neurodegeneration is that glycated proteins can activate a specific receptor for AGE (RAGE), which triggers an inflammatory signalling cascade (Miranda & Outeiro, 2010). Thus, if neuronal-derived glycated proteins are secreted into the extracellular space, it is likely that such proteins or pathological seeds induce neuroinflammation and consequently degeneration through RAGE binding (C Tobon-Velasco, Cuevas, & A Torres-Ramos, 2014; Kierdorf & Fritz, 2013). Increased levels of RAGE were also detected in Parkinson's disease brains and RAGE knockout rescued MPTP/MPP+-induced dopaminergic neuron loss (Dalfó et al., 2005; Teismann et al., 2012).

Alternatively, although glycation was detected under all conditions of seeded aggregation, modification of specific lysine residues on α-synuclein, such as K12, may

result in the deleterious masking of ubiquitination sites as suggested by our mass spectrometry analysis. α-Synuclein was previously shown to be preferentially glycated on lysine residues at the N-terminus, K6, K10, K12, K21, K23, K32, K34, K43, K45 (Vicente Miranda et al., 2017). Therefore, glycation on K12 in my model may prevent conjugation of ubiquitin on K12 and subsequently impair the degradation of misfolded α-synuclein. We identified DJ-1 as an interactor of α-synuclein and observed that this interaction was enhanced in α-synuclein aggregates induced by *de novo* generated fibrils, and weaker in aggregates induced by both PD- and MSA-amplified fibrils (Figure 5.7). On an ultrastructural level, it is likely that aberrantly folded α-synuclein strains can exhibit interactions with overlapping proteins but to varying degrees. The extent to which each strain contributes to the death of neurons is thus unique and specific to its differential interactome. In accordance with these findings, atomic modelling of fibrillar α-synuclein by cryogenic electron microscopy confirmed that the N-terminus of α-synuclein, including K12, is not involved in the amyloid core but rather exposed to the solvent and subject to post-translational modifications like ubiquitination (Guerrero-Ferreira et al., 2019; Schweighauser et al., 2020).

Accordingly, saturating the deglycase or glyoxalase pathways with MGO exacerbated disease phenotypes in my iPSC-based model. Here, $SNCA^{TRIP}$ dopaminergic exposed to *de novo* generated fibrils and supplemented with two pulses of MGO exhibited increased levels of aggregation and fibril-induced neuronal death (Figure 5.13). Dopaminergic neurons in the substantia nigra are considered to be among the most susceptible to oxidative stress due to their high metabolic demand (Biosa et al., 2017). MGO has been shown to modulate dopamine levels and lead to oxidative stress in *in vitro* and *in vivo* models of Parkinson's disease (Szczepanik, de Almeida, Cunha, & Dafre, 2020; Xie et al., 2014). In addition, MGO-induced cytotoxicity was previously shown to trigger α-synuclein pathogenicity via glycation (Vicente

Miranda et al., 2017). Interestingly, chaperone proteins such as small heat shock protein 27 (sHsp27), was shown to be depleted in the presence of MGO and that overexpression of sHsp27 resolved the toxic effects of MGO in cell models of α-synucleinopathy (Vicente Miranda et al., 2020). Altogether, glycation of misfolded α-synuclein or other proximal proteins could overwhelm the glyoxalase pathway, which employs GSH and NADPH to deactivate MGO, thus depleting antioxidant defences or cofactors necessary for their restoration (Jiang et al., 2021). Therefore, by evading potentially protective interactions, for example with DJ-1, assembled α-synuclein may acquire or induce modifications that enhance its neurotoxic effects (Tanudjojo et al., 2021). Further work in this area is needed to confirm the assembly-dependent differential glycation of α-synuclein and assess the effect of α-synuclein glycation in human dopaminergic neurons.

I sought to validate findings in DJ-1 knockout cells described above in a human dopaminergic neuron model. To this end, three DJ-1 knockout clones were generated from $SNCA^{TRIP}$ iPSC clones and characterised for dopaminergic identity (Figure 5.14 and Figure 5.17). Although $SNCA^{TRIP/DJ\text{-}1\ KO}$ cells possessed two disease causing mutations that lead to overexpression of α-synuclein and loss-of-function of DJ-1, the differentiation of these cells into dopaminergic neurons was unimpeded (Figure 5.18). Both α-synuclein and DJ-1 knockout were not lethal in animal models of neurodegeneration, but instead exhibited disease phenotypes later in life or under pharmacological stress conditions (Chandran et al., 2008; Chaprov et al., 2021; Creed et al., 2019; Greten-Harrison et al., 2010; Guschina, Ninkina, Roman, Pokrovskiy, & Buchman, 2021; Kitada, Tong, Gautier, & Shen, 2009; Kyser et al., 2019). These findings suggest that α-synuclein and DJ-1 may be critical determinants of neuronal viability with ageing or other conditions of sustained physiological stress. DJ-1, for example, appears to possess redundant functions with glyoxalase 1 and 2 in the

context of MGO detoxification—however its role may become particularly essential with altered redox states. In Parkinson's disease, the glyoxalase system may thus become saturated due to the brain's dependence on GSH in detoxifying MGO to S-lactoylGSH (Armeni et al., 2014). Here, the deglycase activity of DJ-1 could play a critical role in eliminating glycated α-synuclein, such as in one report demonstrating that DJ-1 attenuated the glycation of mitochondrial complexes in post-ischemic heart tissue (Pantner et al., 2021).

Characterisation of DJ-1 knockout in $SNCA^{TRIP}$ dopaminergic neurons revealed that endogenous α-synuclein levels were elevated at DIV60 but not at DIV30 (Figure 5.19). Increased expression of α-synuclein in the absence of DJ-1 has been reported previously in cell lines and animal models of Parkinson's disease (Burbulla et al., 2017). Likewise, the converse where overexpression of α-synuclein decreases DJ-1 levels, was also shown (S. Lee et al., 2017). These findings demonstrate a potential negative feedback between α-synuclein and DJ-1, which may involve either direct or indirect regulatory mechanisms. For instance, total DJ-1 protein levels were discovered to be significantly reduced in the substantia nigra of sporadic Parkinson's disease patients (Nural et al., 2009)—and concurrently, GSH levels were also found to be significantly reduced in the substantia nigra of diseased patients (Pearce, Owen, Daniel, Jenner, & Marsden, 1997).

DIV60 $SNCA^{TRIP/DJ\text{-}1\ KO}$ neurons exhibited the most significant deficit in mitochondrial respiration compared to $SNCA^{TRIP}$ and healthy control neurons, respectively (Figure 5.20). *PARK* genes, including *PARK7* which encodes DJ-1, have been shown to link mitochondrial dysfunction to α-synuclein pathology in both familial and sporadic cases of Parkinson's disease (W. Li, Fu, Halliday, & Sue, 2021). Although α-synuclein has been implicated in the maintenance of mitochondrial components under physiological conditions, its overexpression has been shown to induce

dopaminergic neuronal death through the release of reactive oxygen species from mitochondria (Ganjam et al., 2019). Moreover, depletion of DJ-1 in cell lines leads to oxidative stress by disrupting the mitochondrial membrane potential and through the accumulation of dysfunctional mitochondria (Ozawa et al., 2020; Trempe & Fon, 2013). Cumulatively, these findings reflect the oxygen consumption rates quantified in dopaminergic neurons at baseline, which suggests that cells harbouring double mutants, *SNCA* triplication and DJ-1 deletion, exhibit significant mitochondrial dysfunction. My model, therefore, strongly implicates mitochondrial impairment in the pathogenesis of Parkinson's disease.

Consistent with the phenotypes observed in DJ-1 knockout HEK293 cells, α-synuclein seeded aggregation and its associated toxicity were enhanced in $SNCA^{TRIP/DJ\text{-}1\ KO}$ dopaminergic neurons compared to their $SNCA^{TRIP}$ line of origin (Figure 5.21a; Figure 5.22). Interestingly, siRNA-mediated knockdown of DJ-1 in both $SNCA^{TRIP}$ and healthy control dopaminergic neurons was also sufficient to increase aggregation in a similar manner as seen in $SNCA^{TRIP/DJ\text{-}1\ KO}$ neurons (Figure 5.21b/c). Validating the effect of DJ-1 levels on seeded aggregation in human neurons suggests that DJ-1 does indeed play an important role in the inhibition of α-synuclein aggregation in healthy and diseased neurons alike. It is also important to note that neuronal death in DJ-1 knockout cells (Figure 5.22b) was quantified at 1-week post-seeding, a timepoint at which fibril-induced death was not observed in $SNCA^{TRIP}$ or control neurons, whereas aggregation was quantified at 2-weeks post-seeding (Figure 5.21a). Aggregation detected in week 2 samples therefore reflect pSYN accumulation in surviving dopaminergic neurons.

Strategies aimed at activating DJ-1 have emerged as a promising therapeutic target (Hijioka, Inden, Yanagisawa, & Kitamura, 2017). Future translational research in this area will benefit from understanding how the interaction between DJ-1 and α-

synuclein mitigates aggregation and rescues toxic phenotypes. For example, the extent of neuroprotection exerted by DJ-1 is dependent on its oxidation state—when activated, DJ-1 was found to counteract the nucleation of α-synuclein seeds through the sequestration of monomeric α-synuclein (Kumar et al., 2019). To further explore the role of DJ-1 in the context of seeded aggregation, I am currently optimising experiments aimed towards deciphering the effect of various pathogenic DJ-1 mutants on aggregation propensity. A number of Parkinson's disease-related DJ-1 mutants have been characterised and shown to interfere with redox sensing (C106A, C46A, C53A) and its detoxification activity (L166P, M261, L10P, A104T, and D149A) (Matsuda et al., 2017). By expressing the above DJ-1 mutants in cell lines and neurons lacking wild-type DJ-1, I hypothesise that certain DJ-1 mutants may exacerbate pSYN accumulation in our models. Discriminating the functional effects of such mutants will ultimately is necessary to enable the development of compounds that modulate the most relevant activity of DJ-1 based on findings derived from DJ-1 mutants.

Chapter 6

Conclusions

The aetiology of Parkinson's disease is complex because it is multifactorial in nature (Spillantini & Goedert, 2018; Tofaris, 2012). Its pathogenesis, likewise, is multifaceted and consists of the dysregulation of multiple cellular systems that are requisites for the performance and maintenance of neuronal function. These distinct pathologies, such as mitochondrial dysfunction, endoplasmic reticulum stress, and impaired protein clearance pathways, converge and trigger the selective degeneration of dopaminergic neurons in the substantia nigra (Henderson, Trojanowski, et al., 2019). In addition, Lewy pathology is most often, but not always, detected in diseased post-mortem brains (Gaig et al., 2007; Johansen et al., 2018). Despite the causal link between Parkinson's disease and its histopathological hallmarks, we do not yet know how and which α-synuclein species are responsible for the death of neurons in diseased human brains.

Research into the identification of molecular targets that counteract the toxicity of aggregated α-synuclein relies on a mechanistic understanding of which species are most harmful. Therefore, to address this challenge, the pathogenesis of Parkinson's disease needs to be examined with different methodologies to understand the biochemical and cellular events that trigger the disease. Throughout my doctoral studies I generated and characterised a robust model of seeded aggregation in iPSC-derived dopaminergic neurons. Using this model, I demonstrated that α-synuclein fibrils amplified from Parkinson's disease and multiple system atrophy were significantly more neurotoxic compared to the conventionally used de novo generated fibrils. Furthermore, biotinylation experiments under seeded aggregation conditions

revealed that DJ-1 was implicated in α-synuclein pathology through its deglycase activity.

Increasing evidence indicates that Parkinson's disease and multiple system atrophy are associated with distinct α-synuclein strains (Burger et al., 2021; Peng, Gathagan, Covell, et al., 2018; Shahnawaz et al., 2020). My data reinforces this notion and suggest that (i) endogenous monomeric α-synuclein which determines abundance of generated assemblies and (ii) conformation which dictates deleterious protein interactions, influence the pathogenicity of said α-synuclein assemblies (Tanudjojo et al., 2021). Hence, strategies aimed towards reducing α-synuclein levels or activating DJ-1 would be promising targets against strain-induced dopaminergic neuronal death. Altogether, my model represents a unique human system to interrogate modifiers of neuronal loss triggered by the intracellular accumulation of brain-amplified α-synuclein conformers.

No curative treatment currently exists for Parkinson's disease and more broadly neurodegenerative diseases—and most clinical trials have been unsuccessful due to poor translational potential of preclinical disease models, lack of disease biomarkers, and phenotypical heterogeneity between patients (Pasteuning-Vuhman, de Jongh, Timmers, & Pasterkamp, 2020). Therefore, iPSC-derived dopaminergic neurons will aid to create scalable high-throughput screening assays with the ultimate goal of identifying novel drug candidates (Sridharan et al., 2019). In this study, I developed a reductionist assay whereby the effect of therapeutic compounds on strain-induced aggregation, viability, or the regulation that SNCA mRNA that I found to be upregulated upon seeded aggregation. In future, iPSC-derived dopaminergic neurons could also be applied in platforms that support a three-dimensional growth environment (brain organoids) and disease-relevant cell to cell interactions (co-culture systems).

Furthermore, functional studies can be performed in dopaminergic neurons to investigate phenotypes resulting from the genetic manipulation of certain genes. CRISPR/Cas9-mediated knockout, as done here for DJ-1, and doxycycline-inducible dCas9-mediated knockdown are amongst the most powerful gene-editing tools to date and are currently being used in our laboratory and others to investigate mechanisms of disease (Brezgin, Kostyusheva, Kostyushev, & Chulanov, 2019; Leng et al., 2021; Tian et al., 2021).

To delineate potentially 'stochastic' events that lead to the pathogenic accumulation of α-synuclein, we employed an integrative "-omics" approach which encapsulated transcriptomic and proteomic analyses to determine aggregation-induced changes in the neuronal model. Our transcriptomic analysis identified multiple hits from our screening experiments, which when visualised through Gene Ontology (http://geneontology.org), converge on biological pathways related to mitochondrial dysfunction, vesicular transport, endoplasmic reticulum stress, and interestingly, non-coding RNA metabolism. These disrupted biological processes shed some light onto the putative functions of α-synuclein and provide future research directions for target validation and subsequent lead optimisation.

An important variable in my model of seeded aggregation is the type of α-synuclein seed used to induce aggregation. Despite exhibiting similar levels of aggregation as measured by levels of pSYN, brain-amplified conformers generated through PMCA were significantly more neurotoxic compared to de novo generated fibrils in human neurons (Tanudjojo et al., 2021). It is likely that de novo fibrils represent a synthetic α-synuclein assembly and thus one which is not physiologically relevant and not tenable in modelling α-synucleinopathies. Phenotypic differences which arise between synthetic and patient brain-amplified conformers, alongside the lack of efficacy in current therapeutics, underlines the necessity to use disease-relevant α-

synuclein strains in drug discovery programs aimed towards the discovery of compounds capable of treating human disease. The full extent to which fibrils amplified with brain homogenate resemble the ones found in brain requires the resolution of their cryo-EM structures. Recently, the cryo-EM structure of fibrils amplified in the presence of sarkosyl-extracted fractions from MSA brain homogenates, using a method different from the one used in this study, were found to exhibit some degree of heterogeneity and differ from the twisted fibrils in the sarkosyl-extracted fractions (Lövestam et al., 2020). This result may be due to the removal by the sarkosyl of relevant factors in the brain homogenate that are required for faithful amplification. Post-translational modifications were shown to mediate the structural diversity of tauopathy strains (Arakhamia et al., 2020). Therefore, distinct α-synuclein strains may also exist as a result of modifications on α-synuclein. Strain diversity is not unique to α-synucleinopathies as growing structural and functional evidence supports the notion that distinct amyloidogenic strains exert different types of pathology in other neurodegenerative disorders such as Alzheimer's disease, amyotrophic lateral sclerosis, Pick's disease, and Huntington's disease (Ayers & Borchelt, 2021; Falcon et al., 2018; Fitzpatrick et al., 2017; Isas et al., 2021; H. H. Lau, Ingelsson, & Watts, 2021). Indeed, several lines of evidence have demonstrated the presence of pathogenic forms of α-synuclein (oligomeric and fibrillar) through conformation-specific antibodies or other techniques (El-Agnaf et al., 2017; Roberts, Wade-Martins, & Alegre-Abarrategui, 2015; Vaikath et al., 2015). A recurrent theme emerges from the above findings, which suggests that the role of strain biology in disease heterogeneity has significant implications on the diagnosis and treatment of patients afflicted with neurodegenerative disorders.

Current hypotheses to counteract α-synuclein aggregate-induced pathology include (i) decreasing endogenous levels of α-synuclein monomer, (ii) increasing

misfolded α-synuclein degradation, (iii) inhibition of α-synuclein oligomerisation, (iv) depolymerisation of aggregate, or (v) antibody-mediated clearance of misfolded α-synuclein (Sardi, Cedarbaum, & Brundin, 2018). However, therapeutic compounds may also include activators or inhibitors that modulate disease-modifying proteins, like DJ-1. Based on the disease mechanism proposed in my model (Chapter 5), enhancing the deglycase activity of DJ-1 may rescue α-synuclein toxicity by increasing its clearance. Under conditions of seeded aggregation, α-synuclein appears to be aberrantly glycated, potentially on residue K12. Therefore, increasing DJ-1 activity or reducing α-synuclein glycation are possible therapeutic avenues.

In the past decade, DJ-1 has emerged as a novel therapeutic target for neurodegeneration; its modulation was shown to be capable of attenuating certain disease phenotypes in cell and animal models (Hijioka et al., 2017; Kitamura et al., 2011; Repici & Giorgini, 2019). Overexpression of DJ-1 in rodent dopaminergic neurons has been consistently shown to exhibit a neuroprotective role, whilst DJ-1 downregulation sensitized neurons to cell death (Antoniou & Borsello, 2010; Gao et al., 2012; Inden et al., 2006; S.-Y. Sun et al., 2012). Hence, as DJ-1 abundance ameliorates disease phenotypes, increasing DJ-1 activity may also be therapeutic. To this end, multiple studies have utilised compounds that inhibit the excessive oxidation of DJ-1 into its inactive form (C106-SO3H) by stabilising its homodimeric form (Huang & Chen, 2021). These compounds, which were identified by in silico screening, prevented dopaminergic cell death, and reduced oxidative stress (Inden et al., 2011; Kitamura et al., 2011; Miyazaki et al., 2008). Although DJ-1 activating compounds revealed positive results, these studies were carried out solely in cell lines and rodent models. Therefore, future work in this area will benefit from proof-of-concept experiments in human systems.

More broadly, hyperglycaemia is a risk factor for Parkinson's disease and diabetic medicines (glitazones, exenatide, metformin, thiamine, glucagon-like peptide-1 receptor agonists, dipeptidyl peptidase 4 inhibitors) were clinically proven to alleviate symptoms in parkinsonian patients (Brauer et al., 2020; Koenig, Vicente Miranda, & Outeiro, 2018). These findings link the role of advanced glycation end-products (AGEs) or other intermediates to the pathogenesis of Parkinson's disease. Glycation and consequently, the presence of AGE, can be modulated (i) by decreasing levels of reducing sugars (e.g. glucose or dicarbonyls), (ii) scavenging AGE precursors such as MGO, or (iii) by enhancing the degradation of reducing sugars. Manipulating AGE levels via diabetic drugs combined with DJ-1 activating compounds may thus be one solution for Parkinson's disease therapies.

Neurodegeneration is an irreversible process and symptoms and signs of Parkinson's disease do not develop until 40-70% of dopaminergic neurons have been lost, therefore treatment should be administered during its prodromal stages (El-Agnaf et al., 2006). Given the growing recognition for the impact of α-synuclein strains, therapeutic or preventive strategies need to evolve towards a personalised medicine approach tailored for strain-specific therapeutics. When genetic screening becomes increasingly widespread, patients who are at risk may one day be diagnosed using early biomarkers (e.g. strain identification through PMCA or detection in extracellular vesicles) and stratified for prognostic care.

Personalised medicine has dramatically transformed the way in which cancer is diagnosed and treated today. My hope is to witness its implementation in patients afflicted from neurodegenerative disorders (Woerman, 2021). This hope is contingent upon the development of strain-specific cellular and animal disease models, which will pave the way for successful clinical translation of diagnostic and therapeutic solutions.

References

Abbott, R., Ross, G., White, L., Tanner, C., Masaki, K., Nelson, J., . . . Petrovitch, H. (2005). Excessive daytime sleepiness and subsequent development of Parkinson disease. *Neurology, 65*(9), 1442-1446.

Abeliovich, A., Schmitz, Y., Fariñas, I., Choi-Lundberg, D., Ho, W.-H., Castillo, P. E., . . . Ryan, A. (2000). Mice lacking α-synuclein display functional deficits in the nigrostriatal dopamine system. *Neuron, 25*(1), 239-252.

Abernathy, D. G., Kim, W. K., McCoy, M. J., Lake, A. M., Ouwenga, R., Lee, S. W., . . . Heuckeroth, R. O. (2017). MicroRNAs induce a permissive chromatin environment that enables neuronal subtype-specific reprogramming of adult human fibroblasts. *Cell stem cell, 21*(3), 332-348. e339.

Abrams, Z. B., Johnson, T. S., Huang, K., Payne, P. R., & Coombes, K. (2019). A protocol to evaluate RNA sequencing normalization methods. *BMC bioinformatics, 20*(24), 1-7.

Adams, C. J., Kopp, M. C., Larburu, N., Nowak, P. R., & Ali, M. M. (2019). Structure and molecular mechanism of ER stress signaling by the unfolded protein response signal activator IRE1. *Frontiers in Molecular Biosciences, 6*, 11.

Adrover, M., Mariño, L., Sanchis, P., Pauwels, K., Kraan, Y., Lebrun, P., . . . Donoso, J. (2014). Mechanistic insights in glycation-induced protein aggregation. *Biomacromolecules, 15*(9), 3449-3462.

Aflaki, E., Borger, D. K., Moaven, N., Stubblefield, B. K., Rogers, S. A., Patnaik, S., . . . Sullivan, P. (2016). A new glucocerebrosidase chaperone reduces α-synuclein and glycolipid levels in iPSC-derived dopaminergic neurons from patients with Gaucher disease and parkinsonism. *Journal of Neuroscience, 36*(28), 7441-7452.

Aguzzi, A., & Lakkaraju, A. K. (2016). Cell biology of prions and prionoids: a status report. *Trends in cell biology, 26*(1), 40-51.

Alberico, S. L., Cassell, M. D., & Narayanan, N. S. (2015). The vulnerable ventral tegmental area in Parkinson's disease. *Basal ganglia, 5*(2-3), 51-55.

Amit, M., & Itskovitz-Eldor, J. (2011). *Atlas of human pluripotent stem cells: derivation and culturing*: Springer Science & Business Media.

Anderegg, A., Poulin, J.-F., & Awatramani, R. (2015). Molecular heterogeneity of midbrain dopaminergic neurons–Moving toward single cell resolution. *FEBS letters, 589*(24), 3714-3726.

Anderson, J. P., Walker, D. E., Goldstein, J. M., De Laat, R., Banducci, K., Caccavello, R. J., . . . Lee, M. (2006). Phosphorylation of Ser-129 is the dominant pathological modification of α-synuclein in familial and sporadic Lewy body disease. *Journal of Biological Chemistry, 281*(40), 29739-29752.

Angelova, P. R., Choi, M. L., Berezhnov, A. V., Horrocks, M. H., Hughes, C. D., De, S., . . . Gandhi, S. (2020). Alpha synuclein aggregation drives ferroptosis: an interplay of iron, calcium and lipid peroxidation. *Cell Death Differ, 27*(10), 2781-2796. doi:10.1038/s41418-020-0542-z

Annerino, D. M., Arshad, S., Taylor, G. M., Adler, C. H., Beach, T. G., & Greene, J. G. (2012). Parkinson's disease is not associated with gastrointestinal myenteric ganglion neuron loss. *Acta neuropathologica, 124*(5), 665-680.

Ansari, K., & Johnson, A. (1975). Olfactory function in patients with Parkinson's disease. *Journal of chronic diseases, 28*(9), 493-497.

Antoniou, X., & Borsello, T. (2010). Cell permeable peptides: a promising tool to deliver neuroprotective agents in the brain. *Pharmaceuticals, 3*(2), 379-392.

Anwar, S., Peters, O., Millership, S., Ninkina, N., Doig, N., Connor-Robson, N., . . . Bannerman, D. M. (2011). Functional alterations to the nigrostriatal system in mice lacking all three members of the synuclein family. *Journal of Neuroscience, 31*(20), 7264-7274.

Appel-Cresswell, S., Vilarino-Guell, C., Encarnacion, M., Sherman, H., Yu, I., Shah, B., . . . Trinh, J. (2013). Alpha-synuclein p. H50Q, a novel pathogenic mutation for Parkinson's disease. *Movement Disorders, 28*(6), 811-813.

Arakhamia, T., Lee, C. E., Carlomagno, Y., Duong, D. M., Kundinger, S. R., Wang, K., . . . Cook, C. N. (2020). Posttranslational modifications mediate the structural diversity of tauopathy strains. *Cell, 180*(4), 633-644. e612.

Arenas, E., Denham, M., & Villaescusa, J. C. (2015). How to make a midbrain dopaminergic neuron. *Development, 142*(11), 1918-1936.

Ariesandi, W., Chang, C.-F., Chen, T.-E., & Chen, Y.-R. (2013). Temperature-dependent structural changes of Parkinson's alpha-synuclein reveal the role of pre-existing oligomers in alpha-synuclein fibrillization. *PloS one, 8*(1), e53487.

Ariga, H., Takahashi-Niki, K., Kato, I., Maita, H., Niki, T., & Iguchi-Ariga, S. M. (2013). Neuroprotective function of DJ-1 in Parkinson's disease. *Oxidative medicine and cellular longevity, 2013*.

Armeni, T., Cianfruglia, L., Piva, F., Urbanelli, L., Caniglia, M. L., Pugnaloni, A., & Principato, G. (2014). SD-Lactoylglutathione can be an alternative supply of mitochondrial glutathione. *Free Radical Biology and Medicine, 67*, 451-459.

Arotcarena, M.-L., Dovero, S., Prigent, A., Bourdenx, M., Camus, S., Porras, G., . . . Kruse, N. (2020). Bidirectional gut-to-brain and brain-to-gut propagation of synucleinopathy in non-human primates. *Brain, 143*(5), 1462-1475.

Athauda, D., Maclagan, K., Skene, S. S., Bajwa-Joseph, M., Letchford, D., Chowdhury, K., . . . Dickson, J. (2017). Exenatide once weekly versus placebo in Parkinson's disease: a randomised, double-blind, placebo-controlled trial. *The Lancet, 390*(10103), 1664-1675.

Ayers, J. I., & Borchelt, D. R. (2021). Phenotypic diversity in ALS and the role of poly-conformational protein misfolding. *Acta neuropathologica, 142*(1), 41-55.

Baba, M., Nakajo, S., Tu, P.-H., Tomita, T., Nakaya, K., Lee, V., . . . Iwatsubo, T. (1998). Aggregation of alpha-synuclein in Lewy bodies of sporadic Parkinson's disease and dementia with Lewy bodies. *The American journal of pathology, 152*(4), 879.

Bacioglu, M., Maia, L. F., Preische, O., Schelle, J., Apel, A., Kaeser, S. A., . . . Pilotto, A. (2016). Neurofilament light chain in blood and CSF as marker of disease progression in mouse models and in neurodegenerative diseases. *Neuron, 91*(1), 56-66.

Bandopadhyay, R., Kingsbury, A. E., Cookson, M. R., Reid, A. R., Evans, I. M., Hope, A. D., . . . Miller, D. W. (2004). The expression of DJ-1 (PARK7) in normal human CNS and idiopathic Parkinson's disease. *Brain, 127*(2), 420-430.

Bandres-Ciga, S., Diez-Fairen, M., Kim, J. J., & Singleton, A. B. (2020). Genetics of Parkinson's disease: an introspection of its journey towards precision medicine. *Neurobiology of disease, 137*, 104782.

Barrett, P. J., & Greenamyre, J. T. (2015). Post-translational modification of α-synuclein in Parkinson′ s disease. *Brain research, 1628*, 247-253.

Barth, M., Bacioglu, M., Schwarz, N., Novotny, R., Brandes, J., Welzer, M., . . . Wuttke, T. V. (2021). Microglial inclusions and neurofilament light chain release follow neuronal α-synuclein lesions in long-term brain slice cultures. *Molecular neurodegeneration, 16*(1), 1-17.

Beach, T. G., Adler, C. H., Sue, L. I., Peirce, J. B., Bachalakuri, J., Dalsing-Hernandez, J. E., . . . Sabbagh, M. N. (2008). Reduced striatal tyrosine hydroxylase in incidental Lewy body disease. *Acta neuropathologica, 115*(4), 445-451.

Beck, R., Fowler, C. J., & Mathias, C. J. (1994). Genitourinary dysfunction in disorders of the autonomic nervous system. *Handbook of Neuro Urology*, 281-301.

Becker, C., Brobert, G. P., Johansson, S., Jick, S. S., & Meier, C. R. (2008). Diabetes in patients with idiopathic Parkinson's disease. *Diabetes Care, 31*(9), 1808-1812.

Bélanger, M., Yang, J., Petit, J.-M., Laroche, T., Magistretti, P. J., & Allaman, I. (2011). Role of the glyoxalase system in astrocyte-mediated neuroprotection. *Journal of Neuroscience, 31*(50), 18338-18352.

Bellucci, A., Zaltieri, M., Navarria, L., Grigoletto, J., Missale, C., & Spano, P. (2012). From α-synuclein to synaptic dysfunctions: new insights into the pathophysiology of Parkinson's disease. *Brain research, 1476*, 183-202.

Benabid, A.-L., Pollak, P., Louveau, A., Henry, S., & De Rougemont, J. (1987). Combined (thalamotomy and stimulation) stereotactic surgery of the VIM thalamic nucleus for bilateral Parkinson disease. *Stereotactic and functional neurosurgery, 50*(1-6), 344-346.

Bendor, J. T., Logan, T. P., & Edwards, R. H. (2013). The function of α-synuclein. *Neuron, 79*(6), 1044-1066.

Berry, B. J., Smith, A. S., Young, J. E., & Mack, D. L. (2018). Advances and current challenges associated with the use of human induced pluripotent stem cells in modeling neurodegenerative disease. *Cells Tissues Organs, 205*(5-6), 331-349.

Bessen, R. A., & Marsh, R. F. (1992). Biochemical and physical properties of the prion protein from two strains of the transmissible mink encephalopathy agent. *Journal of virology, 66*(4), 2096-2101.

Biosa, A., Sandrelli, F., Beltramini, M., Greggio, E., Bubacco, L., & Bisaglia, M. (2017). Recent findings on the physiological function of DJ-1: Beyond Parkinson's disease. *Neurobiology of disease, 108*, 65-72.

Bisaglia, M., Mammi, S., & Bubacco, L. (2009). Structural insights on physiological functions and pathological effects of±-synuclein. *The FASEB Journal, 23*(2), 329-340.

Blauwendraat, C., Nalls, M. A., & Singleton, A. B. (2020). The genetic architecture of Parkinson's disease. *The Lancet Neurology, 19*(2), 170-178.

Blocq, P., & Marinesco, G. (1893). *Sur un cas de tremblement parkinsonien hémiplégique: symptomatique d'une tumeur du pédoncule cérébral*: G. Masson.

Bonifati, V., Rizzu, P., Squitieri, F., Krieger, E., Vanacore, N. a., Van Swieten, J., . . . Meco, G. (2003). DJ-1 (PARK7), a novel gene for autosomal recessive, early onset parkinsonism. *Neurological sciences, 24*(3), 159-160.

Bonifati, V., Rizzu, P., Van Baren, M. J., Schaap, O., Breedveld, G. J., Krieger, E., . . . Joosse, M. (2003). Mutations in the DJ-1 gene associated with autosomal recessive early-onset parkinsonism. *Science, 299*(5604), 256-259.

Borrageiro, G., Haylett, W., Seedat, S., Kuivaniemi, H., & Bardien, S. (2018). A review of genome-wide transcriptomics studies in Parkinson's disease. *European Journal of Neuroscience, 47*(1), 1-16.

Bougea, A., Stefanis, L., Paraskevas, G. P., Emmanouilidou, E., Vekrelis, K., & Kapaki, E. (2019). Plasma alpha-synuclein levels in patients with Parkinson's disease: a systematic review and meta-analysis. *Neurological sciences, 40*(5), 929-938.

Bousset, L., Pieri, L., Ruiz-Arlandis, G., Gath, J., Jensen, P. H., Habenstein, B., . . . Meier, B. H. (2013). Structural and functional characterization of two alpha-synuclein strains. *Nat Commun., 4*(1), 1-13.

Braak, H., & Braak, E. (2000). Pathoanatomy of Parkinson's disease. *Journal of neurology, 247*(2), II3-II10.

Braak, H., de Vos, R. A., Bohl, J., & Del Tredici, K. (2006). Gastric α-synuclein immunoreactive inclusions in Meissner's and Auerbach's plexuses in cases staged for Parkinson's disease-related brain pathology. *Neuroscience letters, 396*(1), 67-72.

Braak, H., & Del Tredici, K. (2008). Neuroanatomy and pathology of sporadic Parkinson's disease.

Braak, H., Del Tredici, K., Bratzke, H., Hamm-Clement, J., Sandmann-Keil, D., & Rüb, U. (2002). Staging of the intracerebral inclusion body pathology associated with idiopathic Parkinson's disease (preclinical and clinical stages). *Journal of neurology, 249*(3), iii1-iii5.

Braak, H., Ghebremedhin, E., Rüb, U., Bratzke, H., & Del Tredici, K. (2004). Stages in the development of Parkinson's disease-related pathology. *Cell and tissue research, 318*(1), 121-134.

Braak, H., Rüb, U., Gai, W., & Del Tredici, K. (2003). Idiopathic Parkinson's disease: possible routes by which vulnerable neuronal types may be

subject to neuroinvasion by an unknown pathogen. *Journal of neural transmission, 110*(5), 517-536.

Braak, H., Sastre, M., Bohl, J. R., de Vos, R. A., & Del Tredici, K. (2007). Parkinson's disease: lesions in dorsal horn layer I, involvement of parasympathetic and sympathetic pre-and postganglionic neurons. *Acta neuropathologica, 113*(4), 421-429.

Bras, J., Guerreiro, R., Darwent, L., Parkkinen, L., Ansorge, O., Escott-Price, V., . . . Honig, L. S. (2014). Genetic analysis implicates APOE, SNCA and suggests lysosomal dysfunction in the etiology of dementia with Lewy bodies. *Human molecular genetics, 23*(23), 6139-6146.

Brauer, R., Wei, L., Ma, T., Athauda, D., Girges, C., Vijiaratnam, N., . . . Foltynie, T. (2020). Diabetes medications and risk of Parkinson's disease: a cohort study of patients with diabetes. *Brain, 143*(10), 3067-3076.

Bray, N. L., Pimentel, H., Melsted, P., & Pachter, L. (2016). Near-optimal probabilistic RNA-seq quantification. *Nat. Biotechnol., 34*(5), 525-527.

Brazdis, R.-M., Alecu, J. E., Marsch, D., Dahms, A., Simmnacher, K., Lörentz, S., . . . Roybon, L. (2020). Demonstration of brain region-specific neuronal vulnerability in human iPSC-based model of familial Parkinson's disease. *Human molecular genetics, 29*(7), 1180-1191.

Breydo, L., Wu, J. W., & Uversky, V. N. (2012). α-Synuclein misfolding and Parkinson's disease. *Biochimica et Biophysica Acta (BBA)-Molecular Basis of Disease, 1822*(2), 261-285.

Brezgin, S., Kostyusheva, A., Kostyushev, D., & Chulanov, V. (2019). Dead Cas systems: types, principles, and applications. *International journal of molecular sciences, 20*(23), 6041.

Brichta, L., & Greengard, P. (2014). Molecular determinants of selective dopaminergic vulnerability in Parkinson's disease: an update. *Frontiers in neuroanatomy, 8*, 152.

Brini, M., Ottolini, D., Calì, T., & Carafoli, E. (2013). Calcium in health and disease. *Interrelations between essential metal ions and human diseases*, 81-137.

Brissaud, É., & Meige, H. (1895). *Gigantisme et acromégalie, par É. Brissaud et H. Meige*: A. Coccoz.

Brundin, P., & Melki, R. (2017). Prying into the prion hypothesis for Parkinson's disease. *Journal of Neuroscience, 37*(41), 9808-9818.

Buchman, V. L., Hunter, H. J., Pinõn, L. G., Thompson, J., Privalova, E. M., Ninkina, N. N., & Davies, A. M. (1998). Persyn, a member of the synuclein family, has a distinct pattern of expression in the developing nervous system. *Journal of Neuroscience, 18*(22), 9335-9341.

Buell, A. K., Galvagnion, C., Gaspar, R., Sparr, E., Vendruscolo, M., Knowles, T. P., . . . Dobson, C. M. (2014). Solution conditions determine the relative importance of nucleation and growth processes in α-synuclein aggregation. *Proceedings of the National Academy of Sciences, 111*(21), 7671-7676.

Burbulla, L. F., Song, P., Mazzulli, J. R., Zampese, E., Wong, Y. C., Jeon, S., . . . Strojny, C. (2017). Dopamine oxidation mediates mitochondrial and lysosomal dysfunction in Parkinson's disease. *Science, 357*(6357), 1255-1261.

Burger, D., Fenyi, A., Bousset, L., Stahlberg, H., & Melki, R. (2021). Cryo-EM structure of alpha-synuclein fibrils amplified by PMCA from PD and MSA patient brains. *bioRxiv*.

Burré, J. (2015). The synaptic function of α-synuclein. *Journal of Parkinson's disease, 5*(4), 699-713.

Burré, J., Sharma, M., & Südhof, T. C. (2014). α-Synuclein assembles into higher-order multimers upon membrane binding to promote SNARE complex formation. *Proceedings of the National Academy of Sciences, 111*(40), E4274-E4283.

Burré, J., Sharma, M., Tsetsenis, T., Buchman, V., Etherton, M. R., & Südhof, T. C. (2010). α-Synuclein promotes SNARE-complex assembly in vivo and in vitro. *Science, 329*(5999), 1663-1667.

Bush, W. D., Garguilo, J., Zucca, F. A., Albertini, A., Zecca, L., Edwards, G. S., . . . Simon, J. D. (2006). The surface oxidation potential of human neuromelanin reveals a spherical architecture with a pheomelanin core and a eumelanin surface. *Proceedings of the National Academy of Sciences, 103*(40), 14785-14789.

Byers, B., Cord, B., Nguyen, H. N., Schüle, B., Fenno, L., Lee, P. C., . . . Palmer, T. D. (2011). SNCA triplication Parkinson's patient's iPSC-derived DA neurons accumulate α-synuclein and are susceptible to oxidative stress. *PloS one, 6*(11), e26159. doi:10.1371/journal.pone.0026159

Byrne, L. M., Rodrigues, F. B., Blennow, K., Durr, A., Leavitt, B. R., Roos, R. A., . . . Langbehn, D. (2017). Neurofilament light protein in blood as a potential biomarker of neurodegeneration in Huntington's disease: a retrospective cohort analysis. *The Lancet Neurology, 16*(8), 601-609.

C Tobon-Velasco, J., Cuevas, E., & A Torres-Ramos, M. (2014). Receptor for AGEs (RAGE) as mediator of NF-kB pathway activation in neuroinflammation and oxidative stress. *CNS & Neurological Disorders-Drug Targets (Formerly Current Drug Targets-CNS & Neurological Disorders), 13*(9), 1615-1626.

Caiazza, M. C., Lang, C., & Wade-Martins, R. (2020). What we can learn from iPSC-derived cellular models of Parkinson's disease. *Progress in brain research, 252*, 3-25.

Campbell, B. C., Li, Q.-X., Culvenor, J. G., Jäkälä, P., Cappai, R., Beyreuther, K., . . . McLean, C. A. (2000). Accumulation of insoluble α-synuclein in dementia with Lewy bodies. *Neurobiology of disease, 7*(3), 192-200.

Candelise, N., Schmitz, M., Llorens, F., Villar-Piqué, A., Cramm, M., Thom, T., . . . Outeiro, T. F. (2019). Seeding variability of different alpha synuclein strains in synucleinopathies. *Annals of neurology, 85*(5), 691-703.

Carlsson, A. (1959). The occurrence, distribution and physiological role of catecholamines in the nervous system. *Pharmacological reviews, 11*(2), 490-493.

Carlsson, A., Waters, N., Holm-Waters, S., Tedroff, J., Nilsson, M., & Carlsson, M. L. (2001). Interactions between monoamines, glutamate, and GABA in schizophrenia: new evidence. *Annual review of pharmacology and toxicology, 41*(1), 237-260.

Carter, J. L., Halmai, J., & Fink, K. D. (2020). The iNs and Outs of Direct Reprogramming to Induced Neurons. *Frontiers in Genome Editing, 2*, 7.
Castellani, R., Smith, M., Richey, G., & Perry, G. (1996). Glycoxidation and oxidative stress in Parkinson disease and diffuse Lewy body disease. *Brain research, 737*(1-2), 195-200.
Castilla, J., Saá, P., Morales, R., Abid, K., Maundrell, K., & Soto, C. (2006). Protein misfolding cyclic amplification for diagnosis and prion propagation studies. *Methods in enzymology, 412*, 3-21.
Cereda, E., Barichella, M., Pedrolli, C., Klersy, C., Cassani, E., Caccialanza, R., & Pezzoli, G. (2011). Diabetes and risk of Parkinson's disease: a systematic review and meta-analysis. *Diabetes Care, 34*(12), 2614-2623.
Cerri, S., Mus, L., & Blandini, F. (2019). Parkinson's disease in women and men: What's the difference? *Journal of Parkinson's disease, 9*(3), 501-515.
Chambers, S. M., Fasano, C. A., Papapetrou, E. P., Tomishima, M., Sadelain, M., & Studer, L. (2009). Highly efficient neural conversion of human ES and iPS cells by dual inhibition of SMAD signaling. *Nature biotechnology, 27*(3), 275-280.
Chandra, S., Fornai, F., Kwon, H.-B., Yazdani, U., Atasoy, D., Liu, X., . . . Castillo, P. E. (2004). Double-knockout mice for α-and β-synucleins: effect on synaptic functions. *Proceedings of the National Academy of Sciences, 101*(41), 14966-14971.
Chandran, J. S., Lin, X., Zapata, A., Höke, A., Shimoji, M., Moore, S. O. L., . . . Price, D. L. (2008). Progressive behavioral deficits in DJ-1-deficient mice are associated with normal nigrostriatal function. *Neurobiology of disease, 29*(3), 505-514.
Chang, C.-W., Yang, S.-Y., Yang, C.-C., Chang, C.-W., & Wu, Y.-R. (2020). Plasma and serum alpha-Synuclein as a biomarker of diagnosis in patients with Parkinson's disease. *Frontiers in neurology, 10*, 1388.
Chaprov, K., Teterina, E., Roman, A. Y., Ivanova, T., Goloborshcheva, V., Kucheryanu, V., . . . Koroleva, I. (2021). Comparative Analysis of MPTP Neurotoxicity in Mice with a Constitutive Knockout of the α-Synuclein Gene. *Molecular Biology, 55*(1), 133-142.
Charcot, J., & Sigerson, G. T. (1879). On paralysis agitans.
Chartier-Harlin, M.-C., Kachergus, J., Roumier, C., Mouroux, V., Douay, X., Lincoln, S., . . . Hulihan, M. (2004). α-synuclein locus duplication as a cause of familial Parkinson's disease. *The Lancet, 364*(9440), 1167-1169.
Chaudhuri, K. R., Healy, D. G., & Schapira, A. H. (2006). Non-motor symptoms of Parkinson's disease: diagnosis and management. *The Lancet Neurology, 5*(3), 235-245.
Chen, B. J., Mills, J. D., Takenaka, K., Bliim, N., Halliday, G. M., & Janitz, M. (2016). Characterization of circular RNA s landscape in multiple system atrophy brain. *Journal of neurochemistry, 139*(3), 485-496.
Chen, H., Zhang, S., Schwarzschild, M., Hernan, M., & Ascherio, A. (2005). Physical activity and the risk of Parkinson disease. *Neurology, 64*(4), 664-669.
Chen, L., & Feany, M. B. (2005). α-Synuclein phosphorylation controls neurotoxicity and inclusion formation in a Drosophila model of Parkinson disease. *Nature neuroscience, 8*(5), 657-663.

Chen, W., Yan, X., Lv, H., Liu, Y., He, Z., & Luo, X. (2020). Gender differences in prevalence of LRRK2-associated Parkinson disease: a meta-analysis of observational studies. *Neuroscience letters, 715*, 134609.

Chiba-Falek, O., Lopez, G. J., & Nussbaum, R. L. (2006). Levels of alpha-synuclein mRNA in sporadic Parkinson disease patients. *Mov Disord., 21*(10), 1703-1708.

Choi, J., Sullards, M. C., Olzmann, J. A., Rees, H. D., Weintraub, S. T., Bostwick, D. E., . . . Li, L. (2006). Oxidative damage of DJ-1 is linked to sporadic Parkinson and Alzheimer diseases. *Journal of Biological Chemistry, 281*(16), 10816-10824.

Choi, M. S., Nakamura, T., Cho, S.-J., Han, X., Holland, E. A., Qu, J., . . . Lipton, S. A. (2014). Transnitrosylation from DJ-1 to PTEN attenuates neuronal cell death in parkinson's disease models. *Journal of Neuroscience, 34*(45), 15123-15131.

Choi, P., Golts, N., Snyder, H., Chong, M., Petrucelli, L., Hardy, J., . . . Wolozin, B. (2001). Co-association of parkin and α-synuclein. *Neuroreport, 12*(13), 2839-2843.

Choi, Y.-G., & Lim, S. (2010). Nε-(carboxymethyl) lysine linkage to α-synuclein and involvement of advanced glycation end products in α-synuclein deposits in an MPTP-intoxicated mouse model. *Biochimie, 92*(10), 1379-1386.

Chu, Y., & Kordower, J. H. (2007). Age-associated increases of α-synuclein in monkeys and humans are associated with nigrostriatal dopamine depletion: is this the target for Parkinson's disease? *Neurobiology of disease, 25*(1), 134-149.

Chu, Y., Muller, S., Tavares, A., Barret, O., Alagille, D., Seibyl, J., . . . Trojanowski, J. Q. (2019). Intrastriatal alpha-synuclein fibrils in monkeys: spreading, imaging and neuropathological changes. *Brain, 142*(11), 3565-3579.

Chung, C.-C., Chan, L., Chen, J.-H., Hung, Y.-C., & Hong, C.-T. (2021). Plasma extracellular vesicle α-synuclein level in patients with parkinson's disease. *Biomolecules, 11*(5), 744.

Chung, C. Y., Khurana, V., Auluck, P. K., Tardiff, D. F., Mazzulli, J. R., Soldner, F., . . . Cho, S. (2013). Identification and rescue of α-synuclein toxicity in Parkinson patient–derived neurons. *Science, 342*(6161), 983-987.

Chung, C. Y., Khurana, V., Yi, S., Sahni, N., Loh, K. H., Auluck, P. K., . . . Carr, S. A. (2017). In situ peroxidase labeling and mass-spectrometry connects alpha-synuclein directly to endocytic trafficking and mRNA metabolism in neurons. *Cell systems, 4*(2), 242-250. e244.

Collinge, J., & Clarke, A. R. (2007). A general model of prion strains and their pathogenicity. *Science, 318*(5852), 930-936.

Connor-Robson, N., Booth, H., Martin, J. G., Gao, B., Li, K., Doig, N., . . . Juhasz, P. (2019). An integrated transcriptomics and proteomics analysis reveals functional endocytic dysregulation caused by mutations in LRRK2. *Neurobiology of disease, 127*, 512-526.

Conway, K. A., Lee, S.-J., Rochet, J.-C., Ding, T. T., Williamson, R. E., & Lansbury, P. T. (2000). Acceleration of oligomerization, not fibrillization, is a shared property of both α-synuclein mutations linked to early-onset

Parkinson's disease: implications for pathogenesis and therapy. *Proceedings of the National Academy of Sciences, 97*(2), 571-576.
Coon, E. A., & Singer, W. (2020). Synucleinopathies. *Continuum (Minneapolis, Minn.), 26*(1), 72.
Courte, J., Bousset, L., Von Boxberg, Y., Villard, C., Melki, R., & Peyrin, J.-M. (2020). The expression level of alpha-synuclein in different neuronal populations is the primary determinant of its prion-like seeding. *Scientific reports, 10*(1), 1-13.
Courtois, E. T., Castillo, C. G., Seiz, E. G., Ramos, M., Bueno, C., Liste, I., & Martínez-Serrano, A. (2010). In vitro and in vivo enhanced generation of human A9 dopamine neurons from neural stem cells by Bcl-XL. *Journal of Biological Chemistry, 285*(13), 9881-9897.
Cox, D., Carver, J. A., & Ecroyd, H. (2014). Preventing α-synuclein aggregation: the role of the small heat-shock molecular chaperone proteins. *Biochimica et Biophysica Acta (BBA)-Molecular Basis of Disease, 1842*(9), 1830-1843.
Creed, R. B., Menalled, L., Casey, B., Dave, K. D., Janssens, H. B., Veinbergs, I., . . . Goldberg, M. S. (2019). Basal and evoked neurotransmitter levels in Parkin, DJ-1, PINK1 and LRRK2 knockout rat striatum. *Neuroscience, 409*, 169-179.
Cummings, J. L. (1992). Depression and Parkinson's disease: a review. *The American journal of psychiatry*.
Dafinca, R., Scaber, J., Ababneh, N. A., Lalic, T., Weir, G., Christian, H., . . . Browne, C. (2016). C9orf72 hexanucleotide expansions are associated with altered endoplasmic reticulum calcium homeostasis and stress granule formation in induced pluripotent stem cell-derived neurons from patients with amyotrophic lateral sclerosis and frontotemporal dementia. *Stem cells, 34*(8), 2063-2078.
Dalfó, E., Portero-Otín, M., Ayala, V., Martínez, A., Pamplona, R., & Ferrer, I. (2005). Evidence of oxidative stress in the neocortex in incidental Lewy body disease. *Journal of Neuropathology & Experimental Neurology, 64*(9), 816-830.
Del Tredici, K., & Braak, H. (2012a). Lewy pathology and neurodegeneration in premotor Parkinson's disease. *Movement Disorders, 27*(5), 597-607.
Del Tredici, K., & Braak, H. (2012b). Spinal cord lesions in sporadic Parkinson’s disease. *Acta neuropathologica, 124*(5), 643-664.
Del Tredici, K., & Braak, H. (2020). To stage, or not to stage. *Current opinion in neurobiology, 61*, 10-22.
Deleersnijder, A., Gerard, M., Debyser, Z., & Baekelandt, V. (2013). The remarkable conformational plasticity of alpha-synuclein: blessing or curse? *Trends in Molecular Medicine, 19*(6), 368-377.
Delenclos, M., Burgess, J. D., Lamprokostopoulou, A., Outeiro, T. F., Vekrellis, K., & McLean, P. J. (2019). Cellular models of alpha-synuclein toxicity and aggregation. *Journal of neurochemistry, 150*(5), 566-576.
Denham, M., Bye, C., Leung, J., Conley, B. J., Thompson, L. H., & Dottori, M. (2012). Glycogen synthase kinase 3β and activin/nodal inhibition in human embryonic stem cells induces a pre-neuroepithelial state that is

required for specification to a floor plate cell lineage. *Stem cells, 30*(11), 2400-2411.

Desplats, P., Spencer, B., Coffee, E., Patel, P., Michael, S., Patrick, C., . . . Masliah, E. (2011). α-synuclein sequesters Dnmt1 from the nucleus: a novel mechanism for epigenetic alterations in Lewy body diseases. *Journal of Biological Chemistry, 286*(11), 9031-9037.

Dettmer, U., Newman, A. J., von Saucken, V. E., Bartels, T., & Selkoe, D. (2015). KTKEGV repeat motifs are key mediators of normal α-synuclein tetramerization: Their mutation causes excess monomers and neurotoxicity. *Proceedings of the National Academy of Sciences, 112*(31), 9596-9601.

Di Loreto, S., Caracciolo, V., Colafarina, S., Sebastiani, P., Gasbarri, A., & Amicarelli, F. (2004). Methylglyoxal induces oxidative stress-dependent cell injury and up-regulation of interleukin-1β and nerve growth factor in cultured hippocampal neuronal cells. *Brain research, 1006*(2), 157-167.

Di Loreto, S., Zimmitti, V., Sebastiani, P., Cervelli, C., Falone, S., & Amicarelli, F. (2008). Methylglyoxal causes strong weakening of detoxifying capacity and apoptotic cell death in rat hippocampal neurons. *The international journal of biochemistry & cell biology, 40*(2), 245-257.

Di Maio, R., Barrett, P. J., Hoffman, E. K., Barrett, C. W., Zharikov, A., Borah, A., . . . Burton, E. A. (2016). α-Synuclein binds to TOM20 and inhibits mitochondrial protein import in Parkinson's disease. *Sci Transl Med., 8*(342), 342ra378-342ra378.

Dickson, D. W. (2012). Parkinson's disease and parkinsonism: neuropathology. *Cold Spring Harbor perspectives in medicine, 2*(8), a009258.

Dickson, D. W., Fujishiro, H., DelleDonne, A., Menke, J., Ahmed, Z., Klos, K. J., . . . Parisi, J. E. (2008). Evidence that incidental Lewy body disease is pre-symptomatic Parkinson's disease. *Acta neuropathologica, 115*(4), 437-444.

Dobson, C. M. (1999). Protein misfolding, evolution and disease. *Trends in biochemical sciences, 24*(9), 329-332.

Dohgu, S., Takata, F., Matsumoto, J., Kimura, I., Yamauchi, A., & Kataoka, Y. (2019). Monomeric α-synuclein induces blood–brain barrier dysfunction through activated brain pericytes releasing inflammatory mediators in vitro. *Microvascular research, 124*, 61-66.

Doi, D., Samata, B., Katsukawa, M., Kikuchi, T., Morizane, A., Ono, Y., . . . Takahashi, J. (2014). Isolation of human induced pluripotent stem cell-derived dopaminergic progenitors by cell sorting for successful transplantation. *Stem cell reports, 2*(3), 337-350.

Dolgacheva, L. P., Berezhnov, A. V., Fedotova, E. I., Zinchenko, V. P., & Abramov, A. Y. (2019). Role of DJ-1 in the mechanism of pathogenesis of Parkinson's disease. *Journal of bioenergetics and biomembranes, 51*(3), 175-188.

Donath, H., Woelke, S., Schubert, R., Kieslich, M., Theis, M., Auburger, G., . . . Zielen, S. (2021). Neurofilament Light Chain Is a Biomarker of Neurodegeneration in Ataxia Telangiectasia. *The Cerebellum*, 1-9.

Dorsey, E., Sherer, T., Okun, M. S., & Bloem, B. R. (2018). The emerging evidence of the Parkinson pandemic. *Journal of Parkinson's disease, 8*(s1), S3-S8.

Drescher, M., Huber, M., & Subramaniam, V. (2012). Hunting the chameleon: structural conformations of the intrinsically disordered protein alpha-synuclein. *ChemBioChem, 13*(6), 761-768.

Du, H.-N., Tang, L., Luo, X.-Y., Li, H.-T., Hu, J., Zhou, J.-W., & Hu, H.-Y. (2003). A peptide motif consisting of glycine, alanine, and valine is required for the fibrillization and cytotoxicity of human α-synuclein. *Biochemistry, 42*(29), 8870-8878.

Duffy, P. E., & Tennyson, V. M. (1965). Phase and electron microscopic observations of Lewy bodies and melanin granules in the substantia nigra and locus caeruleus in Parkinson's disease. *Journal of Neuropathology & Experimental Neurology, 24*(3), 398-414.

Dugger, B. N., & Dickson, D. W. (2010). Cell type specific sequestration of choline acetyltransferase and tyrosine hydroxylase within Lewy bodies. *Acta neuropathologica, 120*(5), 633-639.

Dujardin, S., Bégard, S., Caillierez, R., Lachaud, C., Carrier, S., Lieger, S., . . . Maurage, C.-A. (2018). Different tau species lead to heterogeneous tau pathology propagation and misfolding. *Acta neuropathologica communications, 6*(1), 1-12.

Dunnett, S., Bentivoglio, M., Bjorklund, A., & Hokfelt, T. (2005). Handbook of chemical neuroanatomy. In: Elsevier, Amsterdam.

Durcan, R., Wiblin, L., Lawson, R. A., Khoo, T. K., Yarnall, A., Duncan, G. W., . . . Group, I. P. S. (2019). Prevalence and duration of non-motor symptoms in prodromal Parkinson's disease. *European journal of neurology, 26*(7), 979-985.

Edwards, L., Pfeiffer, R., Quigley, E., Hofman, R., & Balluff, M. (1991). Gastrointestinal symptoms in Parkinson's disease. *Movement disorders: official journal of the Movement Disorder Society, 6*(2), 151-156.

Edwards, T. L., Scott, W. K., Almonte, C., Burt, A., Powell, E. H., Beecham, G. W., . . . Wang, G. (2010). Genome-wide association study confirms SNPs in SNCA and the MAPT region as common risk factors for Parkinson disease. *Annals of human genetics, 74*(2), 97-109.

Ehringer, H., & Hornykiewicz, O. (1960). Verteilung von Noradrenalin und Dopamin (3-Hydroxytyramin) im Gehirn des Menschen und ihr Verhalten bei Erkrankungen des extrapyramidalen Systems. *Klinische Wochenschrift, 38*(24), 1236-1239.

Ehrt, U., Broich, K., Larsen, J. P., Ballard, C., & Aarsland, D. (2010). Use of drugs with anticholinergic effect and impact on cognition in Parkinson's disease: a cohort study. *Journal of Neurology, Neurosurgery & Psychiatry, 81*(2), 160-165.

El-Agnaf, O., Overk, C., Rockenstein, E., Mante, M., Florio, J., Adame, A., . . . Kim, C. (2017). Differential effects of immunotherapy with antibodies targeting α-synuclein oligomers and fibrils in a transgenic model of synucleinopathy. *Neurobiology of disease, 104*, 85-96.

El-Agnaf, O. M., Salem, S. A., Paleologou, K. E., Curran, M. D., Gibson, M. J., Court, J. A., . . . Allsop, D. (2006). Detection of oligomeric forms of α-

synuclein protein in human plasma as a potential biomarker for Parkinson's disease. *The FASEB Journal, 20*(3), 419-425.

Ellis, J. M., & Fell, M. J. (2017). Current approaches to the treatment of Parkinson's Disease. *Bioorganic & medicinal chemistry letters, 27*(18), 4247-4255.

Emmanouilidou, E., Melachroinou, K., Roumeliotis, T., Garbis, S. D., Ntzouni, M., Margaritis, L. H., . . . Vekrellis, K. (2010). Cell-produced α-synuclein is secreted in a calcium-dependent manner by exosomes and impacts neuronal survival. *Journal of Neuroscience, 30*(20), 6838-6851.

Espay, A. J., Kalia, L. V., Gan-Or, Z., Williams-Gray, C. H., Bedard, P. L., Rowe, S. M., . . . Kauffman, M. A. (2020). Disease modification and biomarker development in Parkinson disease: Revision or reconstruction? *Neurology, 94*(11), 481-494.

Falcon, B., Zhang, W., Murzin, A. G., Murshudov, G., Garringer, H. J., Vidal, R., . . . Goedert, M. (2018). Structures of filaments from Pick's disease reveal a novel tau protein fold. *Nature, 561*(7721), 137-140.

Falk, A., Koch, P., Kesavan, J., Takashima, Y., Ladewig, J., Alexander, M., . . . Pollard, S. (2012). Capture of neuroepithelial-like stem cells from pluripotent stem cells provides a versatile system for in vitro production of human neurons. *PloS one, 7*(1), e29597.

Fanciulli, A., & Wenning, G. K. (2015). Multiple-system atrophy. *New England Journal of Medicine, 372*(3), 249-263.

Fanning, S., Haque, A., Imberdis, T., Baru, V., Barrasa, M. I., Nuber, S., . . . Noble, T. (2019). Lipidomic analysis of α-synuclein neurotoxicity identifies stearoyl CoA desaturase as a target for Parkinson treatment. *Molecular cell, 73*(5), 1001-1014. e1008.

Fanning, S., Selkoe, D., & Dettmer, U. (2021). Vesicle trafficking and lipid metabolism in synucleinopathy. *Acta neuropathologica, 141*(4), 491-510.

Fares, M. B., Jagannath, S., & Lashuel, H. A. (2021). Reverse engineering Lewy bodies: how far have we come and how far can we go? *Nature Reviews Neuroscience, 22*(2), 111-131.

Farotti, L., Paolini Paoletti, F., Simoni, S., & Parnetti, L. (2020). Unraveling pathophysiological mechanisms of Parkinson's disease: contribution of CSF biomarkers. *Biomarker Insights, 15*, 1177271920964077.

Fenyi, A., Duyckaerts, C., Bousset, L., Braak, H., Del Tredici, K., Melki, R., & On Behalf Of The Brainbank Neuro-Ceb Neuropathology, N. (2021). Seeding Propensity and Characteristics of Pathogenic αSyn Assemblies in Formalin-Fixed Human Tissue from the Enteric Nervous System, Olfactory Bulb, and Brainstem in Cases Staged for Parkinson's Disease. *Cells, 10*(1). doi:10.3390/cells10010139

Fenyi, A., Leclair-Visonneau, L., Clairembault, T., Coron, E., Neunlist, M., Melki, R., . . . Bousset, L. (2019a). Detection of alpha-synuclein aggregates in gastrointestinal biopsies by protein misfolding cyclic amplification. *Neurobiol Dis., 129*, 38-43.

Fenyi, A., Leclair-Visonneau, L., Clairembault, T., Coron, E., Neunlist, M., Melki, R., . . . Bousset, L. (2019b). Detection of alpha-synuclein aggregates in gastrointestinal biopsies by protein misfolding cyclic amplification. *Neurobiology of disease, 129*, 38-43.

Fernandes, H. J., Hartfield, E. M., Christian, H. C., Emmanoulidou, E., Zheng, Y., Booth, H., . . . Sardi, S. P. (2016). ER stress and autophagic perturbations lead to elevated extracellular α-synuclein in GBA-N370S Parkinson's iPSC-derived dopamine neurons. *Stem cell reports, 6*(3), 342-356.

Fernandes, J. T., Chutna, O., Chu, V., Conde, J. P., & Outeiro, T. F. (2016). A novel microfluidic cell co-culture platform for the study of the molecular mechanisms of Parkinson's disease and other synucleinopathies. *Frontiers in neuroscience, 10*, 511.

Fernandez, H. H., Boyd, J. T., Fung, V. S., Lew, M. F., Rodriguez, R. L., Slevin, J. T., . . . Chatamra, K. (2018). Long-term safety and efficacy of levodopa-carbidopa intestinal gel in advanced Parkinson's disease. *Movement Disorders, 33*(6), 928-936.

Figueroa, J. J., Singer, W., Parsaik, A., Benarroch, E. E., Ahlskog, J. E., Fealey, R. D., . . . Iodice, V. (2014). Multiple system atrophy: prognostic indicators of survival. *Movement Disorders, 29*(9), 1151-1157.

Fiorenzano, A., Sozzi, E., Parmar, M., & Storm, P. (2021). Dopamine Neuron Diversity: Recent Advances and Current Challenges in Human Stem Cell Models and Single Cell Sequencing. *Cells, 10*(6), 1366.

Fiske, M., Valtierra, S., Solvang, K., Zorniak, M., White, M., Herrera, S., . . . DebBurman, S. (2011). Contribution of alanine-76 and serine phosphorylation in α-synuclein membrane association and aggregation in yeasts. *Parkinson’s disease, 2011*.

Fitzpatrick, A. W., Falcon, B., He, S., Murzin, A. G., Murshudov, G., Garringer, H. J., . . . Scheres, S. H. (2017). Cryo-EM structures of tau filaments from Alzheimer’s disease. *Nature, 547*(7662), 185-190.

Flierl, A., Oliveira, L. M., Falomir-Lockhart, L. J., Mak, S. K., Hesley, J., Soldner, F., . . . Jovin, T. M. (2014). Higher vulnerability and stress sensitivity of neuronal precursor cells carrying an alpha-synuclein gene triplication. *PloS one, 9*(11), e112413.

Follett, J., Bugarcic, A., Yang, Z., Ariotti, N., Norwood, S. J., Collins, B. M., . . . Teasdale, R. D. (2016). Parkinson disease-linked Vps35 R524W mutation impairs the endosomal association of retromer and induces α-synuclein aggregation. *Journal of Biological Chemistry, 291*(35), 18283-18298.

Foltynie, T., & Aviles-Olmos, I. (2014). Exenatide as a potential treatment for patients with Parkinson's disease: first steps into the clinic. *Alzheimer's & Dementia, 10*, S38-S46.

Frigerio, R., Fujishiro, H., Ahn, T.-B., Josephs, K. A., Maraganore, D. M., DelleDonne, A., . . . Dickson, D. W. (2011). Incidental Lewy body disease: do some cases represent a preclinical stage of dementia with Lewy bodies? *Neurobiology of aging, 32*(5), 857-863.

Friling, S., Andersson, E., Thompson, L. H., Jönsson, M. E., Hebsgaard, J. B., Nanou, E., . . . Volakakis, N. (2009). Efficient production of mesencephalic dopamine neurons by Lmx1a expression in embryonic stem cells. *Proceedings of the National Academy of Sciences, 106*(18), 7613-7618.

Fujiwara, H., Hasegawa, M., Dohmae, N., Kawashima, A., Masliah, E., Goldberg, M. S., . . . Iwatsubo, T. (2002). α-Synuclein is phosphorylated in synucleinopathy lesions. *Nature cell biology, 4*(2), 160-164.

Fusco, G., Chen, S. W., Williamson, P. T., Cascella, R., Perni, M., Jarvis, J. A., . . . Cremades, N. (2017). Structural basis of membrane disruption and cellular toxicity by α-synuclein oligomers. *Science, 358*(6369), 1440-1443.

Fusco, G., De Simone, A., Gopinath, T., Vostrikov, V., Vendruscolo, M., Dobson, C. M., & Veglia, G. (2014). Direct observation of the three regions in α-synuclein that determine its membrane-bound behaviour. *Nature Communications, 5*(1), 1-8.

Fussi, N., Höllerhage, M., Chakroun, T., Nykänen, N.-P., Rösler, T. W., Koeglsperger, T., . . . Höglinger, G. U. (2018). Exosomal secretion of α-synuclein as protective mechanism after upstream blockage of macroautophagy. *Cell death & disease, 9*(7), 1-14.

Gaig, C., Martí, M. J., Ezquerra, M., Rey, M. J., Cardozo, A., & Tolosa, E. (2007). G2019S LRRK2 mutation causing Parkinson's disease without Lewy bodies. *Journal of Neurology, Neurosurgery & Psychiatry, 78*(6), 626-628.

Gallegos, S., Pacheco, C., Peters, C., Opazo, C. M., & Aguayo, L. G. (2015). Features of alpha-synuclein that could explain the progression and irreversibility of Parkinson's disease. *Frontiers in neuroscience, 9*, 59.

Galvagnion, C., Buell, A. K., Meisl, G., Michaels, T. C., Vendruscolo, M., Knowles, T. P., & Dobson, C. M. (2015). Lipid vesicles trigger α-synuclein aggregation by stimulating primary nucleation. *Nature chemical biology, 11*(3), 229-234.

Ganjam, G. K., Bolte, K., Matschke, L. A., Neitemeier, S., Dolga, A. M., Höllerhage, M., . . . Oertel, W. H. (2019). Mitochondrial damage by α-synuclein causes cell death in human dopaminergic neurons. *Cell death & disease, 10*(11), 1-16.

Gao, H., Yang, W., Qi, Z., Lu, L., Duan, C., Zhao, C., & Yang, H. (2012). DJ-1 protects dopaminergic neurons against rotenone-induced apoptosis by enhancing ERK-dependent mitophagy. *Journal of molecular biology, 423*(2), 232-248.

Garcia-Reitböck, P., Anichtchik, O., Bellucci, A., Iovino, M., Ballini, C., Fineberg, E., . . . Tofaris, G. K. (2010). SNARE protein redistribution and synaptic failure in a transgenic mouse model of Parkinson's disease. *Brain, 133*(7), 2032-2044.

Ghee, M., Melki, R., Michot, N., & Mallet, J. (2005). PA700, the regulatory complex of the 26S proteasome, interferes with α-synuclein assembly. *The FEBS journal, 272*(16), 4023-4033.

Giasson, B. I., Duda, J. E., Murray, I. V., Chen, Q., Souza, J. M., Hurtig, H. I., . . . Lee, V. M.-Y. (2000). Oxidative damage linked to neurodegeneration by selective α-synuclein nitration in synucleinopathy lesions. *Science, 290*(5493), 985-989.

Giasson, B. I., Murray, I. V., Trojanowski, J. Q., & Lee, V. M.-Y. (2001). A hydrophobic stretch of 12 amino acid residues in the middle of α-synuclein is essential for filament assembly. *Journal of Biological Chemistry, 276*(4), 2380-2386.

Giehm, L., Lorenzen, N., & Otzen, D. E. (2011). Assays for α-synuclein aggregation. *Methods, 53*(3), 295-305.

Glat, M. J., Ben-Zur, T., Barhum, Y., & Offen, D. (2016). Neuroprotective effect of a DJ-1 based peptide in a toxin induced mouse model of multiple system atrophy. *PloS one, 11*(2), e0148170.

Goedert, M., Jakes, R., & Spillantini, M. G. (2017). The synucleinopathies: twenty years on. *Journal of Parkinson's disease, 7*(s1), S51-S69.

Goedert, M., Spillantini, M. G., Del Tredici, K., & Braak, H. (2013). 100 years of Lewy pathology. *Nature Reviews Neurology, 9*(1), 13-24.

Gómez-Santos, C., Ferrer, I., Santidrián, A. F., Barrachina, M., Gil, J., & Ambrosio, S. (2003). Dopamine induces autophagic cell death and α-synuclein increase in human neuroblastoma SH-SY5Y cells. *Journal of neuroscience research, 73*(3), 341-350.

Görner, K., Holtorf, E., Waak, J., Pham, T.-T., Vogt-Weisenhorn, D. M., Wurst, W., . . . Kahle, P. J. (2007). Structural determinants of the C-terminal helix-kink-helix motif essential for protein stability and survival promoting activity of DJ-1. *Journal of Biological Chemistry, 282*(18), 13680-13691.

Greffard, S., Verny, M., Bonnet, A.-M., Seilhean, D., Hauw, J.-J., & Duyckaerts, C. (2010). A stable proportion of Lewy body bearing neurons in the substantia nigra suggests a model in which the Lewy body causes neuronal death. *Neurobiology of aging, 31*(1), 99-103.

Greten-Harrison, B., Polydoro, M., Morimoto-Tomita, M., Diao, L., Williams, A. M., Nie, E. H., . . . Buchman, V. L. (2010). αβγ-Synuclein triple knockout mice reveal age-dependent neuronal dysfunction. *Proceedings of the National Academy of Sciences, 107*(45), 19573-19578.

Grey, M., Dunning, C. J., Gaspar, R., Grey, C., Brundin, P., Sparr, E., & Linse, S. (2015). Acceleration of α-synuclein aggregation by exosomes. *Journal of Biological Chemistry, 290*(5), 2969-2982.

Gribaudo, S., Tixador, P., Bousset, L., Fenyi, A., Lino, P., Melki, R., . . . Perrier, A. L. (2019a). Propagation of α-synuclein strains within human reconstructed neuronal network. *Stem cell reports, 12*(2), 230-244.

Gribaudo, S., Tixador, P., Bousset, L., Fenyi, A., Lino, P., Melki, R., . . . Perrier, A. L. (2019b). Propagation of α-Synuclein strains within human reconstructed neuronal network. *Stem Cell Rep., 12*(2), 230-244.

Groveman, B. R., Orrù, C. D., Hughson, A. G., Raymond, L. D., Zanusso, G., Ghetti, B., . . . Caughey, B. (2018). Rapid and ultra-sensitive quantitation of disease-associated α-synuclein seeds in brain and cerebrospinal fluid by αSyn RT-QuIC. *Acta neuropathologica communications, 6*(1), 1-10.

Gründemann, J., Schlaudraff, F., Haeckel, O., & Liss, B. (2008). Elevated α-synuclein mRNA levels in individual UV-laser-microdissected dopaminergic substantia nigra neurons in idiopathic Parkinson's disease. *Nucleic Acids Res., 36*(7), e38.

Guerrero, E., Vasudevaraju, P., Hegde, M. L., Britton, G., & Rao, K. (2013). Recent advances in α-synuclein functions, advanced glycation, and toxicity: implications for Parkinson's disease. *Molecular neurobiology, 47*(2), 525-536.

Guerrero-Ferreira, R., Taylor, N. M., Arteni, A.-A., Kumari, P., Mona, D., Ringler, P., . . . Verasdonck, J. (2019). Two new polymorphic structures of human full-length alpha-synuclein fibrils solved by cryo-electron microscopy. *Elife, 8*, e48907.

Guhathakurta, S., Bok, E., Evangelista, B. A., & Kim, Y.-S. (2017). Deregulation of α-synuclein in Parkinson's disease: Insight from epigenetic structure and transcriptional regulation of SNCA. *Progress in neurobiology, 154*, 21-36.

Guo, J. L., Covell, D. J., Daniels, J. P., Iba, M., Stieber, A., Zhang, B., . . . Trojanowski, J. Q. (2013). Distinct α-synuclein strains differentially promote tau inclusions in neurons. *Cell, 154*(1), 103-117.

Guschina, I. A., Ninkina, N., Roman, A., Pokrovskiy, M. V., & Buchman, V. L. (2021). Triple-knockout, synuclein-free mice display compromised lipid pattern. *Molecules, 26*(11), 3078.

Haenseler, W., Zambon, F., Lee, H., Vowles, J., Rinaldi, F., Duggal, G., . . . Luk, K. C. (2017). Excess α-synuclein compromises phagocytosis in iPSC-derived macrophages. *Sci Rep., 7*(1), 1-11.

Han, S., Li, J., & Ting, A. Y. (2018). Proximity labeling: spatially resolved proteomic mapping for neurobiology. *Current opinion in neurobiology, 50*, 17-23.

Handel, A. E., Chintawar, S., Lalic, T., Whiteley, E., Vowles, J., Giustacchini, A., . . . Bowden, R. (2016). Assessing similarity to primary tissue and cortical layer identity in induced pluripotent stem cell-derived cortical neurons through single-cell transcriptomics. *Human molecular genetics, 25*(5), 989-1000.

Hara, S., Arawaka, S., Sato, H., Machiya, Y., Cui, C., Sasaki, A., . . . Kato, T. (2013). Serine 129 phosphorylation of membrane-associated α-synuclein modulates dopamine transporter function in a G protein–coupled receptor kinase–dependent manner. *Molecular biology of the cell, 24*(11), 1649-1660.

Hartl, F. U., Bracher, A., & Hayer-Hartl, M. (2011). Molecular chaperones in protein folding and proteostasis. *Nature, 475*(7356), 324-332.

Hartmann, C. J., Fliegen, S., Groiss, S. J., Wojtecki, L., & Schnitzler, A. (2019). An update on best practice of deep brain stimulation in Parkinson's disease. *Therapeutic advances in neurological disorders, 12*, 1756286419838096.

Hasegawa, M., Fujiwara, H., Nonaka, T., Wakabayashi, K., Takahashi, H., Lee, V. M.-Y., . . . Iwatsubo, T. (2002). Phosphorylated α-synuclein is ubiquitinated in α-synucleinopathy lesions. *Journal of Biological Chemistry, 277*(50), 49071-49076.

Hasegawa, T., Konno, M., Baba, T., Sugeno, N., Kikuchi, A., Kobayashi, M., . . . Furukawa, K. (2011). The AAA-ATPase VPS4 regulates extracellular secretion and lysosomal targeting of α-synuclein. *PloS one, 6*(12), e29460.

Haston, K. M., & Finkbeiner, S. (2016). Clinical trials in a dish: the potential of pluripotent stem cells to develop therapies for neurodegenerative diseases. *Annual review of pharmacology and toxicology, 56*, 489-510.

Hedrich, K., Djarmati, A., Schäfer, N., Hering, R., Wellenbrock, C., Weiss, P., . . . Heutink, P. (2004). DJ-1 (PARK7) mutations are less frequent than Parkin (PARK2) mutations in early-onset Parkinson disease. *Neurology, 62*(3), 389-394.

Heman-Ackah, S. M., Manzano, R., Hoozemans, J. J., Scheper, W., Flynn, R., Haerty, W., . . . Wood, M. J. (2017). Alpha-synuclein induces the unfolded protein response in Parkinson's disease SNCA triplication iPSC-derived neurons. *Hum. Mol. Genet., 26*(22), 4441-4450.

Henderson, M. X., Cornblath, E. J., Darwich, A., Zhang, B., Brown, H., Gathagan, R. J., . . . Lee, V. M. (2019). Spread of α-synuclein pathology through the brain connectome is modulated by selective vulnerability and predicted by network analysis. *Nature neuroscience, 22*(8), 1248-1257.

Henderson, M. X., Covell, D. J., Chung, C. H.-Y., Pitkin, R. M., Sandler, R. M., Decker, S. C., . . . James, M. J. (2020). Characterization of novel conformation-selective α-synuclein antibodies as potential immunotherapeutic agents for Parkinson's disease. *Neurobiology of disease, 136*, 104712.

Henderson, M. X., Trojanowski, J. Q., & Lee, V. M.-Y. (2019). α-Synuclein pathology in Parkinson's disease and related α-synucleinopathies. *Neuroscience letters, 709*, 134316.

Herva, M. E., Zibaee, S., Fraser, G., Barker, R. A., Goedert, M., & Spillantini, M. G. (2014). Anti-amyloid compounds inhibit α-synuclein aggregation induced by protein misfolding cyclic amplification (PMCA). *Journal of Biological Chemistry, 289*(17), 11897-11905.

Hijioka, M., Inden, M., Yanagisawa, D., & Kitamura, Y. (2017). DJ-1/PARK7: a new therapeutic target for neurodegenerative disorders. *Biological and Pharmaceutical Bulletin, 40*(5), 548-552.

Holec, S. A., & Woerman, A. L. (2021). Evidence of distinct α-synuclein strains underlying disease heterogeneity. *Acta neuropathologica, 142*(1), 73-86.

Holmqvist, S., Chutna, O., Bousset, L., Aldrin-Kirk, P., Li, W., Björklund, T., . . . Li, J. Y. (2014). Direct evidence of Parkinson pathology spread from the gastrointestinal tract to the brain in rats. *Acta Neuropathol, 128*(6), 805-820. doi:10.1007/s00401-014-1343-6

Hoppe, S. O., Uzunoğlu, G., & Nussbaum-Krammer, C. (2021). α-Synuclein Strains: Does Amyloid Conformation Explain the Heterogeneity of Synucleinopathies? *Biomolecules, 11*(7), 931.

Hornykiewicz, O. (1963). Die topische Lokalization und des Verhalten von Noradrenalin und Dopamin (3-Hydroxytyramin) in der Substantia nigra der normalen und Parkinson Kranken Menschen. *Wien. Klin. Wochschr., 75*, 309-312.

Hoyer, W., Cherny, D., Subramaniam, V., & Jovin, T. M. (2004). Impact of the acidic C-terminal region comprising amino acids 109– 140 on α-synuclein aggregation in vitro. *Biochemistry, 43*(51), 16233-16242.

Hsieh, C.-H., Shaltouki, A., Gonzalez, A. E., da Cruz, A. B., Burbulla, L. F., Lawrence, E. S., . . . Wang, X. (2016). Functional impairment in miro degradation and mitophagy is a shared feature in familial and sporadic Parkinson's disease. *Cell stem cell, 19*(6), 709-724.

Hu, B., Zhong, L., Weng, Y., Peng, L., Huang, Y., Zhao, Y., & Liang, X.-J. (2020). Therapeutic siRNA: state of the art. *Signal transduction and targeted therapy, 5*(1), 1-25.

Hu, G., Jousilahti, P., Bidel, S., Antikainen, R., & Tuomilehto, J. (2007). Type 2 diabetes and the risk of Parkinson's disease. *Diabetes Care, 30*(4), 842-847.

Huang, M., & Chen, S. (2021). DJ-1 in neurodegenerative diseases: pathogenesis and clinical application. *Progress in neurobiology*, 102114.

Huh, C. J., Zhang, B., Victor, M. B., Dahiya, S., Batista, L. F., Horvath, S., & Yoo, A. S. (2016). Maintenance of age in human neurons generated by microRNA-based neuronal conversion of fibroblasts. *Elife, 5*, e18648.

Ibanez, P., Bonnet, A., Debarges, B., Lohmann, E., Tison, F., Agid, Y., . . . Group, F. P. s. D. G. S. (2004). Causal relation between α-synuclein locus duplication as a cause of familial Parkinson's disease. *The Lancet, 364*(9440), 1169-1171.

Ikeuchi, T., Kakita, A., Shiga, A., Kasuga, K., Kaneko, H., Tan, C.-F., . . . Iwatsubo, T. (2008). Patients homozygous and heterozygous for SNCA duplication in a family with parkinsonism and dementia. *Archives of neurology, 65*(4), 514-519.

Inden, M., Kitamura, Y., Takahashi, K., Takata, K., Ito, N., Niwa, R., . . . Honda, T. (2011). Protection against dopaminergic neurodegeneration in Parkinson's disease–model animals by a modulator of the oxidized form of DJ-1, a wild-type of familial Parkinson's disease–linked PARK7. *Journal of pharmacological Sciences*, 1110280617-1110280617.

Inden, M., Taira, T., Kitamura, Y., Yanagida, T., Tsuchiya, D., Takata, K., . . . Kiso, Y. (2006). PARK7 DJ-1 protects against degeneration of nigral dopaminergic neurons in Parkinson's disease rat model. *Neurobiology of disease, 24*(1), 144-158.

Isas, J. M., Pandey, N. K., Xu, H., Teranishi, K., Okada, A. K., Fultz, E. K., . . . Chen, J. (2021). Huntingtin fibrils with different toxicity, structure, and seeding potential can be interconverted. *Nature Communications, 12*(1), 1-11.

Ishii, A., Nonaka, T., Taniguchi, S., Saito, T., Arai, T., Mann, D., . . . Hasegawa, M. (2007). Casein kinase 2 is the major enzyme in brain that phosphorylates Ser129 of human α-synuclein: implication for α-synucleinopathies. *FEBS letters, 581*(24), 4711-4717.

Jakes, R., Spillantini, M. G., & Goedert, M. (1994). Identification of two distinct synucleins from human brain. *FEBS letters, 345*(1), 27-32.

Jao, C. C., Der-Sarkissian, A., Chen, J., & Langen, R. (2004). Structure of membrane-bound α-synuclein studied by site-directed spin labeling. *Proceedings of the National Academy of Sciences, 101*(22), 8331-8336.

Jenner, P., Dexter, D., Sian, J., Schapira, A., & Marsden, C. (1992). Oxidative stress as a cause of nigral cell death in Parkinson's disease and incidental Lewy body disease. *Annals of Neurology: Official Journal of the American Neurological Association and the Child Neurology Society, 32*(S1), S82-S87.

Jensen, M. B., Bhatia, V. K., Jao, C. C., Rasmussen, J. E., Pedersen, S. L., Jensen, K. J., . . . Stamou, D. (2011). Membrane curvature sensing by

amphipathic helices: a single liposome study using α-synuclein and annexin B12. *Journal of Biological Chemistry, 286*(49), 42603-42614.

Jensen, P. H., Hager, H., Nielsen, M. S., Højrup, P., Gliemann, J., & Jakes, R. (1999). α-Synuclein binds to tau and stimulates the protein kinase A-catalyzed tau phosphorylation of serine residues 262 and 356. *Journal of Biological Chemistry, 274*(36), 25481-25489.

Jiang, L., Chen, X.-b., Wu, Q., Zhu, H.-y., Du, C.-y., Ying, M.-d., . . . Cao, J. (2021). The C terminus of DJ-1 determines its homodimerization, MGO detoxification activity and suppression of ferroptosis. *Acta Pharmacologica Sinica, 42*(7), 1150-1159.

Jo, J., Yang, L., Tran, H. D., Yu, W., Sun, A. X., Chang, Y. Y., . . . Xiao, B. (2021). Lewy-body Like Inclusions in Human Midbrain Organoid Carrying Glucocerebrosidase and Alpha Synuclein Mutations. *Annals of neurology*.

Johansen, K. K., Torp, S. H., Farrer, M. J., Gustavsson, E. K., & Aasly, J. O. (2018). A case of Parkinson's disease with no Lewy body pathology due to a homozygous exon deletion in Parkin. *Case reports in neurological medicine, 2018*.

Jonikas, M., Madill, M., Mathy, A., Zekoll, T., Zois, C. E., Wigfield, S., . . . Chinnery, P. F. (2018). Stem cell modeling of mitochondrial parkinsonism reveals key functions of OPA1. *Ann Neurol., 83*(5), 915-925.

Jowaed, A., Schmitt, I., Kaut, O., & Wüllner, U. (2010). Methylation regulates alpha-synuclein expression and is decreased in Parkinson's disease patients' brains. *Journal of Neuroscience, 30*(18), 6355-6359.

Jung, B. C., Lim, Y.-J., Bae, E.-J., Lee, J. S., Choi, M. S., Lee, M. K., . . . Lee, S.-J. (2017). Amplification of distinct α-synuclein fibril conformers through protein misfolding cyclic amplification. *Experimental & molecular medicine, 49*(4), e314-e314.

Kalapos, M. P. (1994). Methylglyoxal toxicity in mammals. *Toxicology letters, 73*(1), 3-24.

Kalinderi, K., Bostantjopoulou, S., & Fidani, L. (2016). The genetic background of Parkinson's disease: current progress and future prospects. *Acta Neurologica Scandinavica, 134*(5), 314-326.

Kamath, T., Abdulraouf, A., Burris, S., Gazestani, V., Nadaf, N., Vanderburg, C., & Macosko, E. (2021). A molecular census of midbrain dopaminergic neurons in Parkinson's disease. *bioRxiv*.

Kang, U. J., Boehme, A. K., Fairfoul, G., Shahnawaz, M., Ma, T. C., Hutten, S. J., . . . Soto, C. (2019). Comparative study of cerebrospinal fluid α-synuclein seeding aggregation assays for diagnosis of Parkinson's disease. *Movement Disorders, 34*(4), 536-544.

Kasten, M., Hartmann, C., Hampf, J., Schaake, S., Westenberger, A., Vollstedt, E. J., . . . Dulovic, M. (2018). Genotype-phenotype relations for the Parkinson's disease genes Parkin, PINK1, DJ1: MDSGene systematic review. *Movement Disorders, 33*(5), 730-741.

Kiely, A. P., Asi, Y. T., Kara, E., Limousin, P., Ling, H., Lewis, P., . . . Hardy, J. (2013). α-Synucleinopathy associated with G51D SNCA mutation: a link between Parkinson's disease and multiple system atrophy? *Acta neuropathologica, 125*(5), 753-769.

Kierdorf, K., & Fritz, G. (2013). RAGE regulation and signaling in inflammation and beyond. *Journal of leukocyte biology, 94*(1), 55-68.

Kikuchi, S., Shinpo, K., Moriwaka, F., Makita, Z., Miyata, T., & Tashiro, K. (1999). Neurotoxicity of methylglyoxal and 3-deoxyglucosone on cultured cortical neurons: synergism between glycation and oxidative stress, possibly involved in neurodegenerative diseases. *Journal of neuroscience research, 57*(2), 280-289.

Kim, C., Lv, G., Lee, J. S., Jung, B. C., Masuda-Suzukake, M., Hong, C.-S., . . . Hasegawa, M. (2016). Exposure to bacterial endotoxin generates a distinct strain of α-synuclein fibril. *Scientific reports, 6*(1), 1-12.

Kim, D. I., Birendra, K., Zhu, W., Motamedchaboki, K., Doye, V., & Roux, K. J. (2014). Probing nuclear pore complex architecture with proximity-dependent biotinylation. *Proceedings of the National Academy of Sciences, 111*(24), E2453-E2461.

Kim, D. I., Jensen, S. C., Noble, K. A., Kc, B., Roux, K. H., Motamedchaboki, K., & Roux, K. J. (2016). An improved smaller biotin ligase for BioID proximity labeling. *Molecular biology of the cell, 27*(8), 1188-1196.

Kim, D. I., & Roux, K. J. (2016). Filling the void: proximity-based labeling of proteins in living cells. *Trends in cell biology, 26*(11), 804-817.

Kim, T. W., Piao, J., Koo, S. Y., Kriks, S., Chung, S. Y., Betel, D., . . . Dubose, B. N. (2021). Biphasic Activation of WNT Signaling Facilitates the Derivation of Midbrain Dopamine Neurons from hESCs for Translational Use. *Cell stem cell, 28*(2), 343-355. e345.

Kinumi, T., Kimata, J., Taira, T., Ariga, H., & Niki, E. (2004). Cysteine-106 of DJ-1 is the most sensitive cysteine residue to hydrogen peroxide-mediated oxidation in vivo in human umbilical vein endothelial cells. *Biochemical and biophysical research communications, 317*(3), 722-728.

Kirkeby, A., Grealish, S., Wolf, D. A., Nelander, J., Wood, J., Lundblad, M., . . . Parmar, M. (2012). Generation of regionally specified neural progenitors and functional neurons from human embryonic stem cells under defined conditions. *Cell reports, 1*(6), 703-714.

Kitada, T., Asakawa, S., Hattori, N., Matsumine, H., Yamamura, Y., Minoshima, S., . . . Shimizu, N. (1998). Mutations in the parkin gene cause autosomal recessive juvenile parkinsonism. *Nature, 392*(6676), 605-608.

Kitada, T., Tong, Y., Gautier, C. A., & Shen, J. (2009). Absence of nigral degeneration in aged parkin/DJ-1/PINK1 triple knockout mice. *Journal of neurochemistry, 111*(3), 696-702.

Kitamura, Y., Watanabe, S., Taguchi, M., Takagi, K., Kawata, T., Takahashi-Niki, K., . . . Ariga, H. (2011). Neuroprotective effect of a new DJ-1-binding compound against neurodegeneration in Parkinson's disease and stroke model rats. *Molecular neurodegeneration, 6*(1), 1-19.

Klemann, C. J., Martens, G. J., Sharma, M., Martens, M., Isacson, O., Gasser, T., . . . Poelmans, G. (2017). Integrated molecular landscape of Parkinson's disease. *NPJ Parkinson's disease, 3*(1), 1-7.

Knowles, T. P., Vendruscolo, M., & Dobson, C. M. (2014). The amyloid state and its association with protein misfolding diseases. *Nature reviews Molecular cell biology, 15*(6), 384-396.

Koenig, A., Vicente Miranda, H., & Outeiro, T. F. (2018). Alpha-synuclein glycation and the action of anti-diabetic agents in Parkinson's disease. *Journal of Parkinson's disease, 8*(1), 33-43.

Kordower, J. H., Chu, Y., Hauser, R. A., Freeman, T. B., & Olanow, C. W. (2008). Lewy body–like pathology in long-term embryonic nigral transplants in Parkinson's disease. *Nature medicine, 14*(5), 504-506.

Koros, C., Simitsi, A., & Stefanis, L. (2017). Genetics of Parkinson's disease: genotype–phenotype correlations. *International review of neurobiology, 132*, 197-231.

Kriks, S., Shim, J.-W., Piao, J., Ganat, Y. M., Wakeman, D. R., Xie, Z., . . . Buch, A. (2011). Dopamine neurons derived from human ES cells efficiently engraft in animal models of Parkinson's disease. *Nature, 480*(7378), 547-551.

Krüger, R., Kuhn, W., Müller, T., Woitalla, D., Graeber, M., Kösel, S., . . . Riess, O. (1998). AlaSOPro mutation in the gene encoding α-synuclein in Parkinson's disease. *Nature genetics, 18*(2), 106-108.

Krumova, P., Meulmeester, E., Garrido, M., Tirard, M., Hsiao, H.-H., Bossis, G., . . . Melchior, F. (2011). Sumoylation inhibits α-synuclein aggregation and toxicity. *Journal of Cell Biology, 194*(1), 49-60.

Kubo, S.-i., Nemani, V. M., Chalkley, R. J., Anthony, M. D., Hattori, N., Mizuno, Y., . . . Fortin, D. L. (2005). A combinatorial code for the interaction of α-synuclein with membranes. *Journal of Biological Chemistry, 280*(36), 31664-31672.

Kumar, R., Kumar, S., Hanpude, P., Singh, A. K., Johari, T., Majumder, S., & Maiti, T. K. (2019). Partially oxidized DJ-1 inhibits α-synuclein nucleation and remodels mature α-synuclein fibrils in vitro. *Communications biology, 2*(1), 1-14.

Kurz, A., Rabbani, N., Walter, M., Bonin, M., Thornalley, P., Auburger, G., & Gispert, S. (2011). Alpha-synuclein deficiency leads to increased glyoxalase I expression and glycation stress. *Cellular and molecular life sciences, 68*(4), 721-733.

Kuusisto, E., Parkkinen, L., & Alafuzoff, I. (2003). Morphogenesis of Lewy bodies: dissimilar incorporation of α-synuclein, ubiquitin, and p62. *Journal of Neuropathology & Experimental Neurology, 62*(12), 1241-1253.

Kuwahara, T., Tonegawa, R., Ito, G., Mitani, S., & Iwatsubo, T. (2012). Phosphorylation of α-synuclein protein at Ser-129 reduces neuronal dysfunction by lowering its membrane binding property in Caenorhabditis elegans. *Journal of Biological Chemistry, 287*(10), 7098-7109.

Kuzuhara, S., Mori, H., Izumiyama, N., Yoshimura, M., & Ihara, Y. (1988). Lewy bodies are ubiquitinated. *Acta neuropathologica, 75*(4), 345-353.

Kyser, T. L., Dourson, A. J., McGuire, J. L., Hemmerle, A. M., Williams, M. T., & Seroogy, K. B. (2019). Characterization of motor and non-motor behavioral alterations in the Dj-1 (PARK7) knockout rat. *Journal of Molecular Neuroscience, 69*(2), 298-311.

Lake, B. B., Ai, R., Kaeser, G. E., Salathia, N. S., Yung, Y. C., Liu, R., . . . Chen, S. (2016). Neuronal subtypes and diversity revealed by single-nucleus RNA sequencing of the human brain. *Science, 352*(6293), 1586-1590.

Lam, S. S., Martell, J. D., Kamer, K. J., Deerinck, T. J., Ellisman, M. H., Mootha, V. K., & Ting, A. Y. (2015). Directed evolution of APEX2 for electron microscopy and proximity labeling. *Nature Methods, 12*(1), 51-54.

Landureau, M., Redeker, V., Bellande, T., Eyquem, S., & Melki, R. (2021). The differential solvent exposure of N-terminal residues provides “fingerprints” of alpha-synuclein fibrillar polymorphs. *Journal of Biological Chemistry, 296*.

Langston, J. W. (2006). The Parkinson's complex: parkinsonism is just the tip of the iceberg. *Annals of Neurology: Official Journal of the American Neurological Association and the Child Neurology Society, 59*(4), 591-596.

Lashuel, H. A., Overk, C. R., Oueslati, A., & Masliah, E. (2013). The many faces of α-synuclein: from structure and toxicity to therapeutic target. *Nature Reviews Neuroscience, 14*(1), 38-48.

Lau, A., So, R. W., Lau, H. H., Sang, J. C., Ruiz-Riquelme, A., Fleck, S. C., . . . Meisl, G. (2020). α-Synuclein strains target distinct brain regions and cell types. *Nature neuroscience, 23*(1), 21-31.

Lau, H. H., Ingelsson, M., & Watts, J. C. (2021). The existence of Aβ strains and their potential for driving phenotypic heterogeneity in Alzheimer’s disease. *Acta neuropathologica, 142*(1), 17-39.

Lavedan, C. (1998). The synuclein family. *Genome Res, 8*(9), 871-880. doi:10.1101/gr.8.9.871

Lee Clough, R., & Stefanis, L. (2007). A novel pathway for transcriptional regulation of α-synuclein. *The FASEB Journal, 21*(2), 596-607.

Lee, H.-g., Zhu, X., Takeda, A., Perry, G., & Smith, M. A. (2006). Emerging evidence for the neuroprotective role of alpha-synuclein. *Experimental neurology, 200*(1), 1-7.

Lee, H. J., Kang, S. J., Lee, K., & Im, H. (2011). Human α-synuclein modulates vesicle trafficking through its interaction with prenylated Rab acceptor protein 1. *Biochemical and biophysical research communications, 412*(4), 526-531.

Lee, J.-Y., Kim, H., Jo, A., Khang, R., Park, C.-H., Park, S.-J., . . . Shin, J.-H. (2021). α-Synuclein A53T Binds to Transcriptional Adapter 2-Alpha and Blocks Histone H3 Acetylation. *International journal of molecular sciences, 22*(10), 5392.

Lee, J.-y., Song, J., Kwon, K., Jang, S., Kim, C., Baek, K., . . . Park, C. (2012). Human DJ-1 and its homologs are novel glyoxalases. *Human molecular genetics, 21*(14), 3215-3225.

Lee, M.-H., Thomas, J. L., Su, Z.-L., Yeh, W.-K., Monzel, A. S., Bolognin, S., . . . Lin, H.-Y. (2021). Epitope imprinting of alpha-synuclein for sensing in Parkinson's brain organoid culture medium. *Biosensors and Bioelectronics, 175*, 112852.

Lee, S., Oh, S. T., Jeong, H. J., Pak, S. C., Park, H.-J., Kim, J., . . . Jeon, S. (2017). MPTP-induced vulnerability of dopamine neurons in A53T α-synuclein overexpressed mice with the potential involvement of DJ-1 downregulation. *The Korean Journal of Physiology & Pharmacology, 21*(6), 625-632.

Leng, K., Li, E., Eser, R., Piergies, A., Sit, R., Tan, M., . . . Suemoto, C. K. (2021). Molecular characterization of selectively vulnerable neurons in Alzheimer's disease. *Nature neuroscience, 24*(2), 276-287.

Lesage, S., Anheim, M., Letournel, F., Bousset, L., Honoré, A., Rozas, N., . . . Melki, R. (2013). G51D α-synuclein mutation causes a novel Parkinsonian–pyramidal syndrome. *Annals of neurology, 73*(4), 459-471.

Leverenz, J. B., Quinn, J. F., Zabetian, C., Zhang, J., Montine, K. S., & Montine, T. J. (2009). Cognitive impairment and dementia in patients with Parkinson disease. *Current topics in medicinal chemistry, 9*(10), 903-912.

Lewy, F. H. (1912). Paralysis agitans. I. *Pathologische anatomie. Handbuch der neurologie*.

Li, J.-Y., Englund, E., Holton, J. L., Soulet, D., Hagell, P., Lees, A. J., . . . Björklund, A. (2008). Lewy bodies in grafted neurons in subjects with Parkinson's disease suggest host-to-graft disease propagation. *Nature medicine, 14*(5), 501-503.

Li, W., Englund, E., Widner, H., Mattsson, B., van Westen, D., Lätt, J., . . . Lindvall, O. (2016). Extensive graft-derived dopaminergic innervation is maintained 24 years after transplantation in the degenerating parkinsonian brain. *Proceedings of the National Academy of Sciences, 113*(23), 6544-6549.

Li, W., Fu, Y., Halliday, G. M., & Sue, C. M. (2021). PARK genes link mitochondrial dysfunction and alpha-synuclein pathology in sporadic Parkinson's disease. *Frontiers in Cell and Developmental Biology, 9*.

Lin, K.-J., Lin, K.-L., Chen, S.-D., Liou, C.-W., Chuang, Y.-C., Lin, H.-Y., & Lin, T.-K. (2019). The overcrowded crossroads: mitochondria, alpha-synuclein, and the endo-lysosomal system interaction in Parkinson's disease. *International journal of molecular sciences, 20*(21), 5312.

Lin, L., Göke, J., Cukuroglu, E., Dranias, M. R., VanDongen, A. M., & Stanton, L. W. (2016). Molecular features underlying neurodegeneration identified through in vitro modeling of genetically diverse Parkinson's disease patients. *Cell reports, 15*(11), 2411-2426.

Liu, D. S., Loh, K. H., Lam, S. S., White, K. A., & Ting, A. Y. (2013). Imaging trans-cellular neurexin-neuroligin interactions by enzymatic probe ligation. *PloS one, 8*(2), e52823.

Liu, P., Sun, L., Zhao, X.-l., Zhang, P., Zhao, X.-m., & Zhang, J. (2014). PAR2-mediated epigenetic upregulation of α-synuclein contributes to the pathogenesis of Parkinson' s disease. *Brain research, 1565*, 82-89.

Liu, Y., Ma, X., Fujioka, H., Liu, J., Chen, S., & Zhu, X. (2019). DJ-1 regulates the integrity and function of ER-mitochondria association through interaction with IP3R3-Grp75-VDAC1. *Proceedings of the National Academy of Sciences, 116*(50), 25322-25328.

Lo, T., Westwood, M. E., McLellan, A. C., Selwood, T., & Thornalley, P. J. (1994). Binding and modification of proteins by methylglyoxal under physiological conditions. A kinetic and mechanistic study with N alpha-acetylarginine, N alpha-acetylcysteine, and N alpha-acetyllysine, and bovine serum albumin. *Journal of Biological Chemistry, 269*(51), 32299-32305.

Logan, T., Bendor, J., Toupin, C., Thorn, K., & Edwards, R. H. (2017). α-Synuclein promotes dilation of the exocytotic fusion pore. *Nature neuroscience, 20*(5), 681-689.

Love, M. I., Huber, W., & Anders, S. (2014). Moderated estimation of fold change and dispersion for RNA-seq data with DESeq2. *Genome Biol., 15*(12), 550.

Lövestam, S., Schweighauser, M., Saito, Y., Murayama, S., Tomita, T., Ando, T., . . . Hasegawa, M. (2020). Seeded assembly in vitro does not replicate the structures of α-synuclein filaments from multiple system atrophy. *bioRxiv*.

Ludtmann, M. H., Angelova, P. R., Horrocks, M. H., Choi, M. L., Rodrigues, M., Baev, A. Y., . . . Banushi, B. (2018). α-synuclein oligomers interact with ATP synthase and open the permeability transition pore in Parkinson's disease. *Nat Commun., 9*(1), 1-16.

Luk, K. C., Kehm, V., Carroll, J., Zhang, B., O'Brien, P., Trojanowski, J. Q., & Lee, V. M.-Y. (2012). Pathological α-synuclein transmission initiates Parkinson-like neurodegeneration in nontransgenic mice. *Science, 338*(6109), 949-953.

Luk, K. C., Song, C., O'Brien, P., Stieber, A., Branch, J. R., Brunden, K. R., . . . Lee, V. M.-Y. (2009). Exogenous α-synuclein fibrils seed the formation of Lewy body-like intracellular inclusions in cultured cells. *Proceedings of the National Academy of Sciences, 106*(47), 20051-20056.

Luna, E., Decker, S. C., Riddle, D. M., Caputo, A., Zhang, B., Cole, T., . . . Luk, K. C. (2018). Differential α-synuclein expression contributes to selective vulnerability of hippocampal neuron subpopulations to fibril-induced toxicity. *Acta neuropathologica, 135*(6), 855-875.

Luo, F., Luo, S., Qian, W., Zhang, L., Chen, C., Xu, M., . . . Wang, W. (2020). Developmental deficits and early signs of neurodegeneration revealed by PD patient derived dopamine neurons. *Stem Cell Research, 49*, 102027.

Machiya, Y., Hara, S., Arawaka, S., Fukushima, S., Sato, H., Sakamoto, M., . . . Kato, T. (2010). Phosphorylated α-synuclein at Ser-129 is targeted to the proteasome pathway in a ubiquitin-independent manner. *Journal of Biological Chemistry, 285*(52), 40732-40744.

Maciaczyk, J., Singec, I., Maciaczyk, D., & Nikkhah, G. (2008). Combined use of BDNF, ascorbic acid, low oxygen, and prolonged differentiation time generates tyrosine hydroxylase-expressing neurons after long-term in vitro expansion of human fetal midbrain precursor cells. *Experimental neurology, 213*(2), 354-362.

Mahul-Mellier, A.-L., Burtscher, J., Maharjan, N., Weerens, L., Croisier, M., Kuttler, F., . . . Lashuel, H. A. (2020). The process of Lewy body formation, rather than simply α-synuclein fibrillization, is one of the major drivers of neurodegeneration. *Proceedings of the National Academy of Sciences, 117*(9), 4971-4982.

Majbour, N. K., Vaikath, N. N., van Dijk, K. D., Ardah, M. T., Varghese, S., Vesterager, L. B., . . . Tokuda, T. (2016). Oligomeric and phosphorylated alpha-synuclein as potential CSF biomarkers for Parkinson's disease. *Molecular neurodegeneration, 11*(1), 1-15.

Mak, M. K., Wong-Yu, I. S., Shen, X., & Chung, C. L. (2017). Long-term effects of exercise and physical therapy in people with Parkinson disease. *Nature Reviews Neurology, 13*(11), 689-703.
Malgieri, G., & Eliezer, D. (2008). Structural effects of Parkinson's disease linked DJ-1 mutations. *Protein Science, 17*(5), 855-868.
Maroteaux, L., Campanelli, J. T., & Scheller, R. H. (1988). Synuclein: a neuron-specific protein localized to the nucleus and presynaptic nerve terminal. *Journal of Neuroscience, 8*(8), 2804-2815.
Maroteaux, L., & Scheller, R. (1991). The rat brain synucleins; family of proteins transiently associated with neuronal membrane. *Molecular brain research, 11*(3-4), 335-343.
Martinat, C., Shendelman, S., Jonason, A., Leete, T., Beal, M. F., Yang, L., . . . Zoghbi, H. Y. (2004). Sensitivity to oxidative stress in DJ-1-deficient dopamine neurons: an ES-derived cell model of primary Parkinsonism. *PLoS biology, 2*(11), e327.
Masuda-Suzukake, M., Nonaka, T., Hosokawa, M., Kubo, M., Shimozawa, A., Akiyama, H., & Hasegawa, M. (2014). Pathological alpha-synuclein propagates through neural networks. *Acta neuropathologica communications, 2*(1), 1-12.
Mateos-Aparicio, P., & Rodríguez-Moreno, A. (2020). Calcium dynamics and synaptic plasticity. *Calcium Signaling*, 965-984.
Matsuda, N., Kimura, M., Queliconi, B. B., Kojima, W., Mishima, M., Takagi, K., . . . Ito, Y. (2017). Parkinson's disease-related DJ-1 functions in thiol quality control against aldehyde attack in vitro. *Scientific reports, 7*(1), 1-15.
Matsumoto, L., Takuma, H., Tamaoka, A., Kurisaki, H., Date, H., Tsuji, S., & Iwata, A. (2010). CpG demethylation enhances alpha-synuclein expression and affects the pathogenesis of Parkinson's disease. *PloS one, 5*(11), e15522.
Mattsson, N., Andreasson, U., Zetterberg, H., Blennow, K., & Initiative, A. s. D. N. (2017). Association of plasma neurofilament light with neurodegeneration in patients with Alzheimer disease. *JAMA neurology, 74*(5), 557-566.
Mazzulli, J. R., Zunke, F., Isacson, O., Studer, L., & Krainc, D. (2016). α-Synuclein–induced lysosomal dysfunction occurs through disruptions in protein trafficking in human midbrain synucleinopathy models. *Proceedings of the National Academy of Sciences, 113*(7), 1931-1936.
Mbefo, M. K., Paleologou, K. E., Boucharaba, A., Oueslati, A., Schell, H., Fournier, M., . . . Masliah, E. (2010). Phosphorylation of synucleins by members of the Polo-like kinase family. *Journal of Biological Chemistry, 285*(4), 2807-2822.
McFarland, M. A., Ellis, C. E., Markey, S. P., & Nussbaum, R. L. (2008). Proteomics analysis identifies phosphorylation-dependent α-synuclein protein interactions. *Molecular & Cellular Proteomics, 7*(11), 2123-2137.
Medda, X., Mertens, L., Versweyveld, S., Diels, A., Barnham, L., Bretteville, A., . . . Ebneth, A. (2016). Development of a scalable, high-throughput-compatible assay to detect tau aggregates using iPSC-derived cortical

neurons maintained in a three-dimensional culture format. *Journal of biomolecular screening, 21*(8), 804-815.

Mehta, S. R., Tom, C. M., Wang, Y., Bresee, C., Rushton, D., Mathkar, P. P., . . . Mattis, V. B. (2018). Human Huntington's disease iPSC-derived cortical neurons display altered transcriptomics, morphology, and maturation. *Cell reports, 25*(4), 1081-1096. e1086.

Melki, R. (2015). Role of different alpha-synuclein strains in synucleinopathies, similarities with other neurodegenerative diseases. *Journal of Parkinson's disease, 5*(2), 217-227.

Metzakopian, E., Lin, W., Salmon-Divon, M., Dvinge, H., Andersson, E., Ericson, J., . . . Ang, S.-L. (2012). Genome-wide characterization of Foxa2 targets reveals upregulation of floor plate genes and repression of ventrolateral genes in midbrain dopaminergic progenitors. *Development, 139*(14), 2625-2634.

Milber, J. M., Noorigian, J. V., Morley, J. F., Petrovitch, H., White, L., Ross, G. W., & Duda, J. E. (2012). Lewy pathology is not the first sign of degeneration in vulnerable neurons in Parkinson disease. *Neurology, 79*(24), 2307-2314.

Mills, J., Ward, M., Kim, W., Halliday, G., & Janitz, M. (2016). Strand-specific RNA-sequencing analysis of multiple system atrophy brain transcriptome. *Neuroscience, 322*, 234-250.

Miñones-Moyano, E., Porta, S., Escaramís, G., Rabionet, R., Iraola, S., Kagerbauer, B., . . . Martí, E. (2011). MicroRNA profiling of Parkinson's disease brains identifies early downregulation of miR-34b/c which modulate mitochondrial function. *Human molecular genetics, 20*(15), 3067-3078.

Miranda, H. V., & Outeiro, T. F. (2010). The sour side of neurodegenerative disorders: the effects of protein glycation. *The Journal of pathology, 221*(1), 13-25.

Miranda, H. V., Xiang, W., de Oliveira, R. M., Simões, T., Pimentel, J., Klucken, J., . . . Outeiro, T. F. (2013). Heat-mediated enrichment of α-synuclein from cells and tissue for assessing post-translational modifications. *Journal of neurochemistry, 126*(5), 673-684.

Miyazaki, S., Yanagida, T., Nunome, K., Ishikawa, S., Inden, M., Kitamura, Y., . . . Niwa, M. (2008). DJ-1-binding compounds prevent oxidative stress-induced cell death and movement defect in Parkinson's disease model rats. *Journal of neurochemistry, 105*(6), 2418-2434.

Mollinari, C., Zhao, J., Lupacchini, L., Garaci, E., Merlo, D., & Pei, G. (2018). Transdifferentiation: a new promise for neurodegenerative diseases. *Cell death & disease, 9*(8), 1-9.

Monsellier, E., & Chiti, F. (2007). Prevention of amyloid-like aggregation as a driving force of protein evolution. *EMBO reports, 8*(8), 737-742.

Moors, T. E., Maat, C. A., Niedieker, D., Mona, D., Petersen, D., Timmermans-Huisman, E., . . . Barbour, R. (2018). Detailed structural orchestration of Lewy pathology in Parkinson's disease as revealed by 3D multicolor STED microscopy. *bioRxiv*, 470476.

Mougenot, A.-L., Nicot, S., Bencsik, A., Morignat, E., Verchère, J., Lakhdar, L., . . . Baron, T. (2012). Prion-like acceleration of a synucleinopathy in a transgenic mouse model. *Neurobiology of aging, 33*(9), 2225-2228.

MS Lima, M., F Martins, E., Marcia Delattre, A., B Proenca, M., A Mori, M., Carabelli, B., & C Ferraz, A. (2012). Motor and non-motor features of Parkinson's disease–a review of clinical and experimental studies. *CNS & Neurological Disorders-Drug Targets (Formerly Current Drug Targets-CNS & Neurological Disorders), 11*(4), 439-449.

Münch, G., Lüth, H., Wong, A., Arendt, T., Hirsch, E., Ravid, R. a., & Riederer, P. (2000). Crosslinking of α-synuclein by advanced glycation endproducts—an early pathophysiological step in Lewy body formation? *Journal of chemical neuroanatomy, 20*(3-4), 253-257.

Murakami, K., Miyake, Y., Sasaki, S., Tanaka, K., Fukushima, W., Kiyohara, C., . . . Miki, T. (2010). Dietary glycemic index is inversely associated with the risk of Parkinson's disease: a case–control study in Japan. *Nutrition, 26*(5), 515-521.

Nagakubo, D., Taira, T., Kitaura, H., Ikeda, M., Tamai, K., Iguchi-Ariga, S. M., & Ariga, H. (1997). DJ-1, a novel oncogene which transforms mouse NIH3T3 cells in cooperation withras. *Biochemical and biophysical research communications, 231*(2), 509-513.

Näsström, T., Andersson, P. O., Lejon, C., & Karlsson, B. C. (2019). Amyloid fibrils prepared using an acetylated and methyl amidated peptide model of the α-Synuclein NAC 71–82 amino acid stretch contain an additional cross-β structure also found in prion proteins. *Scientific reports, 9*(1), 1-14.

Nellikka, R. K., Bhaskar, B. R., Sanghrajka, K., Patil, S. S., & Das, D. (2021). α-Synuclein kinetically regulates the nascent fusion pore dynamics. *Proceedings of the National Academy of Sciences, 118*(34).

Nemani, V. M., Lu, W., Berge, V., Nakamura, K., Onoa, B., Lee, M. K., . . . Edwards, R. H. (2010). Increased expression of α-synuclein reduces neurotransmitter release by inhibiting synaptic vesicle reclustering after endocytosis. *Neuron, 65*(1), 66-79.

Neudorfer, O., Giladi, N., Elstein, D., Abrahamov, A., Turezkite, T., Aghai, E., . . . Zimran, A. (1996). Occurrence of Parkinson's syndrome in type 1 Gaucher disease. *QJM: An International Journal of Medicine, 89*(9), 691-694.

Nguyen, T. M. T., Kim, J., Doan, T. T., Lee, M.-W., & Lee, M. (2019). APEX proximity labeling as a versatile tool for biological research. *Biochemistry, 59*(3), 260-269.

Nichols, B. J., & Pelham, H. R. (1998). SNAREs and membrane fusion in the Golgi apparatus. *Biochimica et Biophysica Acta (BBA)-Molecular Cell Research, 1404*(1-2), 9-31.

Nido, G. S., Dick, F., Toker, L., Petersen, K., Alves, G., Tysnes, O.-B., . . . Tzoulis, C. (2020). Common gene expression signatures in Parkinson's disease are driven by changes in cell composition. *Acta neuropathologica communications, 8*(1), 1-14.

Nonnekes, J., Timmer, M. H., de Vries, N. M., Rascol, O., Helmich, R. C., & Bloem, B. R. (2016). Unmasking levodopa resistance in Parkinson's disease. *Movement Disorders, 31*(11), 1602-1609.

Nübling, G. S., Levin, J., Bader, B., Lorenzl, S., Hillmer, A., Högen, T., . . . Giese, A. (2014). Modelling Ser129 phosphorylation inhibits membrane binding of pore-forming alpha-synuclein oligomers. *PloS one, 9*(6), e98906.

Nural, H., He, P., Beach, T., Sue, L., Xia, W., & Shen, Y. (2009). Dissembled DJ-1 high molecular weight complex in cortex mitochondria from Parkinson's disease patients. *Molecular neurodegeneration, 4*(1), 1-9.

O'Shea, I. M., Popal, H., Olson, I. R., Murty, V. P., & Smith, D. V. (2021). Distinct Alterations in Cerebellar Connectivity with Substantia Nigra and Ventral Tegmental Area in Parkinsons Disease. *bioRxiv*.

Oakley, D. H., Klickstein, N., Commins, C., Chung, M., Dujardin, S., Bennett, R. E., . . . Frosch, M. P. (2021). Continuous Monitoring of Tau-Induced Neurotoxicity in Patient-Derived iPSC-Neurons. *Journal of Neuroscience, 41*(19), 4335-4348.

Oliveira, L., Falomir-Lockhart, L. J., Botelho, M., Lin, K., Wales, P., Koch, J., . . . Lingor, P. (2015). Elevated α-synuclein caused by SNCA gene triplication impairs neuronal differentiation and maturation in Parkinson's patient-derived induced pluripotent stem cells. *Cell death & disease, 6*(11), e1994-e1994.

Oosawa, F., & Asakura, S. (1975). *Thermodynamics of the Polymerization of Protein*: Academic Press.

Ostrerova, N., Petrucelli, L., Farrer, M., Mehta, N., Choi, P., Hardy, J., & Wolozin, B. (1999). α-Synuclein shares physical and functional homology with 14-3-3 proteins. *Journal of Neuroscience, 19*(14), 5782-5791.

Oueslati, A. (2016). Implication of alpha-synuclein phosphorylation at S129 in synucleinopathies: what have we learned in the last decade? *Journal of Parkinson's disease, 6*(1), 39-51.

Oueslati, A., Fournier, M., & Lashuel, H. A. (2010). Role of post-translational modifications in modulating the structure, function and toxicity of α-synuclein: implications for Parkinson's disease pathogenesis and therapies. *Progress in brain research, 183*, 115-145.

Oueslati, A., Schneider, B. L., Aebischer, P., & Lashuel, H. A. (2013). Polo-like kinase 2 regulates selective autophagic α-synuclein clearance and suppresses its toxicity in vivo. *Proceedings of the National Academy of Sciences, 110*(41), E3945-E3954.

Outeiro, T. F., Heutink, P., Bezard, E., & Cenci, A. M. (2021). From iPS Cells to Rodents and Nonhuman Primates: Filling Gaps in Modeling Parkinson's Disease. *Movement Disorders, 36*(4), 832-841.

Ozawa, K., Tsumoto, H., Miura, Y., Yamaguchi, J., Iguchi-Ariga, S. M., Sakuma, T., . . . Uchiyama, Y. (2020). DJ-1 is indispensable for the S-nitrosylation of Parkin, which maintains function of mitochondria. *Scientific reports, 10*(1), 1-11.

Paillusson, S., Gomez-Suaga, P., Stoica, R., Little, D., Gissen, P., Devine, M. J., . . . Miller, C. C. (2017). α-Synuclein binds to the ER–mitochondria tethering protein VAPB to disrupt Ca 2+ homeostasis and mitochondrial ATP production. *Acta neuropathologica, 134*(1), 129-149.

Paisán-Ruíz, C., Jain, S., Evans, E. W., Gilks, W. P., Simón, J., Van Der Brug, M., . . . Khan, N. (2004). Cloning of the gene containing mutations that cause PARK8-linked Parkinson's disease. *Neuron, 44*(4), 595-600.

Paleologou, K. E., Kragh, C. L., Mann, D. M., Salem, S. A., Al-Shami, R., Allsop, D., . . . El-Agnaf, O. M. (2009). Detection of elevated levels of soluble α-synuclein oligomers in post-mortem brain extracts from patients with dementia with Lewy bodies. *Brain, 132*(4), 1093-1101.

Pandi, S., Chinniah, R., Sevak, V., Ravi, P. M., Raju, M., Vellaiappan, N. A., & Karuppiah, B. (2021). Association of HLA–DRB1, DQA1 and DQB1 alleles and haplotype in Parkinson's disease from South India. *Neuroscience letters*, 136296.

Panman, L., Papathanou, M., Laguna, A., Oosterveen, T., Volakakis, N., Acampora, D., . . . Joodmardi, E. (2014). Sox6 and Otx2 control the specification of substantia nigra and ventral tegmental area dopamine neurons. *Cell reports, 8*(4), 1018-1025.

Pantner, Y., Polavarapu, R., Chin, L.-S., Li, L., Shimizu, Y., & Calvert, J. W. (2021). DJ-1 attenuates the glycation of mitochondrial complex I and complex III in the post-ischemic heart. *Scientific reports, 11*(1), 1-9.

Pardo Muñoz, M., García Díaz-Barriga, G. A., Straccia, M., Sanders, P., Alberch i Vié, J., Canals i Coll, J. M., & Consortium, H. i. (2017). Developmental alterations in Huntington's disease neural cells and pharmacological rescue in cells and mice. *Nature Neuroscience, 2017, vol. 20, num. 5, p. 648-660*.

Parkinson, J. (2002). An essay on the shaking palsy. *The Journal of neuropsychiatry and clinical neurosciences, 14*(2), 223-236.

Parnetti, L., Farotti, L., Eusebi, P., Chiasserini, D., De Carlo, C., Giannandrea, D., . . . Rossi, A. (2014). Differential role of CSF alpha-synuclein species, tau, and Aβ42 in Parkinson's Disease. *Frontiers in aging neuroscience, 6*, 53.

Parr, C., Yamanaka, S., & Saito, H. (2017). An update on stem cell biology and engineering for brain development. *Molecular psychiatry, 22*(6), 808-819.

Pasanen, P., Myllykangas, L., Siitonen, M., Raunio, A., Kaakkola, S., Lyytinen, J., . . . Paetau, A. (2014). A novel α-synuclein mutation A53E associated with atypical multiple system atrophy and Parkinson's disease-type pathology. *Neurobiology of aging, 35*(9), 2180. e2181-2180. e2185.

Pasteuning-Vuhman, S., de Jongh, R., Timmers, A., & Pasterkamp, R. J. (2020). Towards advanced iPSC-based drug development for neurodegenerative disease. *Trends in Molecular Medicine*.

Pearce, R., Owen, A., Daniel, S., Jenner, P., & Marsden, C. (1997). Alterations in the distribution of glutathione in the substantia nigra in Parkinson's disease. *Journal of neural transmission, 104*(6-7), 661-677.

Peelaerts, W., & Baekelandt, V. (2016). α-Synuclein strains and the variable pathologies of synucleinopathies. *Journal of neurochemistry, 139*, 256-274.

Peelaerts, W., Bousset, L., Baekelandt, V., & Melki, R. (2018). α-Synuclein strains and seeding in Parkinson's disease, incidental Lewy body disease, dementia with Lewy bodies and multiple system atrophy: similarities and differences. *Cell and tissue research, 373*(1), 195-212.

Peelaerts, W., Bousset, L., Van der Perren, A., Moskalyuk, A., Pulizzi, R., Giugliano, M., . . . Baekelandt, V. (2015). α-Synuclein strains cause distinct synucleinopathies after local and systemic administration. *Nature, 522*(7556), 340-344.

Peng, C., Gathagan, R. J., Covell, D. J., Medellin, C., Stieber, A., Robinson, J. L., . . . Luk, K. C. (2018). Cellular milieu imparts distinct pathological α-synuclein strains in α-synucleinopathies. *Nature, 557*(7706), 558-563.

Peng, C., Gathagan, R. J., & Lee, V. M.-Y. (2018). Distinct α-Synuclein strains and implications for heterogeneity among α-Synucleinopathies. *Neurobiology of disease, 109*, 209-218.

Pickrell, A. M., & Youle, R. J. (2015). The roles of PINK1, parkin, and mitochondrial fidelity in Parkinson's disease. *Neuron, 85*(2), 257-273.

Pieri, L., Madiona, K., & Melki, R. (2016). Structural and functional properties of prefibrillar α-synuclein oligomers. *Scientific reports, 6*(1), 1-15.

Plotegher, N., Greggio, E., Bisaglia, M., & Bubacco, L. (2014). Biophysical groundwork as a hinge to unravel the biology of α-synuclein aggregation and toxicity. *Quarterly reviews of biophysics, 47*(1), 1-48.

Poewe, W., & Wenning, G. (2002). The differential diagnosis of Parkinson's disease. *European journal of neurology, 9*, 23-30.

Polymeropoulos, M. H., Lavedan, C., Leroy, E., Ide, S. E., Dehejia, A., Dutra, A., . . . Boyer, R. (1997). Mutation in the α-synuclein gene identified in families with Parkinson's disease. *Science, 276*(5321), 2045-2047.

Popova, B., Galka, D., Häffner, N., Wang, D., Schmitt, K., Valerius, O., . . . Braus, G. H. (2021). α-Synuclein Decreases the Abundance of Proteasome Subunits and Alters Ubiquitin Conjugates in Yeast. *Cells, 10*(9), 2229.

Postuma, R. B., Lang, A. E., Munhoz, R. P., Charland, K., Pelletier, A., Moscovich, M., . . . Altman, R. (2012). Caffeine for treatment of Parkinson disease: a randomized controlled trial. *Neurology, 79*(7), 651-658.

Poulin, J.-F., Caronia, G., Hofer, C., Cui, Q., Helm, B., Ramakrishnan, C., . . . Awatramani, R. (2018). Mapping projections of molecularly defined dopamine neuron subtypes using intersectional genetic approaches. *Nature neuroscience, 21*(9), 1260-1271.

Pranke, I. M., Morello, V., Bigay, J., Gibson, K., Verbavatz, J.-M., Antonny, B., & Jackson, C. L. (2011). α-Synuclein and ALPS motifs are membrane curvature sensors whose contrasting chemistry mediates selective vesicle binding. *Journal of Cell Biology, 194*(1), 89-103.

Pronin, A. N., Morris, A. J., Surguchov, A., & Benovic, J. L. (2000). Synucleins are a novel class of substrates for G protein-coupled receptor kinases. *Journal of Biological Chemistry, 275*(34), 26515-26522.

Prots, I., Grosch, J., Brazdis, R.-M., Simmnacher, K., Veber, V., Havlicek, S., . . . Schütz, O. (2018). α-Synuclein oligomers induce early axonal dysfunction in human iPSC-based models of synucleinopathies. *Proceedings of the National Academy of Sciences, 115*(30), 7813-7818.

Proukakis, C., Dudzik, C. G., Brier, T., MacKay, D. S., Cooper, J. M., Millhauser, G. L., . . . Schapira, A. H. (2013). A novel α-synuclein missense mutation in Parkinson disease. *Neurology, 80*(11), 1062-1064.

Prusiner, S. B. (1998). Prions. *Proceedings of the National Academy of Sciences, 95*(23), 13363-13383.

Prusiner, S. B., Woerman, A. L., Mordes, D. A., Watts, J. C., Rampersaud, R., Berry, D. B., . . . Kravitz, S. N. (2015). Evidence for α-synuclein prions causing multiple system atrophy in humans with parkinsonism. *Proceedings of the National Academy of Sciences, 112*(38), E5308-E5317.

Qin, W., Cho, K. F., Cavanagh, P. E., & Ting, A. Y. (2021). Deciphering molecular interactions by proximity labeling. *Nature Methods, 18*(2), 133-143.

Quinn, N. (1989). Multiple system atrophy--the nature of the beast. *Journal of Neurology, Neurosurgery & Psychiatry, 52*(Suppl), 78-89.

Rabbani, N., & Thornalley, P. J. (2015). Dicarbonyl stress in cell and tissue dysfunction contributing to ageing and disease. *Biochemical and biophysical research communications, 458*(2), 221-226.

Ramsey, C. P., & Giasson, B. I. (2010). L10p and P158DEL DJ-1 mutations cause protein instability, aggregation, and dimerization impairments. *Journal of neuroscience research, 88*(14), 3111-3124.

Recasens, A., Dehay, B., Bové, J., Carballo-Carbajal, I., Dovero, S., Pérez-Villalba, A., . . . Perier, C. (2014). Lewy body extracts from Parkinson disease brains trigger α-synuclein pathology and neurodegeneration in mice and monkeys. *Annals of neurology, 75*(3), 351-362.

Rees, J. S., Li, X.-W., Perrett, S., Lilley, K. S., & Jackson, A. P. (2015). Protein neighbors and proximity proteomics. *Molecular & Cellular Proteomics, 14*(11), 2848-2856.

Reeve, A., Simcox, E., & Turnbull, D. (2014). Ageing and Parkinson's disease: why is advancing age the biggest risk factor? *Ageing research reviews, 14*, 19-30.

Reinert, M.-C., Benkert, P., Wuerfel, J., Michalak, Z., Ruberte, E., Barro, C., . . . Tomic, D. (2020). Serum neurofilament light chain is a useful biomarker in pediatric multiple sclerosis. *Neurology-Neuroimmunology Neuroinflammation, 7*(4).

Repici, M., & Giorgini, F. (2019). DJ-1 in Parkinson's disease: clinical insights and therapeutic perspectives. *Journal of clinical medicine, 8*(9), 1377.

Riaz, S. S., Jauniaux, E., Stern, G. M., & Bradford, H. F. (2002). The controlled conversion of human neural progenitor cells derived from foetal ventral mesencephalon into dopaminergic neurons in vitro. *Developmental brain research, 136*(1), 27-34.

Ribeiro, D., Goya, R. L., Ravindran, G., Vuono, R., Parish, C. L., Foldi, C., . . . Nikkhah, G. (2013). Efficient expansion and dopaminergic differentiation of human fetal ventral midbrain neural stem cells by midbrain morphogens. *Neurobiology of disease, 49*, 118-127.

Richarme, G., Liu, C., Mihoub, M., Abdallah, J., Leger, T., Joly, N., . . . Bouloc, P. (2017). Guanine glycation repair by DJ-1/Park7 and its bacterial homologs. *Science, 357*(6347), 208-211.

Richarme, G., Mihoub, M., Dairou, J., Bui, L. C., Leger, T., & Lamouri, A. (2015). Parkinsonism-associated protein DJ-1/Park7 is a major protein deglycase that repairs methylglyoxal-and glyoxal-glycated cysteine, arginine, and lysine residues. *Journal of Biological Chemistry, 290*(3), 1885-1897.

Rideout, H. J., Dietrich, P., Savalle, M., Dauer, W. T., & Stefanis, L. (2003). Regulation of α-synuclein by bFGF in cultured ventral midbrain dopaminergic neurons. *Journal of neurochemistry, 84*(4), 803-813.

Roberts, R. F., Wade-Martins, R., & Alegre-Abarrategui, J. (2015). Direct visualization of alpha-synuclein oligomers reveals previously undetected pathology in Parkinson's disease brain. *Brain, 138*(6), 1642-1657.

Rockenstein, E., Hansen, L. A., Mallory, M., Trojanowski, J. Q., Galasko, D., & Masliah, E. (2001). Altered expression of the synuclein family mRNA in Lewy body and Alzheimer's disease. *Brain Res., 914*(1-2), 48-56.

Rostami, J., Mothes, T., Kolahdouzan, M., Eriksson, O., Moslem, M., Bergström, J., . . . Falk, A. (2021). Crosstalk between astrocytes and microglia results in increased degradation of α-synuclein and amyloid-β aggregates. *Journal of Neuroinflammation, 18*(1), 1-20.

Roux, K. J., Kim, D. I., Burke, B., & May, D. G. (2018). BioID: a screen for protein-protein interactions. *Curr Protoc Protein Sci., 91*(1), 19.23. 11-19.23. 15.

Roux, K. J., Kim, D. I., Raida, M., & Burke, B. (2012). A promiscuous biotin ligase fusion protein identifies proximal and interacting proteins in mammalian cells. *The Journal of cell biology, 196*(6), 801-810.

Ryan, S. D., Dolatabadi, N., Chan, S. F., Zhang, X., Akhtar, M. W., Parker, J., . . . Talantova, M. (2013). Isogenic human iPSC Parkinson's model shows nitrosative stress-induced dysfunction in MEF2-PGC1α transcription. *Cell, 155*(6), 1351-1364.

Saá, P., & Cervenakova, L. (2015). Protein misfolding cyclic amplification (PMCA): Current status and future directions. *Virus research, 207*, 47-61.

Saborio, G. P., Permanne, B., & Soto, C. (2001). Sensitive detection of pathological prion protein by cyclic amplification of protein misfolding. *Nature, 411*(6839), 810-813.

Sacino, A. N., Brooks, M., Thomas, M. A., McKinney, A. B., Lee, S., Regenhardt, R. W., . . . Borchelt, D. R. (2014). Intramuscular injection of α-synuclein induces CNS α-synuclein pathology and a rapid-onset motor phenotype in transgenic mice. *Proceedings of the National Academy of Sciences, 111*(29), 10732-10737.

Saha, A. R., Hill, J., Utton, M. A., Asuni, A. A., Ackerley, S., Grierson, A. J., . . . Anderton, B. H. (2004). Parkinson's disease α-synuclein mutations exhibit defective axonal transport in cultured neurons. *Journal of cell science, 117*(7), 1017-1024.

Saito, Y. (2014). Oxidized DJ-1 as a possible biomarker of Parkinson's disease. *Journal of clinical biochemistry and nutrition*, 13-108.

Saito, Y., Hamakuba, T., Yoshida, Y., Akazawa, Y. O., Shichiri, M., Noguchi, N., & Niki, E. (2009). *Significant Elevation of Oxidized DJ-1 in Erythrocytes of Early-Stage Parkinson Disease Patients: Potential Application of Oxidized DJ-1 Levels for Diagnosis of PD at Early Stage.* Paper presented at the Free Radical Biology and Medicine.

Saito, Y., Kawashima, A., Ruberu, N. N., Fujiwara, H., Koyama, S., Sawabe, M., . . . Hasegawa, M. (2003). Accumulation of phosphorylated α-synuclein in aging human brain. *Journal of Neuropathology & Experimental Neurology, 62*(6), 644-654.

Salvi, M., Trashi, E., Marin, O., Negro, A., Sarno, S., & Pinna, L. A. (2012). Superiority of PLK-2 as α-synuclein phosphorylating agent relies on unique specificity determinants. *Biochemical and biophysical research communications, 418*(1), 156-160.

Sampathu, D. M., Giasson, B. I., Pawlyk, A. C., Trojanowski, J. Q., & Lee, V. M.-Y. (2003). Ubiquitination of α-synuclein is not required for formation of pathological inclusions in α-synucleinopathies. *The American journal of pathology, 163*(1), 91-100.

Samuel, F., Flavin, W. P., Iqbal, S., Pacelli, C., Renganathan, S. D. S., Trudeau, L.-E., . . . Tandon, A. (2016). Effects of serine 129 phosphorylation on α-synuclein aggregation, membrane association, and internalization. *Journal of Biological Chemistry, 291*(9), 4374-4385.

Sánchez-Pernaute, R., Studer, L., Bankiewicz, K. S., Major, E. O., & McKay, R. D. (2001). In vitro generation and transplantation of precursor-derived human dopamine neurons. *Journal of neuroscience research, 65*(4), 284-288.

Sang, J. C., Hidari, E., Meisl, G., Ranasinghe, R. T., Spillantini, M. G., & Klenerman, D. (2021). Super-resolution imaging reveals α-synuclein seeded aggregation in SH-SY5Y cells. *Communications biology, 4*(1), 1-11.

Sanz, R., Ovando-Roche, P., Udeshi, N. D., Carr, S. A., Chung, C. Y., & Khurana, V. (2019). In Situ Peroxidase Labeling and Mass Spectrometry of Alpha-Synuclein in Rat Cortical Neurons. In *Alpha-Synuclein* (pp. 235-246): Springer.

Sardi, S. P., Cedarbaum, J. M., & Brundin, P. (2018). Targeted therapies for Parkinson's disease: from genetics to the clinic. *Movement Disorders, 33*(5), 684-696.

Satake, W., Nakabayashi, Y., Mizuta, I., Hirota, Y., Ito, C., Kubo, M., . . . Takeda, A. (2009). Genome-wide association study identifies common variants at four loci as genetic risk factors for Parkinson's disease. *Nature genetics, 41*(12), 1303-1307.

Sato, H., Arawaka, S., Hara, S., Fukushima, S., Koga, K., Koyama, S., & Kato, T. (2011). Authentically phosphorylated α-synuclein at Ser129 accelerates neurodegeneration in a rat model of familial Parkinson's disease. *Journal of Neuroscience, 31*(46), 16884-16894.

Schapira, A. H., & Tolosa, E. (2010). Molecular and clinical prodrome of Parkinson disease: implications for treatment. *Nature Reviews Neurology, 6*(6), 309.

Schenck, C. H., Bundlie, S. R., Ettinger, M. G., & Mahowald, M. W. (1986). Chronic behavioral disorders of human REM sleep: a new category of parasomnia. *Sleep, 9*(2), 293-308.

Schmidt, S. I., Bogetofte, H., Ritter, L., Agergaard, J. B., Hammerich, D., Kabiljagic, A. A., . . . Jørgensen, M. L. (2021). Microglia-Secreted Factors Enhance Dopaminergic Differentiation of Tissue-and iPSC-Derived Human Neural Stem Cells. *Stem cell reports, 16*(2), 281-294.

Schöndorf, D. C., Ivanyuk, D., Baden, P., Sanchez-Martinez, A., De Cicco, S., Yu, C., . . . Panagiotakopoulou, V. (2018). The NAD+ precursor nicotinamide riboside rescues mitochondrial defects and neuronal loss

in iPSC and fly models of Parkinson's disease. *Cell reports, 23*(10), 2976-2988.
Schweighauser, M., Shi, Y., Tarutani, A., Kametani, F., Murzin, A. G., Ghetti, B., . . . Hasegawa, K. (2020). Structures of α-synuclein filaments from multiple system atrophy. *Nature, 585*(7825), 464-469.
Senard, J., Rai, S., Lapeyre-Mestre, M., Brefel, C., Rascol, O., Rascol, A., & Montastruc, J. (1997). Prevalence of orthostatic hypotension in Parkinson's disease. *Journal of Neurology, Neurosurgery & Psychiatry, 63*(5), 584-589.
Seppi, K., Ray Chaudhuri, K., Coelho, M., Fox, S. H., Katzenschlager, R., Perez Lloret, S., . . . Chahine, L. (2019). Update on treatments for nonmotor symptoms of Parkinson's disease—an evidence-based medicine review. *Movement Disorders, 34*(2), 180-198.
Sergi, D., Gélinas, A., Beaulieu, J., Renaud, J., Tardif-Pellerin, E., Guillard, J., & Martinoli, M.-G. (2021). Anti-Apoptotic and Anti-Inflammatory Role of Trans ε-Viniferin in a Neuron–Glia Co-Culture Cellular Model of Parkinson's Disease. *Foods, 10*(3), 586.
Sergushichev, A. A. (2016). An algorithm for fast preranked gene set enrichment analysis using cumulative statistic calculation. *bioRxiv*, 060012.
Shahmoradian, S. H., Lewis, A. J., Genoud, C., Hench, J., Moors, T. E., Navarro, P. P., . . . Goldie, K. N. (2019). Lewy pathology in Parkinson's disease consists of crowded organelles and lipid membranes. *Nature neuroscience, 22*(7), 1099-1109.
Shahnawaz, M., Mukherjee, A., Pritzkow, S., Mendez, N., Rabadia, P., Liu, X., . . . Wu, G. (2020). Discriminating α-synuclein strains in Parkinson's disease and multiple system atrophy. *Nature, 578*(7794), 273-277.
Shahnawaz, M., Tokuda, T., Waragai, M., Mendez, N., Ishii, R., Trenkwalder, C., . . . Soto, C. (2017). Development of a biochemical diagnosis of Parkinson disease by detection of α-synuclein misfolded aggregates in cerebrospinal fluid. *JAMA neurology, 74*(2), 163-172.
Shaikh, S., & Nicholson, L. F. (2008). Advanced glycation end products induce in vitro cross-linking of α-synuclein and accelerate the process of intracellular inclusion body formation. *Journal of neuroscience research, 86*(9), 2071-2082.
Shaltouki, A., Hsieh, C.-H., Kim, M. J., & Wang, X. (2018). Alpha-synuclein delays mitophagy and targeting Miro rescues neuron loss in Parkinson's models. *Acta neuropathologica, 136*(4), 607-620.
Shangari, N., & O'Brien, P. J. (2004). The cytotoxic mechanism of glyoxal involves oxidative stress. *Biochemical pharmacology, 68*(7), 1433-1442.
Sharma, M., Burré, J., Bronk, P., Zhang, Y., Xu, W., & Südhof, T. C. (2012). CSPα knockout causes neurodegeneration by impairing SNAP-25 function. *The EMBO journal, 31*(4), 829-841.
Sharma, N., Rao, S. P., & Kalivendi, S. V. (2019). The deglycase activity of DJ-1 mitigates α-synuclein glycation and aggregation in dopaminergic cells: Role of oxidative stress mediated downregulation of DJ-1 in Parkinson's disease. *Free Radical Biology and Medicine, 135*, 28-37.

Shendelman, S., Jonason, A., Martinat, C., Leete, T., & Abeliovich, A. (2004). DJ-1 is a redox-dependent molecular chaperone that inhibits α-synuclein aggregate formation. *PLoS Biol., 2*(11).

Shrivastava, A. N., Bousset, L., Renner, M., Redeker, V., Savistchenko, J., Triller, A., & Melki, R. (2020). Differential membrane binding and seeding of distinct α-synuclein fibrillar polymorphs. *Biophysical journal, 118*(6), 1301-1320.

Shrivastava, A. N., Redeker, V., Fritz, N., Pieri, L., Almeida, L. G., Spolidoro, M., . . . Léna, C. (2015). α-synuclein assemblies sequester neuronal α3-Na+/K+-ATP ase and impair Na+ gradient. *The EMBO journal, 34*(19), 2408-2423.

Siddu, A., David, L. S., Lauinger, N., Chen, X., Saint-Pierre, M., Alpaugh, M., . . . Cicchetti, F. (2020). Beneficial effects of cysteamine in Thy1-α-Syn mice and induced pluripotent stem cells with a SNCA gene triplication. *Neurobiology of disease, 145*, 105042.

Silva, B. A., Breydo, L., & Uversky, V. N. (2013). Targeting the chameleon: a focused look at α-synuclein and its roles in neurodegeneration. *Molecular neurobiology, 47*(2), 446-459.

Simon-Sanchez, J., Schulte, C., Bras, J. M., Sharma, M., Gibbs, J. R., Berg, D., . . . Hernandez, D. G. (2009). Genome-wide association study reveals genetic risk underlying Parkinson's disease. *Nature genetics, 41*(12), 1308-1312.

Singer, W., Schmeichel, A. M., Shahnawaz, M., Schmelzer, J. D., Boeve, B. F., Sletten, D. M., . . . Savica, R. (2020). Alpha-synuclein oligomers and neurofilament light chain in spinal fluid differentiate multiple system atrophy from Lewy body synucleinopathies. *Annals of neurology, 88*(3), 503-512.

Singleton, A., Farrer, M., Johnson, J., Singleton, A., Hague, S., Kachergus, J., . . . Lincoln, S. (2003). [alpha]-synuclein locus triplication causes Parkinson's disease. *Science, 302*(5646), 841-842.

Smith, M. H., Ploegh, H. L., & Weissman, J. S. (2011). Road to ruin: targeting proteins for degradation in the endoplasmic reticulum. *Science, 334*(6059), 1086-1090.

Smolders, S., & Van Broeckhoven, C. (2020). Genetic perspective on the synergistic connection between vesicular transport, lysosomal and mitochondrial pathways associated with Parkinson's disease pathogenesis. *Acta neuropathologica communications, 8*(1), 1-28.

Soldner, F., & Jaenisch, R. (2018). Stem cells, genome editing, and the path to translational medicine. *Cell, 175*(3), 615-632.

Soto, C., & Pritzkow, S. (2018). Protein misfolding, aggregation, and conformational strains in neurodegenerative diseases. *Nature neuroscience, 21*(10), 1332-1340.

Soto, C., Saborio, G. P., & Anderes, L. (2002). Cyclic amplification of protein misfolding: application to prion-related disorders and beyond. *Trends in neurosciences, 25*(8), 390-394.

Spillantini, M. G., Crowther, R. A., Jakes, R., Hasegawa, M., & Goedert, M. (1998). α-Synuclein in filamentous inclusions of Lewy bodies from

Parkinson's disease and dementia with Lewy bodies. *Proceedings of the National Academy of Sciences, 95*(11), 6469-6473.
Spillantini, M. G., & Goedert, M. (2000). The α-synucleinopathies: Parkinson's disease, dementia with Lewy bodies, and multiple system atrophy. *Annals of the New York Academy of Sciences, 920*(1), 16-27.
Spillantini, M. G., & Goedert, M. (2018). Neurodegeneration and the ordered assembly of α-synuclein. *Cell and tissue research, 373*(1), 137-148.
Spillantini, M. G., Schmidt, M. L., Lee, V. M.-Y., Trojanowski, J. Q., Jakes, R., & Goedert, M. (1997). α-Synuclein in Lewy bodies. *Nature, 388*(6645), 839-840.
Sridharan, B., Hubbs, C., Llamosas, N., Kilinc, M., Singhera, F. U., Willems, E., . . . Spicer, T. P. (2019). A simple procedure for creating scalable phenotypic screening assays in human neurons. *Scientific reports, 9*(1), 1-14.
Stephens, A. D., Zacharopoulou, M., Moons, R., Fusco, G., Seetaloo, N., Chiki, A., . . . Phillips, J. J. (2020). Extent of N-terminus exposure of monomeric alpha-synuclein determines its aggregation propensity. *Nature Communications, 11*(1), 1-15.
Stott, S. R., Metzakopian, E., Lin, W., Kaestner, K. H., Hen, R., & Ang, S.-L. (2013). Foxa1 and foxa2 are required for the maintenance of dopaminergic properties in ventral midbrain neurons at late embryonic stages. *Journal of Neuroscience, 33*(18), 8022-8034.
Strohäker, T., Jung, B. C., Liou, S.-H., Fernandez, C. O., Riedel, D., Becker, S., . . . Lee, S.-J. (2019). Structural heterogeneity of α-synuclein fibrils amplified from patient brain extracts. *Nat Commun., 10*(1), 1-12.
Stykel, M. G., Humphries, K., Kirby, M. P., Czaniecki, C., Wang, T., Ryan, T., . . . Ryan, S. D. (2018). Nitration of microtubules blocks axonal mitochondrial transport in a human pluripotent stem cell model of Parkinson's disease. *The FASEB Journal, 32*(10), 5350-5364.
Sulzer, D., Bogulavsky, J., Larsen, K. E., Behr, G., Karatekin, E., Kleinman, M. H., . . . Greene, L. A. (2000). Neuromelanin biosynthesis is driven by excess cytosolic catecholamines not accumulated by synaptic vesicles. *Proceedings of the National Academy of Sciences, 97*(22), 11869-11874.
Sulzer, D., & Edwards, R. H. (2019). The physiological role of α-synuclein and its relationship to Parkinson's Disease. *Journal of neurochemistry, 150*(5), 475-486.
Sun, S.-Y., An, C.-N., & Pu, X.-P. (2012). DJ-1 protein protects dopaminergic neurons against 6-OHDA/MG-132-induced neurotoxicity in rats. *Brain research bulletin, 88*(6), 609-616.
Sun, Y., Chang, Y.-H., Chen, H.-F., Su, Y.-H., Su, H.-F., & Li, C.-Y. (2012). Risk of Parkinson disease onset in patients with diabetes: a 9-year population-based cohort study with age and sex stratifications. *Diabetes Care, 35*(5), 1047-1049.
Suzuki, S., Akamatsu, W., Kisa, F., Sone, T., Ishikawa, K.-i., Kuzumaki, N., . . . Okano, H. (2017). Efficient induction of dopaminergic neuron differentiation from induced pluripotent stem cells reveals impaired mitophagy in PARK2 neurons. *Biochemical and biophysical research communications, 483*(1), 88-93.

Szczepanik, J. C., de Almeida, G. R. L., Cunha, M. P., & Dafre, A. L. (2020). Repeated methylglyoxal treatment depletes dopamine in the prefrontal cortex, and causes memory impairment and depressive-like behavior in mice. *Neurochemical research, 45*(2), 354-370.

Taghavi, F., Habibi-Rezaei, M., Amani, M., Saboury, A. A., & Moosavi-Movahedi, A. A. (2017). The status of glycation in protein aggregation. *International journal of biological macromolecules, 100*, 67-74.

Tagliafierro, L., & Chiba-Falek, O. (2016). Up-regulation of SNCA gene expression: implications to synucleinopathies. *Neurogenetics, 17*(3), 145-157.

Taipa, R., Pereira, C., Reis, I., Alonso, I., Bastos-Lima, A., Melo-Pires, M., & Magalhaes, M. (2016). DJ-1 linked parkinsonism (PARK7) is associated with Lewy body pathology. *Brain, 139*(6), 1680-1687.

Taira, T., Saito, Y., Niki, T., Iguchi-Ariga, S. M., Takahashi, K., & Ariga, H. (2004). DJ-1 has a role in antioxidative stress to prevent cell death. *EMBO reports, 5*(2), 213-218.

Takahashi-Niki, K., Inafune, A., Michitani, N., Hatakeyama, Y., Suzuki, K., Sasaki, M., . . . Ariga, H. (2015). DJ-1-dependent protective activity of DJ-1-binding compound no. 23 against neuronal cell death in MPTP-treated mouse model of Parkinson's disease. *Journal of pharmacological Sciences, 127*(3), 305-310.

Tamgüney, G., & Korczyn, A. D. (2018). A critical review of the prion hypothesis of human synucleinopathies. *Cell and tissue research, 373*(1), 213-220.

Tanji, K., Imaizumi, T., Yoshida, H., Mori, F., Yoshimoto, M., Satoh, K., & Wakabayashi, K. (2001). Expression of α-synuclein in a human glioma cell line and its up-regulation by interleukin-1β. *Neuroreport, 12*(9), 1909-1912.

Tanji, K., Mori, F., Imaizumi, T., Yoshida, H., Matsumiya, T., Tamo, W., . . . Takahashi, H. (2002). Upregulation of α-synuclein by lipopolysaccharide and interleukin-1 in human macrophages. *Pathology international, 52*(9), 572-577.

Tanudjojo, B., Shaikh, S. S., Fenyi, A., Bousset, L., Agarwal, D., Marsh, J., . . . Sims, D. (2021). Phenotypic manifestation of α-synuclein strains derived from Parkinson’s disease and multiple system atrophy in human dopaminergic neurons. *Nature Communications, 12*(1), 1-16.

Tartaglia, G. G., Pechmann, S., Dobson, C. M., & Vendruscolo, M. (2007). Life on the edge: a link between gene expression levels and aggregation rates of human proteins. *Trends in biochemical sciences, 32*(5), 204-206.

Teismann, P., Sathe, K., Bierhaus, A., Leng, L., Martin, H. L., Bucala, R., . . . Schulz, J. B. (2012). Receptor for advanced glycation endproducts (RAGE) deficiency protects against MPTP toxicity. *Neurobiology of aging, 33*(10), 2478-2490.

Telling, G. C., Parchi, P., DeArmond, S. J., Cortelli, P., Montagna, P., Gabizon, R., . . . Prusiner, S. B. (1996). Evidence for the conformation of the pathologic isoform of the prion protein enciphering and propagating prion diversity. *Science, 274*(5295), 2079-2082.

Tenreiro, S., Eckermann, K., & Outeiro, T. F. (2014). Protein phosphorylation in neurodegeneration: friend or foe? *Frontiers in molecular neuroscience, 7*, 42.

Theo, F., Kraus, J., Haider, M., Spanner, J., Steinmaurer, M., Dietinger, V., & Kretzschmar, H. A. (2017). Altered Long Noncoding RNA Expression Precedes the Course of Parkinson's Disease--a Preliminary Report. *Molecular neurobiology, 54*(4), 2869.

Tian, R., Abarientos, A., Hong, J., Hashemi, S. H., Yan, R., Dräger, N., . . . Xu, K. (2021). Genome-wide CRISPRi/a screens in human neurons link lysosomal failure to ferroptosis. *Nature neuroscience*, 1-15.

Tofaris, G. K. (2012). Lysosome-dependent pathways as a unifying theme in Parkinson's disease. *Movement Disorders, 27*(11), 1364-1369.

Tofaris, G. K., Goedert, M., & Spillantini, M. G. (2017). The transcellular propagation and intracellular trafficking of α-synuclein. *Cold Spring Harbor perspectives in medicine, 7*(9), a024380.

Tofaris, G. K., Kim, H. T., Hourez, R., Jung, J.-W., Kim, K. P., & Goldberg, A. L. (2011). Ubiquitin ligase Nedd4 promotes α-synuclein degradation by the endosomal–lysosomal pathway. *Proc. Natl. Acad. Sci., 108*(41), 17004-17009.

Tofaris, G. K., Razzaq, A., Ghetti, B., Lilley, K. S., & Spillantini, M. G. (2003). Ubiquitination of α-synuclein in Lewy bodies is a pathological event not associated with impairment of proteasome function. *Journal of Biological Chemistry, 278*(45), 44405-44411.

Tofaris, G. K., & Spillantini, M. G. (2005). Alpha-synuclein dysfunction in Lewy body diseases. *Mov. Disord., 20*(S12), S37-S44.

Tokuda, T., Qureshi, M., Ardah, M., Varghese, S., Shehab, S., Kasai, T., . . . El-Agnaf, O. (2010). Detection of elevated levels of α-synuclein oligomers in CSF from patients with Parkinson disease. *Neurology, 75*(20), 1766-1770.

Tokuda, T., Salem, S. A., Allsop, D., Mizuno, T., Nakagawa, M., Qureshi, M. M., . . . El-Agnaf, O. M. (2006). Decreased α-synuclein in cerebrospinal fluid of aged individuals and subjects with Parkinson's disease. *Biochemical and biophysical research communications, 349*(1), 162-166.

Tolosa, E., Vila, M., Klein, C., & Rascol, O. (2020). LRRK2 in Parkinson disease: challenges of clinical trials. *Nature Reviews Neurology, 16*(2), 97-107.

Tran, J., Anastacio, H., & Bardy, C. (2020). Genetic predispositions of Parkinson's disease revealed in patient-derived brain cells. *NPJ Parkinson's disease, 6*(1), 1-18.

Traxler, L., Edenhofer, F., & Mertens, J. (2019). Next-generation disease modeling with direct conversion: a new path to old neurons. *FEBS letters, 593*(23), 3316-3337.

Trempe, J.-F., & Fon, E. A. (2013). Structure and function of Parkin, PINK1, and DJ-1, the three musketeers of neuroprotection. *Frontiers in neurology, 4*, 38.

Trétiakoff, C. (1919). Contribution a l'etude de l'Anatomie pathologique du Locus Niger de Soemmering avec quelques deduction relatives a la pathogenie des troubles du tonus musculaire et de la maladie de Parkinson. *Theses de Paris*.

Trexler, A. J., & Rhoades, E. (2009). α-Synuclein binds large unilamellar vesicles as an extended helix. *Biochemistry, 48*(11), 2304-2306.
Trinkle-Mulcahy, L. (2019). Recent advances in proximity-based labeling methods for interactome mapping. *F1000Research, 8*.
Tyanova, S., Temu, T., & Cox, J. (2016). The MaxQuant computational platform for mass spectrometry-based shotgun proteomics. *Nat Protoc., 11*(12), 2301.
Uchiki, T., Weikel, K. A., Jiao, W., Shang, F., Caceres, A., Pawlak, D., . . . Taylor, A. (2012). Glycation-altered proteolysis as a pathobiologic mechanism that links dietary glycemic index, aging, and age-related disease (in nondiabetics). *Aging cell, 11*(1), 1-13.
Ulmer, T. S., Bax, A., Cole, N. B., & Nussbaum, R. L. (2005). Structure and dynamics of micelle-bound human α-synuclein. *Journal of Biological Chemistry, 280*(10), 9595-9603.
Uversky, V. N. (2003). A protein-chameleon: conformational plasticity of α-synuclein, a disordered protein involved in neurodegenerative disorders. *Journal of Biomolecular Structure and Dynamics, 21*(2), 211-234.
Vaikath, N. N., Majbour, N. K., Paleologou, K. E., Ardah, M. T., van Dam, E., van de Berg, W. D., . . . Hattori, N. (2015). Generation and characterization of novel conformation-specific monoclonal antibodies for α-synuclein pathology. *Neurobiology of disease, 79*, 81-99.
Valdinocci, D., Kovarova, J., Neuzil, J., & Pountney, D. L. (2021). Alpha-synuclein aggregates associated with mitochondria in tunnelling nanotubes. *Neurotoxicity Research, 39*(2), 429-443.
Valente, E. M., Abou-Sleiman, P. M., Caputo, V., Muqit, M. M., Harvey, K., Gispert, S., . . . Healy, D. G. (2004). Hereditary early-onset Parkinson's disease caused by mutations in PINK1. *Science, 304*(5674), 1158-1160.
Valera, E., & Masliah, E. (2018). The neuropathology of multiple system atrophy and its therapeutic implications. *Autonomic Neuroscience, 211*, 1-6.
Van der Perren, A., Gelders, G., Fenyi, A., Bousset, L., Brito, F., Peelaerts, W., . . . Baekelandt, V. (2020). The structural differences between patient-derived α-synuclein strains dictate characteristics of Parkinson's disease, multiple system atrophy and dementia with Lewy bodies. *Acta neuropathologica, 139*(6), 977-1000.
van Diggelen, F., Frank, S. A., Somavarapu, A. K., Scavenius, C., Apetri, M. M., Nielsen, J., . . . Otzen, D. E. (2020). The interactome of stabilized α-synuclein oligomers and neuronal proteins. *The FEBS journal, 287*(10), 2037-2054.
Vargas, K. J., Makani, S., Davis, T., Westphal, C. H., Castillo, P. E., & Chandra, S. S. (2014). Synucleins regulate the kinetics of synaptic vesicle endocytosis. *Journal of Neuroscience, 34*(28), 9364-9376.
Veenvliet, J. V., Dos Santos, M. T. A., Kouwenhoven, W. M., Von Oerthel, L., Lim, J. L., Van Der Linden, A. J., . . . Smidt, M. P. (2013). Specification of dopaminergic subsets involves interplay of En1 and Pitx3. *Development, 140*(16), 3373-3384.
Vera, E., Bosco, N., & Studer, L. (2016). Generating late-onset human iPSC-based disease models by inducing neuronal age-related phenotypes through telomerase manipulation. *Cell reports, 17*(4), 1184-1192.

Vicente Miranda, H., Chegão, A., Oliveira, M. S., Fernandes Gomes, B., Enguita, F. J., & Outeiro, T. F. (2020). Hsp27 reduces glycation-induced toxicity and aggregation of alpha-synuclein. *The FASEB Journal, 34*(5), 6718-6728.

Vicente Miranda, H., El-Agnaf, O. M., & Outeiro, T. F. (2016). G lycation in P arkinson's disease and Alzheimer's disease. *Movement Disorders, 31*(6), 782-790.

Vicente Miranda, H., Szegő, É. M., Oliveira, L. M., Breda, C., Darendelioglu, E., de Oliveira, R. M., . . . Oliveira, M. (2017). Glycation potentiates α-synuclein-associated neurodegeneration in synucleinopathies. *Brain, 140*(5), 1399-1419.

Vierbuchen, T., Ostermeier, A., Pang, Z. P., Kokubu, Y., Südhof, T. C., & Wernig, M. (2010). Direct conversion of fibroblasts to functional neurons by defined factors. *Nature, 463*(7284), 1035-1041.

Vilchez, D., Saez, I., & Dillin, A. (2014). The role of protein clearance mechanisms in organismal ageing and age-related diseases. *Nature Communications, 5*(1), 1-13.

Villar-Menéndez, I., Porta, S., Buira, S. P., Pereira-Veiga, T., Díaz-Sánchez, S., Albasanz, J. L., . . . Barrachina, M. (2014). Increased striatal adenosine A2A receptor levels is an early event in Parkinson's disease-related pathology and it is potentially regulated by miR-34b. *Neurobiology of disease, 69*, 206-214.

Volpicelli-Daley, L. A., Gamble, K. L., Schultheiss, C. E., Riddle, D. M., West, A. B., & Lee, V. M.-Y. (2014). Formation of α-synuclein Lewy neurite–like aggregates in axons impedes the transport of distinct endosomes. *Molecular biology of the cell, 25*(25), 4010-4023.

Volpicelli-Daley, L. A., Luk, K. C., & Lee, V. M. (2014). Addition of exogenous α-synuclein preformed fibrils to primary neuronal cultures to seed recruitment of endogenous α-synuclein to Lewy body and Lewy neurite–like aggregates. *Nature protocols, 9*(9), 2135.

Volpicelli-Daley, L. A., Luk, K. C., Patel, T. P., Tanik, S. A., Riddle, D. M., Stieber, A., . . . Lee, V. M.-Y. (2011). Exogenous α-synuclein fibrils induce Lewy body pathology leading to synaptic dysfunction and neuron death. *Neuron, 72*(1), 57-71.

Voronkov, D., Salkov, V., Anufriev, P., & Khudoerkov, R. (2018). Lewy bodies in Parkinson's disease: histological, immunohistochemical, and interferometric examinations. *Arkhiv patologii, 80*(4), 9-13.

Wakabayashi, K., Tanji, K., Odagiri, S., Miki, Y., Mori, F., & Takahashi, H. (2013). The Lewy body in Parkinson's disease and related neurodegenerative disorders. *Molecular neurobiology, 47*(2), 495-508.

Walker, L. C., & Jucker, M. (2015). Neurodegenerative diseases: expanding the prion concept. *Annual review of neuroscience, 38*, 87-103.

Wang, L., Das, U., Scott, D. A., Tang, Y., McLean, P. J., & Roy, S. (2014). α-synuclein multimers cluster synaptic vesicles and attenuate recycling. *Current Biology, 24*(19), 2319-2326.

Wang, X., Park, J., Susztak, K., Zhang, N. R., & Li, M. (2019). Bulk tissue cell type deconvolution with multi-subject single-cell expression reference. *Nat Commun., 10*(1), 1-9.

Wang, Y., Shi, M., Chung, K. A., Zabetian, C. P., Leverenz, J. B., Berg, D., . . . Siderowf, A. D. (2012). Phosphorylated α-synuclein in Parkinson's disease. *Science translational medicine, 4*(121), 121ra120-121ra120.

Welch, J. D., Kozareva, V., Ferreira, A., Vanderburg, C., Martin, C., & Macosko, E. Z. (2019). Single-cell multi-omic integration compares and contrasts features of brain cell identity. *Cell, 177*(7), 1873-1887. e1817.

Wenning, G. K., Colosimo, C., Geser, F., & Poewe, W. (2004). Multiple system atrophy. *The Lancet Neurology, 3*(2), 93-103.

Williams, T., Sorrentino, Z., Weinrich, M., Giasson, B. I., & Chakrabarty, P. (2020). Differential cross-seeding properties of tau and α-synuclein in mouse models of tauopathy and synucleinopathy. *Brain communications, 2*(2), fcaa090.

Wilson, M. A., Collins, J. L., Hod, Y., Ringe, D., & Petsko, G. A. (2003). The 1.1-Å resolution crystal structure of DJ-1, the protein mutated in autosomal recessive early onset Parkinson's disease. *Proceedings of the National Academy of Sciences, 100*(16), 9256-9261.

Woerman, A. L. (2021). Strain diversity in neurodegenerative disease: an argument for a personalized medicine approach to diagnosis and treatment. In: Springer.

Wong, Y. C., & Krainc, D. (2017). α-synuclein toxicity in neurodegeneration: mechanism and therapeutic strategies. *Nature medicine, 23*(2), 1-13.

Wu, X., & Monnier, V. M. (2003). Enzymatic deglycation of proteins. *Archives of biochemistry and biophysics, 419*(1), 16-24.

Xi, J., Liu, Y., Liu, H., Chen, H., Emborg, M. E., & Zhang, S. C. (2012). Specification of midbrain dopamine neurons from primate pluripotent stem cells. *Stem cells, 30*(8), 1655-1663.

Xie, B., Lin, F., Peng, L., Ullah, K., Wu, H., Qing, H., & Deng, Y. (2014). Methylglyoxal increases dopamine level and leads to oxidative stress in SH-SY5Y cells. *Acta Biochim Biophys Sin, 46*(11), 950-956.

Xu, C.-Y., Kang, W.-Y., Chen, Y.-M., Jiang, T.-F., Zhang, J., Zhang, L.-N., . . . Chen, S.-D. (2017). DJ-1 inhibits α-synuclein aggregation by regulating chaperone-mediated autophagy. *Frontiers in aging neuroscience, 9*, 308.

Xu, X., Zhuang, C., Wu, Z., Qiu, H., Feng, H., & Wu, J. (2018). LincRNA-p21 Inhibits Cell Viability and Promotes Cell Apoptosis in Parkinson's Disease through Activating-Synuclein Expression. *BioMed research international, 2018*.

Yamanaka, S. (2012). Induced pluripotent stem cells: past, present, and future. *Cell stem cell, 10*(6), 678-684.

Yin, G., Da Fonseca, T. L., Eisbach, S. E., Anduaga, A. M., Breda, C., Orcellet, M. L., . . . Braus, G. H. (2014). α-Synuclein interacts with the switch region of Rab8a in a Ser129 phosphorylation-dependent manner. *Neurobiology of disease, 70*, 149-161.

Yoshino, H., Hirano, M., Stoessl, A. J., Imamichi, Y., Ikeda, A., Li, Y., . . . Sossi, V. (2017). Homozygous alpha-synuclein p. A53V in familial Parkinson's disease. *Neurobiology of aging, 57*, 248. e247-248. e212.

Zambon, F., Cherubini, M., Fernandes, H. J., Lang, C., Ryan, B. J., Volpato, V., . . . Booth, H. D. (2019). Cellular α-synuclein pathology is associated

with bioenergetic dysfunction in Parkinson's iPSC-derived dopamine neurons. *Human molecular genetics, 28*(12), 2001-2013.

Zanzoni, A., Marchese, D., Agostini, F., Bolognesi, B., Cirillo, D., Botta-Orfila, M., . . . Tartaglia, G. G. (2013). Principles of self-organization in biological pathways: a hypothesis on the autogenous association of alpha-synuclein. *Nucleic acids research, 41*(22), 9987-9998.

Zarbiv, Y., Simhi-Haham, D., Israeli, E., Elhadi, S. A., Grigoletto, J., & Sharon, R. (2014). Lysine residues at the first and second KTKEGV repeats mediate α-Synuclein binding to membrane phospholipids. *Neurobiology of disease, 70*, 90-98.

Zarranz, J. J., Alegre, J., Gómez-Esteban, J. C., Lezcano, E., Ros, R., Ampuero, I., . . . Atarés, B. (2004). The new mutation, E46K, of α-synuclein causes parkinson and Lewy body dementia. *Annals of Neurology: Official Journal of the American Neurological Association and the Child Neurology Society, 55*(2), 164-173.

Zecca, L., Zucca, F., Albertini, A., Rizzio, E., & Fariello, R. (2006). A proposed dual role of neuromelanin in the pathogenesis of Parkinson's disease. *Neurology, 67*(7 suppl 2), S8-S11.

Zhang, L., Shimoji, M., Thomas, B., Moore, D. J., Yu, S.-W., Marupudi, N. I., . . . Dawson, T. M. (2005). Mitochondrial localization of the Parkinson's disease related protein DJ-1: implications for pathogenesis. *Human molecular genetics, 14*(14), 2063-2073.

Zheng, H., Xie, Z., Zhang, X., Mao, J., Wang, M., Wei, S., . . . Chen, H. (2021). Investigation of α-Synuclein Species in Plasma Exosomes and the Oligomeric and Phosphorylated α-Synuclein as Potential Peripheral Biomarker of Parkinson's Disease. *Neuroscience, 469*, 79-90.

Zhou, J., & Troyanskaya, O. G. (2015). Predicting effects of noncoding variants with deep learning–based sequence model. *Nature Methods, 12*(10), 931-934. doi:10.1038/nmeth.3547

Zhou, W., Bercury, K., Cummiskey, J., Luong, N., Lebin, J., & Freed, C. R. (2011). Phenylbutyrate up-regulates the DJ-1 protein and protects neurons in cell culture and in animal models of Parkinson disease. *Journal of Biological Chemistry, 286*(17), 14941-14951.

Zhou, W., Zhu, M., Wilson, M. A., Petsko, G. A., & Fink, A. L. (2006). The oxidation state of DJ-1 regulates its chaperone activity toward α-synuclein. *J Mol Biol. , 356*(4), 1036-1048.

Zimprich, A., Biskup, S., Leitner, P., Lichtner, P., Farrer, M., Lincoln, S., . . . Calne, D. B. (2004). Mutations in LRRK2 cause autosomal-dominant parkinsonism with pleomorphic pathology. *Neuron, 44*(4), 601-607.

Zondler, L., Miller-Fleming, L., Repici, M., Gonçalves, S., Tenreiro, S., Rosado-Ramos, R., . . . Giorgini, F. (2014). DJ-1 interactions with α-synuclein attenuate aggregation and cellular toxicity in models of Parkinson's disease. *Cell Death Dis, 5*(7), e1350-e1350.

Zucchi, E., Bonetto, V., Sorarù, G., Martinelli, I., Parchi, P., Liguori, R., & Mandrioli, J. (2020). Neurofilaments in motor neuron disorders: towards promising diagnostic and prognostic biomarkers. *Molecular neurodegeneration, 15*(1), 1-20.

Appendix

Identification of α-synuclein interacting partners under seeded aggregation using BioID2 in cells expressing Venus-tagged α-synuclein

Differentially interacting proteins in Figure 5.6, log2(fold change)

Gene names	Difference in PD-ampl.	Difference in MSA-ampl.
EPB41	0.643272996	0.289414048
PFN2	3.840896606	3.126547098
WDR36	2.810817719	3.156301498
VARS	1.105524063	1.202516556
HEATR1	2.726649284	2.26091969
GALK1	1.106449127	1.514983177
NOSIP	2.455008268	1.901697755
HMGCS1	1.417414665	2.114103317
FKBP4	3.646332741	3.833918333
EIF4A3	1.146634102	1.324384689
NCAPH	-0.67538929	-0.654156685
CPNE3	0.758464813	0.711929321
FARSA	-1.181218028	-1.0943048
YWHAE	1.869114876	0.62229538
FAM50A;FAM50B	1.003867507	1.665452242
HIST2H2BE;HIST1H2BB;HIST1H2BO;HIST1H2BJ;HIST3H2BB	7.505384684	-0.71138382
HSPD1	1.474725723	0.393995285
OR4A8	-6.926384211	1.329374313
COPG2	-0.456497073	-0.13563323
ME2	0.913674831	0.773460627
SLC25A11	0.559249878	-0.50276947
TNPO1	-0.7466259	0.05506134
C10orf67	-7.285749078	0.128373265
STRBP	-10.79508877	-0.259345412
PARK7	2.033360481	1.831795692
RANGAP1	0.136676788	-0.713551521
CCDC137	-0.69266355	-1.435488343
DHX36	1.917821646	2.296148062
TMED9	2.756979942	2.085141659
NKRF	2.07482338	2.382732391
SEC23B	-0.322254896	0.347132921
LMNB1	4.033214688	3.990785599
PRPS2	2.420772552	4.481084466
EHBP1	-0.033863783	1.698752165
RUVBL2	-0.299655914	-0.468075752

SNCA	-0.106978416	-0.517354012
LIPI	-0.19816494	-0.310462713
MCM3	0.547562599	-0.919047356
ACOT7	2.808835983	2.308461428
PM20D2	1.979314804	2.247620225
GMPPA	1.597122908	2.888806581
ATP6V1B2	4.109274387	3.585407019
GRB2	2.44355154	1.970720291
RPS21	2.089595556	2.524739742
AGFG1	3.287068367	3.564619064
ACAT1	3.917158246	4.817677975
TMEM33	3.353236675	4.059440136
TXNL1	3.706909657	3.427056551
TRMT1L	1.669378281	1.842890739
GLOD4	2.766477466	3.455559492
KMT2A	-1.380934119	-1.005185843
CMBL	3.03462863	3.206371546
PITPNB	3.595602632	2.887109637
CYB5R3	1.918142319	1.957525253
SAE1	4.363570094	4.345683455
SMN1;SMN2	2.352184892	2.696527243

All identified proteins in Figure 5.6, log2(fold change)

Gene names	Difference in PD-ampl.	Difference in MSA-ampl.
GMPPA	1.597122908	2.888806581
KRT2	9.980243206	10.05701828
KRT9	10.613873	10.69090962
RANGAP1	0.136676788	-0.713551521
KRT10	10.04847789	10.11857128
TUFM	0.209841728	0.414096832
ATP6V1B2	4.109274387	3.585407019
CCDC137	-0.69266355	-1.435488343
GRB2	2.44355154	1.970720291
DHX36	1.917821646	2.296148062
TMED9	2.756979942	2.085141659
KRT1	10.12931442	10.20337868
RPS21	2.089595556	2.524739742
NKRF	2.07482338	2.382732391
AGFG1	3.287068367	3.564619064
ACAT1	3.917158246	4.817677975
TMEM33	3.353236675	4.059440136
SEC23B	-0.322254896	0.347132921
TXNL1	3.706909657	3.427056551
TRMT1L	1.669378281	1.842890739
IQGAP1	2.795648575	1.940313697
LMNB1	4.033214688	3.990785599
PSMD6	2.581789017	2.934288979
GLOD4	2.766477466	3.455559492
PRPS2	2.420772552	4.481084466
EHBP1	-0.033863783	1.698752165
KMT2A	-1.380934119	-1.005185843
NAT10	1.347281456	0.992369652
RUVBL2	-0.299655914	-0.468075752
CMBL	3.03462863	3.206371546
PITPNB	3.595602632	2.887109637
SNCA	-0.106978416	-0.517354012
CYB5R3	1.918142319	1.957525253
SAE1	4.363570094	4.345683455
GAPDH	1.122162819	1.429587364
LIPI	-0.19816494	-0.310462713
MCM3	0.547562599	-0.919047356
ACOT7	2.808835983	2.308461428
SMN1;SMN2	2.352184892	2.696527243
PARK7	2.033360481	1.831795692
PM20D2	1.979314804	2.247620225
ALB	6.201372385	6.268909693
U2AF1;U2AF1L4	-1.608863831	-1.412247658

UAP1	1.826955557	2.450246096
NDUFB10	1.760052562	2.617598891
FXR2	1.234823227	1.775304794
EPB41	0.643272996	0.289414048
PFN2	3.840896606	3.126547098
CLIC1	2.940789223	3.638699532
NUP93	2.45713222	2.675575852
PRMT5	2.511096001	3.934526205
PGD	-1.719100475	-2.943896532
SKP1	1.097567558	3.283602238
DNMT1	2.453749776	3.578507185
SPATA5	0.39849472	1.358858585
PHF5A	0.449169159	0.447807312
CDC37	2.111557961	2.175569415
ECHS1	0.445057869	0.77819252
WDR36	2.810817719	3.156301498
EML4	0.442990303	0.323574066
DNAJA2	1.71370244	1.69505465
EPRS	0.829151154	0.893242836
RPS25	-1.126457214	-1.548325539
YARS	1.633089066	1.46750164
VARS	1.105524063	1.202516556
HEATR1	2.726649284	2.26091969
RBM12	3.266259193	3.122189999
NUP155	0.967940331	1.323727608
PSIP1	2.213477135	4.188570976
GALK1	1.106449127	1.514983177
PKM	0.358952522	0.472802162
ZC3HAV1	0.386092186	1.273730755
CGN	2.614938736	2.937187195
NOSIP	2.455008268	1.901697755
TELO2	0.239339471	0.762123704
LBR	1.127080917	1.417980194
PSMC6	0.909459114	0.84027195
PFDN2	0.915404558	0.847159386
DNM1L	3.261577368	3.146549702
AKR1A1	1.796519279	2.214450836
SLC16A1	2.357099533	3.431468964
SRSF10;SRSF12	1.461330414	1.200220108
FBL	-0.628257751	-0.85210228
GORASP2	2.935192823	2.840948939
RBM39	-2.500534177	-3.345848203
TAF6	-0.695782304	-1.089401841
IPO7	2.841866493	3.513078809
CAST	1.785871506	1.730112076
DIDO1	1.234182954	0.873448968

HSPA5	-1.467003822	-1.516992569
HDGF	0.792392254	1.560540557
EXOSC1	1.916445732	2.6225245
FLG2	2.881960869	2.996969581
HMGCS1	1.417414665	2.114103317
BRIX1	0.491664886	0.700456619
FKBP4	3.646332741	3.833918333
SUZ12	0.738517404	1.671487808
LAS1L	1.648558617	1.258858204
NSF	0.084699392	-1.681429386
EEF1G	1.07854557	0.954433441
CAP1	1.066188812	1.07645607
SART1	1.801310539	2.196611404
AARS2	0.424971104	0.999281406
IGF2R	1.66834867	2.851634502
SPG20	0.278800011	0.592748642
RSRC2	0.939473152	1.267337799
CAND1	-0.728129387	-1.119885445
DLST	2.860777855	2.533707976
LDHB	0.508812904	0.461380005
LARP1	2.68268013	2.950199127
HRNR	3.79110384	4.259739637
SRP72	2.524787903	2.023548126
C1QBP	0.855811119	1.226319313
EIF4A3	1.146634102	1.324384689
HNRNPK	0.348014832	0.52410984
G6PD	2.528013587	3.20499599
XPO5	1.310078621	2.327275276
RBM27	-0.399536133	-1.139469147
DBNL	2.237212181	3.002370834
NCAPH	-0.67538929	-0.654156685
RABGAP1	-0.827671885	-1.331261396
MASTL	0.115626693	1.361479878
NUP88	1.40125668	1.058732033
MAP4	-0.419906616	-1.181946754
H1F0	-0.445508003	-0.963561058
PTPN11	1.847688675	1.884451389
HCFC1	-0.871890068	-0.892925262
PCNA	1.365953445	1.453989983
PRPS1	-0.202568054	0.819852829
APOBEC3C	0.158289909	0.353111267
UBE2O	1.336811423	1.863832235
TPT1	1.697340965	1.55991745
HOXA5	1.123064399	1.710476041
SURF6	1.571371078	0.940803528
BOP1	2.4396106	2.514230609

TCEB3	1.844921589	1.825324178
COASY	1.79656148	0.93077302
MDC1	2.837052822	1.673786759
MYH10	0.71883297	0.935729027
VRK1	-0.258497238	-0.326019287
KIF5B	1.09515667	1.037899971
CUL3	0.886173487	1.202360392
FLNB	2.655123711	2.312744141
SMC4	2.847687244	2.972526073
CPNE3	0.758464813	0.711929321
CCT2	0.716056824	0.769812584
PSMD2	1.360060692	0.80365181
PPP1CB	-1.464173317	-1.48374176
FARSA	-1.181218028	-1.0943048
MYBBP1A	0.575011253	1.098316193
SEC24C	2.446928501	2.474025249
ACAD9	1.310697198	1.044312596
GSK3A	0.869582176	0.539259911
PC	-1.242355347	-0.931074142
SMARCA5	0.918344498	1.17054081
IGF2BP3	0.47761178	1.632385015
CCBL2	0.444696546	1.111884356
DDX23	1.980354786	2.198219776
CHERP	-1.366948605	-2.056076527
ADAR	1.304517746	1.215218544
HIST2H2AC;HIST2H2AA3	1.480020046	1.676436782
RIC8A	1.467451811	2.065517902
KPNB1	0.516993523	0.581695557
CAPN1	2.415673494	1.261071563
RPS15A	0.475955963	0.548828125
SNX2	2.62541914	2.054535627
MCCC1	-0.576706886	-0.608971596
ADPGK	0.496172667	1.050858021
DNAJA1	-3.031582594	-3.681319952
PAICS	1.655931473	1.525794029
THUMPD1	-0.350750208	-1.997826576
RAN	0.192938805	0.097241402
SLC25A3	1.111039162	1.105898857
GEMIN5	1.617980719	1.694801092
RPS16	0.060016632	0.456510544
PFKL	-0.765033722	-1.028411865
PDIA3	2.518016815	2.820836067
PRKAR2A	-1.28467083	-1.904384613
ELAVL1	-0.018483162	0.466366768
PRPF40A	-0.927681923	-0.934277534
SNX9	-0.977554321	-0.615581512

ALDOA	1.813459396	1.142302513
GLO1	-1.223995209	-2.404419899
TNKS1BP1	2.657469749	2.68507576
CKB	1.361135483	1.563891411
YWHAZ	0.863103867	1.270942688
TPD52L2	-1.063521385	-1.280958176
TBL3	1.408033133	1.183004856
POLA1	0.356935024	1.038089514
RPS29	-0.990618706	-0.859319687
KIAA1033	0.004134893	-0.576591492
EMD	1.279818535	1.862001657
SRP68	0.232228279	0.252291679
RABL6	-1.220974922	0.607377529
OSBPL9	0.553392529	1.243674755
ACSL4	-1.100793481	1.164995193
CCAR1	1.280168533	1.158667564
CDK9	0.27710557	1.248374939
OAT	0.772621632	1.385177374
ALDH9A1	2.353764772	2.147916079
BPNT1	-1.312432885	-0.920914412
RPS6	0.925322533	1.186294556
HNRNPR	-1.462446213	-1.626725197
ATP5A1	0.421229362	0.361555099
TTF2	-0.890649676	-0.468182445
YWHAE	1.869114876	0.62229538
SLC4A1AP	1.398123741	1.467438698
ACO2	3.334000468	2.777608037
MAP7D3	-1.399202347	-2.156821251
PES1	-1.293453932	-1.709122419
BMS1	0.666882515	1.172631264
PPM1G	1.178837776	1.437239647
DHX38	1.364330173	1.683508992
NAA15	0.968970299	0.670266151
DCXR	0.933594704	1.116293907
PSMA3	-1.424761176	-1.741624594
SRSF9	0.533661842	0.59962368
TLN1	-0.547334671	-0.959671021
SLC25A5	-4.169885039	-4.263249755
FHL1	-1.31443882	-1.189490318
RPL3	-0.228946686	0.635327339
CBX4	-1.049392819	-0.492042303
HBS1L	2.530710459	3.424697638
LSM12	1.290958643	2.103337765
DDX54	0.672063828	0.230966568
EIF4G3	0.113826752	0.562179565
TENM2	0.172781587	0.644309402

PSMD1	-0.084850311	-1.625753403
RPA1	-1.274924278	-0.847118378
FAM50A;FAM50B	1.003867507	1.665452242
RNH1	1.672208786	1.684491158
MYH9	-0.810598373	-0.70983696
SF3B2	0.328041077	0.893930435
RAD21	-0.560375571	-0.839121461
PNO1	0.405407071	0.55653429
NANS	2.508899331	2.396588683
DDX24	0.600924969	1.440962315
SEC31A	0.794997692	1.536162615
ABCE1	-0.65476799	-0.608627319
GTF3C4	0.477494478	-0.727432132
UTP18	1.399721861	1.542146444
HUWE1	1.338694572	1.331867218
FXR1	-0.769339561	-0.712021828
TUBG1;TUBG2	0.910477757	2.063043594
ACACA	2.202507257	2.251067638
HIST2H2BE;HIST1H2BB;HIST1H2BO;HIST1H2BJ;HIST3H2BB	7.505384684	-0.71138382
HSPD1	1.474725723	0.393995285
PHGDH	0.411496162	0.56733799
TFDP2	2.949682713	4.949050903
ARIH2	0.676236272	1.875934958
HDLBP	-0.531149864	-0.786917686
EIF4G2	-1.212827682	-1.465522766
DHX29	-1.423578501	-1.181419611
ERH	-0.509243011	-0.671346664
RPS27L	0.517983079	1.764530301
GTF3C1	0.229498982	0.808213472
ACP1	-0.89387989	-1.799945831
WDHD1	1.063720703	1.707408905
RPL10A	0.488730431	0.731018066
CLIC4	1.540769577	1.401325226
AGPS	1.291288376	1.705875874
PSMC3	1.224541664	0.879487038
TIMM50	0.412261009	0.475205421
ARFGAP1	-1.840052605	-1.584785461
PSMD3	0.482933998	1.026186943
CTTN	0.089339256	-0.355806351
CKAP2	-2.20977354	-2.783427715
TAF15;FUS	-1.356526375	-1.441667557
PPP2R1A	1.951315284	2.757411242
ERP44	0.702632666	1.126988649
DDX46	0.667127609	2.000900269
CCAR2	1.311776161	0.807777405
ZRANB2	1.832350731	1.658670425

TTK	0.938696384	1.31215477
OR4A8	-6.926384211	1.329374313
PIH1D1	0.697548032	0.766228199
AP1M1	1.753017306	1.766901016
TRMT1	1.017025948	1.698506355
PREP	1.726622224	1.471340656
PDCD6IP	3.094527721	3.335621357
AP3D1	0.242555618	0.797436714
TRAP1	-0.1690588	0.74157238
HNRNPAB	-0.835124969	-0.821491241
TARDBP	2.481881618	3.151712894
EEF1D	0.321700096	-0.391691208
HN1	-2.550153494	-2.909855604
CLCC1	0.570287704	0.723208427
SF3A1	-0.583857536	-0.385890007
U2AF2	-1.797649384	-1.857539177
SMC3	-0.49023819	-0.35721302
PDIA6	-3.897310972	-3.652941465
PPAT	2.207494974	2.356055379
ATP6V1H	0.472351313	0.457976222
VDAC1	-0.070784569	1.140618324
LARP7	-2.263465166	-2.261130571
HSP90AB1	1.037920952	1.136594772
FERMT2	0.588551283	0.804807425
SERBP1	-0.621717453	-0.864985466
RPS12	-3.406226397	-3.324044466
EIF2A	-0.68234849	-0.797476053
TMPO	3.268427134	3.264351845
RPL36	1.464741707	1.861193657
UBE2M	-0.011068344	-0.762335777
CEBPZ	2.214625597	1.672026396
RPL6	-0.161125183	0.223694801
ZC3H18	1.325397491	1.9344244
EIF5B	-0.143032074	0.148314476
PCMT1	-3.41526854	-3.498092294
RPS3A	-0.535032272	-0.385903358
TPI1	1.154825211	0.804134369
RPL18	1.08521843	0.999879837
RPS2	-0.030013084	-0.352719307
PITRM1	-0.008905292	0.901128411
CUL1	0.908629775	1.32348001
GART	0.61794281	0.730314255
POLR2H	-0.12034893	0.604693413
TFRC	1.651649475	0.686900854
EIF3E	1.827365756	1.43606174
GSTP1	3.105858088	3.490754843

LIMD1	-1.334204435	-1.414632559
ANXA5	1.056272507	0.875997543
RFC1	2.295075893	1.275123239
MTDH	-1.940850258	-1.916298866
CPNE1	0.983808398	2.245738864
G3BP1	-1.234980583	-1.53473568
HSPH1	-0.115063667	-0.430625916
SRP54	-1.352344275	-1.740525007
HDAC2	-2.265652299	-2.426869988
PFKM	1.185638189	1.063748717
ZNF207	-0.027863026	-2.20892632
EHMT1	-0.328892827	0.803406954
P4HB	-1.205873489	-1.74455452
CKAP5	-0.972923279	-1.465088844
SEC22B	1.258949757	0.576725006
RPS11	0.914060593	1.092795372
SRP9	-2.75974369	-2.833714485
CNN2	2.070780754	2.065485001
HSPA9	0.277778625	0.365297318
LUC7L3	-1.971024513	-2.333342552
PPIL1	2.231173992	1.466294289
DYNC1LI2	-0.980120897	-1.631387711
INTS1	-0.101006746	0.929692745
DDX42	-1.37381494	-1.55227375
RPS27A	-4.575513363	-5.56400919
PCNP	0.127990723	-0.7240448
COPG2	-0.456497073	-0.13563323
CALD1	-1.529195786	-1.368341446
RPL24	-0.349704742	-0.086456299
KPNA1	-1.514042616	-1.576506376
NUP214	-2.017923236	-1.882294536
CD2AP	-0.780061722	-1.382128716
CAPZB	-1.901301384	-1.619708061
DHCR7	2.890417099	3.150761962
ME2	0.913674831	0.773460627
PFAS	-2.597154617	-2.737872124
KPNA2	0.203512192	2.259139776
RPL36A;RPL36A-HNRNPH2;RPL36AL	-5.1126647	-4.855634212
RTCB	2.151467562	1.788340449
PUM1	1.116198182	0.389747143
NEDD1	1.839064598	1.215474129
MCM5	-0.842903137	-0.775914192
SRSF1	0.684675217	0.667899132
UQCRC1	0.047671318	0.253824234
EIF3C;EIF3CL	0.515287399	0.939985275
DNTTIP2	-0.41559577	1.301635027

ADRM1	0.746537209	0.612225533
STT3A	-1.589224815	-0.984592438
HNRNPH2	0.318256974	1.09092176
KRT6B;KRT6C;KRT6A	1.043993473	1.93390727
SND1	0.588298798	2.286086082
GSTM3	0.770906925	1.800678253
UBR4	0.598391533	1.352269173
LDHA	0.720226288	0.796412468
RPL39P5;RPL39	2.33166647	3.091606855
PGM1	0.81765461	1.179191589
YWHAH	2.497460365	1.727751017
CCT5	0.310130119	0.387259483
PHB	-1.564451218	-1.715192795
NHP2L1	0.508194923	0.687028885
GSTO1	-0.772994041	-0.850818634
RPL32	-0.765207291	-0.637616158
IGF2BP2	0.988620758	1.462637901
CCT6A	0.944090843	1.022137642
MATR3	-1.313316345	-0.911278725
CAD	0.184307098	0.197910309
RUVBL1	0.250992775	1.083924294
HNRNPDL	-3.97676146	-3.124597073
TXN	-1.995990753	-1.935655594
HNRNPUL2-BSCL2;HNRNPUL2	-0.925066471	-1.128442287
TRIM25	1.085090637	1.184503794
BOD1L1	1.541222572	1.779126167
EEF1B2	-1.985892296	-1.783410072
RPL15	-0.415676117	-0.268943787
DCAF7	-1.209594965	-1.338579416
MYO1D	0.682620883	1.02818954
PSMC5	0.940054893	0.732897758
ADD1	-2.25346756	-1.922597885
MAP7	1.013725519	1.880920172
RPS17	-2.828152657	-2.898797989
USP7	-2.469292879	-2.324498415
PRPSAP2	0.257872939	1.950572968
ACAT2	-2.112485886	-1.818947792
RPL22	0.077478409	0.348978043
RPL8	0.756375313	0.964317322
NUP205	-0.784804344	-0.467897415
EDC3	0.929569483	0.685569406
FLNA	-0.03561306	-0.095718384
RIF1	-1.122836113	-0.668593407
SNRPD3	-0.285709381	-0.920062065
NDUFAF3	0.214441538	0.306477308
MRPS35	1.618189573	1.036606073

PGK1	-0.434293747	-0.493330956
CCT8	0.407674789	0.421477318
ILKAP;ILKAP3	-0.847632408	-0.707145691
ZC3HAV1L	1.65355444	1.40187335
RSL1D1	-1.152830124	-0.948503494
LIMA1	-1.230766773	-1.662246227
NSUN2	0.615546227	0.758283615
RECQL	1.235169411	1.077598572
LASP1	-1.145118833	-1.155709386
SRRM1	2.234673262	1.962254405
PRPF6	1.413450241	1.715250969
SRCAP	-0.700834155	-0.683929443
RAVER1	-1.707911491	-1.307026863
XRCC5	-0.878838539	-0.598098755
DYNC1I2	1.537707567	1.531245232
RPL29	0.033399582	0.339587212
PYCR2	3.648670197	2.013066411
KARS	1.195504189	0.990279198
PFKP	0.579833031	1.118141174
AIF1L	-0.297632694	-1.855053663
ARCN1	-0.374646187	-0.82185936
PTPN1	0.744453073	1.255783558
TACC3	-0.031916499	0.14215827
HBA2;HBA1	0.293610811	1.175561428
AHCTF1	0.910710096	1.284286261
HSPA8	-4.316401601	-4.12112689
HNRNPH1	-3.977624893	-3.696454048
PTGES3	-3.553248405	-3.380717278
EIF3D	2.270807028	2.271130443
MRTO4	-0.828289986	-0.948658943
XRCC6	-1.026586533	-1.117200851
EDF1	-2.514902115	-3.343805313
RPL26;RPL26L1	0.639995575	0.778770447
CBR1	-0.349200249	-0.261868477
DKC1	2.69964695	2.608049631
DENR	0.478385925	1.543639183
TXLNA	1.893638968	1.523003459
NOP58	-0.66809082	-0.427099228
FARSB	-2.694487095	-1.871817112
ARGLU1	-0.222125053	0.469650269
PPIL4	-0.824165344	-1.526453018
SON	-1.031462669	-1.171823502
EIF2S1	-0.122861862	0.36066246
RPL14	-0.112452507	-0.339898109
UBAP2L	-0.737131119	-0.748685837
PUF60	1.898585081	1.538353205

H1FX	-1.193277359	-0.961253166
NAA10;NAA11	-2.20169878	-1.955543041
TUBA1A;TUBA3C;TUBA3E	0.556254029	1.470364809
SUPT5H	0.645420313	1.80734086
LYAR	-0.760737419	-0.454193115
CNOT1	0.230894089	0.444869995
DPYSL2	0.958875537	1.055338025
RPS27	-3.011140108	-3.020714998
NPM1	-1.385420799	-1.340805054
CALR	0.089835167	-0.893074036
RPSA	1.091853142	0.844622612
SUCLG2	-1.369374275	-0.391902924
PPP1R2;PPP1R2P3	-1.289807916	-1.538734078
ILF2	-0.943887711	-0.622720718
SUGT1	-1.442507744	-1.342959404
DDX3X;DDX3Y	-0.765954018	-0.542088509
SH3GL1;SH3GL2	-1.997196436	-2.041812181
ABCF2	-2.357765913	-1.927653074
CLUH	0.263916731	0.452181697
SART3	-2.022798419	-1.285952449
HADH	-0.852419019	-1.131721616
FLII	1.478880405	1.074575186
CBX5	1.110283852	2.495236635
SRSF11	0.683619499	0.952084541
DDX1	0.399312973	0.668901443
EIF5A;EIF5AL1;EIF5A2	-0.397330284	-0.467817307
RPL21	0.735630035	0.850852013
LRPPRC	-0.033069611	0.298602104
MAT2A	0.61557889	1.146797895
PRPF19	1.911635637	1.433694601
C11orf58;SMAP	-0.177665234	1.042793751
SPTAN1	-1.6381464	-1.755739212
RPL27A	-0.669160843	-0.601783752
SNRPC	-0.810978889	-1.364371657
YWHAQ	0.616634369	0.64328289
PRRC2C	-0.556721687	-0.703888893
SET;SETSIP	-1.93589735	-1.651239872
EPPK1	-1.848172903	-1.867468596
POLR2A	-2.51749897	-0.493884087
RANBP2	0.148919106	0.682010651
CAMSAP3	0.483803272	-0.388052106
GAPVD1	1.272316933	1.888297558
SUPV3L1	-0.778418064	0.833091497
PRRC2A	-0.316926956	-0.912716866
BOLA2B;BOLA2	-2.993219137	-2.640749693
GIGYF2	0.893080711	0.580283165

PSPC1	-1.399777412	-1.095432281
FAU	-0.771868706	-0.55784893
PRPF31	0.834410429	0.427587748
TJP2	-0.993011475	-1.101616859
AKAP12	1.114294052	0.341194153
CSDE1	-0.582304955	-0.532018661
UBA2	-0.699083328	-0.658833504
AAAS	0.481447816	1.093306422
ENO1	0.419387817	0.393750191
ETF1	0.342139244	0.201476097
PRDX6	-0.737960815	-0.999835014
MEPCE	0.106324196	0.409550667
GMPS	-0.145167351	0.111493111
HSP90AA1	-0.96848011	-0.864693642
GPHN	0.975974679	1.233827829
RRP1B	0.26705265	0.422678947
NUFIP2	-0.277741432	-1.290599823
SNRPD2	1.711996794	2.181434155
PGM2	0.535158038	-0.849915504
ALDH18A1	-0.127346992	0.773838997
HNRNPD	0.598823547	0.556824684
DYNC1H1	0.049066544	0.268816948
CCDC59	-0.373706937	-0.695576787
AKAP1	0.226246834	0.943778992
HNRNPH3	0.512162209	0.713496208
PSMD12	0.58823967	0.617952347
MTA2	-1.30603981	-1.404782295
WDR5	0.404891253	0.826810598
G3BP2	-0.737821579	-1.052882195
SNW1	-1.828662157	-1.617976427
DHX15	-0.711247444	-0.584805489
LSM14A	-1.481998205	-1.532891035
NASP	0.675787926	0.414937019
EIF2S2	-0.801245689	-0.68915081
EBNA1BP2	0.498053551	0.878456116
SF3B3	1.857049465	1.443588018
GCN1L1	0.218725204	0.375833511
UHRF1	1.293912888	1.684092999
CFL1	-0.539691925	-0.375800133
EIF3F	-1.711844325	-1.488992572
RPS3	-0.810525894	-0.649285316
CCDC85C	-0.79441452	-1.464071989
RRP12	-1.45481348	-1.032729626
SMC1A	1.148327827	1.221384048
ATXN2	-0.72700882	-1.381567955
RPRD1B	0.417704463	0.908601046

PPP2R2A	-2.321990013	-1.511984825
GAR1	-0.580672026	-1.144078016
FASN	0.045613289	0.19608593
CHTOP	-0.674391985	-1.692597628
APEX1	0.878166199	0.52261734
WDR3	-1.868373036	-0.571508527
TBC1D15	-0.779046774	-0.790973425
TRIM28	-0.54874897	-0.351454735
MLLT4	-1.067119598	-1.643062592
VDAC3	0.661867142	0.512327194
GNL1	0.879757166	0.762878776
OLA1	-0.564557076	-0.457756996
BAZ1B	1.443022728	1.421808243
U2SURP	-1.670130253	-1.450406551
TES	0.159281731	0.365599632
MKI67	-1.229917526	-1.111901283
RIOK2	2.429193139	0.598368049
VIM	0.084258556	0.15986681
TOP1	0.374564171	0.633141518
MRPL14	0.521086574	0.559401155
ABCF3	-0.822989702	-0.488745928
HNRNPA3	-0.159011841	-0.120099068
YWHAB	0.472553253	0.548442841
SLK	0.500782967	0.80059433
RAB6B;RAB6A;RAB39A	-1.236917496	-1.275985718
RPL27	-0.913954735	-0.32638073
CSE1L	0.220099449	0.240466118
PPIB	-0.975834846	-1.02573967
EXOSC9	-1.44506979	-1.084536076
PABPN1	-1.214112878	-0.519035578
PAK2	-1.408617258	-1.358813524
SLC25A11	0.559249878	-0.50276947
PSMD10	0.91255188	0.869654655
YY1	0.282514572	-0.577342153
RPS20	1.147752762	1.096585274
CLTC	-0.432587624	-0.328487396
SF1	-0.745132446	-0.479245186
SMU1	1.178418398	-1.025737643
ARPC2	0.216956139	0.373649597
SYNCRIP	1.461328506	0.452886581
SRSF3	1.400031328	1.816394329
PYGL	-1.330833197	-1.169835806
EIF3B	1.383239985	1.835911512
RAI14	0.506979585	-0.352960467
EIF2S3;EIF2S3L	0.519697189	0.401257515
ILF3	-0.136105537	0.104600906

ACBD3	-0.179063678	1.035143852
AK1	1.815679908	1.586452603
PRSS3	1.565314293	1.238254905
CAPZA1	-0.821806908	-0.619987488
LPP	1.879292727	0.959743857
ZC3H11A	-0.997483253	-0.608469963
DDX6	-1.024296761	-1.058531761
STRAP	1.440024376	-0.419424057
NONO	-0.503530502	-0.53747654
CDV3	0.40046978	0.516736984
GNB2L1	-0.2498703	-0.384810448
PLAA	0.560915709	1.41557169
VAPB	-0.483794212	-0.315054893
EPB41L3	-1.106648445	-0.861029625
MSH2	1.37318325	1.546492338
NEDD8;NEDD8-MDP1	-1.742344737	-1.780316234
RIOK1	1.434906721	1.144885778
EPS15L1	1.845634937	1.361237407
RBM34	0.967017412	1.03755784
RPL23A	0.143823624	0.376342773
DARS	1.058589935	0.422484398
PDS5A	0.842121124	0.88083744
AHCY	0.219445229	-0.443482399
CAPN2	0.965554357	1.176035762
DDX18	-0.299901009	-0.581232071
CIAPIN1	0.506037354	0.521977425
CHORDC1	-0.291359901	-0.316175461
UBA1	0.090370178	0.136015892
IARS	-0.356638908	-0.507147789
STMN2	0.642282486	0.619656563
TTLL12	0.037144661	0.364147186
HAUS6	-2.567549467	-1.120597601
DSTN	0.445887566	-0.426261902
HERC1	0.24010694	0.339324713
PTMA	-0.290019989	-0.267170906
XPOT	-1.883996964	-1.11349678
CACYBP	-0.459733009	-0.454958916
C11orf98	0.474268913	0.660376549
GANAB	1.407437325	0.9346838
WARS	-0.358844638	-0.657833934
ACTR3	0.735376358	0.793375969
FTSJ3	-1.551509857	-1.000170708
HSD17B4	0.370725632	0.279017448
RANBP3	0.491974115	1.21551013
WDR77	1.017757416	0.724319339
NELFA	0.8135252	0.754199982

TRAFD1	0.383687496	0.137986183
MCM7	-0.13436985	0.168434143
VCP	-0.549823761	-0.658349991
DDX39A	-1.934541941	-1.885688066
HN1L	-0.38739109	-0.589664459
RPL28	-0.64048481	-0.546244621
SF3B1	0.614254951	0.372021675
ENSA	0.723355055	0.769762993
RPL7A	0.171218872	0.240986824
PA2G4	0.492506027	0.346430779
DDX20	-1.064992905	-0.961811066
NARS	-1.034821153	-1.121338487
CBS	-1.09616518	-1.197276592
LUZP1	1.122592449	1.327731848
KPNA4	0.31456852	0.739943504
RANBP1	-0.568147659	-0.591629028
COPB2	-1.574323893	-1.510779619
RPL17;RPL17-C18orf32	0.107186317	0.133375168
NEMF	-0.410363078	0.749196649
EPB41L2	-0.857107162	-1.184635162
ZNF598	-0.773450613	-1.105879545
TK1	-0.970770359	-0.628283024
JUN	-0.62422061	-0.651076317
LEMD3	0.030586958	0.898086309
UQCRC2	0.342956543	0.658977747
SQSTM1	2.804838896	0.906030416
KRI1	0.94327426	1.209541082
CXorf56	0.373405933	1.211099625
CUL4B	0.948092461	1.061090231
PABPC4	0.328929901	0.432652473
BUB3	0.145088196	0.310713768
SRPRB	0.906019211	0.953536391
HSD17B10	-0.083902359	-0.266365051
VAPA	-0.300990105	-0.309062004
MDH1	1.698950887	0.791165471
HSP90B1	0.208580017	0.170660019
YTHDF2	-0.983159065	-0.799339294
CNN3	-0.665349007	-0.630177498
RPS9	-0.534487724	-0.338666916
GDI1	0.073943377	1.316052675
40057	-1.657772779	-1.548224211
SREK1IP1	0.587310314	0.396336555
RCC2	0.459275246	0.475831985
UBAP2	0.844704628	0.852399826
AARS	2.090009689	0.857813239
RRBP1	-0.689051151	-0.629331112

CCT7	-0.162538528	-0.133267403
RAP1B;RAP1A	1.817354202	0.79106009
RAB7A	0.934751511	0.721494675
RBM10	-0.695284605	-0.834534407
THOC2	-1.236825943	-1.109875679
HAT1	0.385379791	0.472349167
THRAP3	0.29312706	0.403845787
H2AFY2	0.184053421	0.511796951
TP53	0.466082573	0.361732483
HMGB1;HMGB1P1	0.447188377	-0.12769413
NCAPD2	0.282214165	0.683628082
NSFL1C	0.849359274	1.292749166
NCAPG	-0.259711146	-0.73993516
RPL35	-0.05421257	0.24153614
MYO6	0.463005066	0.23075676
ZNF638	0.97152257	0.982311487
MCM2	-0.024435043	0.751522064
RBM17	0.464788437	0.318241119
TPP2	1.751652002	0.2957201
PFN1	0.07882309	-0.135019302
RBM25	-0.727918625	-0.452147484
PCID2	0.07745719	-1.108463526
EIF4E	-1.371428728	-1.252827406
CNBP	-1.057488441	-0.68838501
USO1	-0.090044618	0.824896574
SFXN1	-1.070736408	-0.921712399
KNOP1	1.250137329	0.683655739
TARS	0.051474571	0.376442909
MRPS27	-0.563881993	-0.381920099
TTC37	0.753616571	0.600238323
SNRPF	0.668016434	0.652809143
ETFB	1.009344101	0.464664817
ATP5F1	0.173240423	-0.209622383
BICD2	0.132975578	-0.173357964
HSPA1B;HSPA1A	-0.018037796	0.161330223
DDX21	-0.583173752	-0.208030701
CEP170	-0.118263721	-0.818268299
MOV10	0.096723557	0.381671906
GSPT1;GSPT2	-0.693268776	-0.319499016
EIF4B	-0.734560966	-1.024724007
EZR	0.773796082	0.420295715
RPLP0;RPLP0P6	-0.088820457	-0.153635025
HTATSF1	-0.458355904	-0.518911362
GLUD2;GLUD1	-0.928745508	-1.040657282
NAE1	-0.53662765	0.396301389
DDX5	-0.402400017	-0.242068291

PGM3	0.442746639	1.02674818
SSB	-0.228100777	-0.296728134
TPR	0.034620285	-0.564423561
PTPN23	0.627738714	0.304309607
UBA6	-0.311118126	-0.120796204
CORO1C	-0.712652206	-0.498441696
RBBP6	-1.028608561	-0.340925217
CCT3	-0.126460075	-0.070835114
PAFAH1B1	0.594658136	0.801783204
SYAP1	0.277008057	0.408494949
SEC61B	0.947980642	0.251987457
CC2D1A	-1.023664236	-0.880622625
TOX4	-0.640286922	-0.78641367
MTA1	-0.40460968	-0.125762939
IKBKAP	-0.793191075	-0.590581536
SNRNP40	-1.312302828	-1.059960604
CCDC50	0.855343103	0.467557907
PEBP1	-0.626058578	-0.760704041
STUB1	-0.090460777	-0.21450901
SFPQ	-0.284085274	-0.149778366
SEPT11;SEPT6	-0.915265083	-0.822692871
COPB1	-0.592835426	-0.621395111
TCP1	-0.196578026	0.12478447
PDLIM5	0.019489765	-0.420008659
LRRC47	-0.158529162	-0.421349049
AIMP2	0.75951314	0.749474287
RCL1	-0.352368474	-0.813536882
RPL30	0.083418846	0.358553886
TCOF1	-0.235853195	-0.182056427
STIM1	1.155804396	0.804651976
USP9X	-1.429568052	-0.780495405
ACIN1	-0.688968658	-0.445890427
RFC3	0.863638639	0.464829087
SMG7	-0.973428845	-0.241971374
KIAA0196	-0.357970715	0.54875195
AASDHPPT	0.137005806	0.27200222
MYL6	0.179455996	-0.674064517
GTPBP4	-0.804363251	-0.696998596
FEN1	1.271766424	-0.411463737
RPAP3	1.189030409	1.008123159
RPN1	-0.293067932	-0.327768326
SRPK1	-2.067808867	-0.983865499
HNRNPM	0.208952904	0.319542885
RPL9	-0.606101036	-0.374504089
GTF2F2	0.354198337	-0.454048038
RRAS2	-0.117521048	-0.282058835

CNP	-0.282835007	-0.323130608
RPL18A	-0.134804726	-0.196279526
HIST1H4A	-0.085315704	-0.241659164
LUC7L	-0.156703949	0.195555687
ZFC3H1	0.761561513	0.177880406
MMTAG2	-0.723136902	-0.544240952
EFTUD2	0.349862099	-0.193020821
PDAP1	-1.596302867	-0.91180563
IPO8	0.652910233	0.555488586
PPIA	0.230212212	0.216874123
PRPF8	-0.224832535	-0.2990942
BLM	-0.344606042	0.244578123
GNL3	-0.738875389	-0.349336624
C19orf43	0.055102348	0.183855057
HSPA6;HSPA7	0.038607597	0.295056343
AHNAK	1.464429855	0.337900162
RPL13	0.052881241	0.14263916
PRDX2	0.08852005	0.283926964
PNP	-0.929176331	-0.373301506
NUP98	-0.114293098	0.388489008
LUC7L2	-0.192452431	-0.093004227
IPO5	0.575376511	0.35997963
SRRM2	1.07080555	1.044132233
SKA3	0.589507341	0.537213802
ZFR	-1.195423365	-0.818720102
TXNDC17	-0.694085836	-0.418660879
CANX	0.416281223	-0.280790806
TRIM33	0.032619953	-0.756140113
APRT	0.259670377	1.011944771
SH3D19	-0.557656765	-0.351962566
FANCI	0.337959886	-0.297148943
GTF3C3	-0.623238444	-0.571887851
TBL2	1.110678673	0.49815917
ANXA4	-0.864946127	-0.41681242
WDR18	-0.545881987	0.660172224
TBC1D5	0.036716461	0.126825333
STAT1	0.345932961	-0.273720026
GPKOW	0.442914963	0.281662941
FSCN1	-0.401644707	0.277356148
NOL6	-0.935393333	-0.551557541
POGZ	0.017576456	0.255663157
PRDX1	0.111372948	0.092292786
PNN	-0.320351005	-0.497575164
CHAMP1	-0.244175911	-0.227675438
ACTR1A	0.35445106	0.3224262
HLA-G2.2;HLA-A;HLA-G;HLA-F;HLA-E;HLA-C;HLA-B;HLA-H	0.385757208	0.402061701

ANXA6	-0.2721138	0.234083414
USP39	0.301438332	0.419591069
SSRP1	-0.783768654	-0.278863907
SNRNP200	-0.348566055	0.160819054
DDX39B	-0.12309742	-0.136981964
DNM2	-0.86658144	-0.641756535
KIF11	-1.132477522	-0.507574081
MCM6	-0.08922863	0.168419838
TROVE2	-0.261308193	-0.528753757
IPO9	-0.036540031	-0.12862587
HNRNPL	0.264673233	0.159894943
MCM4	0.38364315	0.112758636
DNAJC7	-1.49394989	-0.43721199
FAM21A;FAM21C	-1.265640259	-0.332904816
LONP1	0.89595592	0.796476483
GTF2I	0.575732231	0.339484215
PSMD11	0.234490395	0.430528164
COIL	-0.087488174	0.284173012
NCBP1	-0.365107536	-0.597343445
PTBP1	-0.451072693	-0.159988403
CTPS1	-0.214835167	0.223656654
LTA4H	-0.066580772	-0.120001793
RPL5	0.089875221	-0.2162323
ABCF1	-0.685627937	-0.327104568
SAMHD1	0.231574059	0.529782772
NOP2	-0.697727203	0.315972328
MARCKS	0.151087284	0.290148854
CA2	-0.31837368	0.122086525
MTHFD1	-0.008900642	0.054129601
GPN1	0.12792778	0.156504631
FAM120A	0.272956848	0.295325279
CDKN2AIP	0.393962622	0.433821917
CSRP2	0.184001923	0.116806984
UPF1	-0.889767647	-0.343204498
DDX19A;DDX19B	-0.726953506	-0.512816429
EIF4A1	-0.277701378	-0.08617878
GPATCH4	-0.292951107	-0.25592804
SUPT16H	0.487037659	0.275097847
PHF6	0.024721146	0.215527534
TRIP6	-0.088683963	0.36112237
NCOR1	1.062144518	0.126615286
BAIAP2L1	1.105298042	-0.181619167
NUMA1	-0.217906952	-0.088365555
GNAI3	-2.049296498	-0.158607602
RPL4	-0.324612617	-0.12799263
PSMC2	-0.098082542	0.07345295

LIG3	0.167070389	0.281242132
MARS	-0.211989403	0.167881966
ANKHD1;ANKRD17	1.906477332	0.31090796
NUDC	-1.019148827	0.350536466
RPL23	0.152310371	0.141052246
DIS3	-0.106202126	0.132026672
TAGLN2	-0.135910988	-0.297184944
RBM14	-0.295917511	-0.230672836
TNPO1	-0.7466259	0.05506134
SUGP2	-0.446975708	-0.500968933
ZC3H4	-0.059229851	-0.409880638
ATP6V1A	-0.624532461	-0.536456108
ARHGDIA	0.015248299	-0.390010834
XPO1	-0.489561081	-0.128911018
LTV1	0.057971001	0.439600945
RPS8	-0.187842369	0.083337784
RPS23	-0.034414291	-0.030693054
PPA1	0.020073891	0.160651207
CAMSAP1	-1.506805658	-0.13895154
RAB3GAP1	0.204120636	0.162419796
GFPT1	0.482166648	0.399153113
MAP1B	-0.191370964	-0.122977257
NUP50	0.027488708	0.030441284
H2AFY	0.004613876	0.098320961
C10orf67	-7.285749078	0.128373265
ANXA2;ANXA2P2	-0.161445618	-0.153203011
RCC1	-0.285555243	0.622132301
NUCKS1	-0.02833426	0.167257547
IGF2BP1	-0.627263069	-0.113449097
NUP107	0.791603088	0.194523454
EIF3G	-0.10104084	0.088083267
SLC39A7	0.245194435	-0.052975655
NOC2L	-1.072760224	-0.353152633
TPX2	0.430120468	0.25582695
RPL19	-0.021787643	0.102408409
HNRNPU	-0.251576424	0.076353073
NEK9	-0.060636282	-0.191039085
CLTCL1	-0.423184633	0.212770462
SEC23A	-0.479376793	-0.135979652
DDX17	-0.406044006	-0.217853546
HINT1	0.23927021	0.163905144
WAPAL	-0.238462448	-0.181418419
ZC3H14	0.803061485	-0.216254234
DHX9	-0.185487747	0.087658882
AHSA1	0.443949699	0.250083923
PRKDC	-0.043175697	0.08825016

PBDC1	0.982833028	0.103800654
HK1	0.550483704	0.097078323
CCDC43	-0.44244647	-0.361049652
HNRNPF	-0.279087067	-0.058382034
CUL4A	0.279389381	0.149933815
RPL12	0.639987707	-0.527094483
UNC45A	-0.029983521	-0.113715172
EEF2	0.067692757	0.031540871
CHD4	-0.314758301	-0.073308945
ASNS	0.590879321	0.267272472
RAB8A	0.236192703	0.35547924
NCL	0.033084869	-0.061484337
CS	-0.238542318	0.15537715
POLR1A	0.128852725	-0.221515179
MTAP	-0.174048424	-0.271877289
ATIC	-0.255792618	-0.116485596
CCT4	-0.109910011	0.064439774
IGBP1	0.543125153	0.22426796
CTCF	-0.185586452	-0.085483074
SRRT	2.075158119	0.114701271
IK	-0.515510082	0.146975994
RBMX;RBMXL1	1.227834344	0.223683953
TJP1	0.22930932	-0.102677345
ACLY	-0.322650909	-0.070542336
HNRNPA2B1	-0.078984261	-0.035274506
STRBP	-10.79508877	-0.259345412
EIF3I	-0.220959663	-0.069235802
CUX1	0.247219086	0.062854767
STMN1	-1.845103264	-0.199614048
CBX3	0.181312561	-0.119721413
ADNP	-0.066245079	0.112930298
VDAC2	0.548971176	0.110656738
PCCA	0.051246643	-0.079642296
PALM2;PALM2-AKAP2	-1.129826546	-0.080095291
CLINT1	0.438038826	0.149046898
PRMT1	0.075174332	0.051270485
SHMT2	0.514089584	0.16297245
DDOST	-1.039433479	-0.189743757
TOP2A	0.033198357	0.058051109
NACA	2.275392175	-0.122040629
GATAD2A	-0.051339149	0.159552574
IMPDH2	-0.005194664	-0.079227448
RPL7	-0.014692307	0.035949707
HADHA	0.677212715	0.071333885
COPA	0.479523659	0.032035828
ABHD10	-0.093336701	-0.103292823

HSPA4	-0.072203636	-0.07712841
MAP2	-0.030164957	-0.102833748
APBB1	-1.215612769	-0.088778973
HNRNPUL1	-0.135536194	-0.044265747
GDI2	0.102168083	0.041124344
ATXN2L	0.086007118	-0.041938782
NUP153	-0.056853294	-0.032333374
ACTN4	-0.265183449	-0.112262726
NOP56	-0.186306	-0.018864632
EIF4A2	-0.046175957	-0.041485786
SKIV2L2	-0.295134783	-0.062212229
GARS	0.291954756	-0.080670595
RPL37A	-0.304123878	0.084170341
MIF	-0.383125305	-0.087254524
HNRNPLL;HNRPLL	0.184422731	-0.17404449
MAGED2	-0.752583504	0.048428535
NIFK	-0.263233185	-0.013260841
PABPC1	-0.378611565	0.027694702
QARS	0.086057663	-0.027248383
FDPS	-0.502122283	0.054295182
KHSRP	0.071486473	0.029698372
PWP2	-0.874461055	0.028938055
MSH6	0.513816595	-0.082739115
39326	-1.041218758	0.079103708
PARP1	-0.318119049	0.003969193
TCEB1	0.44181633	0.015915871
UCHL1	0.004471779	-0.00455761
RALY	0.009245634	-0.035000563
RPS14	-0.727807045	0.022244453
ZYX	0.626857758	-0.020947456
RPL35A	-0.347500801	-0.006232262
EIF4G1	0.135103226	-0.007210732
DDX27	-0.340929985	-0.012624741
RAB3GAP2	-0.022809982	-0.005842209
FKBP15	0.734267235	-0.007990479
TXLNG	-0.21794796	0.008657455
LARS	-0.326868057	0.004656792
PCBP1	0.253484726	-0.000937462
EPS15	-0.515411615	-0.002445459